Investigations of extracellular vesicles in triple-negative breast cancer

A thesis submitted to the University of Dublin, Trinity College

towards a degree of Doctor of Philosophy

June 2021

Niamh McNamee

Based on research carried out under the supervision of

Prof. Lorraine O'Driscoll

School of Pharmacy & Pharmaceutical Sciences,

Trinity Biomedical Science Institute,

Trinity College Dublin.

Declaration

I declare that this thesis has not been submitted as an exercise for a degree at this or any other university and it is entirely my own work, unless where otherwise indicated. I agree to deposit this thesis in the University's open access institutional repository or allow the Library to do so on my behalf, subject to Irish Copyright Legislation and Trinity College Library conditioned of use and acknowledgement

Signed: 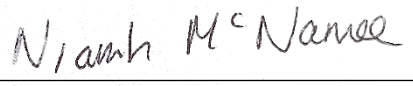

Acknowledgements

Firstly, I would like to thank my supervisor, Prof. Lorraine O'Driscoll. I have learned a lot throughout my 3.5 years in your group. From the very first day you have been a great mentor and was always there to help at literally any time of the day. Thanks to everyone in the School of Pharmacy. Everyone was so welcoming.

The LOD group is a fantastic group of people and a great place to work every day. I definitely could not have got through the last year especially, without everyone. To Delva, we have worked together every day for the past three years and we have also become great friends. Thanks for always calming me down when things didn't work out and reminding me that there was a solution. We really do make a great team, but we can also make great lab work schedules! You are a great scientist and friend and I know whatever you do, you will be great at it. To Jessie, I could always be sure that you would be in the office first in the morning when I arrived and we could have our usual morning coffee chat, probably about western blots! Thanks for being there whenever I needed it and all the help you have given me over the years. I know your PhD will be fantastic. To Sarai, you are so generous with your time and would help anyone, no matter how busy you were yourself. You are such a brilliant researcher and I can't wait to see what you do in the future. To Roisin, we have made a great team since you have started your PhD. I can always rely on you to take my mind of the lab stuff. You are a great team member and I know you will be an amazing scientist. To the Postdocs, Anindya you are a brilliant scientist and I have learned so much from you. Any time I had a problem you would always listen and help me figure out what to do. You give the best advice and you are a great teacher. Dimitris, since you have started you have been such a great help. You never hesitated to give advice whenever I asked and was always available. Thanks to everyone in the LOD group, you are an amazing bunch of people!

To my family, I could not have gotten this far without all of you. You have been there at every step of the way. To mam, thanks for all the dinners you have cooked me after a long day in the lab, even if I complained about them! To Dad, thanks for listening to me complain when my experiments didn't work out as I had planned during the drive home over the past 3.5 years, I could tell you didn't understand what I was talking about most of the time but you always seemed to give right advice. To Sean, thanks for always making my problems seem so silly. To Claire, thanks for being my commuting buddy for the last few years. To my twin sister Ciara, you have made sure that I have got this far and without your constant advice, help and support I know that I would not be where I am today.

To my grandparents, nanny and grandad, thanks for asking about my research every time I called to see you. Thanks for all the encouragement throughout my education. To Gran, you are such a kind, smart and funny person. You always know how to cheer me up. This thesis is dedicated to you!

Table of Contents

List of Figures

List of Tables

Thesis Abstract

Breast cancer is the most commonly diagnosed cancer worldwide accounting for 11.7% of the newly diagnosed 19.3 million cases in 2020. In Ireland breast cancer accounted for 10.8% of cancer cases and 23.8% of female cancers. Triple-negative breast cancer (TNBC), a subtype of breast cancer that lacks expression of the oestrogen receptor (ER), the progesterone receptor (PR) and the human epidermal growth factor receptor 2 (HER2), accounts for 10-20% of all breast cancers. It is heterogeneous in nature, and unlike the other subtypes, has no identified molecular targets for improving treatment options. TNBC is often an aggressive cancer, commonly associated with younger women, and with poor overall survival.

The main focus of this project was the role of extracellular vesicles (EVs) in TNBC. EVs are described as mini-maps of their cell of origin and are involved in cell-to-cell communication. In TNBC, initially our group and subsequently others have shown that EVs were able to pass on "aggressive" traits to recipient cells, prevent cancer cell death by exporting chemotherapeutic drugs, re-programme the tumour microenvironment, support pre-metastatic niche formation, and enhance the metastasis of TNBC cells. Thus, this project started by separating four EV sub-populations from the heterogeneous pool of EVs released from TNBC cells, in order to identify which sub-populations are most responsible for the transfer of the negative effects. We found that all four sub-populations played a part in the transfer of increased cell proliferation, migration, invasion and *anoikis* resistance. No one sub-population was responsible; rather the total heterogeneous population. Therefore, the next logical step was to investigate ways which we might block the release of EVs from the TNBC cells, in an effort to prevent the spread of these undesirable traits. Using proposed EV inhibitors including calpeptin, Y27632, manumycin A, and GW4869- at non-toxic concentrations- we quantified and characterised any EVs that continued to be released after inhibitor treatment. We found that EV quantities were substantially inhibited after treatment. Specifically, calpeptin ($p<0.0001$), Y27632 ($p<0.0001$), combo 1 ($p<0.0001$), manumycin A ($p=0.001$), GW4869 ($p<0.0001$) and combo 2 ($p<0.0001$) all significantly decreased EV release. GW4869 caused the greatest levels of decrease with 98% reduction in EV release compared to the control. Furthermore, the TNBC EVs that were still released after inhibitor treatment did not stimulate migration of recipient TNBC cells when compared to EVs released from TNBC cells not treated with an inhibitor. Specifically, BT549 migration was significantly reduced when cells were treated with the highest dose of EVs released following calpeptin ($p=0.036$), Y27632

(*p=0.007*), combo 1 (*p=0.005*), manumycin A (*p=0.005*), GW4869 (*p=0.005*) and combo 2 (*p=0.017*) treatment.

Venous thromboembolism (VTE), a subset of thromboembolism, is the second leading cause of cancer-related fatality, with cancer patients accounting for 20% of all VTE cases. We identified that two TNBC cell line variants and their corresponding EVs can induce platelet aggregation. Our global proteomic profiling of the EVs cargo identified a number of proteins (including platelet derived growth factor receptor β (PDGFRβ), Protein Cyr61, mucin 18 (MUC18), urokinase plasminogen activator receptor (uPAR), CD97 and glypican-1) that may be involved in this platelet aggregation.

Additionally, EVs may be used as diagnostic tools. However, the methods typically used for EV separation and characterisation, by the EV Community, are not realistically translatable to clinical utility. Therefore, we compared multiple methods of EV separation from serum (breast cancer patients and age-matched healthy controls) with the intention of finding a method that would result in reasonably pure, intact, EVs that were not contaminated with serum-derived proteins; but with a particular interest in potential future clinical utility. To do this, we evaluated differential ultracentrifugation, magnetic immunobeads capture, size exclusion chromatography, nickel-based separation, and precipitation with poly(ethylene glycol) (PEG). To conclude, we found that a magnetic immunobead approach provided an EV separation method that resulted in a higher purity when compared to other methods tested. Although, every method has its disadvantages, this method provides an easy, reliable, and fast method of EV separation that could be realistically translated into a hospital setting.

In conclusion, our results demonstrate that TNBC EVs may play a role in the many facets of TNBC disease, but that the increased migration associated with the TNBC EVs may be reduced through their inhibition. Although our results are preliminary, some EV protein cargo was identified that may be targetable to inhibit VTE in cancer patients or help identify patients who are most at risk of developing VTE. There are many different methods of EV separation for patient-derived blood-based samples. We have demonstrated that EVs from serum can be separated using a user-friendly, easy method that would be realistically translated to patient care.

List of Abbreviations

2-DG 2-Deoxy-D-Glucose

2-DG-6-P 2-Deoxy-D-Glucose-6-Phosphate

A4F Asymmetrical-Flow Field-Flow Fractionation

AChE acetylcholinesterase

ADSCs Adipose-derived stem cells

AMPK AMP-activated protein kinase

APOs Apoptotic bodies

ApoB Apolipoprotein B

AR Androgen receptor

ARF6 Adenosine diphosphate (ADP)-ribosylation factor 6

ASCs Adipose stem cells

ATE Arterial thromboembolism

AU Arbitrary units

BCA Bradford colorimteric assay

BMDCs Bone marrow derived cells

BL Basal-like

BLIA Basal-like immune-activated

BLIS Basal-like immunosuppressed

BPD Benign pancreatic disease

BSA Bovine serum albumin

CAF Cancer associated fibroblast

CAT Cancer associated thrombosis

CEA Carcinoembryonic antigen

CK cytokeratin

CM Conditioned medium

CP Chronic pancreatitis

CRC Colorectal cancer

CSCs Cancer stem cells

Cyr61 Cysteine-rich angiogenic inducer 61

DIFF UC Differential ultracentrifugation

DMEM Dulbecco's modified eagles' medium

DNMT1 DNA methyltransferase 1

DOACs Direct oral anticoagulants

dUC Density-gradient ultracentrifugation

EBV Epstein-Barr virus

ECAR Extracellular acidification rate

ECM Extracellular Matrix

ED Effective dose

EGF Epidermal growth factor

EGFR Epidermal growth factor receptor

EMT Epithelial-to-mesenchymal transition

EQ ExoQuick^{TC}

ER Endoplasmic reticulum

ER Estrogen receptor

ERK Extracellular signal-regulated kinase

ESC Endometrial stromal cell

ESCRT Endosomal-sorting complex required for transport

EVs Extracellular vesicles

FBS Foetal bovine serum

FC Flow cytometry

FIX Factor IX

FVa Factor Va

FVIII Factor VIII

FVIIa Factor VIIa

FX Factor X

GBM Glioblastoma

GE Genetic expression

GECs Glioblastoma-derived endothelial cells

GEFs Guanine nucleotide exchange factors

GP Glycoprotein

GPCR G-Protein coupled receptor

GTPase Guanosine triphosphatase

H3Cit Citrullinated histone H3

HCC Hepatocellular carcinoma

HER2 Human epidermal growth receptor

Hrs Hepatocyte growth factor-regulated kinase substrate

HSPs Heat shock proteins

HTF-1 Anti-human TF antibody

HTR Hormone therapy resistance

HUVECs Human umbilical vein endothelial cells

IARC International Agency for Research on Cancer

ICAM-1 Intercellular adhesion molecule-1

IFCM Imaging flow cytometry

ILVs Intraluminal Vesicles

IM Immunomodulatory

IPMN Intraductal papillary mucinous neoplasm

LAR luminal Androgen Receptor

lEV Large EVs

LFQ Label-free quantification

LMWH Low molecular weight heparin

M Mesenchymal

mEVs Medium EVs

MLC2 Myosin light chain 2

MMPs Matrix metalloproteinases

MP Microparticle

MSCs Mesenchymal stem cells

MSL Mesenchymal Stem Like

MT1-MMP Membrane type-1 matrix metalloproteinase

mtDNA Mitochondrial DNA

mTNBC metastatic TNBC

mTORC1 Mammalian Target of Rapamycin Complex 1

MUC18 Mucin 18

MV Microvesicles

MVBs Multivesicular bodies

NBI Nickel-based isolation

NET Neutrophil nuclear trap

NK Natural killer

NLR Neutrophil-to-lymphocyte

NSCLC Non-small cell lung cancer

nSMase neutral Sphingomyelinase

NTA Nanoparticle tracking analysis

OCR Oxygen consumption rate

OS Overall survival

PADs Peptidylarginine deiminases

PAI-1 Plasminogen activator inhibitor type-1

PARP poly (ADP-ribose) polymerase

PBST Phosphate buffered saline/tween

PCPL Pancreatic cancer precursor lesion

PD-1 Programmed cell death 1

PDAC Pancreatic ductal adenocarcinoma

PD-L1 Programmed death-ligand 1

PDGFRβ Platelet-derived growth factor receptor β

PEG Polyethylene glycol

PFS Progression free survival

PLR Platelet-to-lymphocyte

Poly-HEMA Poly (2-hydroxymethyl methacrylate)

PR Progesterone receptor

PrP Prion protein

PSGL1 P-selectin glycoprotein ligand 1

PVDF Polyvinylindene fluoride

REF Rat embryonic fibroblast

ROCK Rho associated protein kinase

ROS Reactive oxygen species

SEC Size-exclusion chromatography

sEVs Small EVs

SFX Sufisoxazole

SI Signal Intensity

TAMs Tumour associated macrophages

TAT Thrombin-anti-thrombin

TCIPA Tumour cell induced platelet aggregation

TCIPS Tumour cell induced platelet secretion

TE Thromboembolism

TEI Total exosome isolation

TEM Transmission electron microscope

TF Tissue factor

TFMPs Tissue factor-bearing microparticles

TGFβ Transforming growth factor β

TNBC Triple Negative Breast Cancer

TNF Tumour necrosis factor

TPA Tissue polypeptide antigen

TSG101 Tumour Susceptibility Gene 101

tTG Tissue transglutaminase

UC Ultracentrifugation

uPA Urokinase plasminogen activator

uPAR Urokinase plasminogen activator receptor

Vsp4 Vacuolar protein sorting 4

VTE Venous thromboembolism

vWF von Willebrand factor

Chapter 1: Introduction

Parts of this Introduction have been published in the following peer-reviewed paper:

McNamee N, O'Driscoll L. Extracellular vesicles and anti-cancer drug resistance. *Biochem Biophys Acta Rev Cancer*. 2018;1870(2):123-136. Doi: 10.1016/j.bbcan.2018.07.003.

1.1 Breast cancer

There were 19.3 million new cancer cases recorded in 2020. Breast cancer was the most commonly diagnosed cancer worldwide accounting for 11.7% of the newly diagnosed. In Ireland, breast cancer accounted for 10.8% of cancer cases and 23.8% of female cancers (accessed information from IACR.FR website). In 2000, Five subtypes of breast cancer, also known as the "five intrinsic subtypes" were identified (See Table 1.1) by applying first generation cDNA microarrays in human breast tumour samples and were separated based on their gene expression profile [1, 2]. They consist of luminal A, luminal B, HER2, basal-like and normal-like. Of all breast cancers luminal A is the most common, representing 50-60% of breast tumours [3]. They are characterised by the expression of estrogen receptor (ER) and the progesterone receptor (PR) and are negative for the human epidermal growth receptor (HER2) receptor. Luminal B represents 15-20% of breast cancers and are slightly more aggressive than luminal A cancers [4]. Approximately 30% of luminal B tumours are HER2 receptor positive, However, this clinical marker is not sensitive enough to distinguish luminal B tumours from luminal A tumours alone. A study distinguished luminal A and B from each other by the immunochemistry analysis of Ki-67, a marker of proliferation encoded by the *MKI67* gene [5]. The study established that luminal A tumours had a low expression of Ki-67 compared with luminal B which had a high expression. This contributes to the worse prognosis associated with luminal B tumours. In addition, Luminal B tumours tend to have a higher percentage of lymph node involvement compared with luminal A [6]. Luminal breast cancers respond to endocrine therapies such as tamoxifen which inhibits the transcriptional activity of the ER [7].

HER2-enriched breast cancers have an amplification of the HER2 oncogene and overexpression of the HER2 receptor gives this subtype a more aggressive clinical and biological behaviour compared to the other subtypes that do not have HER2 expression [3]. This subset accounts for 15-20% of all breast cancers [8]. The development of trastuzumab, a monoclonal antibody that blocks the HER2 receptor, has improved the treatment of HER2-positive breast cancer [9]. It must be noted that some patients experience resistance to this form of treatment [10].

Normal-like tumours represent 5-10% of all breast cancers but are poorly understood. This subgroup may be based on the contamination of breast cancer cells with healthy tissue [3]. They have similar expression profile as luminal A tumours but have a poorer prognosis [11].

Another subtype, called claudin-low (see Table 1.1) has been identified by the low expression of genes involved in tight junctions and cell-cell adhesion such as claudins 3 and 4, Occludin and E-cadherin [12]. Clinically they have a poor prognosis with the approximately 70% of claudin-low tumours being negative for ER, PR and HER2. They have high epithelial-to-mesenchymal transition marker expression (i.e. vimentin and N-cadherin) and immune-related genes (e.g. *CD4, CD79a*) [13].

Subtype	Associated molecular signature
Luminal A	ER and/or PR^+, $HER2^-$, low Ki-67
Luminal B	ER and/or PR^+, $HER2^+$, High Ki-67 ER and/or PR^+, $HER2^+$, Low Ki-67
HER2+	ER^-, PR^-, $HER2^+$
TNBC	ER^-, PR^-, $HER2^-$
Normal-like	ER^- and/or PR^+, $HER2^-$, low Ki-67
Claudin-low	ER^-, PR^-, low E-Cadherin

Table 1.1: Breast cancer subtypes and their molecular signatures

1.1.1 Triple Negative Breast Cancer

Triple negative breast cancer (TNBC) is a subtype of breast cancer that lacks the expression of the ER, PR and the HER2 receptor. TNBC accounts for 10%-20% of all breast cancers. There is substantial heterogeneity associated with TNBC which can be divided into subgroups based on IHC staining and gene expression profiles. TNBCs can be basal-like in nature based on their genetic makeup, getting its name from it similarity to basal epithelial cells which have reduced immunohistochemical staining for ER, PR, HER2 but are positive for basal cytokeratins (CKs) such as CK5/6, CK14 and CK17 [14, 15]. However, as shown by Bastien *et al.* [16] 57% of TNBC tumours were classified as basal-like demonstrating that caution should be taken when characterising TNBC as it is not totally synonymous with the basal-like subtype. This will have ramifications for patients in the clinic and will hopefully lead to a more personalised approach during treatment plans.

Due to the lack of molecular targets, a poor prognosis is usually associated with TNBC compared with other breast cancer subtypes. Treatment options are limited for this group of cancers along with a high chance of distant recurrence and disease progression [17]. Sorlie *et al*. [18] concluded that basal-like tumours had an association with BRCA-1 mutations and that this mutated allele may preferentially give rise to the TNBC phenotype. A study in 2007 including 1,601 breast cancer patients concluded that less than 30% of patients with metastatic TNBC survived more than 5 years despite receiving

adjuvant therapy, displaying a more aggressive clinical course [19]. Bauer *et al.* also observed that TNBC is diagnosed in younger women and it is more prevalent in Hispanic and non-Hispanic black women [20]. Overall, TNBC is characterised by a tumour that is larger in size, has a higher chance of lymph node involvement at diagnosis, increased aggressiveness, shorter survival, and is similar to BRCA-1 mutated breast cancer [2, 18, 21-23]. Currently the main treatment option for TNBC is chemotherapy including taxanes, anthracyclines, cyclophosphamide, fluorouracil and platinum agents such as cisplatin [24]. With "precision medicine" being the aim for modern day treatment, giving patients a personalised treatment plan based on the genetic makeup of their tumour, a recent phase Ib/II clinical trial, FUTURE published its results [25]. The FUTURE trial is one of the first trials for TNBC that employs personalised medicine approach to stratify TNBC patients into precision treatment arms based not only on the IHC molecular profiling of their tumours and also based on genomic sequencing of their tumour biopsies. This allowed a targeted therapy approach for refractory metastatic TNBC patients with some treatment arms including anti-PD-1 immune checkpoint inhibitor, SHR-1210 plus nab-paclitaxel, androgen receptor inhibitor plus CDK4/6 inhibitor or PARP inhibitor. Overall, the study demonstrated that using sequencing to develop a targeted treatment plan was feasible and a promising strategy for the highly aggressive metastatic TNBCs.

1.1.1.1 Triple Negative Breast Cancer subtypes

In 2011 Lehmann *et al.* [26] published a study that characterised six distinct subtypes of TNBC based on their genetic expression (GE) profiles. Through the analysis of publicly available GE of 587 TNBC tumours, they illustrated that the six subtypes had individual biology and this in turn led to their varying responses to therapies. Their cluster analysis revealed the following subtypes: two basal-like (BL1 and BL2), an immunomodulatory (IM), a mesenchymal (M), a mesenchymal stem-like (MSL) and finally a luminal androgen receptor (LAR) subtype. BL1 subtypes had increased expression of cell cycle components along with elevated DNA damage response and proliferation pathways suggested by the expression of genes such as *CHEK1, NBN, EXO1, MSH2 and MCD1.* BL2 subtype displayed separate gene ontologies involved in growth factor signalling (i.e. signalling pathways such as the EGF, NGF, MET and WnT/β-catenin pathways) and energy pathways such as glycolysis. It had increased expression of growth factor receptors such as EGFR and MET. The IM subgroup has gene signatures corresponding to immune processes including immune cell signalling (e.g. TH1/TH2 pathway, NK cell pathway, DC pathway), cytokine signalling (e.g. IL-7 and IL-12 pathways), antigen processing and presentation and immune signal transduction pathways (e.g. NFKB and JAK/STAT pathways). The M

group displayed gene ontologies which are components of cell motility and cell differentiation pathways along with extracellular matrix (ECM) receptor interactions. MSL TNBCs share similar genes with the M subtype in relation to cell motility and cell differentiation involvement along with a set of unique ontologies linked to growth factor signalling such as the epidermal growth factor receptor (EGFR) and ERK1/2 signalling, G protein-coupled receptor signalling as well as ABC transporter and adipocytokine signalling. It also displayed genes involved in angiogenesis such as *VEGFR2, TEK, TIE1* and *EPAS1*. One major difference discovered during the analysis between the M and the MSL subgroups was the MSL subtype expressed low levels of proliferation genes but had an increased set of genes associated with stem cells (e.g. *ABCA8, ENG, ALDHA1, BMP* and *THY1*) and mesenchymal stem cell-specific markers (e.g. *BMP2, ENG, ITGAV, NGFR, PDGFRB, THY1* and *VCAM1*). In addition, it also had a claudin-low gene signature, similar to the claudin-low subtype of breast cancer described by Herschkowitz *et al.* [12]. The LAR tumours were subdivided based on the identification of high androgen receptor (AR) signalling. AR mRNA expression was 9-fold greater than all other subtypes and genes of downstream factors of AR were detected (e.g. *ALCAM, FASN, APOD* and *CLDN8*).

In 2016, Lehmann and colleagues redefined the six molecular TNBC subtypes after they confirmed, by laser-capture microdissection and RNA isolation for gene expression analysis, that infiltrating stromal cells were contributing to the MSL and IM subtypes and therefore the original TNBC subclassification was narrowed down to contain four subtypes; BL1, BL2, M and LAR [27].

Meanwhile, others have reported a different subtype classification that has also been used to distinguish between the heterogenous subtypes of TNBC. Burstein *et al.* [28], using 198 TNBC tumours, performed DNA and mRNA profiling analyses, revealing the presence of four distinct TNBC subtypes including luminal androgen receptor (LAR), mesenchymal (MES), basal-like immunosuppressed (BLIS) and basal-like immune-activated (BLIA). Each subtype had specific molecular biomarkers that defined each group, such as MUC1 in the AR tumours and PDGFRA and c-Kit in MES tumours. BLIS had the worst prognosis and immunosuppressive characteristics with downregulation of B and T cell signalling. The immunosuppressive protein VTCN1 was detected as a specific marker of BLIS subgroup. BLIA subgroup had the best prognosis and distinguished by STAT signalling and cytokines.

1.1.1.2 TNBC cell line Hs578T and its isogenic subclone

The Hs578T cell line is one of the many used to study TNBC *in vitro* (including in this project). It belongs to the MSL TNBC subtype. It was originally isolated from a primary carcinoma of the breast [29]. The Hs578T cell line is invasive in 3D culture and grows in stellate projections that connect multiple cell

colonies. The cells have mutations in the *TP53, HRAS* and *CDKN2A* genes [30]. In 2008, a more invasive variant of the Hs578T cells was established by Hughes *et al.* [31] and designated Hs578Ts(i)$_8$. It was developed by seeding Hs578T cells on a Matrigel invasion chamber. The cells that invaded through the Matrigel were detached and expanded in a culture flask. The cells were then plated on another invasion chamber and allowed to invade and expanded for a second time. This was repeated eight times in total, when the cells increased their invasive capabilities 3-fold and were 2.5-fold more migratory than the parental, Hs578T cells. It was shown that this new variant could also produce tumours in nude mice while the less tumorigenic Hs578T parent cells could not. It was postulated it may be due to the higher stem cell population seen in the Hs578Ts(i)$_8$ cells compared to the Hs578T cells [31]. Our research group investigated this further and found that Hs578Ts(i)$_8$ cells have an increased proportion of $CD44^+/CD24^+$, i.e. cancer stem cells (CSCs) compared to the parental Hs578T cells, which could be reduced by 2-Deoxy-D-Glucose (2-DG) treatment *in vitro* [32]. Other TNBC cell lines used in this project include; MDA-MB-468 (BL1 subtype), MDA-MB-231 (MSL subtype), HCC1143 (BL1 subtype) and BT549 (M subtype) [26, 33].

1.2. Extracellular Vesicles

Approximately 30 years ago, exosomes were described as involved in reticulocyte maturation by transporting transferrin receptor out of the cell [34]. Building on this knowledge, over recent years increasing evidence indicates that substantial cargos of information are released from cells via lipid bilayer-enclosed vesicles typically termed exosomes and microvesicles. These vesicles are proposed to be tailor-made specialised mini-maps of their cell of origin; are transported in the bloodstream and other body fluids; and much evidence indicates them to be involved in cell-to-cell communication. Exosomes and microvesicles now collectively termed extracellular vesicles (EVs), are often defined and sub-grouped based on size, cellular origin (exosomes ~30nm-120nm, endosomal origin; microvesicles/ectosomes >120-1000nm, from the cell membrane) [35]. It should be noted that some reports use additional or alternative terms including, but not limited to, ectosomes, microparticles, oncosomes, melanosomes and prostasomes; all of which are EVs and/or apoptotic bodies. However, once outside the cell and released into the environment (for example, the bloodstream) we cannot be certain if the EVs originated from the cells' endosomal region or directly from the cell membrane. Furthermore, EV size distinctions are not absolute i.e. there is no known reason why vesicles budding from the cell membrane cannot be <120nm. In diseases such as cancer, regardless of the size and origin of EVs released, arguably the problems that EVs contribute to when released are of much importance to understand. Evidence from pre-clinical and clinical specimens' studies, by ourselves and

others, strongly associate EVs with transmitting anti-cancer drug resistance and cancer cell traits from cell-to-cell in multiple cancer types.

Microvesicles (MVs) are released by direct budding and fission of the cell membrane (see Fig. 1.1) [36]. The translocation of phosphatidylserine to the outer membrane of the cell induces MV release by causing alterations in the cell morphology and promoting membrane curvature and detachment from the cell [37]. Enzymes such as flippases and scramblases are involved in switching lipids from one side of the membrane to the other [38]. Ca^{2+} levels regulate these enzymes as well as calpain, affecting membrane rigidity and symmetry and the contraction of the actin cytoskeleton, enabling MV formation and budding [39]. Cholesterol has also been shown to play a role in MV release as the inhibition of lipid raft formation by methyl-beta-cyclodextrin reduced EV release and cholesterol [40]. Cargo released from the cell in MVs is thought to be selective and mediated by the GTP-binding protein, adenosine diphosphate (ADP)-ribosylation factor 6 (ARF6) [36]. Shedding of the MVs is also controlled by actin-myosin contraction and induction of extracellular signal-regulated kinase (ERK), inducing a signalling cascade resulting in the contraction of actinomyosin and eventual MV release [41]. This can also be mediated by Rho family members such as RhoA, which can act on Rho associated protein kinases (ROCK) and ERK [42].

Exosomes are formed through an intracellular pathway (see Fig. 1.1). Cell membrane invagination and fusion of endocytic vesicles results in the formation of early endosomes. These endosomes undergo maturation to form late endosomes [43]. Intraluminal vesicles (ILVs) are formed within the late endosome following invagination of the endosome membrane which are then called multivesicular bodies (MVBs). The endosome sorting complex required for transport (ESCRT) machinery is required for MVB formation and is made up of ESCRT-0, I, II and III as well as accessory proteins such as the ATPase vacuolar protein sorting 4 (Vsp4) [44]. They orchestrate the recognition and sorting of protein cargoes into ILVs. ESCRT-0 and -I recognise ubiquitinated proteins and target them for ILVs integration. The recruitment of ESCRT-III and then ESCRT-II results in vesicle abscission and release, forming MVBs [45-47]. Adaptor proteins help to synchronise the sorting of cargoes into ILVs. For example, Vsp4 allows the dissociation of the ESCRT-ubiquitinated protein complexes and recycles ESCRT-III after ILV formation [47, 48]. An alternative, ESCRT-dependent pathway has been described, involving the syndecan-ALIX-syntenin axis [49]. ALIX, an ESCRT accessory protein brings ESCRT-III into a complex that can initiate ILV formation. This complex contains syndecans that are acted upon by heparinases, allowing their interaction with syntenins and intraluminal budding in endosomes [50]. ESCRT-independent pathways have also been discovered and seem to be dependent upon certain lipids and ceramide. Lipid rafts on the endosome membrane contain both cholesterol and sphingolipids. The

sphingolipids undergo a conversion to ceramide by the action of neutral sphingomyelinase (nSMase) which forms larger microdomains in the membrane and induces budding and the formation of ILVs [51]. Inhibition of nSMase activity reduced the release of exosomes while also increasing MV budding [52]. Tetraspanin CD63 has been shown to play a role in melanosome formation, specialised endosomal structures in pigment cells, in a unique pathway, independent from ESCRT ubiquitination [53].

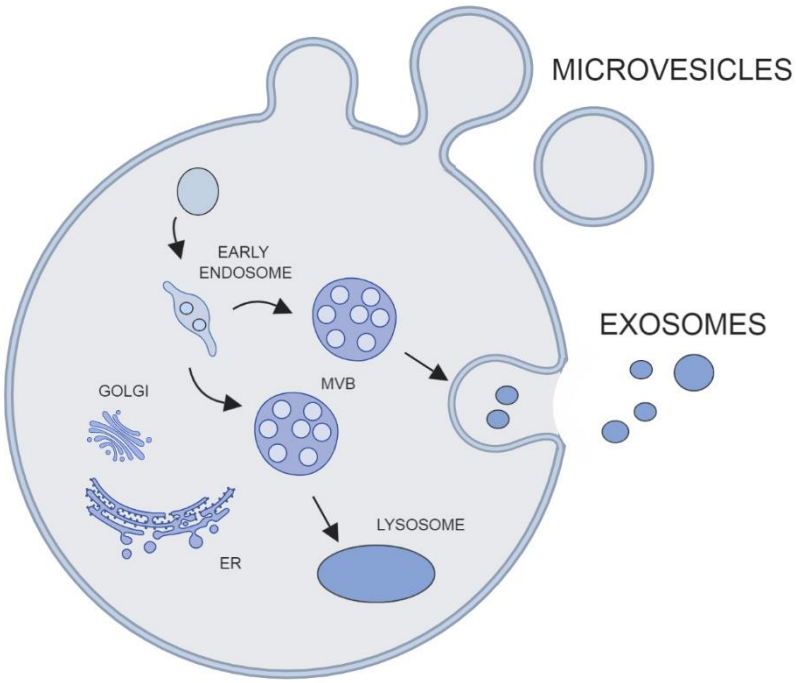

Figure 1.1: Biogenesis of microvesicles and exosomes, collectively termed extracellular vesicles

The biogenic pathway of microvesicles (MVs) involve the budding of vesicles directly from the cell membrane. Exosomes are formed through an intercellular pathway through the formation of multivesicular bodies (MVBs) which can be targeted to the lysosome for breakdown or to the cell membrane and eventual release into the extracellular environment. ER=Endoplasmic reticulum.

1.2.1 EV sub-populations

Over the past ten years, researchers have begun to subdivide EVs into either small, medium, or large vesicles, based on their size. This is a preferred terminology among EV researchers rather than MVs or exosomes as EVs budding from the cell membrane can be of varying sizes and therefore, do not satisfy the old classification that MVs only bud from the cell membrane and are bigger than 120 nm in diameter.

1.2.1.1 Large EVs

Apoptotic bodies (APOs): Cells that undergo apoptosis release EVs, called APOs that bleb from the cell membrane [54]. They are reported to have a wide range of sizes from approximately 500 nm to 2000 nm. Their content is thought to be randomly packaged by the apoptotic cell. However, other researchers have shown that APOs can contain distinct RNA and DNA profiles, with cells releasing different populations of apoptotic bodies, with some containing RNA and no DNA and *vice versa* [55]. APOs can contain larger amounts of RNA compared with other EV subpopulations such as small EVs, in particular rRNA [56]. APOs can have an effect in many physiological processes that occur in the body, however, they can also play a role in pathological conditions. Holmgren *et al.* [57] demonstrated that APOs from an Epstein-Barr virus (EBV)-positive Burkitt's lymphoma cell line, BL41/95 can transfer their contents, including EBV DNA into human foetal fibroblast (HF) cells, inducing the expression of EBV markers such as EBV-encoded nuclear RNAs, EBER1 and EBER2. APOs can also transfer harmful oncogenes, increasing the tumorgenicity of the recipient cells. The uptake of APOs from H-ras^{v12}-and c-myc transfected rat embryonic fibroblast (REF) cells conferred anchorage independence to recipient mouse embryonic fibroblast (MEF) cells that had inactivated p53 (i.e. MEF p53$^{-/-}$) and the loss of their contact inhibition. When cells were treated with APOs from normal REF cells, their growth was not affected as focus formation was not detected. This study showed that APOs can act as delivery systems for oncogenic material, however, it should be noted that after four weeks of culture, PCR detection of H-ras^{v12} and c-myc was lost with the authors demonstrating that genes involved in hygromycin, which offer a positive selection advantage, could be propagated after four weeks of culturing [58].

Large oncosomes (LOs): The term "oncosome" was originally coined by the authors investigating MVs that contained oncoproteins. They were first identified in 2008 as vesicles that were released by glioblastoma cells and contained an oncogenic variant of the EGFRvIII receptor. The authors demonstrated that these vesicles transferred the oncoprotein to the cell membrane of other tumours that had previously lacked it, thus propagating the cancer phenotype *via* intercellular communication carried out by the oncosomes [59]. This terminology was further developed and subsequently used for another subtype of EVs called "large oncosomes", as their size was atypically large with a diameter of 1-10 µm. These large vesicles were released by prostate cancer cells that had underwent a fast "amoeboid" migration and in response to induced oncogenic signalling through oncoprotein transfection such as MyrAkt1 and the precursor form of EGFR ligand HB-EGF [60]. They are cancer-specific and contain cargoes that enhance the transformation of their target cells [61]. In addition, LOs can contain distinct miRNA cargoes depending if their cell of origin is tumorigenic or non-tumorigenic. It was discovered that LOs from the tumorigenic RWPE-2 cell line contained miRNA (miR-1227) that

was transferred into recipient fibroblast cells and induced their migration [62]. LOs released from the prostate cancer cell line LNCaP that expressed the oncogene, MyrAkt1, contained MyrAkt1 on their surface and could induce the migration of mouse endothelial cells and DU145, another prostate cancer cell line in *vitro* [63]. This was also replicated *in vivo*, with MyrAkt1-positive LOs isolated from mice that had been injected sub-cutaneously with LNCaP/MyrAkt1 cells and subsequently developed tumours, able to stimulate the migration of normal endothelial cells.

1.2.1.2 Medium EVs

Microvesicles (MVs) is the name given to vesicles that fall into the "medium category" as they are in the size range of 120-1000 nm. They originate from the cell membrane by outward budding and are released into the extracellular space by fission [64]. In the cancer setting, MVs have a role to play in tumour progression, especially in metastasis and priming of metastatic niches. For example, MVs interact with nearby stromal cells and other tumour cells to enhance tumour migration and the creation of premetastatic niches. Sidhu *et al.* [65] reported that MVs released by tumour cells interact with fibroblast cells and deliver EMMPRIN, a transmembrane glycoprotein, initiating the production of matrix metalloproteinases (MMPs), allowing tumour cell invasion and metastasis to occur. In another study, EMMPRIN-positive MVs isolated from plasma correlated with a worse prognosis in a cohort of cancer patients and at elevated levels with advanced tumours [66]. MVs released from CD105-positive CSCs of a renal carcinoma increased the invasion of normal human umbilical vein endothelial cells (HUVECS). These EV carried pro-angiogenic factors, such as VEGF, FGF, MMP2 and MMP9. The MVs were injected into SCID mice along with K1 cells, previously isolated from renal carcinoma. After 5 weeks, there was a substantial increase in lung metastases along with increased MMP9 expression in the lung tissue, demonstrating that the MVs contributed to the formation of premetastatic niche [67]. Prostate cancer MVs isolated from PC3 and LNCaP cell lines also activated fibroblasts in the stroma, upregulating MMP9, increasing their migration and resistance to apoptosis. Interestingly, the MV-activated fibroblasts released their own MVs which were able to further increase the migration and invasion capabilities of the prostate cancer cells [68]. MVs have been shown to transfer the oncogenic receptor, EGFR, into endothelial cells; leading to the activation of MAPK and Akt pathways and triggering pro-angiogenic signalling [69]. MVs can also carry oncogenic proteins. CD133-containing MVs originating from KRAS mutant HCT116 colon cancer cells delivered the mutated KRAS to nearby non-tumorigenic, HEK293A cells and activated KRAS signalling. They also increased the migration and invasion of recipient HEK293A cells [70]. Similarly, colorectal cancer cells,

SW480 released MVs containing integrins, NOTCH1/2 and EGFR while SW620 derived MVs contained cancer progression proteins such as FGFR4, MACC1, and PAK1 which are involved in cell invasion, metastasis and signal transduction, respectively. The MVs capable of being taken up by NIH3T3 fibroblasts and increasing their invasive potential [71].

1.2.1.3 Small EVs

Small EVs are approximately 30-150 nm in diameter. Due to the similarity in diameter between exosomes and MVs, size cannot reliably distinguish among the two. Exosomes are formed through an intracellular pathway involving the generation of early endosomes which mature into late endosome or multivesicular bodies (MVBs). While doing so, they accumulate intraluminal vesicles (ILVs) as the endosomal membrane undergoes invagination. The MVBs fuse with the cell membrane and the ILVs are subsequently released into the extracellular space as exosomes [72]. The endosomal-sorting complex required for transport (ESCRT) is responsible for sorting cargoes into the ILVs [73]. As with the other types of vesicles, exosomes can also harbour oncogenic material facilitating oncogenesis.

Increased exosome-like EV release from RAS-3 cells was attributed to oncogenic transformation of rat intestinal epithelial cells by H-*ra*s. These exosomes were shown to transfer oncogenic H-*ras* double-stranded DNA to recipient cells, promoting increased proliferation in the receiving non-tumorigenic fibroblast RAT-1 cells [74]. In a separate study, prostate cancer exosomes from PC-3 and RWPE-1 cells were taken up by patient adipose-derived stem cells (pASCs) promoting the neoplastic reprogramming of the ASCs and tumour formation *in vivo*. Further analysis revealed that the exosomes caused the up-regulation of the oncomiRNAs miR-125b and miR-130b, resulting in the expression of mutated H-*ras* and K-*ras* in the treated pASCs, inducing their transformation [75]. Exosomes released from prostate cancer cells, PC3 and LNCaP under hypoxic conditions have also been reported to increase the invasiveness and stemness of the recipient prostate cancers cells PC3 and LNCaP and also increased the cancer-associated fibroblast (CAF) phenotype in prostate stromal cells through the increase in lytic enzymes such as MMP2 and MMP9 [76]. Exosomes have been implicated in the suppression of immune cells and blocking the tumour cells of immune attack. Our group published a study that demonstrated HER2-positive breast cancer cells HCC1954, EFM192A and SKBR3 which overexpress neuromedin U (NmU) had increased levels of tumour suppressor proteins, $TGF\beta_1$ and PD-L1 and this was transferred into the EVs which they released [77]. Interestingly, lapatinib and neratinib-resistant HCC1954 derived EVs had increased $TGF\beta_1$ and PD-L1 levels compared to parental HCC1954 EVs and the drug-resistant EVs could increase $TGF\beta_1$ in the drug-sensitive cells. EVs isolated from serum of

patients with HER2-overexpressing tumours showed that there was higher TGFβ_1 levels in EVs from non-responders (NR) when compared to patients that had a complete response (CR) or partial response (PR) to neo-adjuvant therapy of trastuzumab with or without lapatinib. Cereghetti *et al.* [78] demonstrated that tumour derived exosomes can deliver miRNAs that inhibit T cell development. As shown with MVs, exosomes can also prepare and recruit cells that form part of the pre-metastatic niche. In addition, exosomes from melanoma cells educated and mobilized bone marrow derived cells (BMDCs) *in vivo* and increased the metastatic burden by delivering MET oncogene to the BMDCs [79]. Overall, there is a substantial amount of evidence of exosomes role in tumour development, growth and progression.

1.2.1.4 Protein components of EV sub-populations

One of the main methods of distinguishing different sub-populations of EVs is the use of immunoblotting to determine specific combination of protein markers. These proteins are often involved in their biogenesis. Distinct sets of proteins can determine the sub-population of EVs being studied. Small EVs, such as exosomes, are enriched for proteins involved in endosomal formation during exosome release [80]. For example, exosomes can be identified by the presence of the tumour susceptibility gene 101 (TSG101), a protein component of the ESCRT1 complex which recognises cargo and sorts them into the ILVs in the maturing MVB [81]. Membrane-bound tetraspanins such as CD9, CD63 and CD81 have been identified in small EVs, however, it should be noted that CD9 and CD63 can be present in non-exosomal EV pellets and that small EVs can also be devoid of all three tetraspanins [82]. In the same study, *bona fide* exosomes were established by the presence of TSG101, tetraspanins and syntenin proteins while protein that were considered true exosomes markers such as flotillins, heat-shock proteins 70 and MHC class I/II molecules were found in all sub-populations [82]. Syntenin is implicated in another exosomal pathway as an adaptor protein with syndecans and ALIX (a component of the ESCRT machinery) that results in the formation of exosomes [83].

In terms of large and medium vesicles or microvesicles, the markers are less well defined. ARF6 has been validated as a marker which helps the shedding of microvesicles from tumour cell surface [41]. ARF6 is a member of the ARF family of GTP-binding proteins and has been shown to regulate membrane trafficking, cytokinesis and cytoskeleton remodelling [84]. Other markers include proteins involved in the cellular secretory pathways through the endoplasmic reticulum and/or Golgi apparatus. These include GRP94 which is highly enriched in large EVs and have been identified in the secreting cells from which the large EVs were isolated. It should be noted that some consider GRP94

as a negative EV marker. A proteomic study revealed that actinin-4 and mitofilin are specific markers for large and medium sized EVs and are not present in small EVs [82]. The Di Vizio group reported that cytokeratin 16 may be a potential marker for tumour-specific large oncosomes [61].

Table 1.2 lists some of the proteins that have been found in each sub-population and includes protein markers that are used in this project. MISEV guidelines published in 2018 gave a clear overview of which proteins should be present EVs and how to distinguish what sub-population is under investigation with categories including (A) transmembrane proteins, (A) cytosolic proteins, (C) non-EV co-isolated structures, (D) proteins associated with other intracellular compartments other than the plasma membrane and (E) endosome and secreted protein recovered with EVs [85]. Contaminating proteins listed category (C) include apolipoproteins, albumin in plasma or serum EVs and uromodulin in urine EVs

EV marker	MISEV category	Large EVs	Medium EVs	Small EVs
CD9	A	✓	✓	
CD81	A	✓	✓	✓
CD63	A	✓	✓	✓
TSG101	B			✓
Syntenin	B			✓
Flotillin	B	✓	✓	✓
ARF6	B	✓		✓
Mitofilin	D	✓	✓	
Actinin-4	D	✓	✓	
Cytokeratin 18	D	✓		
GRP94	D	✓	✓	

Table 1.2: Protein markers in EV sub-populations according to MISEV2018 guidelines

TSG101 = tumour susceptibility gene 101, ARF6 = adenosine diphosphate (ADP)-ribosylation factor 6

1.2.2 EVs in TNBC

There have been a number of studies which demonstrate EVs' role in cancer progression in TNBC. Our group first reported EVs involvement in propagating the disease, demonstrating that EVs from the Hs578Ts(i)$_8$ cell line could transfer "aggressive" phenotypic traits to recipient cells that resembled their

cell of origin i.e. Hs578Ts(i)$_8$, including increased proliferation, migration and invasion as well as stimulation of endothelial tubule formation by HUVECs [86]. Another paper published by our group showed that there was a lower level of miR-134 in the aggressive TNBC cell line Hs578Ts(i)$_8$ compared to the less aggressive, parental cell line Hs578T and their corresponding EVs. By transfecting the Hs578Ts(i)$_8$ cell line with miR-134 or through the delivery of miR-134 *via* EVs loaded with miR-134, they were able to demonstrate a reversal of aggressiveness with a reduction in cell proliferation and increased sensitivity to cisplatin [87]. In 2017, a study with senescence-induced Cal51 TNBC cells resulted in the release of more EVs (i.e. EVs < 200 nm) when compared to control Cal51 TNBC cells. These EVs **exported the chemotherapeutic** fluorescent paclitaxel analogue, flutax-2, from the cells; preventing death of the cancer cells. The EVs also contained key proteins from the Cal51 cells that are involved in cell proliferation, ATP depletion, apoptosis, maintaining ATP levels within the cells, and inhibiting the onset of cell death. This is advantageous to cancer, removal of molecules from the TNBC cells via EVs may explain how senescent cells remain viable even during chemotherapy treatment [88]. In another such study, EVs (i.e. exosomes) isolated from the TNBC cell line, HCC1806 conditioned medium increased the proliferation of the non-tumourigenic cells MCF10A. The TNBC EVs induced the chemoresistance of the MCF10A cells to both doxorubicin and docetaxel [89]. EVs from TNBC have also been associated with the **reprogramming the tumour microenvironment**. Rabe *et al.* [90] demonstrated, using bone marrow-derived macrophages (BMDMs) isolated from C57Bl/6 mice, that EVs (i.e. EVs < 200 nm) from BM1 (i.e. the bone-metastatic variant of MDA-MB-231) and LMB (i.e. mouse TNBC cell line E0771-LMB) TNBC cells reprogrammed tumour associated macrophages (TAMs) *via* activation of TLR2 and TLR3, advancing them towards a more invasive phenotype, stimulating the release of cytokines from the TAMs that increased tumour cell metastasis. Additionally, TNBC cell MDA-MB-231 derived EVs (i.e. isolated using Exo-spin exosome purification kit) were found to enable axillary **lymph node metastasis** in an orthotopic TNBC model *via* the polarisation of RAW264.7 macrophages into pro-inflammatory M2 macrophages, with the increase in polarisation markers such as arginase-1 compared with phosphate buffer saline (PBS) control [91]. In a recent study, TNBC SUM159 cells were shown to **establish pre-metastatic niche** in the lungs of mice compared with non-TNBC cell line, MCF-7. After more in-depth investigation they found that EVs isolated (i.e. small EVs isolated by filtration and SEC) from the TNBC cell lines MDA-MB-231, SUM159 and LRCP17 promoted the expression of pre-metastatic niche markers, fibronectin and periostin, in lung fibroblasts at the RNA and protein level [92]. A study in 2020 confirmed a role for stage-II and stage-III breast cancer patient-derived EVs (i.e. a heterogeneous pool of EVs) in promoting the **migration and invasion on MDA-MB-231** cells by inducing MMP-2 and MMP-9 secretion from the TNBC cells and through the activation of Src signalling pathway [93]. EVs from the plasma of healthy women with no family history

of breast cancer were also used alongside the breast cancer EVs and demonstrated that they did not induce MDA-MB-231 migration. Overall, it has been established that EVs released from TNBC cells have a role to play in all steps of cancer progression and metastasis.

1.2.3 Inhibition of EV release

An extensive literature review has been published by our group on this topic [94]. Ongoing research is underway to identify new targets to prevent or decrease the release of EVs, in order to prevent cancer progression. Drugs and inhibitors with the potential to prevent EV release are also being investigated for eventual clinical use or for research purposes. For example, sulfisoxazole (SFX) was shown to inhibit small EVs release from breast cancer cell line MCF-7 and MDA-MB-231, but not the EVs from the normal breast cell line, MCF10A [95]. SFX decreased the expression of several RABs such as Rab5 and Rab27a, and cellular CD63. Endothelin receptor A is also a target for SFX and found to be involved in small EV biogenesis.

Several drugs were tested for their ability to inhibit EV release, with the conclusion that chloramidine and bisindolylmaleimide-I were the most effective, as they reduced the release of both exosomes and MV-sized vesicles [96]. They also show the combination of both drugs improve the efficacy of 5-fluorouracil in breast and prostate cancer cells, MCF-7 and PC-3. In a similar study, using PC-3 and PNT2, a normal prostate cell line, the cellular targets of chloramidine was elucidated by the demonstration that chloramidine targets and inhibits peptidylarginine deiminases (PADs), specifically PAD2 and PAD4, preventing MV release [97]. PADs are involved in post-translational modification, catalysing protein-bound arginine residues to citrullines that are essential for physiological functions [98].

The inhibitors used in this study include calpeptin and Y27632, proposed to have the ability to inhibit the release of MVs or vesicles that bud directly from the cell membrane. Manumycin A and GW4869 were also used. They have been claimed to inhibit the release of exosomes or EVs that are formed and secreted through an endosomal pathway.

1.2.3.1 Calpeptin

Calpeptin is a drug that was initially developed to assess the physiological role of calpains, its cellular target [99]. Calpains are a family of well-conserved calcium dependent cysteine proteinases with 14 known calpain gene isoforms [100]. μ-calpain (calpain-1) and m-calpain (calpain-2) are the most extensively studied with a role in controlling proteolytic activity being the main one [101]. When calcium levels rise, Ca^{2+} binds to the calpains, initiating a conformational change and activation of the protein which play a role in many different cellular processes such as cell differentiation, cell proliferation, cytokine processing, migration and apoptosis [102]. They have also been implicated in cancer, becoming dysregulated in many cancers and promoting cancer aggression and progression [103]. Because of their role in these cellular processes and therefore, their actions in cytoskeleton remodelling, it has been suggested that they play a part in MV release and budding (see Fig. 1.2).

A combination of docetaxel and calpeptin inhibited MV release by PC3 cells by more than fifty percent when compared to PC3 cells treated with docetaxel alone. There was higher intracellular docetaxel concentration with calpeptin treatment compared to no calpeptin treatment as the drug was not able to be secreted out of the cell, with reduced MV release, resulting in more cell death [104]. When an *in vivo* xenograft PC-3 mouse model was treated with 10 mg/kg of calpeptin, it enabled a 100-fold lower dose of docetaxel and methotrexate to be used as treatment.

Dash *et al.* [105] investigated and demonstrated that prion protein (PrP) fragment (106-126) activates platelets causing an increase in intracellular calcium levels and therefore, up-regulated calpain activity leading to more shedding of platelets microparticles. However, when they preincubated the platelets with calpeptin, they saw a decrease in calpain activity and an attenuation of platelet microparticle release. This implicates both PrP ability to activate calpain activity and calpeptin's ability to inhibit MV secretion. In activated platelets, calpains cause the hydrolysis of actin-binding proteins such as talin and cytoskeleton proteins. A study investigated whether MVs shed from activated, pro-coagulant platelets released MVs with procoagulant activity [106]. The level of calpain activation correlated positively with the hydrolysis of actin-binding proteins and the amount of pro-coagulant-containing MV shedding when platelets were activated with agonists such as thrombin and collagen. However, when the platelets were pre-incubated with calpeptin before addition of the agonists, the hydrolysis of actin-binding proteins was almost completely abrogated and pro-coagulant-rich MV shedding was reduced.

1.2.3.2 Y27632

Y27632 is a drug that inhibits Rho associated protein kinases (ROCK)1 and ROCK2, serine-threonine kinases by competing with ATP for binding. ROCK1 and ROCK2 are downstream Rho effectors that play a role in the cell migration, cell contraction, cell polarity and lamella formation [107] and have therefore been implicated in MV release (see Fig. 1.2). They have many cellular substrates including myosin light chain 2 (MLC2) involved in actomyosin contractility and can phosphorylate LIM kinases, which phosphorylate and inhibit cofilin, the actin-depolymerisation protein, leading to actin reorganisation [108, 109].

Studies have shown that the use of Y27632 to decrease MV shedding. One such study, using MDA-MB-231 and epidermal growth factor (EGF)-activated Hela cells, demonstrated that RhoA was responsible for MV release [42]. With ROCK1 and ROCK2 being downstream targets for RhoA, Y27632 was used to block these proteins, with the reduction in MV formation on the cell surface and collection from their condition medium, confirming this. The activation of ROCK downstream targets (e.g. LIMK) was also prevented with Y27632 treatment, establishing a role for actin cytoskeleton remodelling in MV shedding.

Y27632 prevented actin reorganisation and stress fibre formation in hCMEC/D3 cells with and without treatment with tumour necrosis factor (TNF) [110]. The cells also had a changed morphology and less protrusions at the cell surface after Y27632 treatment, even with TNF stimulation. The number of MVs produced per cell was reduced to resting, basal levels in conjunction with Y27632 treatment. A study performed in HUVEC cells to investigate the role of MV release in cell survival, discovered that treatment of the cells with Y27632 promoted the accumulation of caspase-3 in the cells in the presence of apoptotic agent staurosporin and more than 90% of the adherent cultures detached [111]. The inhibition of MV release by Y27632 indicated that the endothelial cells use this mechanism of shedding for survival when under stress, releasing MVs as a way to remove caspase-3 from the cells, increasing their survival.

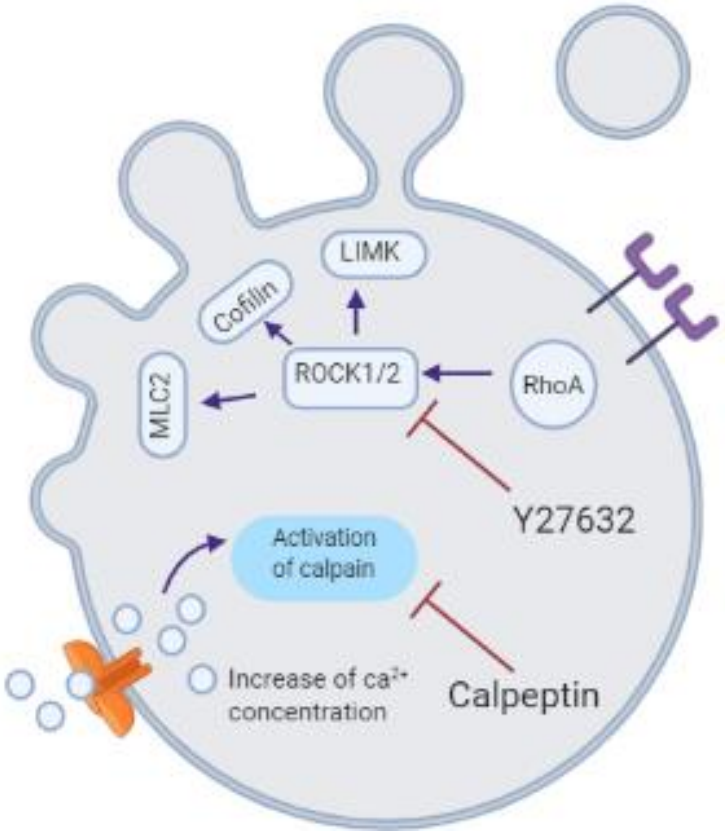

Figure 1.2: Actions of calpeptin and Y27632 on microvesicle release

Larger vesicles are released from cells through both actin-myosin contraction and through activating pathways such as ERK. Activation of calpains act on their substrate proteins and initiate the reorganisation of the cytoskeleton, causing the budding or pinching off of vesicles from the cell membrane. Y27632 inhibits ROCK1/2 which are upstream effectors of many proteins involved in actin polymerisation and contraction. Calpeptin inhibits the actions of calpain and therefore larger microvesicle release.

1.2.3.3 Manumycin A

Manumycin A, an antibiotic derived from *Streptomyces parvulus*, is an inhibitor of farnesyltransferases, specifically Ras farnesyltransferase. With the involvement of Ras, a family of small guanosine triphosphatases (GTPase), in exosome formation through the ESCRT-dependent pathway, manumycin A is reported to inhibit exosome release (see Fig. 1.3). Ras can undergo several post-translational modification in order to regulate its activity, through multiple processes including activation by guanine nucleotide exchange factors (GEFs), ubiquitylation, acetylation and also farnesylation [112]. The addition of the farnesyl group modifies Ras and is mediated by Ras farnesyltransferase. It is this modification that is targeted by manumycin A.

Neurogenesis was inhibited by the blockage of exosome release under manumycin A treatment [113]. The investigators in this study hypothesised that exosomes were involved in the transfer of miR-193a

from differentiated, F11 rat cells to undifferentiated F11 cells, forming neural cells. They found that this transfer and ultimately the differentiation of neural cells, were inhibited by the Manumycin A-induced reduction in exosomes.

Datta *et al.* [114] established that manumycin A decreased exosome release in prostate cancer cells, C4-2B, 22RV1 and PC-3 cells by 50%, 65% and 60%, respectively, with a combination of manumycin A and GW4869 exerting an even bigger effect on exosome release. Ras signalling was found to be the target of manumycin A and reason behind reduced exosome biogenesis. The study also reports the downregulation of hnRNP H1 expression is another mode of action of manumycin A. The same group of researchers showed that hnRNP H1, a splicing factor involved in pre-mRNA biogenesis, plays a role in sorting Ras into the cargo of exosomes in prostate cancer cells [115].

Interestingly, exosomes released by renal tubular BUMPT cells that had undergone a wound-healing assay were reported to have a negative effect on wound healing, something that has not been widely studied [116]. By treating the cells with manumycin A or GW4869 they demonstrated a decrease in exosome release but an increase in wound-healing and EGFR activation, revealing a role for exosomes released during the healing process having a negative effect on the wound-healing and antagonising the activation of EGFR.

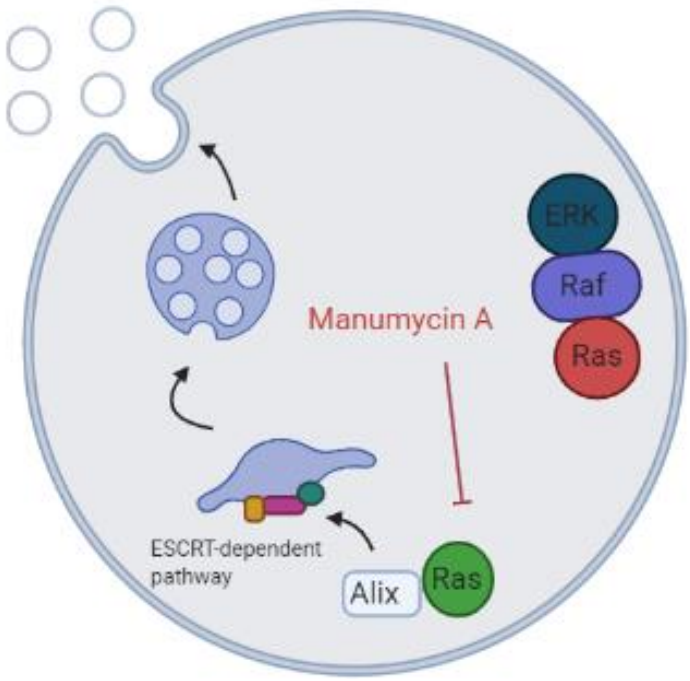

Figure 1.3: Actions of manumycin A on the ESCRT-dependent pathway of exosome biogenesis

Manumycin A effects the release of vesicles by the ESCRT-dependent pathway. Ras has been implicated in biogenesis and secretion of tumour-derived exosomes. Manumycin A, a farnesyltransferase inhibitor, blocks the activation of ras by farnsylation, preventing the release of the exosomes. Exosomes secreted from glioblastomas cells had detectable ras in complex with Vsp4 and ALIX [117].

1.2.3.4 GW4869

GW4869 is a hydrophobic, cationic inhibitor of neutral sphingomyelinase (nSMase) located on the cell membrane (see Fig. 1.4) nSMase acts by converting sphingomyelin to ceramide, a bioactive lipid that is involved in several cellular processes [118]. The conversion to ceramide creates spontaneous negative curvature in the cell membrane and budding to form ILVs through an ESCRT-independent pathway. Therefore, GW4869 appears to be an inhibitor of small EVs or exosomes.

Essandoh *et al.* [119] investigated if GW4869 could be used as a way to combat the pro-inflammatory effect of EVs released from LPS-stimulated RAW264.7 macrophages. GW4869 reduced exosome biogenesis in LPS-treated macrophages. The level of proinflammatory cytokines, TNF-α, Il-1β and Il-6 were reduced in the supernatants of macrophages treated with GW4869 upon LPS-stimulation compared to the controls of supernatants of macrophages treated with LPS. This was backed up with an *in vivo* study in wild-type mice with an injection of either PBS or GW4869 followed by a dose of LPS. Serum exosomes were significantly higher in LPS treated mice compared to PBS control. However, pre-treatment with GW4869 significantly decreased serum exosomes numbers compared to LPS + PBS mice along with a decrease in pro-inflammatory cytokines. These results were also replicated in a sepsis mouse model, reducing myocardial inflammation.

One interesting study, determined that GW4869 has the ability to prevent the spread of a ZIKA virus infection by decreasing the release of exosomes from ZIKA virus-infected astrocytes in a dose-dependent manner [120]. It also reduced the ZIKA virus RNA in infected astrocytes.

GW4869 treatment has been shown to reduce chemoresistance [121]. Exosomes were first separated from the conditioned medium of fibroblasts derived from normal colon tissues, 18Co and cancer-associated fibroblast (CAF). These exosomes were used to treat cancer stem cells (CSCs) from colorectal cancer cells, SW620 and XhCRC respectively, which resulted in the primed CSCs being able to form more spheres compared with control CSCs under treatment with 5-Fluorouracil and oxaliplatin. Separation of EVs after pre-treatment with GW4869, resulted in reduced chemoresistance of the CSCs. A second study demonstrated that GW4869 was able to overcome cisplatin resistance in ovarian cancer cells [122]. Exosomes separated from ovarian cancer cells SKOV3 had higher DNA methyltransferase 1 (DNMT1) mRNA compared to normal endometrial stromal (ESC) cells. SKOV3 cells treated with endogenous exosomes and DNMT1 levels were measured. DNMT1 doubled in the SKOV3 cells which also had increased survival under cisplatin treatment. However, when SKOV3 cells were treated with GW4869 and the separated exosomes used to treat SKOV3 cells, the recipient cells had

no induction of DNMT1 and the cisplatin resistance previously seen had been abolished with GW4869 treatment. A study showed that GW4869 decreased the number of EVs pelleted at 100,000g (P100) but significantly increased the EVs pelleted at 14,000 g (P14) [123]. The P100-EVs had a decrease in EV number with an average size of less than 100 nm according to NTA analysis, whereas P14-EVs between the size of 150-200 nm were increased after GW4869 treatment. P14-EVs also had an altered lipid composition with higher amount of sphingomyelin in the lipid bilayer. Although GW4869 decreased smaller EVs, it caused more EV budding directly from the plasma membrane and altered the protein and metabolite profile of the two populations of EVs.

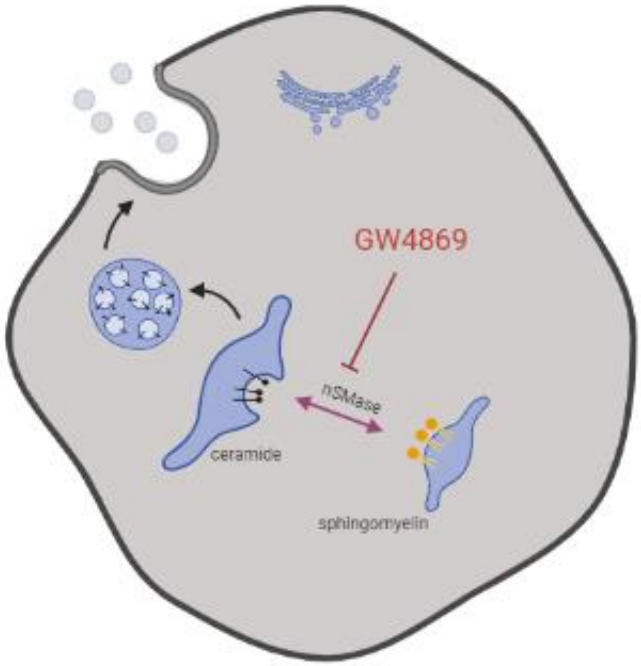

Figure 1.4: GW4869 actions on exosome biogenesis through an ESCRT-independent pathway

An ESCRT-independent pathway resulting in the release of small EVs involves the formation of ceramide from the phospholipid sphingomyelin. nSMase, an enzyme is involved in the conversion, initiating the formation of ILVs through budding of the membrane. GW4869 inhibits the activity of nSMase.

1.3 Platelets' role in cancer

Platelets are a component of blood that are involved in blood coagulation. They have no nucleus and are cell fragments. They are the first cells to respond in the wound healing process and homeostasis. When an injury occurs, for example to a blood vessel wall, platelets respond, becoming activated by receptor recognition of extracellular matrix components. They begin immediately changing shape and undergo degranulation in order to release their contents. Their contents include proteins, growth

factors and bioactive lipids that in turn recruit more platelets and immune cells initiating the blood clotting process to fill in the wound with a "platelet plug" [124].

Platelet receptor, glycoprotein (GP) Ib/V/IX induces actin cytoskeleton reorganisation upon binding to von Willebrand Factor (vWF), promoting both platelet-vessel wall contraction and platelet-platelet adhesion. The platelets are then tethered to the vessel wall and roll along, creating more contacts with platelet integrins (including $\alpha_{IIb}\beta_3$, $\alpha_2\beta_1$) to allow the platelets to become stationary. Stationary platelets can now release their contents and vWF on their surface is detached recruiting further platelets by GP Ib/V/IX recognition [125]. In a parallel pathway, the coagulation cascade results in the formation of fibrin which strengthens the platelet plug. Tissue factor (TF)**,** a transmembrane protein involved in clot formation, initiates the cascade by binding to factor VIIa (FVIIa) after it is exposed to coagulation factors upon blood vessel injury [126]. The TF:VIIa complex cleaves and activates factor X (FX) (i.e. to form FXa) and factor IX (FIX). Activated FXa, with its cofactor factor Va (FVa) (i.e. prothrombinase complex) cleave prothrombin to form thrombin. Fibrinogen is consequently cleaved to fibrin by thrombin [127]. Thrombin also activates factor XIII, which forms covalent bonds between fibrin fibres creating crosslinks.

During cancer progression, platelet activation and the coagulation cascade become heightened and dysregulated. There are multiple mechanisms that have been studied in which tumour cells exploit platelets to increase their survival and use them to their advantage to spread throughout the body (see Fig. 1.5). One example of the exploitation of platelets is the use of platelets as a "protective shield". Niewswandt *et al.* [128] demonstrated that **platelets protect tumour cells** from natural killer (NK) cells. They found, by using mouse cell lines *in vitro*, that platelets bound to 33% of gated tumour cells and large aggregates were present. However, when antiaggregating agents, hirudin and anti-P-selectin antibodies were added the number of tumour cells with platelets bound was reduced to 3% and 9%, respectively, and the formation of large aggregates was prevented. Additionally, *in vivo* they found that in normal NK cell-bearing mice, 5.5.% of tumours had colonised the lungs. However, platelet-depletion prevented tumour cells metastasising to the lungs, with only 0.2% reaching the secondary organ, indicating the platelets protected the tumour cells from NK cell lysis. Platelets have also been shown to **dampen down the immune response,** with one study determining that platelet-secreted transforming growth factor β (TGFβ) and lactate had the ability to prevent the anti-cancer effects of $CD4^+$ and $CD8^+$ T cells [129]. They can facilitate the metastasis of tumour cells while inducing the resistance to *anoikis*, a form of cell apoptosis that occurs when cells detach from the extracellular matrix and into the bloodstream. By incubating cancer cells (e.g. SKOV3, HEYA8 and OCAR8) with increasing number of platelets under *anoikis* conditions, they discovered that platelets increased the survival of the detached cancer cells [130]. **Epithelial-mesenchymal transition (EMT)** can be induced

by tumour cell-platelet interactions. Colon cancer cells, (MC38GFP) isolated from a C57BL/6 mouse and breast carcinoma cells, (Ep5) spontaneously transformed by the v-Ha-Ras oncogene, (EpRas) were pre-incubated *in vitro* with platelets before they were injected into mice. The cancer cells primed with platelets resulted in a higher number of lung metastases [131]. The tumour cells treated with platelets had increased EMT markers such as N-cadherin, snail, and vimentin as well as matrix metalloproteinases (MMPs) including MMP9. It was shown that TGFβ released from activated platelets upregulated the TGFβ and NF-kappaB pathways in tumour cells which enhanced *in vivo* metastases. Another role of platelets in cancer progression is the increased **resistance to cell death**. Bottsford-miller *et al.* [132] established that in ovarian cancer patients who had thrombocytosis (i.e. >450,000 platelets/µl plasma) at diagnosis resulted in worse median progression free survival (PFS) and median overall survival (OS). The co-culture of ovarian cancer cell lines A2780, HeyA8, and SKOV3-ip1 with platelets resulted in a reduction in apoptosis. For example, incubation of A2780 cells with platelets caused a reduction in apoptosis from 10.7% to 5.7% compared with serum-free medium incubation. With the addition of docetaxel, apoptosis was reduced from 46.6% to 37.1%. The researchers established that the platelets did not require direct contact with the cancer cells to exert this anti-apoptotic effect with a barrier of 0.4 µm placed between cells and platelets *in vitro* over 72 hrs. *In vivo* experiments in nude mice, demonstrated that tail vein platelet transfusion, simulating the effects of excess platelets, resulted in a 1.9-fold increased tumour weight compared to the untreated control. However, by pre-incubating platelets with aspirin before the transfusion the anti-apoptotic effect of the platelets was inhibited. Anti-platelet antibodies, which sequester circulating platelets decreased the mouse tumour weight by 65%, indicating that platelets increase chemo-resistance in ovarian cancer. Platelets were also shown to increase the survival of 59M ovarian cancer cells, Caco-2 colonic cancer cells, and CRL2014 human gingival fibroblasts under paclitaxel and 5-FU treatment by inhibiting apoptosis [133]. One mechanism of survival identified, was the up-regulation of anti-apoptotic genes in 59M and Caco-2 cells (e.g. BCL3 and NF-κB1) by platelets. Another involved the proteins secreted, thrombospondin-1 and RANTES, which were identified by proteomic analysis on the secretome of paclitaxel-treated Caco-2 cells with platelets. Lastly, platelets can also promote **angiogenesis**. Platelets from glioblastoma (GBM) patients (*n=22*) were reported to promote angiogenesis of glioblastoma-derived endothelial cells (GECs) and platelets from GBM patients had higher levels of VEGF compared to healthy controls (*n=18*) [134]. Platelets have various pro-angiogenic factors stored in their α-granules such as VEGF, PDGF, and EGF. Breast cancer cells incubated with platelet releasate (i.e. activated platelets through receptor stimulation) had increased proliferation through a VEGFR-2 and integrin dependent manner [135]. The combination of platelet releasate and

breast cancer cells enhanced tube formation of HUVECs *in vitro* while an *in vivo* model showed increased angiogenesis in breast cancer tumours supplemented with platelet releasate.

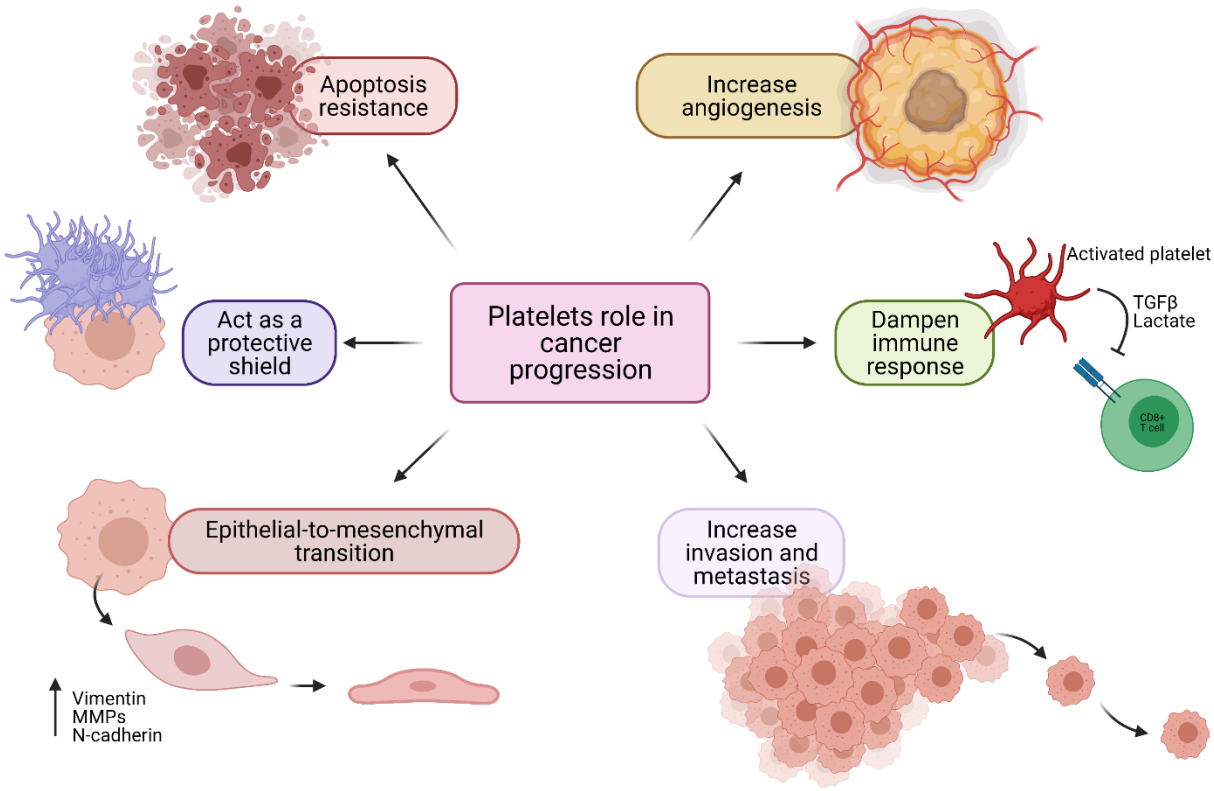

Figure 1.5: Platelets' role in cancer growth and progression

Platelets are involved in many aspects of the growth, progression, and spread of cancer cells. They enhance some of the "cancer hallmarks", such as resistance to apoptosis and contribute to the epithelial-mesenchymal transition. They can evade the immune system by dampening the response and increasing the invasiveness of the cancer cells. They aggregate around the tumour cells preventing them from being killed by drug treatments. Lastly, they can increase angiogenesis in the tumour microenvironment through the release of pro-angiogenic factors.

Tumour-cell induced platelet aggregation (TCIPA) is a well described phenomenon whereby cancer cells cause platelet aggregation, offering an advantage of tumour cell survival in the bloodstream and eventual metastasis. One of the main focusses of TCIPA studies is the environment in which TCIPA occurs *in vitro,* with many studies reporting different conditions in which platelet aggregation occurs. One study dissected the conditions required for platelet aggregation to occur in the presence of MDA-MB-231, MCF-7 and Caco2 cells [136]. Firstly, they established that autologous plasma (0.05% v/v), from which the washed platelets were isolated, was required for aggregation to occur in the presence of the cancer cells and washed platelets. When serum was used instead of plasma, aggregation did not occur, leading to an assumption this was due to serum not containing coagulation factors such as fibrinogen and serine proteases. Thrombin was produced during the aggregation induced by the

cancer cells and TF was identified on all three cancer cell lines. The researchers found that the tumour cells were capable of forming platelet aggregates through the binding of fibrinogen to integrin αIIbβ3 and the formation of fibrin network that may entrap the tumour cells. Similarly, pancreatic cancer cells, PC 3, PC 44, ASPc1, BxPC 3 and Capan 2, were used to demonstrate that the TCIPA was thrombin-dependent and fibrin clot formation was detected at peak aggregation [137]. Mitrugno *et al.* [138] showed that metastatic prostate and colon cancer cells, PC3M-luc and Caco-2, respectively, directly interacted with platelets to induce their activation and caused the secretion of platelet granules. This phenomenon is called tumour cell-induced platelet secretion (TCIPS) and preceded platelet aggregation. Caco-2 cells, were also found to induce platelet aggregation through ADP and MMP-2 release [139]. This mechanism was also observed with MCF-7 cells which were stably transfected with membrane type-1 matrix metalloproteinase (MT1-MMP) and integrin subunit β3 [140]. Increased TCIPA was induced by the transfected cells by activating pro-MMP2 to its activated form, MMP2, implicating a role of MMP2 in aggregation. Additionally, a panel of lung cancer cells (e.g. H596, H69, A549 and U1812) *in vitro*, including both large-cell lung cancer and squamous-cell lung cancer induced aggregation though thrombin and ADP. The thrombin inhibitor, hirudin, blocked this TCIPA [141]. TCIPA is, therefore, a phenomenon that is detected by multiple cancers and could represent a target for treatment of cancer.

In the context of TNBC, one retrospective study (*n=57* patient number) investigated if neutrophil-to-lymphocyte ratio (NLR) and platelet-to-lymphocyte (PLR) could be used as a predictive biomarker during treatment in patients with metastatic TNBC (mTNBC) undergoing platinum-based chemotherapy [142]. The researchers found a link between high NLR and PLR and worse progression free survival (PFS) in mTNBC patients. Specifically, they discovered that platelets above 300000/µl of blood was significantly associated with shorter PFS. Another study, reviewing and analysing immune-related gene expression signatures derived from the literature reported that higher platelet counts in TNBC were associated with higher aggressiveness score of the tumour and a poorer outcomes [143].

1.3.1 Thromboembolism associated with cancer

The association between thromboembolism (TE) and cancer has been widely reported. Cancer patients may have a higher risk of developing arterial thromboembolism (ATE) and venous thromboembolism (VTE). There are several risk assessments or scoring systems that provide an estimation of the risk of the patients developing TE. The Khorana score is one such predictive model, which includes a scoring system that ranges form 0-6 with a score of 0.3-0.8% indicating low risk, 1-2% indicating an intermediate risk and ≥3% indicating a high risk of VTE [144]. The PROTECT score, is

a modified version of the Khorana which take treatment with chemotherapy agents, carboplatin, cisplatin and gemcitabine into account [145].

Of all cases of VTE, cancer patients account for 20%, with patients undergoing chemotherapy treatment representing 13% of the VTE burden [146]. VTE is the second leading cause of cancer-related deaths with **risk factors including patient-related** (e.g. age and comorbidities), **cancer-related** (e.g. primary site and histological type of cancer) and **treatment-related** (i.e. agents with a strong correlation with VTE include platinum, fluorouracil and antiangiogenic agents) risk factors [147]. A meta-analysis revealed that pancreatic and brain cancers had the highest risk of developing VTE [148]. Results published from the Vienna Caner and Thrombosis Study, reported that tumour grade was associated with VTE. Patients with higher grade tumours were reported to have a significantly higher risk, with the probability of developing VTE after 6 months being 8.2% in patients with high-grade tumours compared with 4% in patients with low-grade tumours [149]. A retrospective study studying the association of TE in NSCLC patients (*n=784*) and platinum-based therapy (i.e. cisplatin and carboplatin) found that 69 TE events occurred in 63 patients, with 39 patients developing VTE alone and 21 developing ATE alone [150]. Patients who had experienced a TE event during their treatment had a significantly shorter overall survival (OS) compared to patients that had no TE. Lechner *et al.* [151] found that cisplatin-induced apoptosis of endothelial cells caused a release of pro-coagulant endothelial microparticles and increasing pro-coagulant activities through the generation of thrombin

Hypofibrinolysis has been shown to be a risk factor for thrombotic complications. This is caused by increased levels of plasminogen activator inhibitor type 1 (PAI-1). PAI-1 inhibits the conversion of plasminogen to plasmin which normally breaks down fibrin clots, maintaining tissue homeostasis. It inhibits the enzymes, tissue plasminogen activator (i.e. t-PA) and urokinase (i.e. u-PA). PAI-1 was significantly elevated in the plasma of GBM cancer patients (*n=250*) compared to healthy controls (*n=270*), suggesting it may be a biomarker for thrombosis [152]. A study comparing patients that developed VTE (*n=102*) *versus* those that had not (*n=113*), reported that PAI-1 level were significantly higher in VTE patients and PAI-1:tPA ratio was 1.9 fold higher [153]. Furthermore, it has been observed that bevacizumab, a VEGF monoclonal antibody, increased the levels of PAI-1 in a mouse xenograft model of lung carcinoma [154]. The treatment resulted in larger venous thrombi compared with vehicle-treated mice. PAI-1 expression was higher in the tumours after bevacizumab treatment and it was suggested that the increase in PAI-1 was due to bevacizumab blocking the inhibitory effects of VEGF on PAI-1. The researchers further demonstrated that PAI-1 inhibitor, PAI-039, significantly reduced the weight of thrombi in tumour-bearing mice.

1.3.1.1 Treatment of thromboembolism associated with cancer

Some studies that have investigated the use of thromboprophylaxis for the treatment of patients at a higher risk of developing TE with anti-coagulants. Low molecular-weight heparin (LMWH) is the current standard treatment for VTE in cancer patients. Direct oral anti-coagulants agents (DOACs) are shown to be just as effective, but the safety and efficacy has not been fully explored. There have been clinical trials performed to investigate DOACs efficacy in cancer patients with recurrent VTE and to compare them with LMWHs. There was a relatively recent update of recommendations for the clinical treatment of VTE in cancer patients [155]. It recommended that cancer patients with recurrent VTE, undergo six months of treatment with LMWH, edoxaban, or rivaroxaban, as they have better efficacy over vitamin K antagonists. It also states that there is an increased risk of bleeding when using DOACs in gastrointestinal tract malignancies. Beyond the six months of treatment, an assessment of risk-benefit profile needs to be performed intermittently.

The oral inhibitor of factor Xa, **Apixaban,** was tested for its efficacy in cancer patients with an intermediate-to-high risk of VTE (i.e. Khorana score of ≥2) in the AVERT trial after an initial pilot study showing it was well-tolerated in cancer patients receiving chemotherapy [156, 157]. The trial was a double-blind, placebo-controlled, test comparing apixaban with placebo and included patients who were either recently diagnosed with cancer or their cancer had progressed after remission and were starting a course of chemotherapy. During the treatment, VTE occurred in 3 of 288 patients (1%) in the apixaban group and 20 of 275 patients (7.3%) in the placebo group. Adverse events were reported with just 1 event in the apixaban group and 2 events in the placebo group being attributed to the trial regimen. Another factor X inhibitor, edoxaban, a direct oral anti-coagulant, was included in a randomised prospective clinical trial and compared with dalteparin, a LMWH in cancer patients, named the Hokusai VTE Cancer trial [158]. Edoxaban was found to be non-inferior to subcutaneous dalteparin when comparing recurring venous thromboembolism and major bleeding events

The SAVE-ONCO trial compared **semuloparin**, an ultra-low-molecular-weight heparin with factor Xa activity to placebo in patients that had metastatic or locally advanced lung, pancreas, stomach, colon or rectum, bladder or ovary cancer [159]. Treatment with semuloparin resulted in a reduction in deep-vein thrombosis with it occurring in 20 of 1608 (1.2%) patients in the semuloparin group compared with 55 of 1604 (3.4%) in the placebo group. While on the treatment regime 1.2% of patients receiving semuloparin had a major bleeding event compared with 1.1% in patients receiving the placebo.

Zwicker *et al.* [160] conducted a randomised prospective, phase II trial of **enoxaparin**, low-molecular-weight-heparin with cancer patients that had high levels of plasma tissue factor-bearing microparticles

(TFMPs) and therefore a higher risk of VTE. Out of 66 patients enrolled, 34 had high levels of TFMPs and 32 had lower levels of TFMPs. High TFMPs patients were split into two groups, 23 were randomly selected to receive enoxaparin with 11 underwent observation without thromboprophylaxis with VTE incidence 5.6% and 27.2%, respectively. In addition, patients with low levels of TFMPs had a 7.2% rate of VTE without receiving enoxaparin. This study demonstrated that enoxaparin reduces thrombosis in patients that have high levels of TFMPs and the authors stated that they are moving forward to conduct a placebo controlled, randomised trial to confirm the above results.

However, there still remains risks associated with this treatment in cancer patients. Due to the risk of thrombosis in cancer patients, the treatment with anti-coagulants are usually given for a longer time period. It has been reported that cancer patients have higher bleeding complications compared to other patients that receive anti-coagulant that do not have an active cancer. An analysis of patient data undergoing anti-coagulant treatment with LMWH and warfarin determined that cancer patients had a higher risk of TE event and bleeding complications during anti-coagulant therapy compared to patients without cancer, with VTE four times higher and bleeding risk twice as high [161].

1.3.1.2 Biomarkers of thromboembolism

There are many **biomarkers** of VTE which can be used to monitor the treatment of VTE and to determine the VTE risk of an individual. In a study using tissue microarrays from pancreatic cancer patients, 54% of tumours were found to have a high expression of **TF** (66 of 120 samples). More importantly, of the patients with high TF, VTE occurred in 26.3% of patients compared with just 4.5% of patients with low TF expression [162]. **Clotting factor VIII (FVIII)** plays a role in the clotting cascade, acting as a co-factor in the activation of thrombin. In a study with 840 patients, the probability of VTE occurring within 6 months was calculated at 14% of patients with high VFIII levels and only 4% of patients with normal levels [163]. A study conducted enrolling patients that had varying levels of pancreatic diseases, including chronic pancreatitis (CP), intraductal papillary mucinous neoplasm of the pancreas (IPMN) and pancreatic ductal adenocarcinoma (PDAC), investigated if there are biomarkers of VTE in PDAC [164]. Compared to CP and IPMN, PDAC had significantly higher levels of fibrinogen, interleukin-6 (Il-6), factor VIII, D-dimers, von Willebrand factor (VWF) and extracellular DNA. In addition, PDAC compared to IPMN had significantly higher MV-TF. Metastatic status correlated with elevated levels of MV-TF activity, D-dimers and thrombin-anti-thrombin (TAT) complexes. PDAC patients underwent an observation period of 6-months during which 22% had

experienced VTE. TAT complexes, D-dimers, cancer antigen CA19-9 and MV-TF activity were all significantly higher in these patients. It has been reported that the probability of developing VTE after 6-months was 74.3% among patients with elevated MV-TF activity, compared with 21.7% in those with lower MV-TF activity. However, assessing the performance of all biomarkers indicated that CA19-9 had the highest sensitivity and specificity at predicting VTE in PDAC patients.

Citrullinated histone H3 (H3Cit) was shown to be a potential biomarker of VTE [165]. Cancer patients (*n=946*) that had elevated levels of H3Cit also had higher levels of previously reported biomarkers such as FVIll and prothrombin fragment 1 + 2. In a 2-year follow up, patients that had developed VTE had statistically and constantly higher H3Cit.

1.3.1.3 Extracellular vesicles procoagulant potential

Extracellular vesicles have also been proposed as potential biomarkers as pro-coagulant proteins have been detected on or within them. It should be noted that EVs are also proposed as a risk factor in the development in VTE. Microparticles released from many different cells such as platelets, endothelial cells and tumour cells have been shown to carry pro-coagulant proteins with much attention on TF. Zwicker et al. [164] conducted a study using platelet-poor plasma from n=96 patients diagnosed with a range of cancers such as breast, colon, ovarian, renal cell and pancreatic. An association was found between high levels of TF-bearing microparticles and VTE in cancer patients. A fibrin generation test was used to assess the correlation between the level of TF-bearing EVs and VTE risk in 648 cancer patients [165]. High TF-EVs was more consistently associated with pancreatic cancer compared to other cancers including breast, colorectal and lung cancer. 50% of pancreatic patients had a high fibrin generation measurement and this was associated with a four-fold increase risk of developing VTE compared to just 1.5-fold increased risk with other cancers.

A study involving cancer patients (i.e. included patients diagnosed with pancreatic, colorectal, prostate, bone and breast cancers) (n=51) that had presented with a VTE, cancer patients (n=49) that had no VTE, and healthy individuals (n=37) were compared by their MP-TF activity [166]. Patients that developed VTE had significantly higher MP-TF activity compared to cancer patients with no thrombosis. Median survival of patients with elevated MP-TF activity was 3.5 months compared with 13 months for patients with normal levels of MP-TF activity. However, the researchers point out that patients who developed VTE during chemotherapy treatment had a normal MP-TF activity and, thus, this suggested that cancer cells may provide an indirect cause of the elevated MP-TF activity.

Cancer cell EVs have been implicated in cancer-associated thrombosis. By using a mouse model, it was shown that tumour-derived microparticles (MPs) isolated from pancreatic cancer (Panc02) and Lewis lung carcinoma (LLC1) cells, as termed in this particular study, were able to bind to activated platelets with P-selectin on their surface by P-selectin glycoprotein ligand 1 (PSGL1) carried on the MPs [166]. Researchers found that the MPs, and not the cancer cells were able to accelerate thrombi growth *in vivo* by accumulating at the site of injury and proposed to promote platelet aggregation in a TF-dependent manner.

TF associated with MPs released by MDA-MB-231 and L3.6pl tumour cells had pro-coagulant activity *in vitro* and in mice with the presence phosphatidylserine (PS) also involved in their pro-coagulant activity [167]. MPs from MDA-MB-231 cells significantly increased thrombin generation of human plasma. However, blocking TF and PS with anti-human TF antibody (HTF-1) and annexin V, respectively, abolished the pro-coagulant activity of the MDA-MB-231 MPs. *In vivo* experiments were performed with MPs from MDA-MB-231 and L3.6pl cells, as well as a PBS control. Human TF antigen was detected in cell-free plasma obtained from mice injected with MPs after just 5 mins but was not detected in PBS control mice. Again, this was blocked by prior incubation of plasma with TF antibody.

Prostate cancer cells, DU145 and PC3, were used to determine the coagulant activity of prostate cancer EVs [168]. TF was knocked down in DU145 cells and subsequently treated with EVs isolated from parental DU145 cells that was shown to contain TF. The resulting incubation of DU145 cells with EVs increased the pro-coagulant activity by the increase in TF in the EV-treated cells. Furthermore, it was demonstrated using EVs from DU145 cells *versus* the more oncogenic cell line DU145 EGFRvIII and also, PC3 cells *versus* their more metastatic variant PC3MLN4, that the greater the metastatic potential of the cells, the more thrombogenic is the corresponding EVs. This was measured by FXa activity and thrombin generation.

Pancreatic adenocarcinoma MVs from the cell line BxPc-3 and L3.6pl had TF activity and bound to washed platelets *in vitro*, increasing the TF activity of platelets and reduced the lag time for thrombin generation [169]. Confirming a role for TF in the platelet activation seen, the preincubation of MVs with HTF-1 or active site-inhibited recombinant FVIIa (FVIIai) before demonstrating an inhibition of platelet activation. Thrombin inhibitor, Hirudin, P2Y12 receptor inhibitor 2 MesAMP and ADP scavenger, apyrase also reduced platelet activation. Furthermore, platelet aggregation was attributed to MV associated TF and thrombin, with both HTF-1 and hirudin preventing aggregation. *In vivo* study experiments with BxPc-3 MVs showed an increase in thrombus formation, size and reduced survival in tumour-bearing mice and IVC stenosis mouse model. HFT-1 again reduced thrombus formation, size and increased survival.

EVs derived from platelets have been used to determine the role of TF and PS in the generation of thrombus and thrombotic events. **Platelet-derived EVs** has also been implicated in thrombosis. Heijnen *et al.* [170] observed that platelets released two types of EVs, both, microvesicles and exosomes, with different characteristics between the two. It was found that prothrombin and factor X only bound to microvesicles, suggesting that microvesicles have more coagulating activity compared with exosomes and where the prothrombinase complex may form. CD63 was also reported to be enriched on platelet exosomes, leading to the conclusion that exosomes may be involved in signalling away from the site of platelet activation.

Glutamate is often found in α- granules of activated platelets which when released, can initiate a positive feedback loop by interacting with glutamate receptors on the platelets [171]. Gautan *et al.* [172] demonstrated that by exposing platelets to glutamate, a significant increase in EV release occurred by inducing an increased uptake of Ca^{2+} by the platelets, activating RhoA-GTPases activity and therefore cytoskeleton remodelling and vesicle shedding. Glutamate also increased thrombogenic peptide synthesis, i.e. PAI-1 and HIF-2α.

The coagulant activity of EVs rely on the exposure of the anionic phospholipid, PS, on the EV surface which can stimulate the formation of coagulant complexes on the EV surface. Platelet-derived EVs were found to increase thrombin generation in vesicle-free human plasma in a dose-dependent manner, which was inhibited by the blocking of phosphatidylserine with annexin V [173].

Improvements in blood collection and plasma preparation can have an impact in the coagulation potential of plasma EVs [174]. With a second additional washing centrifugation step, isolating platelet-depleted plasma rather than platelet-poor plasma and blood collection into plastic tubes rather than glass tubes, demonstrated that healthy donor plasma EVs did not cause coagulation, which is the opposite of what had been reported by the same group in 2001 [175]. This clearly shows that the handling of plasma EVs needs to be standardised and previous reports of coagulation by EVs from healthy donors need to be carefully evaluated, as the pro-coagulant activity may be down to residual platelets left over and not platelet-derived EVs.

Overall, EVs released from tumour cells may play a role in VTE development. Therefore, by identifying potential pro-coagulant targets either on the surface or within the EVs and, subsequently, blocking or inhibiting their actions may prove beneficial to the cancer patients and reduce their risk of cancer-associated thrombosis.

1.4 Aims of project

Previous research performed by our group, showed that the heterogeneous population of EVs released from aggressive TNBC cells (Hs578Ts(i)$_8$) compared to the more docile, isogenic parental TNBC cells (Hs578T) can transmit aggressive phenotypic characteristics to recipient cells. The overall aim of this project was to use *in vitro* models of TNBC and patients' samples to further understand the involvement of EVs in TNBC and to investigate ways of exploiting this information on TNBC EVs.

This aim involved achieving the following objectives:

1. Investigating if a particular sub-population(s) of the Hs578Ts(i)$_8$ EVs was responsible for the transmission of aggressive phenotypic traits or if this was caused by the full heterogeneous population of EVs.
2. Establishing if the release of EV sub-population(s) from the Hs578Ts(i)$_8$ cell line variant, that are responsible for the undesirable cell-to-cell communication could be blocked -or at least partially inhibited- with previously proposed EV inhibitors; calpeptin, Y27632, manumycin A and GW4869; some in combinations. If a total block of EV release could not be achieved, the plan was to determine if there was any difference in the effects of the EVs that continued to be released.
3. Develop a quick "first check" screening method for EV analysis in solution (conditioned medium, in this case), using imaging flow cytometry to identify potential EV inhibitors in a TNBC cell line panel- rather than requiring the laborious separation of EVs from CM, for this purpose.
4. Considering that venous thromboembolism is a major contributor to death for cancer patients, investigate the role of TNBC cell line variants, Hs578T and Hs578Ts(i)$_8$, and their corresponding EVs in platelet aggregation. Subsequently perform proteomic profiling of the EVs to identify proteins that may be involved in platelet aggregation and which may be useful therapeutic targets.
5. Perform an EV separation methods comparison on breast cancer patients' sera and their age-matched controls' sera to identify an EV separation method that results in intact EVs and that would realistically be easily translated for use in a clinical setting towards patient care.

Chapter 2: Materials and Methods

2.1 Cell culture

Six triple-negative breast cancer (TNBC) cell line variants were cultured. Hs578T cell line and its isogenic sub-clone Hs578Ts(i)$_8$ were grown in Dulbecco's Modified Eagles Medium (DMEM) (Sigma-Aldrich, Cat. #: D5671) at 37 °C, 5% CO_2 containing 10% foetal bovine serum (FBS) (Gibco, Cat. #: 10270106), 2mM L-Glutamine (Sigma-Aldrich, Cat. #: 10516) and 10 µg/ml insulin (Sigma-Aldrich, cat # 19278). MDA-MB-468 and MDA-MB-231 cell lines were grown in Dulbecco's Modified Eagles Medium (DMEM) (Sigma-Aldrich, Cat. #: D5671) at 37 °C, 5% CO_2 containing 10% foetal bovine serum (FBS) (Gibco, Cat. #: 10270106) and 2mM L-Glutamine (Sigma-Aldrich, Cat. #: 10516). BT549 and HCC1143 cell lines were grown in Roswell Park Memorial Institution (RPMI) medium (Sigma-Aldrich, Cat. #: R0883) at 37 °C, 5% CO_2 containing 10% FBS and 2mM L-Glutamine. When performing experiments with 2-Deoxy-D-Glucose (2-DG) (Sigma-Aldrich, Cat. #: D8375) and/or metformin (Sigma-Aldrich, Cat. #: D150959) cell line variants were grown in low glucose DMEM (Sigma-Aldrich, Cat. #: D5546). *Mycoplasma* testing was routinely performed by reverse-transcriptase polymerase chain reaction (RT-PCR) (ATCC, Cat. #: 30-1012K) every three months. All cell culture conditions are summarised in Table 2.1.

Triple-negative breast cancer cell line	Cell culture medium
Hs578T	DMEM, 10% Foetal bovine serum, 2mM L-Glutamine, 10µg/mL insulin
Hs578Ts(i)$_8$	DMEM, 10% Foetal bovine serum, 2mM L-Glutamine, 10µg/mL insulin
BT549	RPMI-1640, 10% Foetal bovine serum, 2mM L-Glutamine
HCC1143	RPMI-1640, 10% Foetal bovine serum, 2mM L-Glutamine
MDA-MB-468	DMEM, 10% Foetal bovine serum, 2mM L-Glutamine
MDA-MB-231	DMEM, 10% Foetal bovine serum, 2mM L-Glutamine

Table 2.1: Triple-negative breast cancer cell line culture conditions

2.2 Isolation of extracellular vesicles

2.2.1 Heterogeneous EV population

FBS was depleted of extracellular vesicles (EVs) by ultracentrifugation at 120,000g for 18 hrs at 10°C (dFBS).

Hs578Ts(i)$_8$ were seeded at 5 x 10^5 cells per T175 flask (Corning, Cat. #: 431080). The following day the medium was replaced with DMEM media supplemented with 10% dFBS with 1% penicillin/streptomycin (Sigma-Aldrich, Cat. #: P4458), and grown for another 5 days. Conditioned medium (CM) was collected from each flask, the cell viability was noted, and the starting cell number was counted. The CM was centrifuged at 2,000g for 20 minutes at 4°C as a pre-clearing step. The CM was filtered using a PES 0.45µm filter (Fisher, Cat. #: 15216869). The CM was transferred into 39ml Quickseal tubes (Beckman Coulter, Cat. #: 342414) and centrifuged in a Type 70 Ti fixed angle rotor (Beckman Coulter, Cat. #: 337922) at 110,000g for 75 minutes. The pellet was washed with 39ml of PBS and re-centrifuged at the same speed before resuspending the pellet in 150 µl of PBS and storing the EVs in Protein LoBind tubes (Eppendorf, Cat. #: 0030 108.116) at -80°C. (see Fig 2.1 for protocol overview).

2.2.2 EV sub-populations

Hs578Ts(i)$_8$ were seeded at 5 x 10^5 cells per T175 flask. The following day the medium was replaced with DMEM media supplemented with 10% dFBS and 1% penicillin/streptomycin and grown for another 5 days. EVs were isolated by differential ultracentrifugation. Conditioned medium (CM) was collected from each flask and the starting cell number was counted. The CM was centrifuged at 300g for 10 minutes at 4°C (X3) as a pre-clearing step to remove cellular debris. The CM was transferred to new 50ml tubes and centrifuged at 2,000g for 20 minutes at 4°C (2K pellet). The CM was transferred to Quickseal 39ml tubes (Beckman coulter, Cat. #: 342414) and centrifuged in a Type 70 Ti fixed angle rotor (Beckman coulter, Cat. #: 337922) at 10,000g for 30 minutes (10K pellet). The CM was transferred to new Quickseal tube and centrifuged in a Type 70 Ti rotor at 100,000g for 70 minutes (100K pellet). Finally, the CM was transferred to another Quickseal tube and centrifuged in a 70 Ti rotor at 200,000g for 65 minutes (200K pellet). All pellets were washed with 20-39ml of PBS and re-centrifuged at the same speed before resuspending pellet in 150 µl of PBS and storing the EV sub-populations in Protein LoBind tubes (Eppendorf, Cat. #: 0030 108.116) at -80°C (see Fig. 2.1 for

protocol overview). If pellets were needed for immunoblotting the EVs were lysed as described in section 2.3.

2.2.3 Extracellular vesicles treated with proposed EV inhibitors

[This EV isolation protocol was established by PhD student Mariadelva Catalano]

Hs578Ts(i)$_8$ cells were seeded at 1.5 x 10^6 cells per T175 flask. The following day the medium was replaced with DMEM media supplemented with 10% dFBS and 1% penicillin/streptomycin and grown for another 48 hours in the presence of the proposed EV inhibitors at a concentration determined by performing toxicity assays. CM was centrifuged at 300g for 10 mins to remove cellular debris. This was repeated three times in total, using a fresh 50 mL falcon tube each time. The CM was concentrated from approximately 125mL to 1.5mL using a tangential flow filtration (TFF) based device (Hansabiomed, Cat. #: HBM-TFF/1). The 1.5mL of concentrated CM was then loaded onto an OptiPrep™ (Sigma, Cat. #: D1556) density gradient using a bottom-up approach, to separate EVs based on their density. In 17 mL Ultraclear UC tubes (Beckamn Coulter, Cat. #: 344061), 1.5 mL of CM was diluted with 60% OptiPrep and PBS to form the bottom layer of 40% (8 mL in total). 30% (2.5 mL), 20% (2.5 mL), 10% (2.5 mL) and 5% (2 mL) of OptiPrep was loaded on top, in subsequent layers. The density gradient was ultracentrifuged at 186,000g for 18.5 hours at 4°C in a SW 32.1 Ti swinging rotor (Beckman Coulter, Cat. #: 369651). Fractions of 1mL were collected from top to bottom. Fraction 3-9 were pooled and ultracentrifuged in a Quickseal 39ml tubes (Beckman coulter, Cat. #: 342414) in a Type 70 Ti fixed angle rotor (Beckman coulter, Cat. #: 337922) at 120,000g for 120 minutes. This was repeated a second time and the final pellet was resuspended in 150µl or 200 µl of sterile PBS. EVs were stored in Protein LoBind tubes (Eppendorf, Cat. #: 0030 108.116) at -80°C (see Fig. 2.1 for protocol overview).

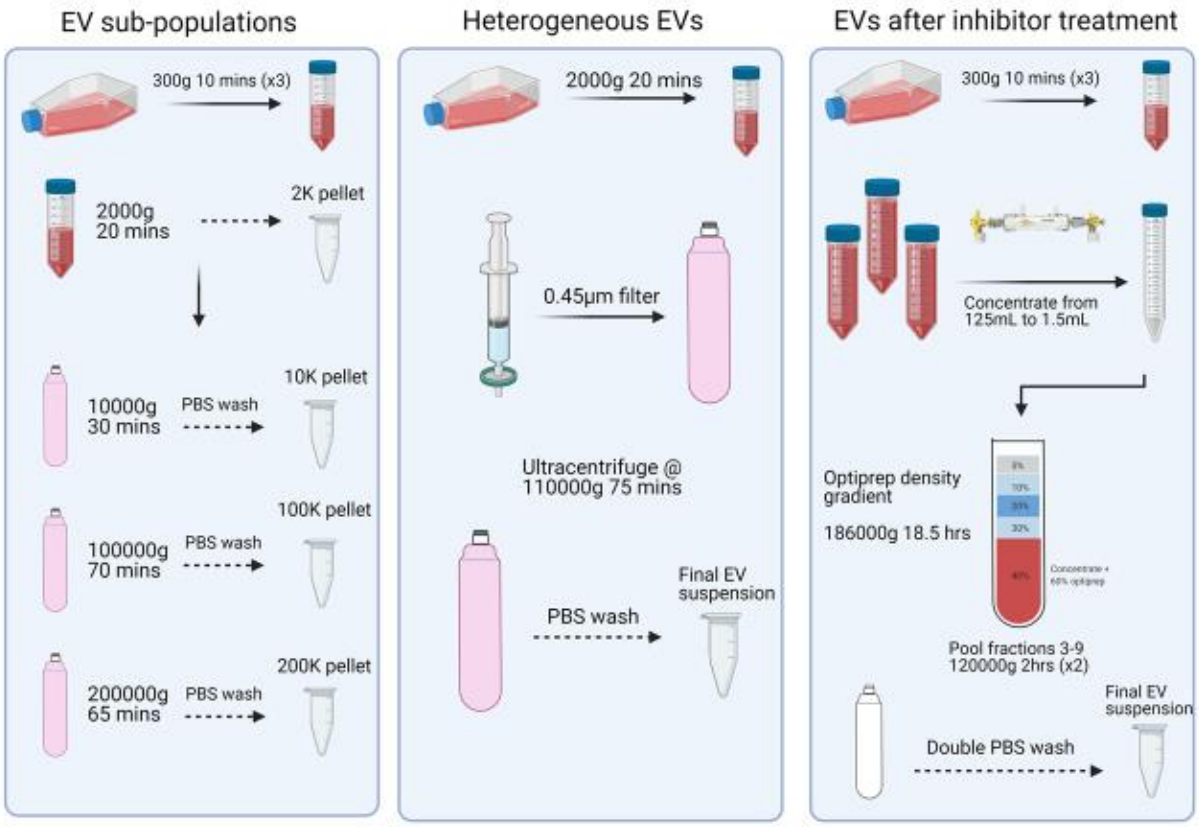

Figure 2.1: Overview of EV separation protocol used in this study

2.3 Collection of protein lysate of cells isolated along with extracellular vesicles

Hs578Ts(i)$_8$ cells were seeded at 1x10^5 cells per T75 flask (Corning, Cat. #: 431464U). The following day the medium was changed to 10% dFBS DMEM medium. After 5 days of incubation the medium was removed from the flask and the cells were washed twice with 1ml of ice-cold PBS. 1ml of PBS was added to the flask and the cells were scraped using a sterile cell scraper (Fisher Scientific, Cat. #: 08-100-241). Cells were centrifuged at 10,000g at 4°C for 5 mins. The supernatant was removed and the pellet was resuspended in 50 µl of cell lysis buffer (Invitrogen, Cat. #: FNN0011) and 1X proteinase inhibitor (Roche, Cat. #: 05892970001). Cell lysate was incubated on ice for 30 mins, vortexing every 10 mins for 10 seconds. After 30 minutes, the sample was centrifuged at 16,000g at 4°C for 10 minutes. The supernatant was transferred to a new tube and stored at -20 °C until required. EV pellets were lysed using this protocol for immunoblotting by using 1:1 of EVs suspension and lysis buffer.

2.4 Characterisation of EV pellets

2.4.1 Protein quantification of EV pellets

Two methods of protein were used during the course of this study i.e. the standard bicinchoninic acid (BCA) assay and the microBCA assay. The sensitivity of the microBCA is greater and was used when the protein concentration was low

2.4.1.1 Bicinchoninic acid (BCA) assay

Cell lysate, EV lysate and intact EV protein content was quantified using the Bio-Rad protein assay Dye reagent (Bio-Rad, Cat. #: 500-0006). Bovine serum albumin (BSA) standards of 800-12.5 µg/ml were prepared in PBS and used to calculate the protein content of the samples. Lysed and intact EVs from each pellet were diluted 1:2 in PBS and whole cell lysates were diluted 1:5 in PBS. 10 µl of standards and sample was added to a 96-well plate in duplicate. Bio-Rad Dye reagent was diluted 1:5 in dH_2O and 200µl added to each standard and sample. Absorbance was read at 570 nm using a FluoStar Optima microplate reader (Serial #: 08-100-241) and protein levels were calculated from a standard curve.

2.4.1.2 Micro BCA ™ Protein assay kit

Protein concentration of serum EVs was measured using the Micro BCA ™ protein assay kit (Thermo Scientific, Cat. #: 23235). Briefly, 10µl of EVs were diluted with 140µl of PBS (i.e. 1 in 15 dilution) and added to 96-well plate. 150µl of standards (40-2µg/mL) were also added and plate was mixed on plate shaker for 30secs. Plate was sealed and incubated at 37°C for 2hrs. Absorbance was read at 560 nm using a FluoStar Optima microplate reader (Serial #: 08-100-241) and protein levels were calculated from a standard curve.

2.4.2 Immunoblotting of EV-associated markers

For all immunoblotting performed in this project, total protein was resolved on either 10% or 8% bis-acrylamide gels for protein SDS-PAGE electrophoresis, along with a molecular weight marker, SeeBlue Plus2 Pre-stained standard (Invitrogen, Cat. #: LC5925). Separated proteins were transferred to polyvinylidene fluoride (PVDF) membranes (BioRad, Cat. #: 162-0177) using semi-dry transfer at 20V for 1 hr. Following transfer, blots were incubated in blocking buffer (5% BSA) (Sigma-Aldrich, Cat. #: A9413) in PBS) at room temperature for 1 hr. Blots were then washed in PBS/0.01 % Tween 20 (PBST) for 5 min (x3 times). Primary antibodies were prepared in 3% BSA in PBST. Membranes were incubated in primary antibodies overnight at 4°C under constant rocking. Membranes were subsequently washed in PBST (3 times) and incubated in secondary horseradish peroxidase-conjugated secondary antibodies for 1 hr at room temperature under constant rocking. Membranes were again washed in PBST (3 times) and proteins were visualized by Super Signal® West Pico chemiluminescence substrate (Thermofisher, Cat. #: 34080) or Super Signal® West Femto maximum sensitivity substrate (Thermofisher, Cat. #: 3409s). Proteins were detected using a chemidoc exposure system (BioRad laboratories). All antibody conditions and catalogue numbers are detailed in Table 2.2.

Primary Antibody	Company, Cat#	Dilution	Antibody condition	Secondary Antibody
GRP94	Cell Signalling, 2104S	1 in 2000	3% BSA in PBST	Rabbit
Actinin-4	Abcam, ab108198	1 in 1000	3% BSA in PBST	Rabbit
TSG101	Abcam, ab83	1 in 1000	3% BSA in PBST	Mouse
CD63	Abcam, ab68418	1 in 500	3% BSA in PBST	Rabbit
CD81	Santa Cruz, 5A6	1 in 200	3% BSA in PBST	Mouse
CD9	Abcam, ab92726	1 in 1000	3% BSA in PBST	Rabbit
Flotillin	Abcam, ab133497	1 in 1000	3% BSA in PBST	Rabbit
Syntenin-1	Abcam, ab133267	1 in 1000	3% BSA in PBST	Rabbit
Albumin	Abcam, ab190806	1 in 2000	3% BSA in PBST	Rabbit
Calnexin	Abcam, ab92573	1 in 1000	3% BSA in PBST	Rabbit
All secondary antibodies were diluted 1 in 1000 in 3% BSA in PBST				

Table 2.2: Antibody dilutions and conditions for EV immunoblotting

2.4.3 Nanoparticle tracking analysis (NTA) of EV pellets

Nanoparticle tracking analysis (NTA) was performed using the NTA NS300 system (NanoSight, Nanosight, Amesbury, UK). EV size distribution and concentration can be determined using NTA system which measures nanoparticles from 10nm to 2000nm. The concept the NTA system uses includes both light scattering and Brownian motion, upon nanoparticle impact on laser beams, the beams are scattered and visualized by 20X magnification. Brownian motion of the particles is observed by capturing 30 frames/sec. Filtered PBS (0.45µm filter, Pall Corporation, Cat. #: 4654) was used as a negative control. EV samples were diluted appropriately using filtered PBS, loaded onto the NTA using a NanoSight syringe pump and five 60sec videos were taken. The size of the particles was determined using the NTA software.

2.4.4 Transmission electron microscopy (TEM) of EV pellets

[TEM imaging of EVs was performed in the Advanced Microscopy Laboratory in Trinity College Dublin, with the help of Dr. Eoin Mc Carthy and Mr. Neal Leddy]

A 10µL sample of EV suspension was placed onto parafilm (Sigma-Aldrich, Cat. #: P7793). A formvar carbon-coated nickel grid (Ted Pella Inc, Cat. #: 01813) was placed on top (coated side facing the droplet) of the EV suspension droplet. The grid was incubated for 60min at room temperature, washed in 30µL of PBS (x3 times) on parafilm for 5min. Absorbent paper was used to remove excess PBS from the washing steps. A droplet of paraformaldehyde (2%) was placed on parafilm and the grid was placed on top and fixed for 10min. The PBS washing steps were repeated. The grid was then contrasted in 2% uranyl acetate (BDH, Cat. #: 230550) and all images were taken using the JEOL JEM-2100 transmission electron microscope at 120kV.

2.4.5 Flow cytometry analysis of EV markers

[Antibody preparations and Imaging flow cytometry (IFCM) was performed by Postdoctoral researcher Dr. Anindya Mukhopadhya]

EV surface antigens were exposed to antibodies diluted in 0.22 µm-filtered PBS with 2% dFBS supplemented with protease inhibitor and phosphatase inhibitor (IFCM buffer). The antibodies used were anti-CD63 conjugated with FITC (1:150) (Biolegend, Cat. #: 353006), CD9-PE (1:5000) (Biolegend, Cat. #: 312106), CD81-PE-Cy7 (1:150) (Biolegend, Cat. #: 349512) and ADAM10-APC (1:150) (Biolegend, Cat. #: 352706). The EVs were incubated with the antibodies for 45 mins at room temperature in the dark, and washed using a 300kDa filter (Nanosep, Cat. #: 516-8531), resuspended in 50µl IFCM buffer and acquired within 2hrs on the ImageStream X MK II imaging flow cytometer (Amnis/Luminex, Seattle, USA) at 60x magnification and low flow rate. EV-free IFCM buffer, unstained EVs, single-stained controls and fluorescence minus one (FMO) controls were run in parallel. Fluorescence was within detection linear range in the following channels: FITC was measured in channel 2 (B/YG_480-560 nm),PE in channel 3 (B/YG_560-595 nm), PE-Cy7 in channel 6 (B/YG_ 745-780 nm) and APC in channel 11 (R/V_642-745 nm). Brightfield in channel 1 and 9 (B/YG_435-480 and R/V_560-595 nm filter, respectively) and side scatter channel (SSC) in channel 12 (R/V_745-780 nm filter). Data analysis performed using IDEAS software v6.2 (Amnis/Luminex, Seattle, USA). EVs were gated as SCC-low vs fluorescence, then as non-detectable brightfield (Fluorescence vs Raw Max Pixel Brightfield channel), gated EVs were confirmed in IDEAS Image Gallery.

2.5 Toxicity of proposed EV inhibitors

2.5.1 Cytotoxicity assay of proposed EV inhibitors

Hs578Ts(i)$_8$ cells were seeded at 3 x 10^3 in 96-well plate and allowed to attach overnight. Cells were treated with calpeptin (Apexbio, Cat. #: A4411), Y27632 (Apexbio, Cat. #: A3008), GW4869 (Selleckchem, Cat. #: S7609) and manumcyin A (Sigma, Cat. #: M6418) the next day in 10% dFBS medium and cultured for 48 hrs. Acid phosphatase assay was used to determine the cell viability. Cell medium was removed and cells were subsequently washed in 100µl PBS (twice) (Sigma-Aldrich, Cat. #: P8537). 1M sodium acetate buffer was prepared (500 mL dH20, 4.1g sodium acetate (Sigma Aldrich, Cat. #: S5636), 500µl triton X (Sigma-Aldrich, Cat. #: T8787), pH to 5.5) and subsequently used for the phosphatase substrate buffer. Fresh phosphatase substrate buffer was prepared prior to use using 0.27g of 10mM p-nitrophenol phosphate (VWR chemicals, Cat. #: 27963.101) per 100mL sodium acetate buffer. 100µL of phosphatase substrate was added to each well. The plates were wrapped in aluminium foil and placed in an incubator at 37°C/5% CO_2 for 1.5hr. After the incubation period, 50µL 1M NaOH (Sigma Aldrich, Cat.#: S5881) was added to each well to stop the reaction. The absorbance was read at 405nm using the FlouStar Optima microplate reader (BMG Labtech, serial #: 413-2103).

2.5.2 Apoptosis assay (Annexin V/PI Flow cytometry)

Toxicity of the inhibitors was also investigated using annexin V-FITC (IQ Products, Cat. #: IQP-120F) and propidium iodide (PI) staining (BD Biosciences, Cat. #: 550474). Hs578Ts(i)$_8$ cells were seeded at 5 x 10^4 in 6-well plate. The next day the cells were treated with proposed EV inhibitors at the chosen concentration determined by acid phosphatase assay in 10% dFBS medium. 48hrs later the conditioned medium was collected. The cells were trypsinised and placed with the CM and centrifuged at 1200rpm for 5 mins. The pellet was resuspended in 500µl of 1X Binding Buffer (BB) (for 20X BB: 2.6g of HEPES (10.9mM), 8.18g of NaCl (140 mM), 0.28g of $CaCl_2$ (2.5 mM), pH 7.4) and centrifuged at 600g for 5mins. Annexin V-FITC was diluted 1:33.3 with BB and 38µl was used to resuspend the pellet. Cells incubated on ice for 20 mins. 500µl of BB was added and centrifuged at 600g for 5 mins at 4°C. Pellet was resuspended in 500µl of BB and 5µl of PI was added. Apoptosis was analysed on 1 x 10^4 events using the BD Accuri™ C6 flow cytometer.

2.6 EV-treated functional assays

2.6.1 EV sub-population studies

2.6.1.1 Proliferation assay

Hs578T cells were seeded at 2 x 10^3 cells/well in a 96-well plate in 10% dFBS-containing medium i.e. FBS had been ultracentrifuged overnight to remove any EVs in the FBS, and allowed to attach overnight. The following day the cells were treated with EV sub-populations of 0.5, 1 and 2 µg. 72 hrs post-treatment an acid phosphatase assay was performed to measure proliferation as described in section 2.5.1.

2.6.1.2 Migration assay

Hs578T cells were seeded at 4 x 10^4 cells/well in a 24-well plate in 10% dFBS-containing DMEM medium and allowed to grow overnight. Next day the wells were scratched with a p200 pipette tip down the centre of the well. The medium was removed from the wells and they were washed (X2) with 500 µl of 10% dFBS-containing medium. EV sub-populations were added to the appropriate wells at 1, 2 and 4 µg in 1% dFBS medium. Images were taken (X3 for each well) along the scratch with a 10X objective lens using the Olympus IX81 inverted microscope just after treatment (0hrs) and after 24 hrs. ImageJ was used to measure the wound closure.

2.6.1.3 Invasion assay

Extracellular matrix (ECM) (Sigma-Aldrich, Cat. #: E1270) diluted with serum-free DMEM medium at a concentration of 1 mg/ml was thawed at 4°C overnight. Polyester (PET) membrane transwell inserts with a pore size of 8 µm (Falcon, Cat. #: 353097) were coated with the ECM by adding 200µl to each insert and placing them in a 24-well plate. The plate was incubated at 37°C, 5% CO_2 overnight. The following day, the inserts were washed (X2) with 200µl serum-free DMEM media. Hs578T cells were seeded at 2 x 10^4 cells/well in 200 µl 10% dFBS-containing medium. The following day, the medium inside the chambers was changed to 1% dFBS. EV sub-populations were added to the chambers at 1, 2 and 4 µg. 500 µl of 10% dFBS was added to the bottom of each well of the 24-well plate. 72 hrs post-treatment, the inside of each insert was washed with a PBS-soaked Q-tip. Inserts were stained with 0.1% crystal violet (Sigma, Cat. #: C3886) for 10 mins while rocking. Following the staining, inserts were

washed (X3) with PBS for 10 mins. Images of the cells that had invaded were taken using a 10X objective lens using the Olympus IX81 inverted microscope. To evaluate the percentage of invading cells, inserts were placed in 10% acetic acid (Sigma, Cat. #: 338826) for 10 mins to elute the crystal violet and the absorbance was read at 570 nm using a FluorStar Optima microplate reader.

2.6.1.4 *Anoikis* assay

24-well plate was coated with 200µl of 12 mg/ml poly (2-hydroxyethyl methacrylate) [poly-HEMA] (Sigma-Aldrich, Cat. #: P3932) and left in a biosafety cabinet overnight. The following day the same process was repeated. As a control, wells were coated with 95% ethanol in place of the poly-HEMA. Hs578T cells were seeded at 5 x 10^4 cells/well in 500µl of 10% dFBS-containing medium and treated with EV sub-populations at 2.5, 5 and 10 µg. 72 hrs post-treatment 50µl of Alamar blue dye (Invitrogen, Cat. #: DAL1100) was added to each well and the plate covered in tin-foil and incubated at 37°C, 5% CO_2 for 3.5hrs. Cell survival was determined by reading the plate at an absorbance of 570nm using a FluoStar Optima microplate reader.

2.6.2 EVs still released after EV inhibitor treatment

2.6.2.1 Proliferation assay

Recipient TNBC cell lines were seeded in a 96-well plate in 10% FBS medium and allowed to attach overnight (see Table 2.3 for seeding densities). Densities were chosen to give well confluency in control cells after 72 hrs. The following day the cells were treated with EVs separated from different inhibitor treatments in 200µl 10% dFBS medium, 72 hrs post-treatment an acid phosphatase assay was performed, as described in section 2.5.1, to measure proliferation.

2.5.2.2 Migration assay

Recipient TNBC cells were seeded in a 24-well plate in 10% FBS medium and allowed to grow overnight (see Table 2.3 for seeding densities). Seeding densities were chosen to allow cell confluency after 24 hrs so a scratch could be clearly visible in the centre of the well. The following day the wells were scratched with a p200 pipette tip down the centre of the well. The medium was removed from the wells and they were washed (twice) with 500µl of 1% dFBS medium. EVs released after treatment with

inhibitors were added to the appropriate wells in 500µl 1% dFBS-containing medium. Images were taken three for each well) along the scratch with a 10X objective lens using the Olympus IX81 inverted microscope just after treatment (0hrs), after 24 hrs and 48 hrs, depending on the cell line being imaged. ImageJ was used to measure the wound closure.

TNBC recipient cell line	Proliferation assay	Migration assay
Hs578T	3×10^3	4×10^4
MDA-MB-468	6×10^3	22.5×10^4
BT549	4×10^3	3×10^4

Table 2.3: TNBC cells seeding densities for proliferation and migration assays

2.7 Flow cytometry screening of Triple-Negative Breast Cancer EV release

A small-scale screening assay was set-up to determine if potential EV inhibitors have an effect on EV release. In a 24-well plate format, TNBC conditioned medium was collected and screened using the Amnis ImageStream Flow Cytometer.

2.7.1 Toxicity of drugs on TNBC cell lines

Acid phosphatase assay previously described in section 2.5.1 was used to determine the viability of TNBC cell lines following 48hrs drug treatment. The following drugs were tested; GW4869 (Selleckchem, Cat. #: S7609), manumycin A (Sigma, Cat. #: M6418), sulfisoxazole (Apexbio, Cat. #: B2043), carboplatin (Apexbio, Cat. #: A2171), neratinib (Sequoia Research products Ltd., Cat. #: SRP06000n) and COTI-2 (Selleckchem, Cat. #: S8580). See Table 2.4 for seeding density.

2.7.2 Isolation of conditioned medium (CM)

Hs578Ts(i)$_8$, MDA-MB-231, HCC1143, BT549 and MDA-MB-468 cells were used for the study and cultured as previously described (see section 1.1). TNBC cells were seeded in 24-well plates in 10% FBS medium, see Table 2.4 for seeding densities. After 24hrs, the medium was removed and replaced with 500µl of 10% dFBS medium with or without the drugs being tested. After 48hrs, the CM was collected, the cells were counted and cell viability was measured. The CM was then cleared from debris by

centrifuging at 300g for 5 mins at 4°C. This was repeated another two times, changing the Eppendorf each time. Once cleared, the CM was aliquoted and stored at -80°C until required.

TNBC cell lines	Seeding density for 96-well plate	Seeding density for 24-well plate
$Hs578Ts(i)_8$	3×10^3	1.5×10^4
BT549	4×10^3	2×10^4
HCC1143	5×10^3	3×10^4
MDA-MB-468	6×10^3	1×10^5
MDA-MB-231	6×10^3	5×10^4

Table 2.4: TNBC cells seeding densities for toxicity and screening assays

2.7.3 Screening of conditioned medium on Amnis ImageStream

CM from each TNBC cell line was screened for the presence of CD9 (ExBio, Cat. #: 1P-208-T100). The CD9 antibody was diluted in PBS (1:25) and centrifuged at 16,000g for 15 mins at 4°C to remove antibody aggregates. The CM was thawed on ice and 25µl was added to 25µl of prepared CD9 antibody. The CM was incubated for 2hrs at room temperature in the dark. After incubation the CM-antibody sample was washed in 300kDa filter (Nanosep, Cat. #: 516-8531) and centrifuged at 2,500g for 3 mins to remove any unbound antibody. The cleaned CM-antibody sample was resuspended in PBS, placed in a new Eppendorf and acquired within 2hrs on ImageStream X MK II imaging flow cytometer at 60X magnification and low flow rate. PBS and unstained controls were run in parallel. All samples were screened for 5 mins. Once screened, 4% of NP-40 (EMD Millipore, Cat. #: 492016) was added at 1:1 ratio with the sample and was re-screened, as the NP-40 control.

Data analysis was performed using IDEAS software v6.2. EVs in the CM were detected based on brightfield detection and SSC visibility (i.e. previously published [176]). Large EVs (lEVs) were gated events with clear brightfield and SSC signals, medium EVs (mEVs) events with low/no brightfield and lower but clearly visible SSC signals, small EVs (sEVs) have no visible brightfield and no/very low SSC signals. All three sub-populations of EVs were looked at individually and combined when calculating the final EV numbers present in each sample.

2.8 Platelet aggregation study

[Platelet aggregation experiments were performed in collaboration with Laura de la Fuente Rodriguez and Assoc. Prof. Maria J Santos-Martinez]

The platelet aggregation experiments were performed with the Hs578T cells and the isogenic sub-clone Hs578Ts(i)$_8$. EVs were separated from the cell line variants using the protocol outlined in section 2.2.1.

2.8.1 Blood collection and preparation of platelets

Approval for this study was obtained from the School of Pharmacy and Pharmaceutical Sciences Research Ethics Committee to Dr. Maria J Santos-Martinez (2015-06-01 MS). Following informed consent, blood was withdrawn from healthy volunteers who had not taken any medication known to interfere with platelets function for at least 2 weeks prior to the study.

Washed platelets (WP) were prepared by differential centrifugation just before each experiment. Briefly, blood was drawn and added to a 50ml falcon tube with 3.15% sodium citrate (9:1). The tube was gently inverted and centrifuged at 250g for 20 mins. The upper yellow layer, the platelet rich plasma (PRP) was removed and placed in a new 50ml tube. Prostacyclin (PGI_2), stock concentration was 1 mg/ml, was added to the PRP to prevent activation of the platelets and centrifuged at 900g for 10 mins. The platelet poor plasma (PPP) was gently removed without disturbing the pellet. The surface of the platelet pellet was then washed three times with 1ml of Tyrode's buffer (Sigma, Cat. #: T2937). The platelets were resuspended in Tyrode's buffer and placed in a new tube. The platelet concentration was measured using a Beckman Coulter Z1 series Coulter Counter (Labplan, Ireland), and the platelet suspension was adjusted with Tyrode's buffer to have a final concentration of 2.5 x 10^8 platelets/ml. Platelets were allowed to sit at room temperature for 1hr before using for the experiment.

2.8.2 Preparation of TNBC cells for aggregation experiments

Hs578T and Hs578Ts(i)$_8$ cell line variants were prepped when their cell confluency was 80%-90% in a T75 flask. 3ml of DPBS/EDTA (7mM) was added to the flask to wash the cells after removing the cell culture media. Next, 7 ml of DPBS/EDTA was added to the flask to detach the cells. Cells were then collected in a 50ml falcon tube and centrifuged at 300g for 5 mins. The supernatant was removed, and

the resultant cell pellet was resuspended in 10ml of Tyrode's solution and centrifuged at 300g for 5 mins. The cell pellet was resuspended in 1ml of Tyrode's solution. The cells were counted using the Beckman Coulter Z1 series Coulter Counter (Labplan, Ireland) and left to rest on ice for 1-2 hrs before using for the experiment.

2.8.3 Light transmission aggregometry (LTA) experiments

Platelet aggregation was measured using an eight-channel Platelet Aggregation Profiler Model PAP-8E from (Biodata Corporation, Ireland). The percentage of platelet aggregation was calculated by the Aggro-Link software where the amount of light passing through a cuvette with Tyrode's salt solution (blank) was considered as 100% of aggregation.

Platelet aggregation was measured using light transmission aggregometry (LTA). Washed platelets (WP) (i.e. 2.5 x 10^8 platelets/ml) were placed in each channel under stirring for 1 min at 37°C. Cells or EVs were then added to the cuvettes at the various concentrations and platelet response monitored by the software for 30 mins. For the controls instead of adding cells or EVs, Tyrode's solution and PBS was used, respectively. At the beginning of each set of experiments with a new donors' platelets, 2 µg/ml of collagen was added to the WP to confirm the ability of the WP to aggregate.

2.8.4 Fixing and imaging of aggregated platelets

Following the aggregometer experiments with TNBC cell line variants or their corresponding EVs, the platelet suspensions were fixed with 2% paraformaldehyde (Sigma, Cat. #: P6148) for 30 mins. The samples were then mounted on a microscope slide, using a cytospin (Cytospin 4, Thermo Shandon, Fisher Scientific, Ireland) The images were analysed by phase-contrast microscopy at a magnification of 10X using an Olympus CKX41 microscope (Mason Technology Ltd., Ireland)

2.9 Global proteomic profiling of EVs

[Mass spectrometry analysis was performed by Dr. Eugene Dillon at UCD mass spectrometry core facility and raw data was returned for analysis]

EVs separated from the Hs578T and Hs578Ts(i)$_8$ cell line variants were analysed by mass spectrometry (MS) to identify potential key proteins that may be involved in platelet aggregation (see Fig. 2.2 for experimental design and overview).

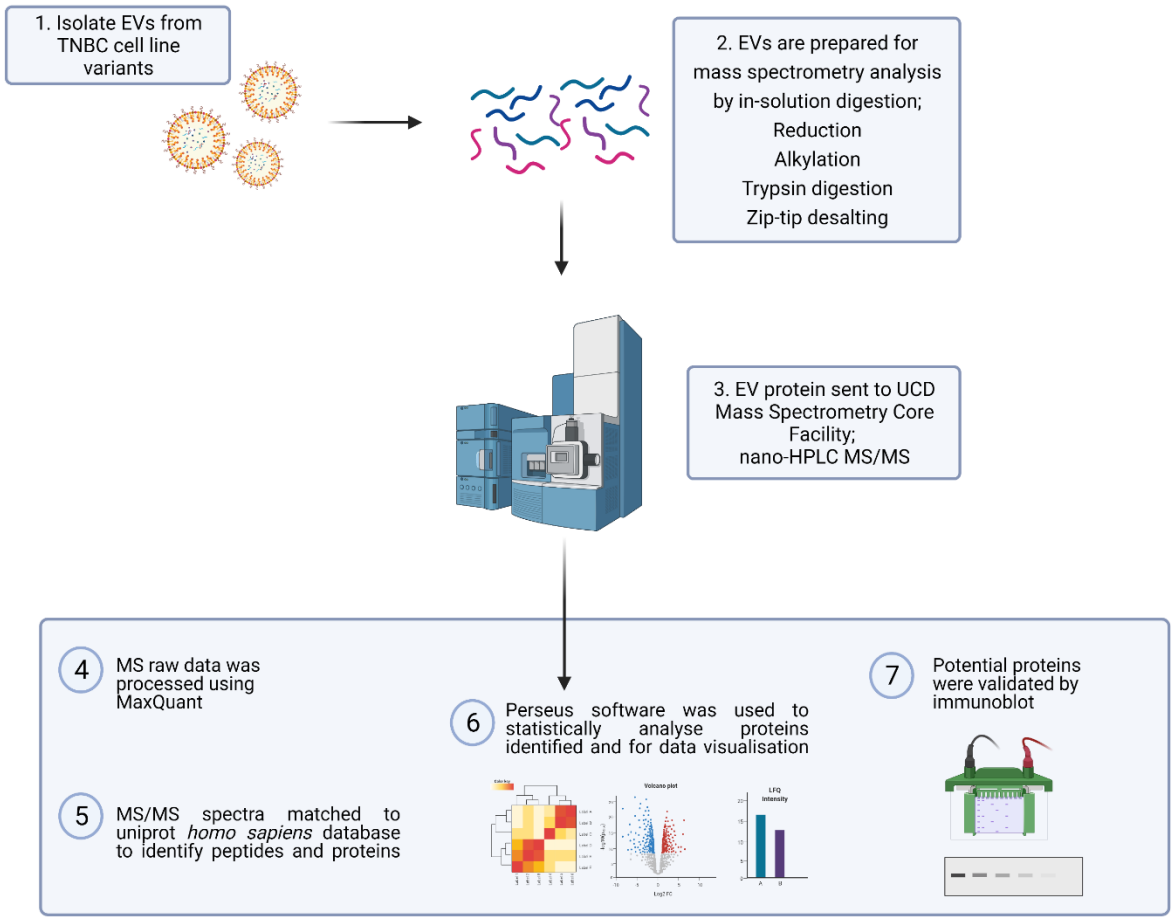

Figure 2.2: Overview of proteomic profiling of EVs

2.9.1 In-solution digestion preparation of EVs for MS

50ug of EV protein were prepped for MS analysis. Fresh solution of 100 mM DL-dithiothreitol (DTT) (Sigma, Cat. #: D0632) was prepared by adding 15.4mg in 1ml of HPLC-grade water (Sigma-Aldrich, Cat. #: 900682) . This was added to each sample to give a final concentration of 5mM. Samples were vortexed and heated at 60°C for 5 mins to remove the disulphide bonds. Reduced samples were briefly centrifuged to gather the condensate. For alkylation of the samples, 200mM of iodoacetamide (Sigma, Cat. #: I1149) (37mg in 1ml water) was added to the samples to give a final concentration of 10mM, vortexed and incubated in the dark for 30 mins. 50µl of reduced and alkylated sample was added to one vial of trypsin singles (Sigma, Cat. #: T7575), vortexed and allowed to digest overnight at 37°C on a thermomixer at 350rpm. To stop the digest, acetic acid (Sigma, Cat. #: 338826) was added to the sample (i.e. a volume of 1% of the sample volume). Digested proteins were bound and desalted using C18 ZipTips (Merck Millipore, Cat. #: ZTC18S096), washing the samples with 0.1% Trifluoroacetic acid (TFA) (Sigma, Cat. #: T0699) (100µl of TFA in 900µl water). Once washed, the samples were eluted from the ZipTip and dispensed in 12µl of 50% acetonitrile (Sigma, Cat. #: 494445)in 0.1% TFA (300µl of acetonitrile, 300µl 0.1% TFA). The samples were then dried using a Speedvac vacuum concentrator and resuspended in 10µl of MS buffer (2.5% acetonitrile, 0.5% acetic acid).

2.9.2 Mass spectrometry

Peptide fractions (*n=3*) were analysed on a quadrupole Orbitrap (Q-Exactive, Thermo Scientific) mass spectrometer equipped with a reversed-phase NanoLC UltiMate 3000 HPLC system (Dionex LC Packings, now Thermo Scientific). Peptide samples were loaded onto C18 reversed phase columns (10 cm length, 75 µm inner diameter) and eluted with a linear gradient from 1 to 27% buffer B containing 0.5% AA 97% ACN in 60 min at a flow rate of 250 nL/min. The injection volume was 5 µl. The mass spectrometer was operated in data dependent mode, automatically switching between MS and MS2 acquisition. Survey full scan MS spectra (m/z 300 – 1200) were acquired in the Orbitrap with a resolution of 70,000. MS2 spectra had a resolution of 17,500. The twelve most intense ions were sequentially isolated and fragmented by higher-energy C-trap dissociation.

2.9.3 Protein Identification

Raw data from the Orbitrap Q-Exactive was processed using MaxQuant version 1.6.3.4 [177, 178], incorporating the Andromeda search engine [179].To identify peptides and proteins, MS/MS spectra were matched to the Uniprot *homo sapiens* database (2018_12) containing 73,928 entries. All searches were performed with tryptic specificity allowing two missed cleavages. The database searches were performed with carbamidomethyl (C) as fixed modification and acetylation (protein N terminus) and oxidation (M) as variable modifications. Mass spectra were searched using the default setting of MaxQuant namely a false discovery rate of 1% on the peptide and protein level. For the generation of label free quantitative (LFQ) ion intensities for protein profiles, signals of corresponding peptides in different nano-HPLC MS/MS runs were matched by MaxQuant in a maximum time window of 1 min [180].

2.9.4 Analysis of data using Perseus software

The data generated using MaxQuant was uploaded into Perseus software v1.6.15.0 to identify EV proteins and perform statistical analysis and visualisation. Data were filtered and transformed into log scale. Rows were categorised into Hs578T EVs or Hs578Ts(i)$_8$ EVs. To increase the confidence of the data set, proteins that were identified in at least three out of the six EV samples were analysed further, filtering for the valid values. A two-sample t-test was performed to compare the cell line variant-derived EVs with a threshold of 0.05, identifying proteins that are significantly different. Hierarchical clustering was performed by generating z-scores of normalised LFQ intensities. Values were then clustered using the Euclidean distance method (see Fig. 2.3 for overview of analysis performed with Perseus).

FunRich, a functional enrichment software tool (v3.1.3), was used to analyse the cellular component and biological pathways associated with proteins identified in the EVs [181]. Vesiclepedia and ExoCarta databases were explored.

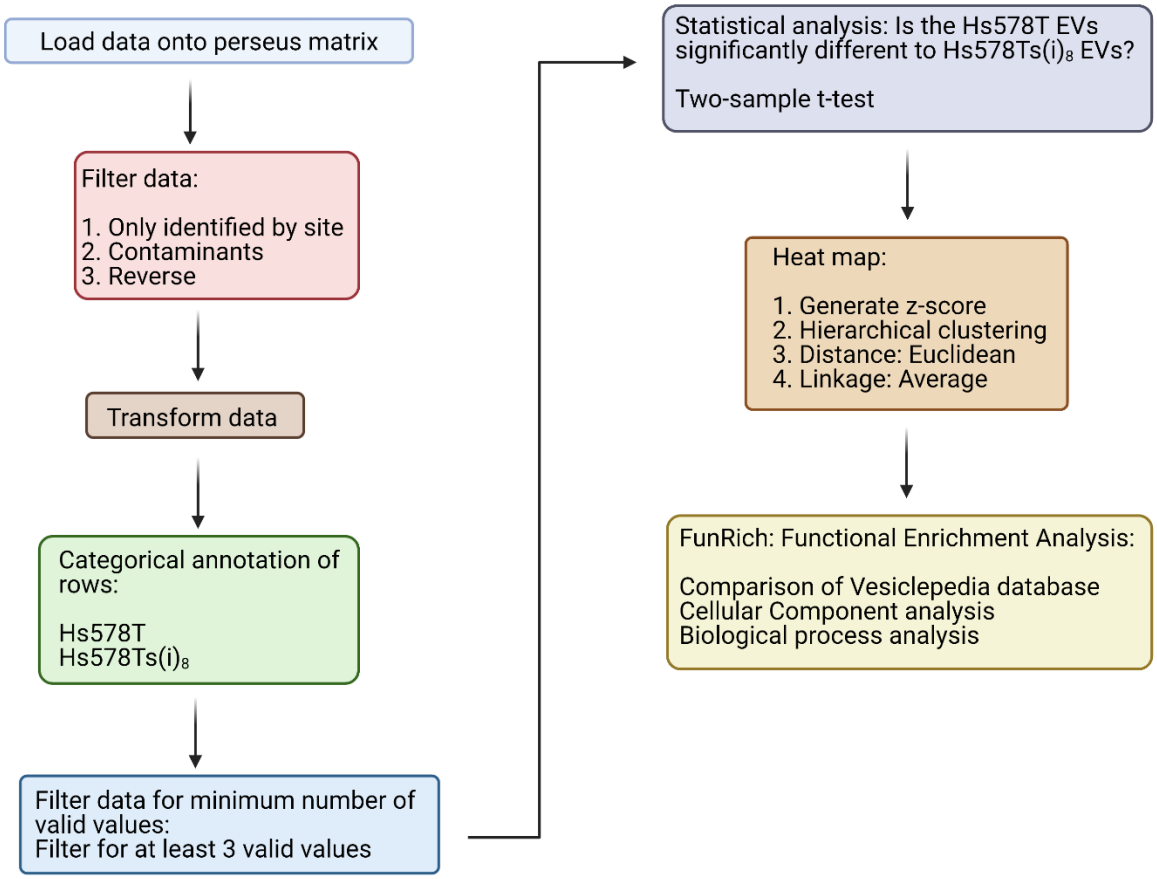

Figure 2.3: Overview of Perseus software analysis of EV proteomic data

2.9.5 Validation of identified proteins

Proteins identified as potential candidates for the platelet aggregation by proteomic profiling were validated using immunoblot.

Non-lysed vesicles that were prepped in both reducing (i.e. β-mercaptoethanol added to loading buffer and heated at 95° C for 5 min) and non-reducing (i.e. no β-mercaptoethanol added to loading buffer and heated at 95° C for 5 min) conditions were resolved on either 8% or 10% bis-acrylamide gels for Protein SDS-PAGE electrophoresis as described in section 2.4.2. All antibody conditions and catalogue numbers are detailed in Table 2.5.

Primary Antibody	Company, Cat#	Dilution	Antibody condition	Secondary Antibody
Platelet-derived growth factor receptor β	R and D systems, MAB1263	1µg/ml	3% BSA in PBST	Mouse
Glypican-1	Abcam, ab199343	1 in 1000	3% BSA in PBST	Rabbit
Urokinase plasminogen activator receptor	R and D systems, MAB807	1µg/ml	3% BSA in PBST	Mouse
CD97	R and D systems, MAD2529	1µg/ml	3% BSA in PBST	Mouse
MUC18/MCAM/CD146	R and D systems, MAB932	1µg/ml	3% BSA in PBST	Mouse
Protein Cyr61	R and D systems, MAB4055	1µg/ml	3% BSA in PBST	Mouse
All secondary antibodies were diluted 1 in 1000 in 3% PBST				

Table 2.5: Antibody dilutions and conditions for platelet aggregation study

2.10 Isolation of breast cancer patient serum EVs

2.10.1 Serum collection

Blood was taken from 104 individuals attending the Breast Care Clinic at St. Vincent's University Hospital, Dublin, for their first visit. Ethics approval was obtained from the St. Vincent's University Hospital Ethics Committee. Blood was collected in non-heparinised tubes prior to any other intervention and it was allowed to clot for 30 mins minimum to 60 mins maximum, according to the All-Ireland Oncology Research Group (ICORG)/Cancer Trials Ireland established SOP. Centrifugation was carried out at room temperature for 10 min at 1000 g. Serum was aliquoted and stored at -80 °C. At a later time, it was revealed which individuals were diagnosed with cancer ("patients") and which were not i.e. who breast mass was benign and non-cancerous ("controls").

2.10.2 Methods used for serum EV study

Six methods were compared when separating EVs from breast cancer patient serum and age-matched healthy controls. Initially, a pool of ER^+ breast cancer patient serum and their age-matched healthy controls were created by thawing the serum on ice and centrifuging the pooled serum at 2,500g for 15 mins at 4°C as a pre-clearing step. The cleared serum was aliquoted into 600µl and stored at -80°C until further required. Each method of separation used one aliquot of both ER^+ breast cancer serum and the corresponding age-matched healthy control aliquot.

2.10.2.1 Optiprep density gradient ultracentrifugation

Serum was thawed on ice and EVs were separated using a bottom-up density gradient. 500ul of serum was mixed with Optiprep (60%) to create a 40% iodixanol suspension (4mL) and placed in an Ultraclear ultracentrifuge tube. A discontinuous gradient was formed by overlaying the serum suspension with 30% (4 mL), 20% (4 mL), 10% (3.5 mL) and 5% (1 mL) iodixanol solutions. The gradient was centrifuged at 186,000g for 18 hrs at 4°C in a SW32.1 Ti swinging rotor. Afterwards, 1 mL fractions were taken from the top of the tube and the density was measured by calculating the refractive index. Fractions 8-10, corresponding to a density of 1.08g/ml - 1.13g/ml were pooled and diluted with PBS in a QuickSeal ultracentrifuge tube (Beckman coulter, Cat. #: 342414) and centrifuged at 120,000g for 2 hrs at 4°C. The resulting pellets were centrifuged a second time, finally being resuspended in 125 µl of PBS and stored at -80°C.

2.10.2.2 Differential ultracentrifugation

Serum was thawed on ice and ultracentrifuged at 100,000g for 60 mins in Open-top Polyallomer tubes (Beckman coulter, Cat. #: 326823) in the SW 32 Ti swinging rotor at 4°C. The supernatant was removed, and the pellet was further washed with PBS. The final pellet was resuspended in 125µl PBS and stored at -80°C.

2.10.2.3 Poly(ethylene glycol)

Serum was thawed on ice and mixed 1:1 with PEG buffer, with a final 10% w/v of PEG. PEG buffer contains: 20% w/v PEG6000 (Sigma, Cat. #: 81260) in 200 mM NaCl (Sigma, Cat. #: 1376), 10 mM EDTA (Invitrogen, Cat. #: 15575-038), 200mM Tris-HCL (sigma, Cat. #: T3253), pH 7.0. Samples were rotated end-over-end for 1 hr at 4°C and then centrifuged at 4000g for 15 mins at 4°C. The supernatant was carefully removed, and the pellet was resuspended in PBS and washed by centrifugation at 120,000g for 2 hrs at 4°C. The pellet was resuspended in 125ul of PBS.

2.10.2.4 Size exclusion chromatography

Serum was thawed on ice and EVs were separated using Izon qEVoriginal 70nm (Izon, Cat. #: SP1) columns on the automatic fraction collector. Briefly, the column was equilibrated using 10mL of 0.22µm filtered PBS. Once equilibrated, 500µl of serum was loaded onto the column and fractions of 0.5mL were collected, immediately. Once the sample had run through, PBS was loaded on top of the column to continue fraction collection. In total, 26 fractions were collected. The first 3mL of collected fractions are called the void volume, i.e. no EVs. Fractions 7-9 were pooled based on manufacturer's instructions. After fraction collection, the column was flushed with 15mL of PBS before loading the next sample. Separate columns were used for ER^+ patient serum and age-matched healthy control serum. Once finished, the columns were flushed with 0.05% w/v sodium azide (Sigma, Cat. #: 71289) solution, used as an anti-bacterial solution. The columns were stored at 4°C until required. The 1.5mL of fractions were concentrated using 10 kDa Pierce protein concentrator, PES 10 MWCO (Sigma, Cat. #: 88513) to a final volume of 125µl.

2.10.2.5 Nickel-based isolation

2.10.2.5.1 Bead functionalisation

This isolation protocol was taken from a previously published protocol [182]. Nickel Sepharose beads (GE Healthcare, Cat. #: 17-5268-01) were transferred to 50ml tube and centrifuged at 800g for 2 mins at room temperature. Supernatant was discarded and 25ml of water (Lonza, Cat. #: 17-724Q) was used to homogenously resuspend the beads by gentle inversion of the tube. This was centrifuged at 800g for 2 mins at room temperature. The supernatant was removed and 25ml of Buffer S was added

to resuspend the pellet and remove nickel ions from the beads. Beads were incubated for 5 mins at room temperature and centrifuged at 800g for 2 mins. Supernatant was removed and pellet was resuspended in Buffer N, incubated for 5 mins at room temperature and centrifuged at 800g for 2 mins. This step functionalises the beads and confers a positive charge to the matrix. The functionalised beads were washed again in 25ml water, centrifuged at 800g for 2 mins. Supernatant was discarded and beads resuspended in 25ml PBS and centrifuged at 800g for 2 mins. This was repeated two more times with the supernatant removed with a serological pipette at a slow constant aspiration speed to avoid disturbing the pellet. Final bead pellet was resuspended in 25ml of PBS to obtain a final bead concentration of 20mg/ml. The functionalised beads were stored at 4°C.

2.10.2.5.2 EV capture

Serum was thawed on ice and diluted to 2ml with PBS. 50µl of functionalised nickel beads (i.e. 1:40 ratio of bead:serum volume) were added to the surface of the serum drop by drop and incubated for 30 mins at room temperature with gentle rotation. Serum was centrifuged at 800g for 2 mins at room temperature and supernatant was removed.

2.10.2.5.3 EV elution

Elution buffer was prepared by diluting 200µl of solution A and 200µl solution B in 600µl of 0.22µm filtered PBS. 50µl of elution buffer was added to the bead pellet and transferred to a protein lo-bind Eppendorf. The EV solution was incubated at 28°C using a thermomixer at 600rpm, keeping the beads in suspension and allowing the bound EVs to dissociate. Beads were pelleted down by centrifuging at 800g for 30 seconds. The supernatant containing the EVs was transferred to a new Eppendorf. The elution was repeated a second time to fully elute all EVs bound to the nickel beads. The final EVs were brought to a volume of 125µl PBS.

Buffer S: PBS+ 0.5M NaCl (Sigma, Cat. #: 450006) +50mM EDTA (Invitrogen, Cat. #: 15575-038), pH8.0. Filter with 0.2µm filters. Store at room temperature.

Buffer N: 0.4M $NiSO_2$ (Sigma, Cat. #: 227676) in pure water. Filter with 0.2µm filters. Store at 4°C.

Solution A (5X): PBS + 16mM EDTA. Filter with 0.2µm filters. Store at 4°C.

Solution B (5X): PBS + 10mM NaCl + 225µM citric acid (Sigma, Cat. #: 251275). Filter with 0.22µm filters. Store at room temperature.

2.10.2.6 Stemcell Technologies EasySep Pan extracellular vesicles kit

EVs positive for CD9, CD81 and/or CD63 were separated using the Stemcell Easy Sep kit (Stemcell technologies, Cat. #: 17891), following manufacturer's instructions. Briefly, serum was thawed on ice was placed in 5mL polystyrene round-bottom tube (BD Falcon, Cat. #: 352054) with 25 µl of selection cocktail (i.e. combination of monoclonal antibodies in PBS, Cat. #: 17891C) and incubated at room temperature for 10 mins. Rapid spheres™ (i.e. suspension of magnetic particles in water, Cat. #: 50201) were vortexed for 30 secs and 50 µl was added to the serum and incubated at room temperature for 10 mins. PBS was added to the serum to a volume to 2.5mL, gently mixed and incubated in the EasySep™ magnet (Stemcell technologies, Cat. #: 18000) at room temperature for 5 min. Supernatant was poured from the tube and 2.5mL PBS was added and incubated at room temperature for 1 min. This was repeated another two times to wash the sample. The final EVs were collected by removing the tube from the magnet and resuspending in 125 µl of PBS.

2.10.2.7 Miltenyi Biotec Macsplex Exosome isolation kit

EVs positive for CD9, CD81 and /or CD63 were separated using the exosome isolation kit, Pan (Miltenyi Biotec, Cat. #: 130-110-912) with MicroBeads specific for CD9, CD81 and CD63. Briefly, serum was thawed on ice and 50µl of MicroBeads were added to the serum and incubated for 1hr at room temperature. µ columns were placed under the magnet of the µMACS separator (Miltenyi Biotec, Cat. #: 130-042-602) and prepped by adding 100µl of equilibration buffer. After, the column was rinsed with 100µl of isolation buffer. This is repeated three times. Serum sample was added to the column and allowed to run through, with the EVs captured in the magnetic field and retained in the column. The column was washed with 200µl of isolation buffer, this was repeated four times. The µ column was removed from the magnetic field and placed onto a 1.5mL Eppendorf. 100µl of isolation buffer is added and the magnetically labelled EVs are flushed out, pushing the plunger into the column. A further 25µl of isolation buffer was added to the final pool of EVs to adjust final volume to 125µl.

2.10.3 Characterisation of serum EVs

To choose the most suitable method for serum EV separation, EVs were characterised with various methods previously described in Section 2.4.

2.10.3.1 Apolipoprotein B ELISA

Apolipoprotein B was quantified in whole, non-lysed EVs using the human ApoB ELISA (Abcam, Cat. #: ab190806). Performed according to the manufacturers' instructions using 500ng of EVs and TNBC cell lysate as a positive control, using equal volumes of PBS and sample diluent supplied with the ELISA kit to bring volume to 50µl.

2.10.3.2 Glypican-1 and Gremlin 1 ELISA

Twenty age-matched pairs of breast cancer patient serum and healthy control EVs were isolated using the Stemcell isolation kit (see section 2.10.1.6) and lysed prior to glypican-1 (Assay genie, Cat. #: HUFI02075) and gremlin 1 (Assay genie, Cat. #: HUFI01783) ELISA. 10 µg and 5 µg of EV protein was used for glypican-1 and gremlin 1 ELISA, respectively. Both ELISAs were performed according to manufacturer's instructions.

2.11 Statistical analysis

Statistical analysis of the data was performed using GraphPad Prism. Graphs were generated using GraphPad Prism 9. *P-values* were generated using Student's t-test or ANOVA for multiple comparisons where $P<0.05$ was considered statistically significant.

Chapter 3: Extracellular vesicles sub-populations of triple-negative breast cancer and their effects on recipient cells

3. Abstract

There is increasing attention to extracellular vesicles (EVs) and their ability to increase tumour progression through cell-to-cell communication. Furthermore, there is substantial evidence that cancer cells release heterogeneous EV populations including, sub-populations of EVs and that all EVs in a heterogeneous pool are not necessarily the same. Previous work by our group demonstrated that the total populations of EVs from triple-negative breast cancer (TNBC) Hs578Ts(i)$_8$ cells could transfer aggressive traits from the aggressive cancer cells to recipient cells. Advancing on that earlier research, this study involved the separating and characterising of EV sub-populations of the heterogeneous EV population released from Hs578Ts(i)$_8$ cells. The effects of these EV sub-populations compared to the total heterogeneous EV population were investigated. This involved treating the less aggressive parental cell line variant, Hs578T with the EVs and evaluating the effect of the EVs on Hs578T proliferation, migration, invasion and *anoikis* resistance, all of which are processes that cancer cells use in order to undergo metastasis and propagate at secondary sites *in vivo.*

By separating, characterising, and comparing individual four EV sub-populations with their heterogeneous pool of EVs, it was established that all sub-populations seem to act together to deliver their pro-carcinogenic messages to recipient cells. There was no substantial difference in the effects caused by the EV sub-populations compared to the heterogeneous pool of EVs on Hs578T proliferation, migration, invasion and *anoikis*. No one single sub-population was solely responsible for the phenotypic effects transferred to the Hs578T cells.

In conclusion, to reduce the negative effects of TNBC EVs, a strategy to inhibit the release of all EV sub-populations would seem to be required, rather than trying to target one specific sub-population.

3.1 Introduction

Previous work by our research group, demonstrated that treatment of recipient cells with the heterogeneous EV population from the more aggressive Hs578Ts(i)$_8$ cell line variant increased the proliferation, migration, invasion and decreased the *anoikis* resistance of the less aggressive Hs578T cell line variant [183]. A more recent study has demonstrated that EVs isolated by differential ultracentrifugation from ten breast cancer cell line conditioned medium were able to distinguish between breast cancer subtypes, ER/PR+, HER2+ and TNBC. HER2+ and TNBC were significantly different from each other with TNBC EVs enriched in proteins involved in cancer cell migration, invasion and EMT processes whereas HER2+ EVs were enriched in proteins involved in metabolism, ERBB signalling and translation initiation [184].

There are continuous efforts in the EV research community to maintain a stringent nomenclature. It has been stated that the term of EVs is more correct when a piece of work has not definitively defined their separated vesicles as exosomes or microvesicles. There is also a consensus among many EV researchers that the terms, small EVs (sEVs), medium EVs (mEVs) and large EVs (lEVs), are most suitable, this because it is considered that small vesicles that were previously assumed to be exosomes, formed through an intracellular pathway and due to their small size (i.e. <150nm), may actually be small EVs that have bud from the cell membrane. Therefore, by using sEVs, mEVs and lEVs terminology, there is more agreement between EV researchers. This classification of EVs is predominately based on EV size and the ultracentrifugation speed at which they are isolated. By taking this approach, protein markers associated with each subtype have been identified [82].

Studies have shown that different EV sub-populations can have different effects. For example, neuroblastoma, SH-SY5Y and SK-N-BE2 cancer cell derived mEVs (or as the authors refer to them, ectosomes) isolated by 10,000g ultracentrifugation were less tumourigenic when compared to sEV, (referred as, exosomes), isolated by Optiprep density gradient. Here tumorigenicity was reported as increased proliferation and migration of SK-N-BE2 cells, treated with mEVs and sEVs isolated from SH-SY5Y cells [185]. Whereas lEVs, (or as authors refer to them, microvesicles and apoptotic bodies) separated from C57BL/6 derived melanoma cells, B16-F1 and B16-OVA conditioned medium by differential ultracentrifugation, were shown to have transmit a higher pro-coagulant phenotype than sEVs (referred as, exosomes) in terms of fibrin formation and thrombin generation [186]. Therefore, it seems that EV sub-populations may have differing influences. However, there are no studies describing the effects of TNBC EV sub-populations on recipient cells.

We set out to determine if the sub-populations released from TNBC cell line variant, Hs578Ts(i)$_8$, were individually responsible for the increase of cancer phenotypic characteristics of the parental cell line variant, Hs578T, by comparing four different EV sub-populations

3.2 Aims of study

The aim of this study was to expand on work performed by our research group [183], and to successfully separate out four EV sub-populations based on their size (nm) and EV protein markers that they carry from a heterogeneous pool of EVs from the TNBC cell line variant Hs578Ts(i)$_8$ using differential ultracentrifugation

Subsequently we aimed to determine if one EV sub-population was responsible for transfer of aggressive traits to parental cell line variant, Hs578T, previously seen with the heterogeneous pool of EVs or if all EVs within the heterogeneous pool may casually be involved.

3.3 Results

3.3.1 Characterisation of extracellular vesicle (EV) sub-populations

EV sub-populations were isolated as described in section 2.2.2. As illustrated in Fig. 3.1 (A), the size and concentration of EVs in each pellet suspension were determined by nanoparticle tracking analysis (NTA). The 100K and 200K vesicles, termed, sEVs had a mean EV size of 125 nm ± 34 nm and 88 nm ± 14 nm, respectively, with 200K EVs having a significantly smaller size compared to the 100K EVs (*p=0.047*). The vesicles in the 10K pellet suspension termed mEVs, had an average EV size of 170 nm ± 72 nm. These were significantly bigger compared to 200K EVs (*p=0.005*). Finally, the 2K pellet, expected to be representative of lEVs had an average size of 134 nm ± 34 nm (Fig. 3.1 (A)).

NTA analysis also measured the concentration of EVs in each pellet suspension. Overall, the Hs578Ts(i)$_8$ cell line variant released a higher quantity of sEVs compared to mEVs and lEVs, with the 100K pellet containing a significantly higher concentration of vesicles compared to the 2K (*p=0.009*) and 10K (*p=0.011*) pellets (Fig. 3.1 (B)). The 200K pellet also had a significantly higher concentration of EVs compared to the 2K (*p=0.008*) and 10K (*p=0.009*) pellets (Fig. 3.1 (B)).

Protein content, an albeit somewhat controversial surrogate marker for EVs, was measured. The 200K pellet had significantly higher concentration of protein compared to the 2K (*p=0.011*), 10K (*p=0.002*) an the 100K (*p=0.010*) pellets (Fig. 3.1 (C)).

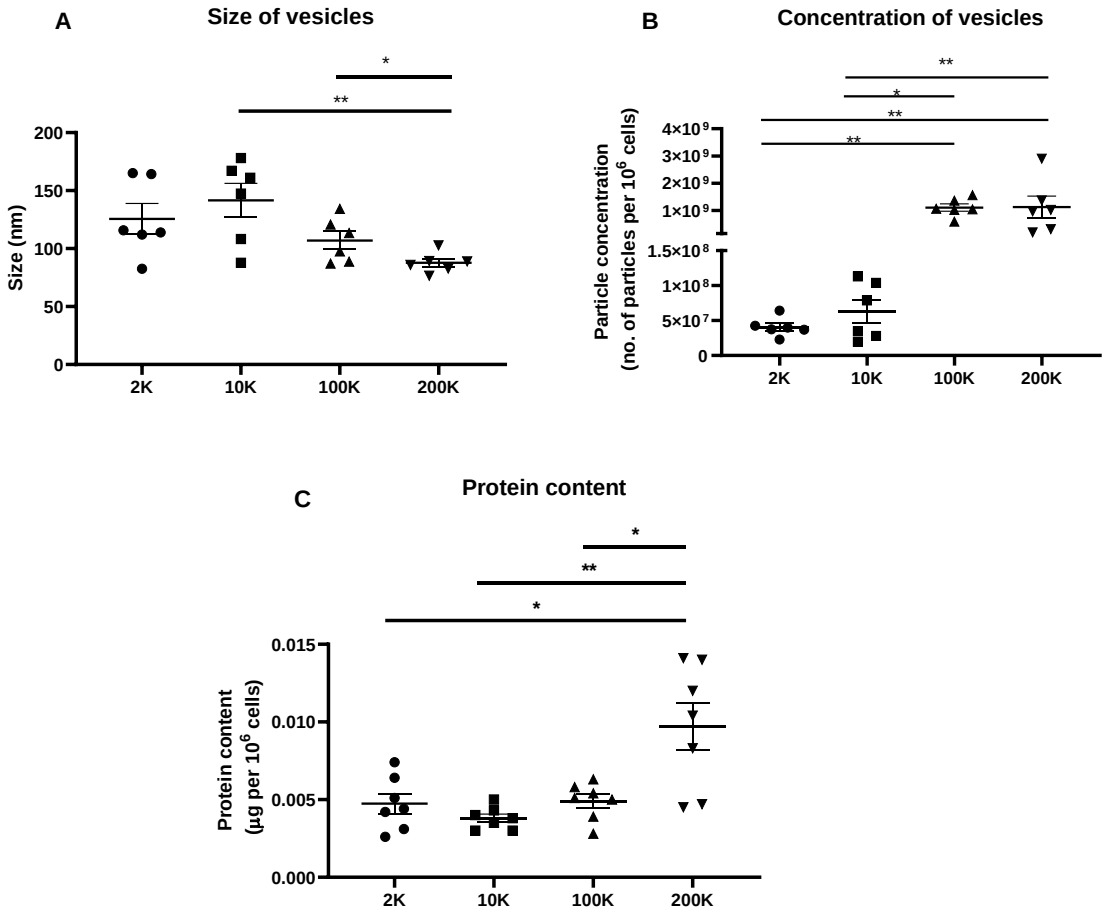

Figure 3.1: Nanoparticle tracking analysis and BCA on EV sub-populations

NTA analysis determined the (A) diameter (nm) and (B) concentration (vesicles released per 10^6 cells) of the isolated vesicles in each pellet suspension. BCA assay determined the (C) protein content (µg per 10^6 cells) of each sub-population. Graphs presented as mean ± SEM and represents (A) *n=6* (B) *n=6* and (C) *n=7* biological repeats. Note biological repeats here means EV isolation. One-way ANOVA was used as statistical test. *P<0.05, **P<0.01.

Immunoblot analysis was performed on the four EV sub-populations. GRP94 and Actinin-4, markers of mEVs and lEVs, according to MISEV2018 [187], were detected in the 2K and 10K pellets; with actinin-4 significantly higher in the 2K pellet compared to the 10K pellet (*p=0.005*) (Fig 3.2 (A and B)). TSG101 and Syntenin, markers associated with sEVs, were mostly contained in the 100K and 200K pellets (Fig. 3.2 (C and D)). TSG101 was significantly higher in the 200K pellet compared to the 2K (*p=0.042*) and 10K pellets (*p=0.010*). Syntenin was at significantly higher amounts in the 100K (*p=0.0003*) and 200K pellet (*p=0.0002*) compared to the 10K. CD81, a tetraspanin was highest in the 100K pellet, with a significantly higher amount compared to the 10K (*p=0.0007*) and 200K pellets (*p=0.0005*) (Fig 3.2 (E)). A representative immunoblot is also shown (Fig. 3.2 (F)).

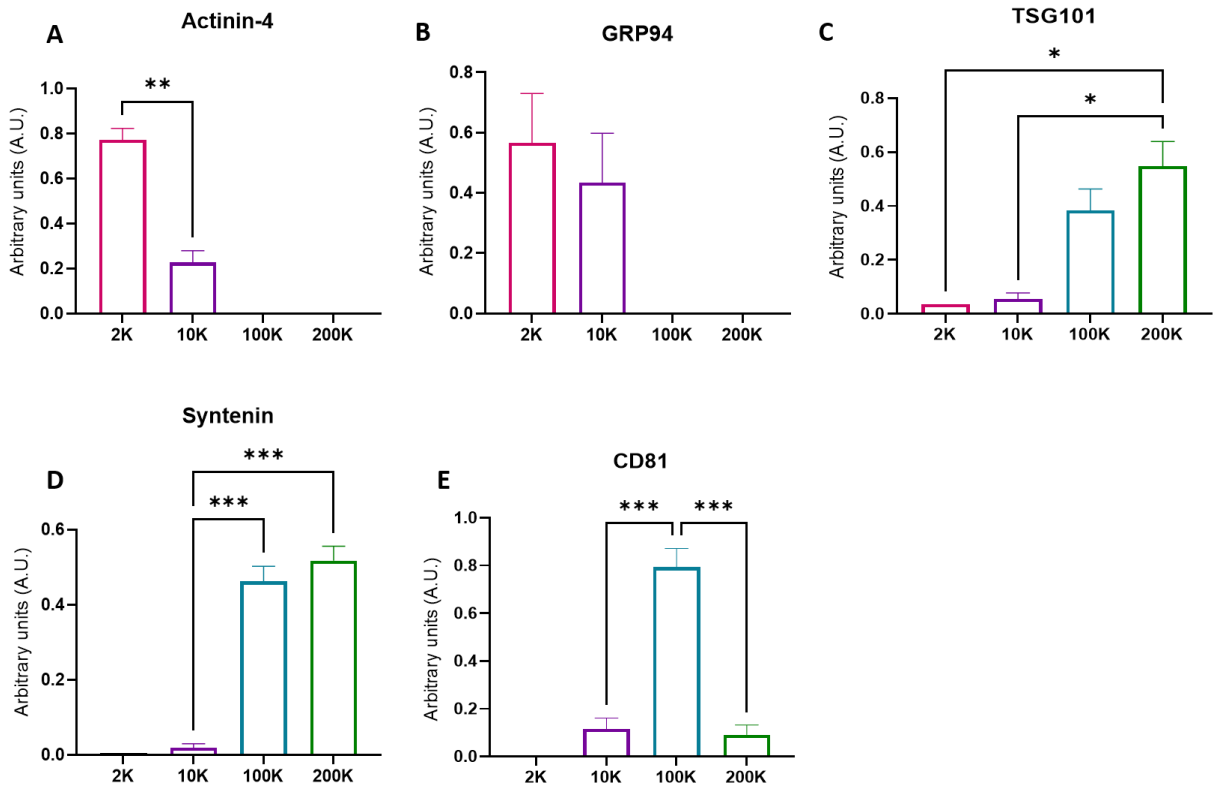

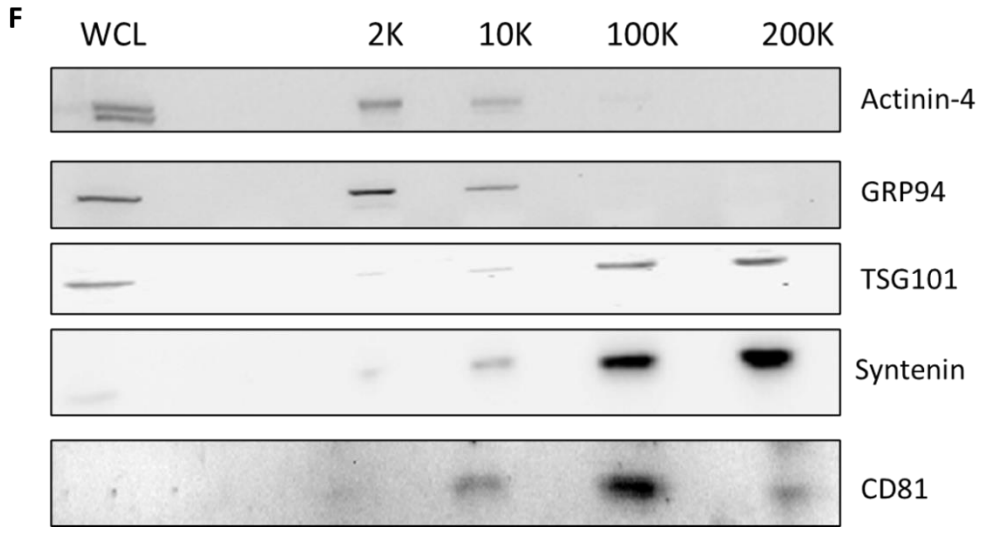

Figure 3.2: Immunoblot analysis of protein markers in isolated EV sub-populations

Densitometry analysis of EV sub-population protein markers. EV markers detected include (A) actinin-4, (B) syntenin, (C) GRP94, (D) TSG101 and (E) CD81. Arbitrary units (AU) were calculated using imageJ by measuring the signal intensity of each protein band. AU of individual EV markers were calculated by signal intensity (SI) of EV marker/Total sum of SI (2k+10K+100K+200K). (F) Representative immunoblot is shown. Graphs presented as mean ± SEM. One-way ANOVA was used as statistical test. *P<0.05, **P<0.01, ***P<0.001.

To further confirm the successful isolation of EV sub-populations, transmission electron microscopy (TEM) analysis was performed, with representative images shown in (Fig 3.3).

In agreement with NTA results shown in Fig. 3.1 (B), the 2K pellet had a small number of EVs. The 10K pellet contained a mixed population of vesicles in terms of size, containing both small and medium vesicles, conflicting with the average size of 170 nm, obtained by NTA analysis. The 100K had a homogeneous population of EVs, with a rounded shape and size of approximately 100 nm. The 200K pellet also contained a homogeneous population of vesicles with the smallest diameter of ≤100 nm.

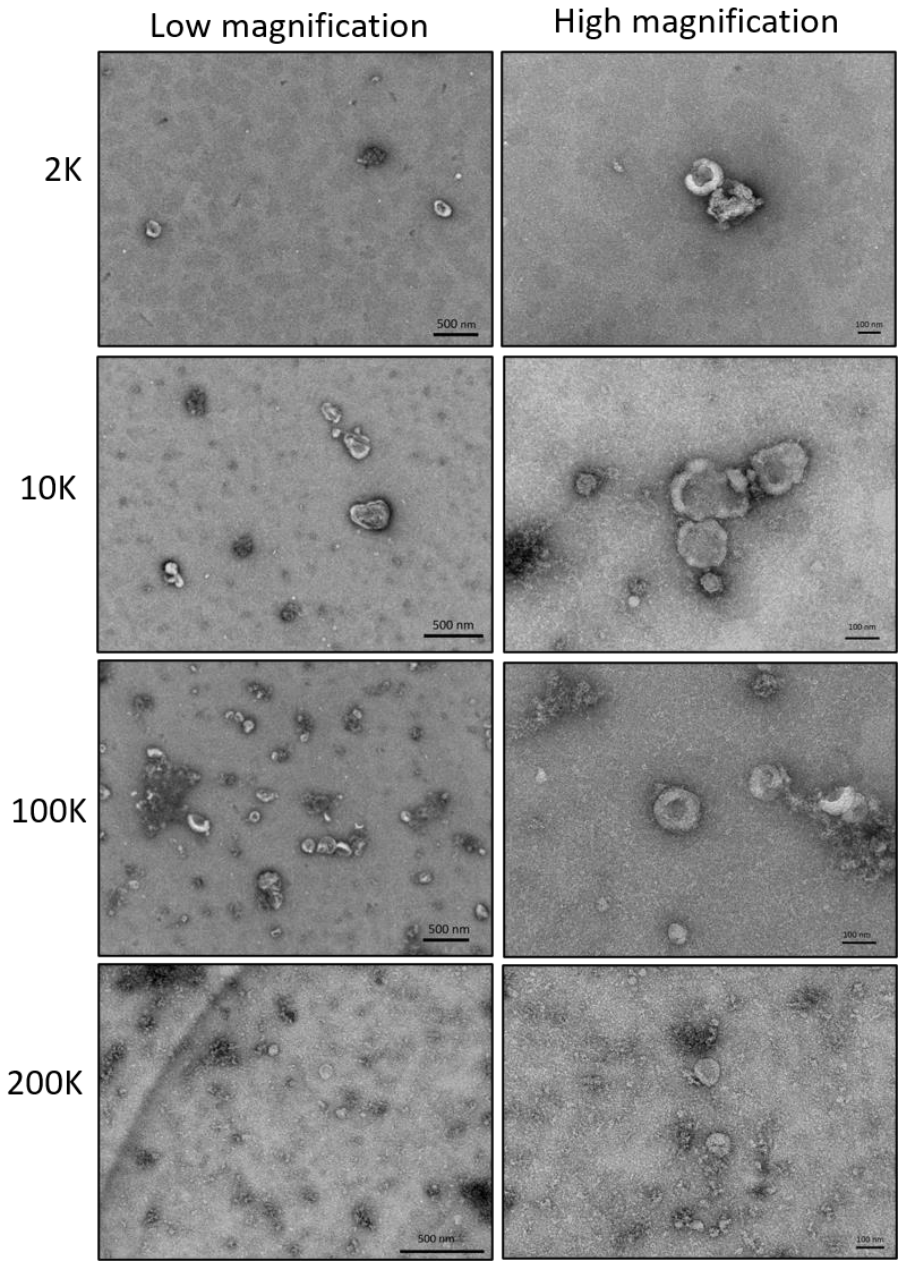

Figure 3.3: TEM analysis of EV sub-populations

TEM images of the EV sub-populations. A low magnification (scale bar of 500 nm) and a high magnification (scale bar of 100 nm) of representative EVs were taken for each EV sub-population.

3.3.2 Effects of treatment of Hs578T cell line variant with Hs578Ts(i)$_8$-derived EV sub-populations

EV sub-populations isolated from conditioned medium of the more aggressive Hs578Ts(i)$_8$ cell line variant were investigated to see if they transmit Hs578Ts(i)$_8$'s more aggressive phenotype to the more docile Hs578T cell line variant. The Hs578T cells were also treated with the heterogeneous EV population of EVs (i.e. all sub-populations isolated together), as in the original study [183] on which this work was based, and so acting as "comparator" against which to evaluate the influences of the four individual sub-populations. The effect of Hs578Ts(i)$_8$-derived heterogeneous EV population and the EV sub-populations on Hs578T cell proliferation, migration, invasion and *anoikis* resistance was investigated (see section 2.6.1 for assay setups).

Hs578Ts(i)$_8$ EV sub-populations affected the proliferation of the Hs578T cells. O'Brien *et al.* [183] demonstrated that the heterogenous pool of EVs released by Hs578Ts(i)$_8$ cells, increased the proliferation of recipient breast cancer cells, SKBR3, MDA-MB-231 and HCC1954. Although it was shown in Fig. 3.1 (C), protein is not a good surrogate marker for measuring EV quantity, to keep experimental setup somewhat consistent with the previous study, Hs578T cells were treated with EVs based on protein amount.

Increased proliferation was evident following treatment with the 2K and 10K sub-populations (Fig. 3.4 (A-B)). The 2K sub-population significantly increased proliferation of the Hs578T cells compared to the growth rate of untreated cells (Fig. 3.4 (A)). This was evident after the addition of 0.5 µg (*p=0.001*), 1 µg (*p<0.0001*) and 2 µg (*p<0.0001*) of the 2K vesicles. The 10K sub-population caused a subtle increase in Hs578T proliferation compared to the control, however, no significance was reached (Fig. 3.4 (B)). Treatment with the 100K sub-population had no effect on Hs578T cell proliferation (Fig. 3.4 (C)). The 200K sub-population increased proliferation with 0.5 µg and 1 µg but with 2 µg, decreased proliferation compared to the control (Fig. 3.4 (D)). Following treatment with 1 µg of the heterogeneous EV population of EVs, an inhibition of Hs578T proliferation is evident compared to the control (Fig. 3.4 (E)). When all EV sub-populations are compared together, only the 2K sub-population caused significant increased proliferation compared to the untreated control (*p=0.018*) (Fig. 3.4 (E)).

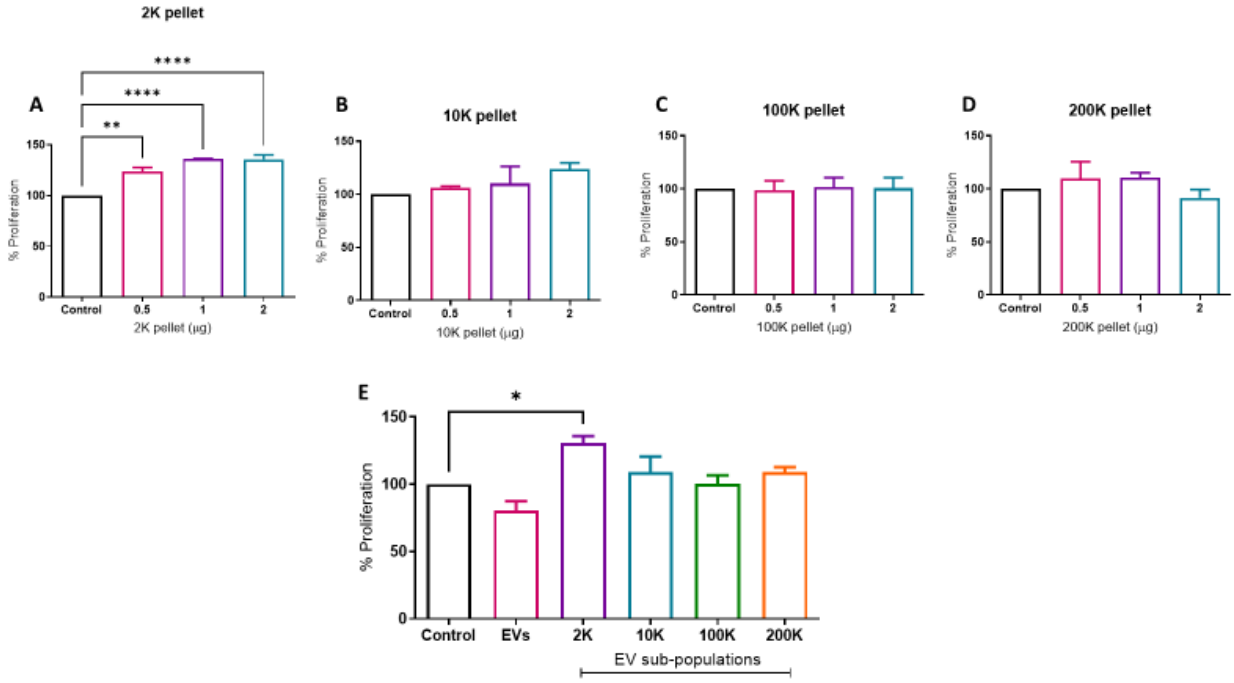

Figure 3.4: Effect of Hs578Ts(i)$_8$ EV sub-populations on Hs578T cell proliferation

Hs578T cells were treated with the heterogeneous EV population or EV sub-populations isolated from the Hs578Ts(i)$_8$ cell line variant including the (A) 2K, (B) 10K, (C) 100K and (D) 200K sub-populations. (E) Compares the effect of the heterogeneous EV population and the four sub-populations after the addition of 1 µg of each. Control is Hs578T cells that were not treated with any EV. All graphs represent *n=4* biological repeats as mean ± SEM. One-way ANOVA was used as statistical test. *P<0.05 **P<0.01, ****P<0.0001.

The heterogenous EV study by our group had previously shown that Hs578Ts(i)$_8$ EVs increased migration of SKBR3, MDA-MB-231 and HCC1954 cells [183].

Here all EV sub-populations isolated from the Hs578Ts(i)$_8$ cell line variant's conditioned medium significantly increased the migration of the Hs578T cells, after 24 hrs treatment. A higher protein amount of EVs were used for migration assays because a higher number of cells are seeded for a migration assay when compared to proliferation assay. The 2K sub-population significantly increased migration compared to untreated control cells (Fig. 3.5 (A)). This was evident at 2K vesicle quantities of 1 µg (*p=0.032*), 2 µg (*P=0.009*) and 4 µg (*p=0.007*). The 10K sub-population significantly increased Hs578T migration (Fig. 3.5 (B)). This was evident at the quantities of 2 µg (*p=0.006*) and 4 µg (*p=0.001*). The 100K sub-population also significantly increased migration at all quantities, including 1 µg (*p=0.004*), 2 µg (*p=0.002*) and 4 µg (*p=0.0002*) (Fig. 3.5 (C)). In addition, the 200K sub-population significantly increased migration at 1 µg (*p=0.0004*), 2 µg ($p<0.0001$) and 4 µg (*p<0*.0001) (Fig. 3.5 (D)).

The heterogeneous EV population exerted a greater increase in Hs578T migration. However, when compared to the effects of 2 µg of the four EV sub-populations, it was evident that no one single sub-population caused more migration in the Hs578T cells compared with the others. 2 µg of the heterogeneous EV population significantly increased Hs578T migration (*p<0.0001*) compared to the untreated control (Fig. 3.5 (E)). It was also not more significant than any sub-population. Using phase contrast microscopy, the relative increase in Hs578T migration can be seen (Fig. 3.6).

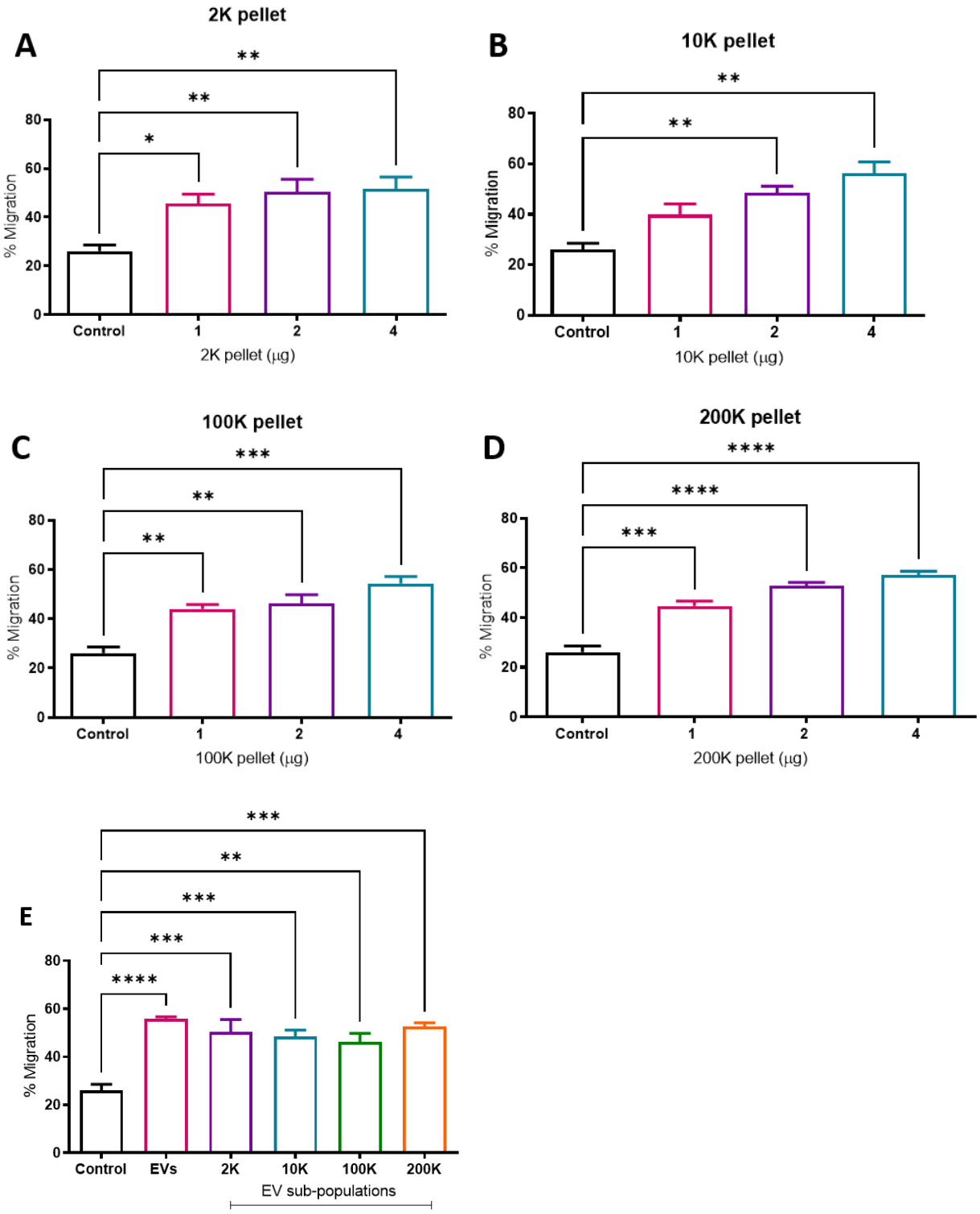

Figure 3.5: Effect of the Hs578Ts(i)$_8$ EV sub-populations on Hs578T cell migration

Hs578T cells were treated with the heterogeneous EV population or EV sub-populations; isolated from the Hs578Ts(i)$_8$ cell line variant conditioned medium, including the (A) 2K, (B) 10K, (C) 100K and (D) 200K sub-populations. (E) Compared the effect of the heterogeneous EV population and the sub-populations at a quantity of 2 µg. All graphs represent n=3 biological repeats as mean ± SEM. One-way ANOVA was used as statistical test. *P<0.05, **P<0.01, ***P<0.001, ****P<0.0001.

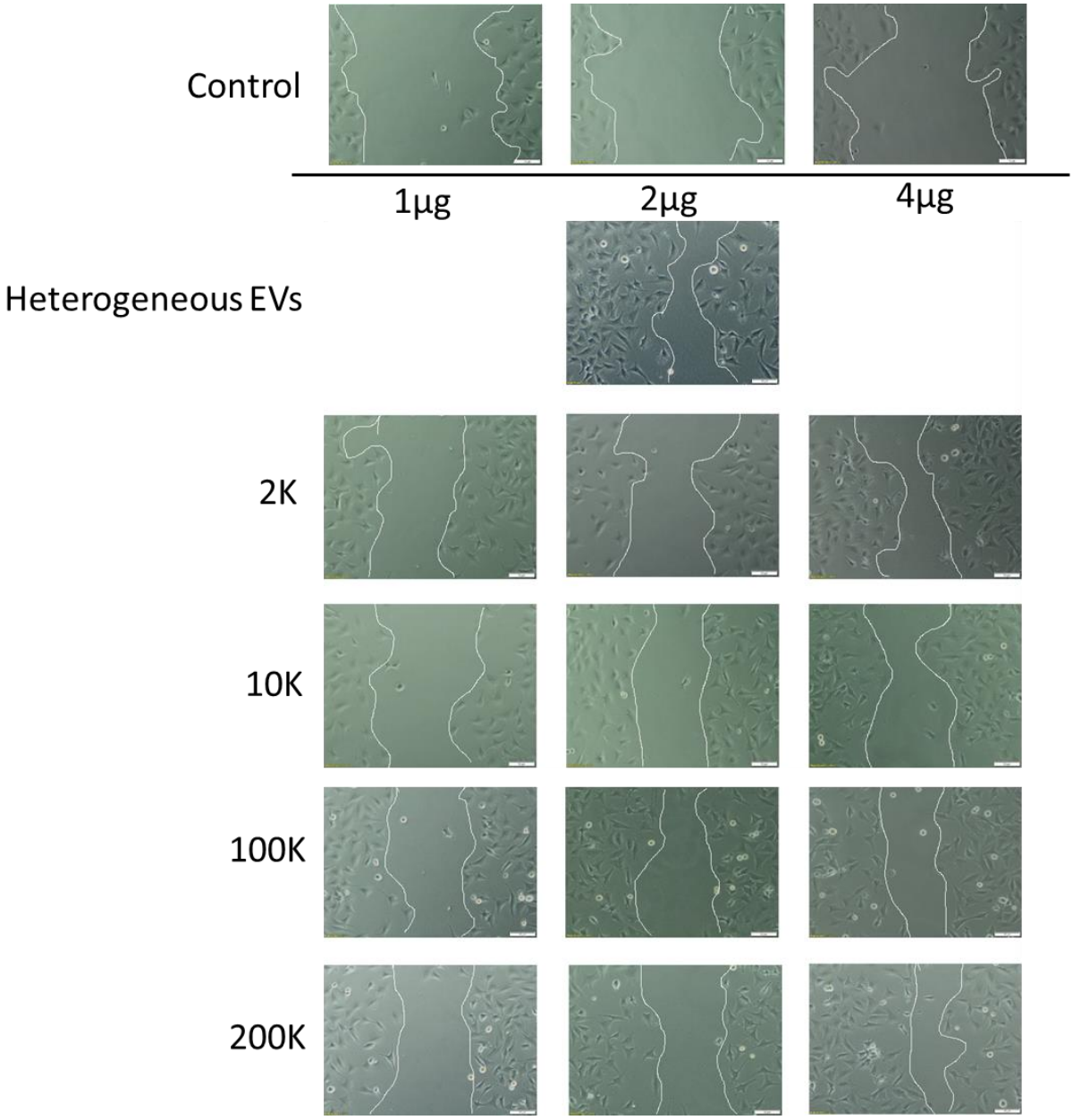

Figure 3.6: Representative migration assay images of Hs578T cells

Representative migration assay images of Hs578T cell line variant following 24hrs treatment with the Hs578Ts(i)$_8$-derived heterogeneous EV population or increasing amounts of EV sub-populations. Control is Hs578T cells not treated with any EVs. Images were taken at a 100X magnification. Scale bar is 10 µm.

O'Brien *et al.* [183] demonstrated that the heterogenous EVs isolated from Hs578Ts(i)$_8$ conditioned medium increased the invasion of SKBR3, MDA-MB-231 and HCC1954 cells.

Here, EV sub-populations had a limited, insignificant effect on Hs578T cell invasion. The 2K sub-population increased invasion at 1 µg and 2 µg, although not significant (Fig. 3.7 (A)). The 10K sub-population inhibited Hs578T invasion with a quantity of 1 µg, but increased Hs578T invasion when treated with of 2 µg and 4 µg (Fig. 3.7 (B)). The 100K sub-population increased Hs578T invasion at the quantities of 1 µg and 2 µg, although not significantly. However, 4 µg of the 100K sub-population resulted in an inhibition of invasion compared to the untreated control (Fig. 3.7 (C)). The 200K sub-population showed the greatest ability to increase Hs578T cell invasion with all three amounts increasing invasion compared to the untreated control (Fig. 3.7 (D)). However, no significance was achieved.

The increase in Hs578T invasion when treated with 2 µg of the heterogeneous EV population was similar to the effect of each single sub-population alone at a concentration of 2 µg (with the exception of the 100K sub-population) (Fig. 3.7 (E)). The relative invasion of the crystal violet stained Hs578T cells was visualised with a phase contrast microscope (Fig. 3.8).

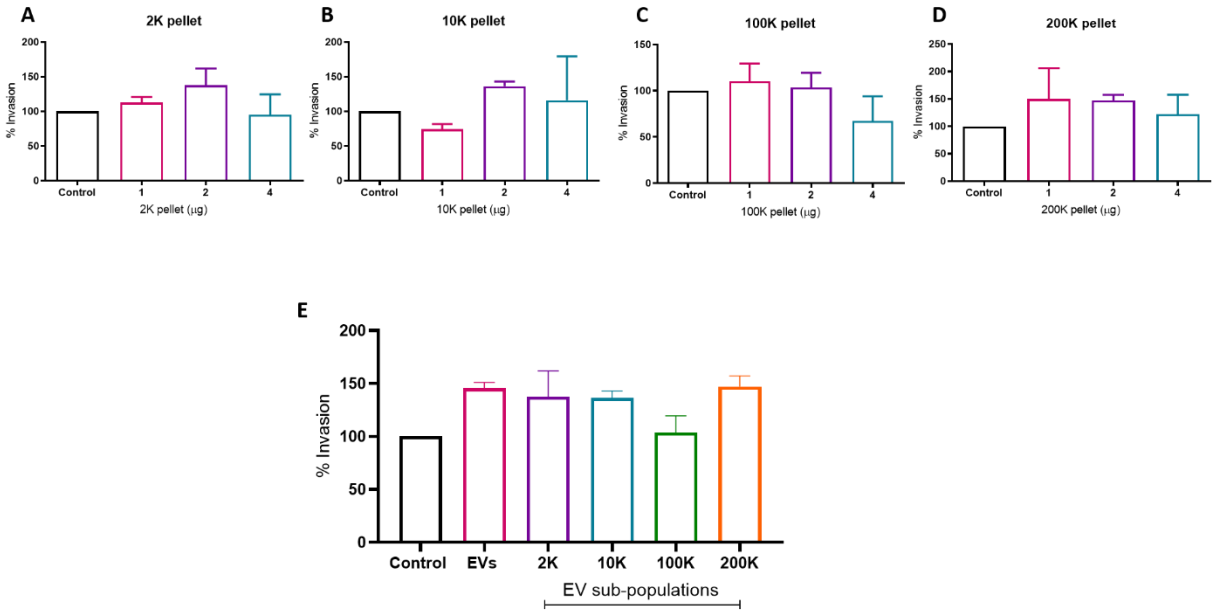

Figure 3.7: Effect of Hs578Ts(i)$_8$ EV sub-populations on Hs578T cell invasion

Hs578T cells were treated with the heterogeneous EV population or EV sub-populations isolated from the Hs578Ts(i)$_8$ cell line variant including the (A) 2K, (B) 10K, (C) 100K and (D) 200K sub-populations. (E) Compared the effect of the heterogeneous EV population and the sub-populations at an amount of 2 µg. All graphs represent n=3 biological repeats as mean ± SEM.

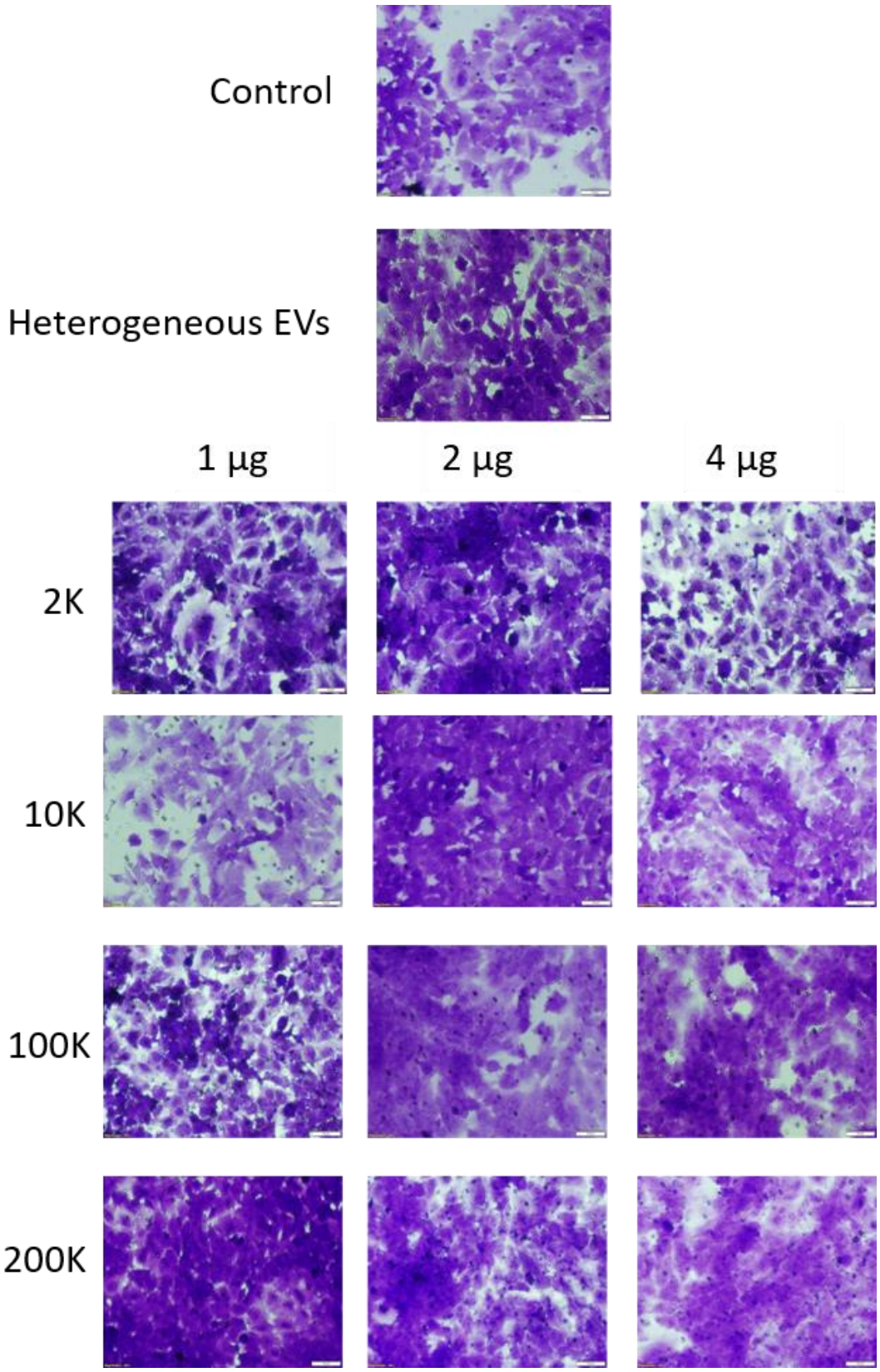

Figure 3.8: Representative invasion assay images of Hs578T cells

Representative invasion images of Hs578T cells treated with 2 µg of the heterogeneous EV population or increasing amounts of EV sub-populations for 72 hrs. Control is untreated Hs578T cells. Images were taken at a 100X magnification. Scale bar is 10 µm.

Previously, our group showed that the heterogenous EVs from Hs578Ts(i)$_8$ conditioned medium, conferred a greater *anoikis* sensitivity to SKBR3, MDA-MB-231 and HCC1954 cells [183].

EV sub-populations separated from the Hs578Ts(i)$_8$ cell line variant, conditioned medium had a limited, insignificant effect on *anoikis* sensitivity in the Hs578T cells when compared to the untreated control (Fig. 3.9 (A-D)).

Furthermore, treatment with 5 µg of the heterogeneous EV population demonstrated that there are similar levels of *anoikis* between the different sub-populations and compared to the heterogeneous EV (Fig 3.9 (E)).

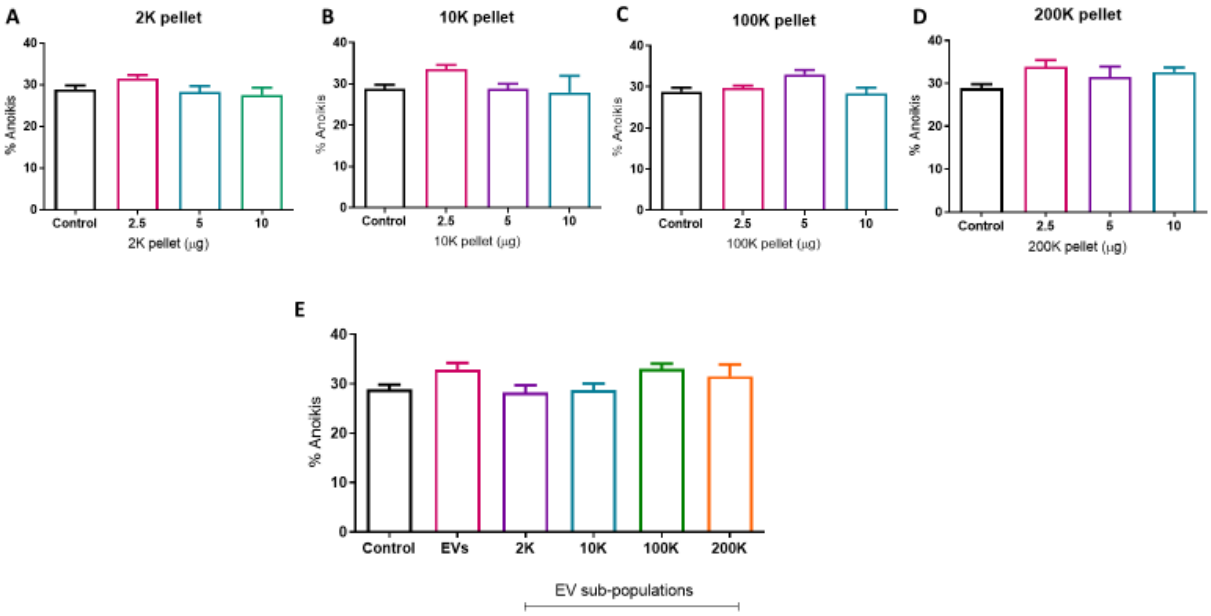

Figure 3.9: Effect of Hs578Ts(i)$_8$ EV sub-populations on Hs578T *anoikis*

Hs578T cells were treated with the heterogeneous EV population or EV sub-populations; isolated from the Hs578Ts(i)$_8$ cell line variant, conditioned medium including the (A) 2K, (B) 10K, (C) 100K and (D) 200K sub-populations. (E) Compared the effect of the heterogeneous EV population and the sub-populations at an amount of 5 µg. All graphs represent n=3 biological repeats as mean ± SEM.

3.4 Discussion

3.4.1 Separation of EV sub-populations

The triple-negative breast cancer cell line variant, Hs578Ts(i)$_{8,}$ releases a heterogeneous population of vesicles. Four EV sub-populations were separated from its conditioned medium and compared on their sizes, quantities, and characteristic protein markers.

It was expected that the 2K pellet would represent the lEV sub-population, however, although it displays lEV protein markers, it had particles of 134 ± 34 nm. TEM analysis corroborated the NTA results, demonstrating that vesicles in the 2K pellet suspension were smaller in size than expected and there was no evidence of any larger vesicles. Very few studies have analysed vesicles that sediment at 2,000g. Kowal *et al.* [82] demonstrated that the 2K pellet contained vesicles abundant with GRP94 and actinin-4. The majority of these vesicles had a diameter of >200 nm and were identified as not being cell fragments released by dying or necrotic cells. Vesicles that were obtained here in the 2K pellet from the Hs578Ts(i)$_8$ cells also contained GRP94 and actinin-4 but had a much smaller diameter suggesting that either low-speed centrifugation may pellet out cell debris from the cancer cells or that the difference in sizes are due to the cell of origin, as Kowal *et al.* investigated sub-populations of vesicles released by dendritic cells. Other studies have included a centrifugation step of 2,000 g as a "cleaning" step to remove cellular debris before the isolation of other vesicles from a wide range of cell types including astrocytes [188], chronic lymphocytic leukaemia cells [189] glioblastoma cells and cerebrospinal fluid [190].

Of all the sub-population analysed, the 10K pellet showed the highest level of heterogeneity, in terms of size; with a size range, from mEVs to sEVs sizes based on NTA, giving an average size slightly larger than the sEVs isolated in the 100K pellet. The range in vesicle size was demonstrated by TEM analysis, with the presence of both small and medium vesicles. Muralidharan-Chai *et al.* [41] reported seeing similar heterogeneity in vesicles isolated by centrifugation at 10,000g with diameters ranging from 300 nm to 900 nm. Similar to our results and using the same isolation protocol, Kowal *et al.* [82] also showed that the majority of the vesicles isolated at 10,000 g and 100,000 g had a size range between 150 nm to 50 nm. The 10,000 g pellet had a higher number of larger vesicles compared to the vesicles isolated at 100,000 g and therefore, had an average size larger than the 100,000 g pellet vesicles. Interestingly, the 10K pellet vesicles also contained markers of sEVs commonly called exosomes. This demonstrates that exosomes may co-sediment with mEVs at 10,000g. This has been reported in EVs isolated from melanoma cells [191]. Overall, the vesicle size in the 10K pellet is relatively small compared to vesicles isolated by others at the same speed. For example, Vagner *et al*. [192] isolated vesicles with a diameter of 1-5.5 µm from prostate cancer cells, PC3 and prostate plasma samples. We

have not identified any studies relating to TNBC mEVs, that have been isolated at 10,000g to be able to compare with. This is also the first study reporting the isolation of EV sub-populations from the Hs578Ts(i)$_8$ cells.

The 100K pellet represents sEVs. The Hs578Ts(i)$_8$ cells release a larger amount of these vesicles than any other of the other sub-populations as determined by the NTA when comparing to the other sub-population's particle concentrations. These sEVs displayed some of the most common exosomal markers, which are involved in their biogenesis and do not contain the markers of lEVs. With TEM analysis and an average size of 125 nm measured by NTA they are similar to exosomes isolated by other researchers [91, 189].

The 200K sub-population is an additional EV sub-population that has not been as extensively characterised when compared to other populations, with 200,000g not commonly reported as a means for EV isolation. This population of vesicles represent the smallest in diameter, as shown by NTA and TEM analysis, released from the Hs578Ts(i)$_8$ cells' but they contain the highest amount of protein and contain exosomal markers. This sub-population of vesicles may represent the newly termed, large exosomes (EXO-L) [193]. Zhang *et al.* concluded that exosomes can be split into two sub-populations, called large-exosomes (EXO-L) and small-exosomes (EXO-S). The isolated EXO-L had a mean diameter of 90-120 nm and contained Alix, CD81 and TSG101 protein markers. Vesicles of the 200K pellet from the Hs578Ts(i)$_8$ cells have an average size of 88 ± 14 nm and display both CD81 and TSG101 exosome markers, similar to the EXO-L described.

It is clear that the Hs578Ts(i)$_8$ cell line variant releases a variety of vesicles in terms of their size, protein content and their quantity. A range of EV sub-populations have been successfully isolated from the Hs578Ts(i)$_8$ cells using differential ultracentrifugation.

3.4.2 Effects of treatment of Hs578T cell line variant with Hs578Ts(i)$_8$-derived EV sub-populations

EVs are known to be major players in cell-to-cell communication, in a multitude of processes, including acting as information carriers for cancer cells, propagating the oncogenesis to recipient cell. An important process activated in cancer cells, in order to promote tumour progression, is their increase in proliferation and migration in order to invade through the extracellular matrix to gain access to the bloodstream and eventually metastasise to secondary locations in the body.

Our first investigation involved analysing the effect of Hs578Ts(i)$_8$-derived EV sub-populations on Hs578T proliferation. The 2K and 10K sub-populations increased Hs578T proliferation compared to the proliferation of untreated control cells. The 100K and 200K sub-populations had a limited effect, with the 200K sub-population causing a decrease in proliferation compared to the proliferation of the untreated control cells. Unexpectedly, when Hs578T cells were treated with the heterogeneous EV population an inhibition in proliferation occurred when compared to the growth rate of the untreated control cells. Previously, our group showed that the Hs578Ts(i)$_8$ EVs significantly increased Hs578T proliferation [183]. This conflicting result may be due to different experimental controls used, with Hs578T EVs acting as a control in the original experiment compared to untreated Hs578T cells in my experiments.

In the literature, there is a trend reported that cancer cell derived EVs cause an increased proliferative effect in their target cells by means of bioactive cargo transfer. An interesting study demonstrated that microvesicles (or mEVs) isolated from the human leukaemia cell line, K562, which is positive for BCR-ABL and carries the t(9;22) translocation, increased the proliferation of mesenchymal stem cells (MSCs). It was shown that the MVs transferred the BCR-ABL mRNA into the recipient MSCs, which may cause the increase in proliferation in correlation to MV dosage (i.e. a sequential dilution of MVs was added to the MSC medium, from undiluted MVs and MVs diluted 1:2 to 1:10 dilution) [194]. MVs derived from colorectal cancer cells contained mRNA transcribing cell cycle-related genes such as CCNA2, NEK2, CDK8 and PBK. Upon endothelial cell treatment, the MVs upregulated the cell cycle activity in the cells and cell proliferation [195].

We next compared the different EV sub-populations' abilities to either decrease or increase migration of the Hs578T cell line when compared to the heterogeneous EV population. Overall, every sub-population significantly increased the migratory potential of the parental cells. However, treatment with heterogeneous EV populations had a similar effect compared to each sub-population alone, with the exception of the 200K sub-population, which increased the migration of the Hs578T cells to the same extent as the heterogeneous population (when using 2 µg of each). This may be an indication that all EVs act together to play a role in increasing cell migration and have a more potent effect compared to each EV sub-population alone. Although not investigating individual sub-populations, others have found the EVs released by cancer cells can increase the migration of their recipient cells such as an invasive bladder cancer [196], lung cancer [197] and hepatocellular carcinoma (HCC) [198]. Harris *et al.* [199] demonstrated that EVs from low (i.e. MCF-7), moderate (i.e. Rab27b/MCF-7, MCF-7 cells that overexpress Rab27b) and highly metastatic (i.e. MDA-MB-231) breast cancer cell lines proportionally increased the migration of recipient cells, with the highly metastatic cell-derived EVs

having the greatest effect compared to the other two sets of EVs isolated from lower metastatic potential.

We subsequently evaluated the ability of the EV sub-populations compared to the heterogeneous EV population to influence the invasiveness of the Hs578T cells. Overall, the sub-populations caused an increase Hs578T invasion were treated with 2 µg of each. However, when Hs578T cells were treated with the higher concentration of EV sub-populations, (i.e. 4 µg) there was a decrease in cell invasion an indication that different bioactive cargoes are packaged and released by the Hs578Ts(i)$_8$ cells *via* the different EV sub-populations, causing different effects on the recipient cells depending on the EV sub-population. It may also be an indication that non-EV inhibitory proteins may be co-sedimented with the EVs. When compared to the heterogeneous EV population (i.e. 2 µg), no individual sub-population is responsible for the invasion seen.

Other studies have reported the effect of EVs in changing the invasiveness of their secondary cells by the transmission of a particular cargo or set of cargoes. In particular, miRNAs have been proposed as regulators of cancer cell invasion and transported *via* EVs. MiR-93 carried by exosomes increased the invasion of HCC cells, SKHEP1 and HUH7, by targeting CDKN1A, TIMP2, TP53INP1. In addition, HCC patients (*n=85*) had a higher level of serum exosomal miR-93 [200]. Exosomes containing miR-1246 and miR-342-3p isolated from a highly metastatic oral cancer cell line, HOC313, were reported to increase the invasion of its less metastatic, parental cell line [201]. In the context of breast cancer, exosomes from the metastatic TNBC cell line, MDA-MB-231 increased the invasion of the non-tumorigenic cells, HMLE, *via* miR-10b and the downregulation of one of its targets, HOXD10 [202]. In contrast, our group established that miR-134-transfected Hs578Ts(i)$_8$ cells, released exosomes that were enriched in miR-134 and upon treatment of non-transfected Hs578Ts(i)$_8$ cells, they observed a decrease in migration and invasion which may be due to the downregulation of STATB and Hsp90 [87].

Finally, the effect of Hs578Ts(i)$_8$ EV sub-populations on *anoikis* of the Hs578T cells was evaluated in comparison to the effect of the heterogeneous EV population, as our group previously reported that the Hs578Ts(i)$_8$ are more sensitive to *anoikis* compared to Hs578T cells [183]. *Anoikis*, is a form of cell death that occurs when the cell detaches from the extracellular matrix. It is a barrier that cancer cells overcome in order to metastasise to order parts of the body [203]. We found that the Hs578Ts(i)$_8$-derived EVs sub-populations had a limited effect on *anoikis* of the parental cell line compared to untreated Hs578T cells. However, treatment of the Hs578T cells with the heterogeneous EV population caused a bigger increase in *anoikis* compared to the untreated control cells. Out of all EV sub-populations, only the 100K and 200K sub-population increased the *anoikis* to the same extent as the heterogeneous population with no single sub-population exhibiting a greater effect. Interestingly,

the 2K and 10K sub-populations decreased *anoikis* of the Hs578T cells compared to the heterogeneous EV population, therefore, increasing *anoikis* resistance. This may be an indication that within the heterogeneous EV population the 100K and 200K sub-populations have a more potent effect compared to the effect of the 2K and 10K sub-populations. Other groups have reported that EVs can reduce *anoikis* in cancer cells, thereby increasing their survival in anchorage-independent condition, as seen in non-small cell lung cancer (NSCLC) [204]. Urciuoli *et al.* [205] also reported increased survival when murine fibroblast NIH3T3 cells were treated with EVs isolated from osteosarcoma cells. A study published by our group in 2012, established that docetaxel-resistant prostate cancer cell lines, 22RV1RD and DU145RD showed a decrease in *anoikis* when compared to their drug-sensitive parental cell lines [206]. Although, they did not investigate whether this decrease in *anoikis* could be transferred *via* the resistant cell-derived exosomes, the researchers demonstrated that exosomes from DU145RD cells could transfer docetaxel resistance to drug-sensitive DU145, 22RV1 and LNCap cells. Oushy *et al.* [207] used a soft agar assay to investigate what effects EVs derived from glioblastoma cells had on the colonisation ability of normal human astrocytes. Although this study used agar instead pf poly-HEMA, they demonstrated a substantial increase in astrocyte growth in soft agar when glioblastoma EVs were added compared to untreated astrocytes and reduced their dependence on matrix anchorage for tumour growth.

Recently, other researchers have elucidated roles for EV sub-populations, including the separation of large and small EVs from metastatic melanoma tissue, a protocol that allows for separation of EV sub-populations that are directly from patient tumours (*n=27*) and reflect a true cancer microenvironment [208]. High density (HD) and low density (LD) exosomes were isolated by loading the sEV pellet (i.e. after 110,000g) on bottom of sucrose density gradient. These two sub-populations differed from larger EVs isolated by 10,000g ultracentrifugation and also from each other when analysed by mass spectrometry for proteins and investigating their RNA profiles by high resolution electrophoresis [191]. Sub-populations have also been distinguished based on their DNA cargo [209]. In this separate study, HD and LD sEVs isolated by density gradient were shown to have separate DNA profiles. LD sEVs, with small amounts of DNA, were thought to represent the classic exosome formed through intracellular pathway; HD sEVs, enriched in DNA, may be EVs that were formed and released *via* other cellular components such as cell membrane. Two differing sub-populations of EVs were also separated using two techniques of differential ultracentrifugation and immune-affinity isolation for the surface marker, intercellular adhesion molecule-1 (ICAM-1) [210]. Larger EVs positive for ICAM-1 induced more inflammation in recipient endothelial cells, whereas the smaller EVs positive for ICAM-1 were able to recruit monocytes. When ICAM-1 was depleted by removing the positive EVs, both functions were lost.

3.5 Conclusion

The results in this study indicates that the heterogeneous EV population released from the Hs578Ts(i)$_8$ cell line variant transfers their aggressive phenotype to Hs578T cells in terms of cell migration. Hs578T cell invasion and *anoikis* was also affected but not significantly. Following the separation of the heterogeneous EV population into four individual sub-populations, it is evident that no single sub-population is responsible for the effects observed. It is evident that all EV sub-populations are responsible, acting together, to transfer these phenotypic effects. Therefore, it would seem that a strategy to prevent tumour progression *via* EV signalling may need to consider blocking the release of all EVs from cancer cells.

Chapter 4: Investigation of the use of proposed inhibitors of EV release to block EV release from triple-negative breast cancer cells

4 Abstract:

As we established that no single sub-population of Hs578Ts(i)$_8$ EVs was responsible for the transfer of aggressive effects to the parental Hs578T cell line variant, we then wanted to determine if we could inhibit to block- or at least reduce- such undesirable cell-to-cell communication by EVs. To investigate this, we evaluated the proposed inhibitors of EV release including calpeptin, Y27632, manumycin A and GW4869, some in combination. These inhibitors have been used in other studies. However, have not been investigated all together and thoroughly investigated as per MISEV2018 guidelines. While other studies also induced EV release with treating with cell activators or apoptotic agents with the inhibitors, we investigated the constitutive inhibition of EVs from TNBC cells.

The EVs released following inhibitor treatment were characterised and their effects on recipient TNBC cell lines, Hs578T and BT549 were investigated. We found that EVs were substantially inhibited after treatment. The EV inhibitors significantly decreased the release EVs from Hs578Ts(i)$_8$ cells. Specifically, calpeptin (*p<0.0001*), Y27632 (*p<0.0001*), combo 1 (*p<0.0001*), manumycin A (*p=0.001*), GW4869 (*p<0.0001*) and combo 2 (*p<0.0001*) all significantly decreased EV release with GW4869 having the biggest effect, decreasing EV release by 98% compared to the untreated control cells. The effect of the EVs that were still released had a limited effect on recipient cell proliferation, however, BT549 migration was significantly reduced when cells were treated with the highest dose of EVs released following calpeptin (*p=0.036*), Y27632 (*p=0.007*), combo 1 (*p=0.005*), manumycin A (*p=0.005*), GW4869 (*p=0.005*) and combo 2 (*p=0.017*) treatment.

In conclusion, the proposed EV inhibitors decreased EV release while the EVs that were still released could not stimulate the cell migration of BT549 cells, demonstrating a change in the EV profile released from the Hs578Ts(i)$_8$ cells and a change in the transfer of phenotypic traits.

4.1 Introduction

Tumour-derived EVs have been reported to transfer their cargo to recipient cells, changing the profile and tumorigenic potential, increasing migration, invasion and metastasis of the cancer cells as well as their resistance to chemotherapy drugs. Cancer cells seem to use EVs as a way to transport selective cargoes to recipient cells. A proteomic analysis of three different breast cancer cells, MCF-7, MDA-MB-231 and T47D was performed and demonstrated that proteins are selectively packaged from cells into EVs (should be noted that EVs were isolated using 22,000g ultracentrifugation speed) which differed depending on the breast cancer subtype [211]. EVs can become the transmitter of resistance if the cancer cells become resistant to their treatment and can also interact with resident immune cells to develop metastatic niche. Our group was the first to demonstrate, that prostate cancer cells, DU145, that were resistance to docetaxel could transit this resistance to docetaxel-sensitive cell lines, DU145, 22RV1, and LNCap *via* their exosomes [206]. Keklikoglou *et al.* [212] demonstrated that small EVs (i.e. isolated by 134,000g ultracentrifugation) augmented lung metastasis in a paclitaxel-induced mammary tumour metastasis mouse model. They also showed that paclitaxel and docetaxel delivered systemically increased the metastatic capacity of EVs released from the 4T1 tumour *in vivo*. Paclitaxel treatment enriched annexin A6 in the released EVs, increasing the pro-metastatic abilities of the EVs in establishing lung metastases through monocyte expansion. Another study, documented that MDA-MB-231 EVs transfer adhesion proteins to recipient breast cancer cells, MDA-MB-231 and T47D, increasing the migration and invasion of those cells [213].

A strategy for dampening down these effects by inhibiting the release of EVs from cancer cells, thereby preventing the spread and transfer of their oncogenic secretory cargo, is needed. One reported strategy involved blocking EV surface CD9 and CD63 with antibodies, reducing metastasis in mice that harboured orthotopic MDA-MB-231-luc-D3H2LN tumours, through the uptake and removal of cancer EVs by macrophages [214]. There are also multiple inhibitors reported to have an effect on EV release. In this study four proposed inhibitors are investigated which are included in a review published by our group [94]. GW4869, (an inhibitor of neutral sphingomyelinases) and manumycin A, (an antibiotic that blocks ras farnesyltransferases) are proposed to inhibit small EV formation and their release. Calpeptin, (a calpain inhibitor) and Y27632, (known to prevent ROCK signalling by outcompeting ATP) are proposed to inhibit the release of medium sized EVs. The novelty of this study is by its comprehensive analysis of more than one inhibitor and their effects on EV release.

Other studies have investigated these inhibitors and their use as potential EV inhibitors; However, the majority of the studies do not full the "Minimal information for studies of EVs" (MISEV) guidelines which were updated in 2018 [187]. The MISEV guidelines provide information to researchers on the requirements needed to claim the involvement of EVs or sub-populations of EVs to a particular biological function. In these guidelines, it states that multiple methods of EV characterisation must be used and in particular for EV quantification, it gives various methods including protein and lipid concentration, particle number quantification and/or total RNA concentrations. After reviewing the EV characterisation methods employed by other studies, it came to our attention that full characterisation was almost never achieved as per MISEV2018 guidelines (see Table 4.1). For example, Matsumoto *et al.* [215] concluded that GW4869 inhibited the release of EVs by observing a decrease in protein concentration, which is not synonymous with EV numbers. Brassart *et al* [216], investigated the effects of elastin degradation products on cancer cell metastasis and shedding of EVs. The researchers demonstrated that the pre-treatment of fibrosarcoma, HT-1080 cells with Y27632 could inhibit blebbing. However, the only method used by the researchers to determine a decreased in blebbing was the counting of membrane blebs under a phase contrast optical microscope. There were no other methods used in combination to confirm their observation. A study investigating miR-21 in adipose derived stem cell (ADSCs) exosomes and the increase of HaCat cell (i.e. representative keratinocyte cell line isolated from adult skin) proliferation when these exosomes were added to HaCat cells, used GW4869 to inhibit exosome release from ADSCs [217]. However, there was no characterisation performed after the treatment with GW4869 as the authors assumed that GW4869 was inhibiting by pre-treating the ADSCs with GW4869 before co-culturing them with HaCat cells.

The concentration and incubation times of the inhibitors are an important consideration for these experiments. The inhibitors cannot be toxic to the cells being investigated as this will influence the release of EVs due to cell death and not the specific actions of the inhibitors. Incubation time must also be considered, in order to make the *in vitro* experimental setup clinically relevant and to ensure that there is enough time for the inhibitors to act. Allowing enough incubation time, will let the inhibitory actions of the inhibitors take place, but also allow other compensatory mechanisms to take effect, something that may occur if these inhibitors were administered to patients. In this study, Hs578Ts(i)$_8$ cells were treated for 48hrs with each inhibitor before the CM was collected, to allow for the total effects of the inhibitors to be effective. This is the first reported study to treat the TNBC Hs578Ts(i)$_8$ cells with the proposed EV inhibitors. It is also the first time the combination of manumycin A and GW4869 is investigated.

Toxicity assays for the inhibitors used in the studies below were not always reported (see Table 4.1), and therefore, did not demonstrate that the decrease in EV release is definitely due to the actions of

the inhibitors, as the concentrations used were not proven to be non-toxic for the specific cells being studied. For example, Mallick *et al.* [105] used a concentration of 80 µM of calpeptin when treating platelets without any toxicity reported. In addition, the platelets are only treated with calpeptin for 30 minutes. A study investigating the use of GW4869 at decreasing EVs and therefore, the decrease in muscle degeneration, used highly different doses of GW4869 when treating C_2C_{12} myoblast cells *in vitro* (8 µM) and treating C57BL/6 mice *in vivo* (100 µM) [218]. No toxicity assays were reported for either of the two experiments and EV reduction was measured by AchE activity, which has been shown not to be a universal EV marker. Another observation of previous studies using the inhibitors was that activators or stressors were used in many cases to induce the release of EVs or to induce membrane blebbing, Under these conditions, the inhibitors seemed to have a significant effect at lowering down EV release. For example, Kim *et al.* [219] exposed human endothelial cells (EA.hy9262) to isoflurane, an anaesthetic, which subsequently had increased CD73+ Annexin V+ microparticle (MP) release compared to endothelial cells treated with carrier gas. When Y27632 was used in combination with isoflurane there was a significant decrease in microparticle CD73 activity. However, under basal conditions when isoflurane was not used, Y27632 did not substantially decrease MP CD73 activity. The human microvascular endothelial cell line, HMEC-1, was pre-incubated with Y27632 before being stimulated with thrombin for 18 hours, in order to elucidate the mechanisms that control thrombin-induced MP release from the endothelial cell line. Y27632 significantly decreased MP release from thrombin stimulated HMEC-1 [220]. However, it was observed that at basal levels, with no thrombin treatment, Y27632 only partially inhibited MP release, with higher concentrations of Y27632 increasing MP release. This study demonstrated that Y27632 only had a significant effect when HMEC-1 cells were artificially stimulated. In our study, we wanted to look at the effect of the inhibitors under basal conditions with no pre-conditioning with EV inducers, something which reflects a more realistic *in vivo* environment.

Cell type	**EV isolation method(s)**	**Inhibitor**	**EV release measurement**	**Extra treatments**	**Concentration of inhibitor**	**Comments**	**Ref.**
Jurkat, U937, MCF-7, HaCat		Y27632	Membrane blebbing	Induction of apoptosis with anti-Fas antibody (7C11)	10 µM 1hrs pre-incubation	No toxicity reported	[221]
HUVEC	17,570g No washing	Y27632 Calpeptin	Annexin V FACS SEM on blebbing cells	Sturosporin Il-1α	30 µM of Y27632-2hrs pre-incubation 200 µM of calpeptin- 1hr pre-cubation	No toxicity reported	[222]
NIH3T3		Y27632	Blebbing cells	TNFα	10 µM 2 hrs incubation	No toxicity reported	[223]

MDA-MB-231, HeLa, U87	Differential ultracentrifugation No washing	Y27632	Blebbing cells Immunoblot	EGF Starvation	5 µM	No toxicity reported	[42]
HCAECs HMEC-1	17,500g No washing	Y27632	Flow cytometry (CD62E, CD105, CD51, CD106, CD31 and CD53)	TNFα Thrombin Starvation	10 µM 24 hrs incubation	No toxicity reported	[224]
HMEC-1		Y27632	Annexin V staining flow cytometry	Thrombin	0-10 µM 1 hr pre-incubation		[220]
EA.hy926	20,000g No washing	Y27632	Annexin V and CD73 flow cytometry	Isoflurane	10 µM 30 mins pre-incubation		[219]
hCMEC/D3 BBB EC	18,000g No washing	Y27632	Annexin V or CD105 flow cytometry SEM	Many different including TNFα	5 µM 2 hrs pre-treatment		[110]
Many different including HT-1080, MDA-MB-231, A375, HUH-7 and HT-29	100,000g No washing	Y27632	Blebbing cells BCA Optical microscopy TEM Hsp90 immunoblot	EDP	25 µM	No NTA	[216]
HUVEC		Y27632	CD31 flow cytometry	LPS with/without tetramethylpyrazine	10 µM 30 mins pre-incubation		[225]
Platelets	180,000g No washing	Y27632	Annexin V and CD61 flow cytometry TEM	Collagen High glucose level	10 µM 10 mins pre-incubation		[226]
HEK293 Human astrocytoma cell line, U373MG		Y27632	NK-1R-GFP positive vesicles by flow cytometry	Undecapeptide substance P	10 µM 20 mins pre-incubation		[227]
F11	150,000g No washing	Manumycin A	NTA Immunoblot GFP-CD63 exosomes		5 µM	No toxicity reported	[113]
BUMPT	100,000g	Manumycin A GW4869	NTA Immunoblot TEM		1 µM of Manumycin A 10 µM of GW4869 2 hrs pre-incubation	No toxicity reported	[116]
C4-2B RWPE-1 PC3 22RV1	Differential ultracentrifugation ExoEasy kit	Manumycin A	NTA qNANO Flow cytomtery		0-500 nM		[114]
Platelets	100,000g No washing	Calpeptin	Annexin V and CD41a flow cytometry	A23187 Collagen Toxin B	9-70 µM 30 mins pre-incubation	No toxicity reported	[228]
Rat hepatocytes		Calpeptin	Phase-contrast microscopy TEM	TBHP $CaCl_2$ EGTA	30 µM 30 mins pre-incubation	No toxicity reported	[229]
Platelets		Calpeptin	Flow cytometry	A23187 Thrombin Collagen	10-300 µM 5 ins pre-incubation	No toxicity reported	[230]
Platelets		Calpeptin	Annexin V and CD41a flow cytometry	A23187 $CaCl_2$ PrP	80 µM 30 min treatment	No toxicity reported	[105]
Platelets	Filtration or 100,000g No washing	Calpeptin	Immunoblot	A23187 Collagen	10-20 µg/ml	No toxicity reported	[106]
PC3	15,000g	Calpeptin	NTA	Docetaxel Mitoxantrone	20 µM		[104]

			Annexin V Flow cytometry		45 mins pre-incubation		
HEK293 SH-SY5Y	130,000g No washing	Calpeptin	Shedding with confocal microscopy Flow cytometry	Many different including cytoskeleton destabiliser	60 µM	No toxicity reported	[231]
THP-1	160,000g or 25,000g No washing	Calpeptin	Annexin V and CD63 flow cytometry TEM		0-100 µM 30 mins treatment		[232]
Platelets		Calpeptin	Calcein-labelled MVs Annexin V flow cyotmetry	Many different	50 µM	No toxicity reported	[233]
Platelets		Calpeptin	Blebbing Annexin V flow cytometry	Many different including convulxin	30 µM 5 mins pre-incubation	No toxicity reported	[234]
B16BL6	0.22 µm filtration 100,000g	GW4869	BCA NTA qNANO immunoblot		5 µg/ml	Used immunoblot to measure EV reduction	[215]
SKOV3	ExoQuick	GW4869	Immunoblot DNMT1 detection by PCR		Not mentioned		[122]
CAF-1	ExoQuick	GW4869	TEM Immunoblot Particle anlayser Light transmission spectroscopy for CD63-GFP quantification	1 µM gemcitabine	20 µM		[235]
PC9	ExoQuick	GW4869	TEM BCA Annexin V flow cytometry Immunoblot		5-20 µM	Used BCA to measure reduction in EVs	[236]
Rov and Mov cells	100,000g	GW4869	TEM Immunoblot	Prions	10 µM 26 hrs incubation	No toxicity reported	[237]
HsC LX-2		GW4869	Immunoblot		10 µM	No toxicity reported	[238]
Cardiac fibroblasts isolated from, neonatal rat	Differential ultracentrifugation	GW4869	TEM Immunoblot BCA	Many different such as angiotensin II	10 µM and 40 µM 48hrs incubation	No toxicity reported	[239]
GT1-7	Differential ultracentrifugation	GW4869	TEM AchE activity qNANO Immunoblot	Prions	4 µM 48 hrs incubation		[240]
MDA-MB-231 SKBR3 Mouse L-cells	14,000g and 100,000g	GW4869	NTA TEM Immunoblot Flow cytometry	Scratch assay	5 µM 16 hrs incubation		[123]
HT29 HCT116	Life technology isolation kit	GW4869	TEM Immunoblot	$CoCl_2$ to mimic hypoxia	Not mentioned	Use immunoblot to measure EV reduction	[241]
HBMECs	Anti-CD63 beads or 130,000g	GW4869	MicroBCA CD63 ELISA NTA TEM		10 µM and 20 µM 4hrs pre-incubation	Use immunoblot to measure EV reduction	[242]

Mouse umbilical MSCs	12,000g and 120,000g	GW4869	NTA TEM Immunoblot		5 µM 48 hrs incubation		[243]
ADSCs	100,000	GW4869	TEM CD63 and CD81 Flow cytometry		1 µM 8 hrs incubation	No characterisation of EVs after GW4869 treatment	[217]
Mice microglia slice culture	0.22 µm filtration 100,000g	GW4869	Immunoblot	LPS INFγ	1 µM and 10 µM 96 hrs incubation		[244]
Human pleural MM cancer cells, H2373, H2595, HP-1 and Hmeso	ExoQuick	GW4869	TEM Immunoblot NTA		40 µM 72 hrs incubation	No toxicity reported	[245]
HT29 and SW480	100,000g	GW4869	TEM NTA Immunoblot		10 µM 24 grs incubation		[246]
THP-1	100,000g No washing	GW4869	TEM NTA Immunoblot		10 µM 2 hrs pre-incubation		[247]
HUVECs	PEG isolation and 120,000g	GW4869	BCA Zetasizer TEM Immunoblot		10 µM	No toxicity reported	[248]
VSC 4.1 neurons	Differential ultracentrifugation	GW4869	NTA TEM Immunoblot		Not mentioned	No toxicity reported. BCA used to measure EV reduction	[249]
Primary stem cells derived from patient's dental pulp tissue	Differential ultracentrifugation	GW4869	NTA BCA TEM Immunoblot		10 µM 12 hrs pre-incubation	BCA used to measure EV reduction	[250]
Primary stem cells derived from patient's dental pulp tissue	Differential ultracentrifugation	GW4869	NTA BCA TEM Immunoblot		Not mentioned	No toxicity reported. No characterisation of EVs released after GW4869 treatment	[251]
Human endometrial adenocarcinoma cell line, Ishikawa	100,000g Concentration with Vivaspin 100K MWCO Exo-Spin kit	GW4869	TEM EXOCET AchE activity		0.1 µM, 1 µM, 10 µM, 20 µM 48 hrs incubation	EV release measured by AchE activity and immunoblot	[252]
A549	ExoQuick	GW4869	NTA TEM		10 µM 24hrs pre-incubation	No toxicity reported	[253]
661W cells	10,000g and 150,000g	GW4869	NTA Zetasizer TEM Immunoblot		1.25 mg/kg in mice (injected daily for 5 days) 20 µM in 611W cells- 4 hrs incubation		[254]
THP-1 cells differentiated into macrophages	0.22 µm filtration 100,000g	GW4869	NTA TEM AFM Immunoblot		10 μmol^{-1} 48 hrs incubation	No toxicity reported. Did not show NTA data	[255]
Cal51 TNBC cells	0.22 µm filtration 120,000g	GW4869	NTA Immunoblot	Pre-treatment with paclitaxel	5 µM 48hrs incubation	No toxicity reported	[88]

	Exospin for GW4869 treated cell derived CM			to induce senescence			
Patient serum C_2C_{12} cells C57BL/6 mouse models	ExoQuick TEI kit	GW4869	Immunoblot Flow cytometry		100 µM in mice (injected once) 8 µM in cells for 72 hrs	No toxicity reported. EV concentration measured by BCA and AchE activity	[218]
BEAS-2b cells	Differential ultracentrifugation and sucrose density gradient	GW4869	Immunoblot Flow cytometry		5 µM 1 hrs pre-incubation	No toxicity reported. Immunoblot used to measure EV reduction	[256]
A431, MDA-MB-231, BxPC3, Panc1, PC3, DLD-1, CaCo-2	Differential ultracentrifugation	GW4869	NTA		10 µM 24 hrs incubation		[257]
5TGM1-Murine multiple myeloma cells	0.22 µm filtration Concentration with 150kDa ExoQuick Density ultracentrifugation	GW4869	BCA Zetasizer Immunoblots TEM		2.5 µM, 5 µM, 10 µM *in vitro* (24 hrs incubation) 2.5 mpk *in vivo* (Treated intraperitoneally 3 times per week)	No toxicity reported. Immunoblot used to measure EV reduction	[258]
Mixed glial cells from mice	Differential ultracentrifugation and sucrose density gradient	GW4869	BCA		C75B1/6 mice injected with 4 µg/g daily for 5 days 10 µM, 20 µM, 40 µM	Immunoblot used to measure EV reduction	[259]
Human renal tubular epithelial cells, HK-2	ExoQuick	GW4869	NanoFCM TEM Immunoblots	LPS	40 µM -24 hrs incubation	Toxicity performed using reduction of tetraspanins (CD9, CD63, CD81) by immunoblot. Used HK-2 cell lysate and supernatant to measure EV reduction	[260]
Adult mouse cardiomyocytes	0.22 µm filtration 120,000g	GW4869	BCA Zetasizer Immunoblot AchE kit		TG (diabetes) mouse model (FVB/N mice) injected with 1 µg/g daily for 5 days	No toxicity reported. No characterisation after GW4869 treatment	[261]

Table 4.1: Details of previous studies that used the EV inhibitors used in this project

ADSCs=Adipose derived stem cells, AFM=Atomic force microscopy, BCA=Bradford colorimetric assay, EDP=Elastin degradation products, EGF=Epidermal growth factor, LPS=lipopolysaccharide NTA=Nanoparticle tracking analysis, TEM=Transmission electron microscopy, TNFα=Tumour necrosis factor α

During the study of proposed EV inhibitors, it came to our attention that there was an unmet need for an easy and reliable method to determine the effects of potential inhibitors on EV release without the need for a full EV isolation. It has been shown that EV release can be influenced by chemotherapy *in vitro*. For example, Aubertin et al. [262] demonstrated that photodynamic therapy with Foscan m-THPC and doxorubicin caused an increase in EV release from prostate cancer cells, PC3 and that the EVs released contained the drug inside them. These EVs were then able to transfer the drug into recipient endothelial cells. In an *in vivo* study, circulating EVs isolated from breast cancer patient plasma were significantly increased post neoadjuvant therapy compared to both pre-neoadjuvant therapy and healthy controls [263]. Therefore, we wanted to develop a easy method in which to test a panel potential inhibitors or test chemotherapy drugs that are already in use, in shorter timeframe than it would take to fully isolated EVs using an isolation method such as density gradient ultracentrifugation.

4.2 Aims of study

The primary aim here was to investigate if proposed EV inhibitors, calpeptin, Y27632, GW4869 and manumycin A- when used at non-toxic concentrations- could inhibit EV release from TNBC cell line variant, Hs578Ts(i)$_8$. We aimed to quantify and characterise all EVs still released after inhibitor treatment and their subsequent effects on recipient TNBC cell line proliferation and migration, according to MISEV guidelines. The use of toxicity assay to determine the correct concentration and multiple methods to characterise the EVs made sure that definitive conclusions could be made of the results.

The secondary aim was to develop a fast, small-scale screening protocol that did not require a full EV separation, to determine if potential EV inhibitors could decrease the release of EVs from a panel of TNBC cell lines; using use imaging flow cytometry to measure any changes in EVs released.

4.3 Results

4.3.1 Toxicity of proposed EV inhibitors

Triple-negative breast cancer cell line variant, Hs578Ts(i)$_8$ was used to investigate the use of proposed EV inhibitors, calpeptin, Y27632, manumycin A and GW4869, in decreasing the release of EVs. Firstly, a cytotoxicity assay was used to identify a concentration that would not be toxic to the Hs578Ts(i)$_8$ cell line variant over 48hrs treatment (Fig. 4.1 (A-D)). The following concentrations were chosen (Fig. 4.1 (E)), 20 µM calpeptin, 10 µM Y27632, 5 µM GW4869 and 2 µM manumycin A, for the Hs578Ts(i)$_8$ cells.

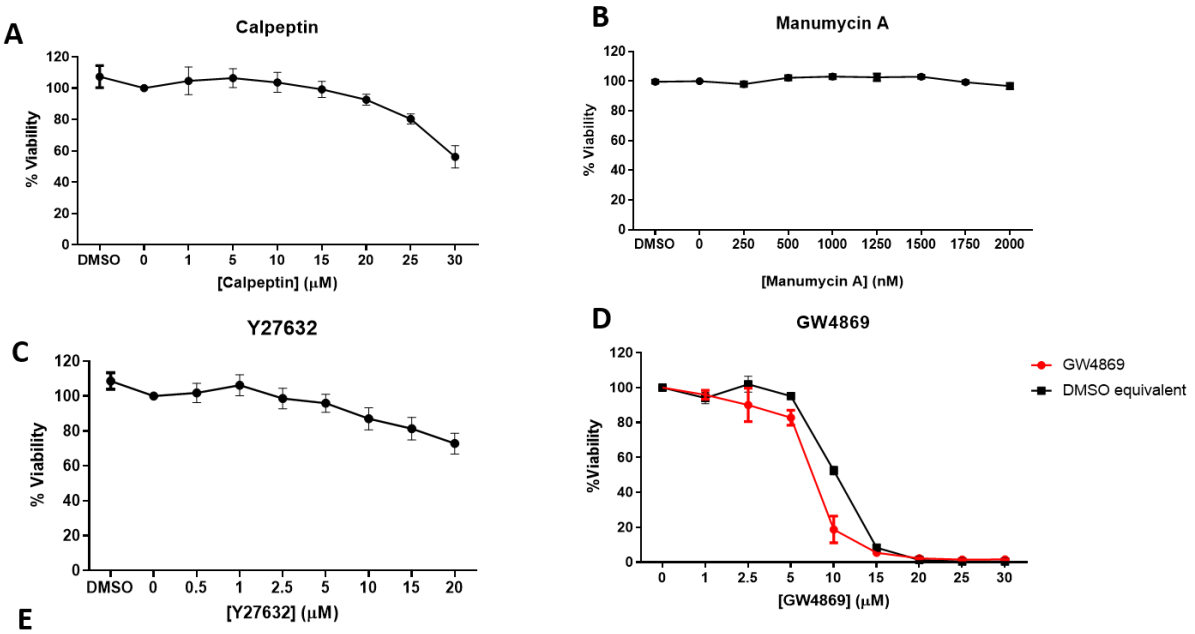

E

Potential Inhibitor	Concentration chosen	Viability (%) (*n=3*) ± SEM
Calpeptin	20 µM	92.7 ± 4.9
Y27632	10 µM	87.0 ±8.9
GW4869	5 µM	82.8 ± 6.0
Manumycin A	2 µM	96.7 ± 2.6

Figure 4.1: Cytotoxicity assay with proposed EV inhibitors on Hs578Ts(i)$_8$ cell line variant

Cytotoxicity assay were performed on the Hs578Ts(i)$_8$ cell line variant using (A) calpeptin, (B) Manumycin A, (C) Y27632 and (D) GW4869. (E) The concentrations chosen are displayed along with the percent of viability at that given concentration. Graphs represent mean ± SEM of *n=3* independent biological experiments.

Subsequent experiments were performed to confirm that appropriate inhibitor concentrations were being used. Using annexin V/propidium iodide (Annexin V/PI) flow cytometry (FC), the viability of Hs578Ts(i)$_8$ cells was measured after 48hrs treatment with each individual inhibitor alone and the combination of calpeptin and Y27632 together (i.e. Combo 1) and the combination of GW4869 and manumycin A together (i.e. Combo 2).

Annexin V/PI FC analysis confirmed that the inhibitors did not result in cell toxicity at their chosen concentrations in the Hs578Ts(i)$_8$ cell line (Fig. 4.2 (A)). Representative dot plots shown, demonstrate the levels of cell death after treatment with all inhibitors in the Hs578Ts(i)$_8$ cells (Fig. 4.2 (B)). Cells were also treated with 1 µM of Staurosporine, as a positive control of apoptosis.

A

Potential inhibitor	Viable cells (%)	Necrotic cells (%)	Apoptotic cells (%)
Control	98.8 ± 0.4	0.5 ± 0.4	0.7 ± 0.1
Calpeptin	98.3 ± 0.9	1.0 ± 0.9	0.8 ± 0.05
Y27632	97.7 ± 1.0	1.0 ± 0.8	1.3 ± 0.2
Combo 1	97.4 ± 1.1	1.3 ± 1.0	1.4 ± 0.1
GW4869	99.0 ± 0.1	0.3 ± 0.1	0.7 ± 0.05
Manumycin A	98.1 ± 0.6	0.9 ± 0.4	1.0 ± 0.1
Combo 2	97.4 ± 0.4	1.0 ± 0.2	1.7 ± 0.1
Staurosporine (1µM)-Positive control	23.4 ± 13.6	1.8 ± 1.6	74.8 ± 2.2

B

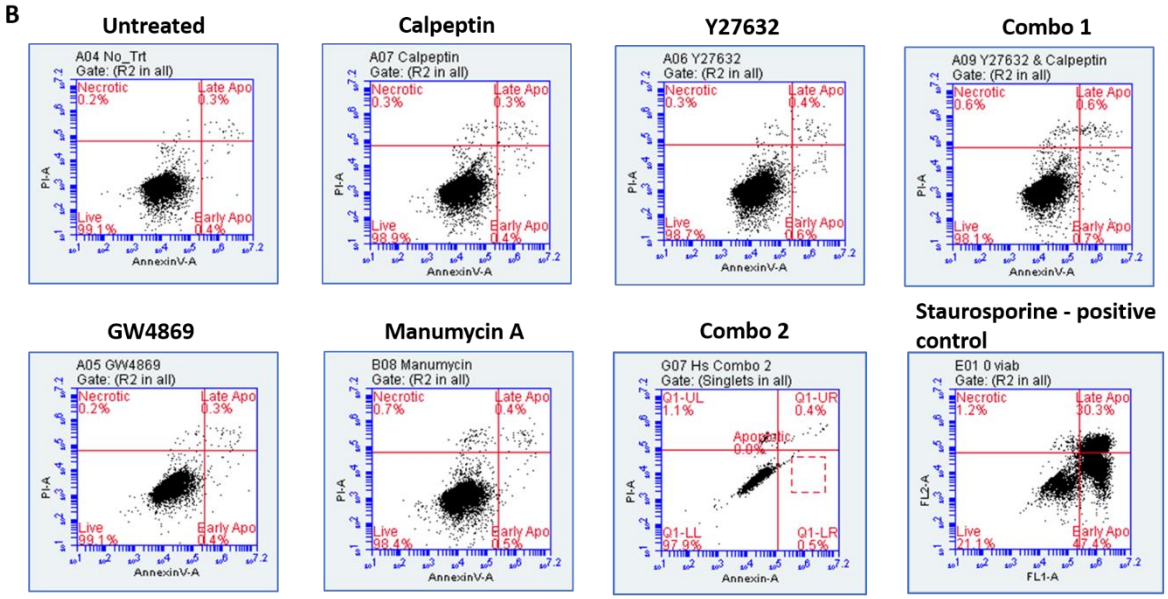

Figure 4.2: Annexin/Propidium iodide flow cytometry analysis of Hs578Ts(i)$_8$ cell line variant

A second type of viability test was performed using Annexin V/PI staining. (A) Table shows the % of viable, necrotic and apoptotic cells of mean ± SEM of *n=3* independent experiments. Staurosporine (1 µM) was used as a positive control of apoptosis. (B) Representative dot plots generated during analysis of the effect of inhibitors on Hs578Ts(i)$_8$ cells.

The effect of the proposed inhibitors on cancer cell migration and invasion was also investigated. Manumycin A significantly (*p=0.014*) decreased migration (Fig. 4.3 (A)). Calpeptin and GW4869 also decreased migration. However, significance was not reached. Representative wound closure images are shown (Fig. 4.3 (B)). Invasion was significantly (*p=0.005*) decreased by GW4869 (Fig. 4.3 (C)). Calpeptin and manumycin A also decreased invasion but to a lesser extent. Representative crystal violet stained cells that had invaded are shown (Fig. 4.3 (D)).

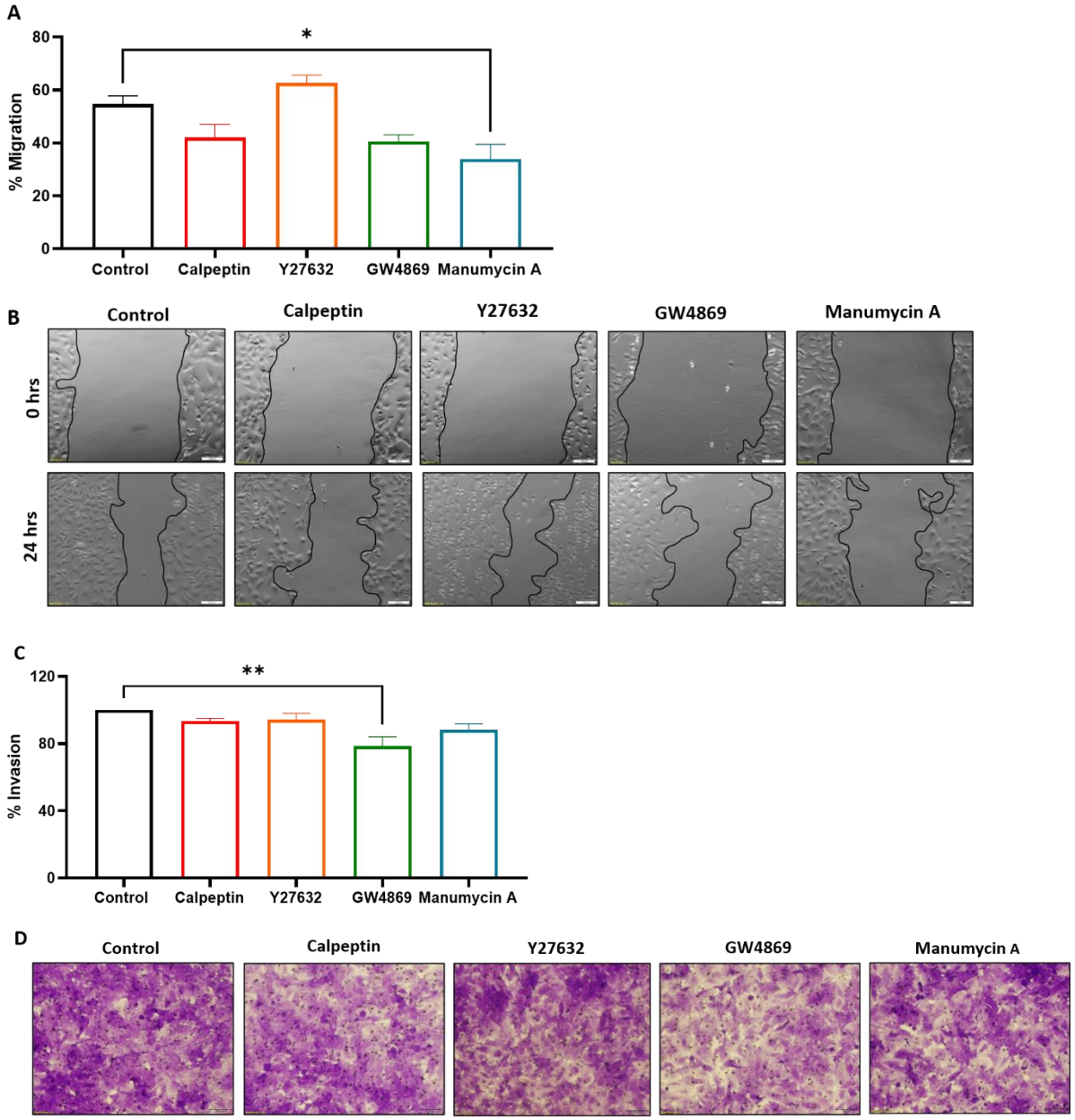

Figure 4.3: Anti-cancer effects of proposed EV inhibitors

Hs578Ts(i)$_8$ cell (A) migration and (C) invasion was investigated with proposed EV inhibitor treatment versus untreated control for 24 hrs. Representative (B) wound closure images and (D) crystal violet-stained invaded cells are shown. Both sets of images are taken at 10X magnification and scale bars are 100 µm. Graphs represent mean ± SEM of *n=3* independent biological experiments. One-way ANOVA was used as statistical test. *P<0.05, **P<0.01.

4.3.2 Characterisation of EVs following inhibitor treatment

Initial characterisation of EVs following the second EV isolation procedure included NTA analysis of EVs released after inhibitor treatment. All inhibitors decreased EV release from the Hs578Ts(i)$_8$ cells. These included, calpeptin (*p<0.0001*), Y27632 (*p<0.0001*), combo 1 (*p<0.0001*), manumycin A (*p=0.001*), GW4869 (*p<0.0001*) and combo 2 (*p<0.0001*) (Fig. 4.4 (A)). The percentage of decrease is shown (Fig. 4.4 (B)). There was no significant change in the size (nm) of the EVs released following inhibitor treatment, although GW4869 increased EV size a little more than any other treatment (Fig. 4.4 (C)). Protein measurement of the EVs after treatment demonstrated that combo 2 caused a significant increase (*p=0.030*) (Fig. 4.4 (D)).

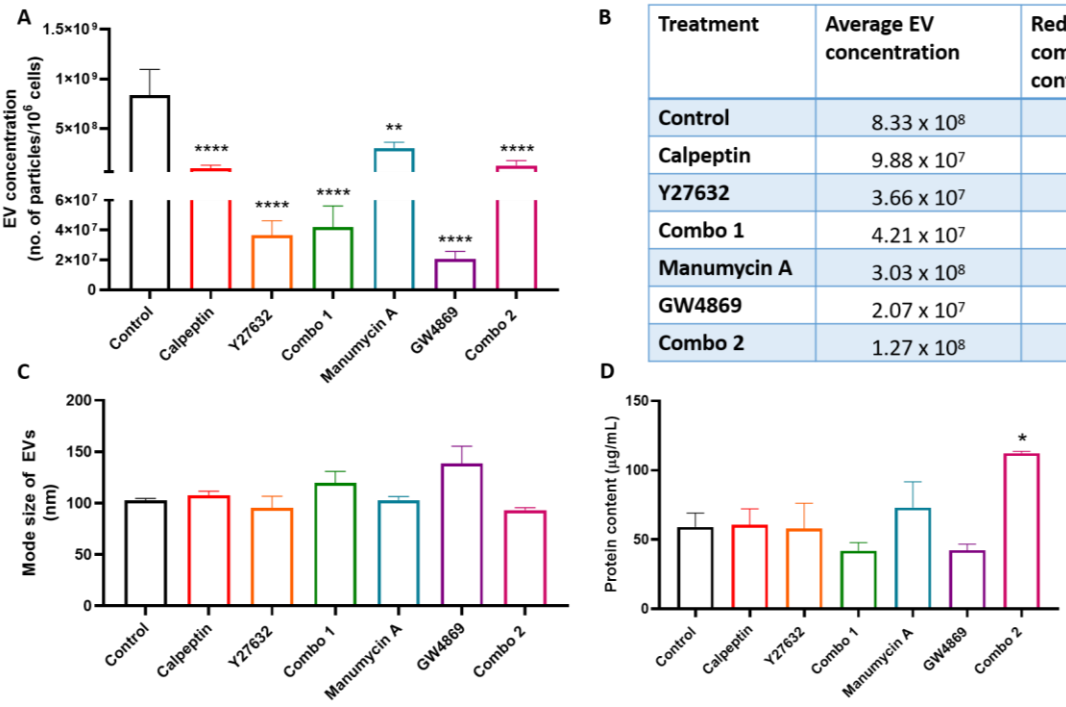

Treatment	Average EV concentration	Reduction compared to control
Control	8.33 x 10^8	-
Calpeptin	9.88 x 10^7	-88%
Y27632	3.66 x 10^7	-96%
Combo 1	4.21 x 10^7	-95%
Manumycin A	3.03 x 10^8	-64%
GW4869	2.07 x 10^7	-98%
Combo 2	1.27 x 10^8	-85%

Figure 4.4: Particle and protein measurements of Hs578Ts(i)$_8$ EVs after inhibitor treatment of cells

The release of EVs were measured by (A) NTA and (B) the % of release was calculated compared to the untreated control. The (C) size of EVs released was measured by NTA and (D) the protein (µg/mL) was measured by BCA. Graphs (A) and (C) represent mean ± SEM of *n=4* independent biological experiments. Graph (D) is representative of mean ± SEM of *n=3* independent biological experiments. One-way ANOVA was used as statistical test for *P<0.05, **P<0.01, ****P<0.0001.

Immunoblot analysis was performed on EVs released from Hs578Ts(i)$_8$ cells. Calnexin was used as a negative control, demonstrating the purity of the separated EVs. CD63 was carried in all EVs following inhibitor treatment. Syntenin, a cytosolic protein is also present in all EVs after inhibitor treatment. There is limited effect on EV markers after treatment when compared to EVs released after no inhibitor treatment.

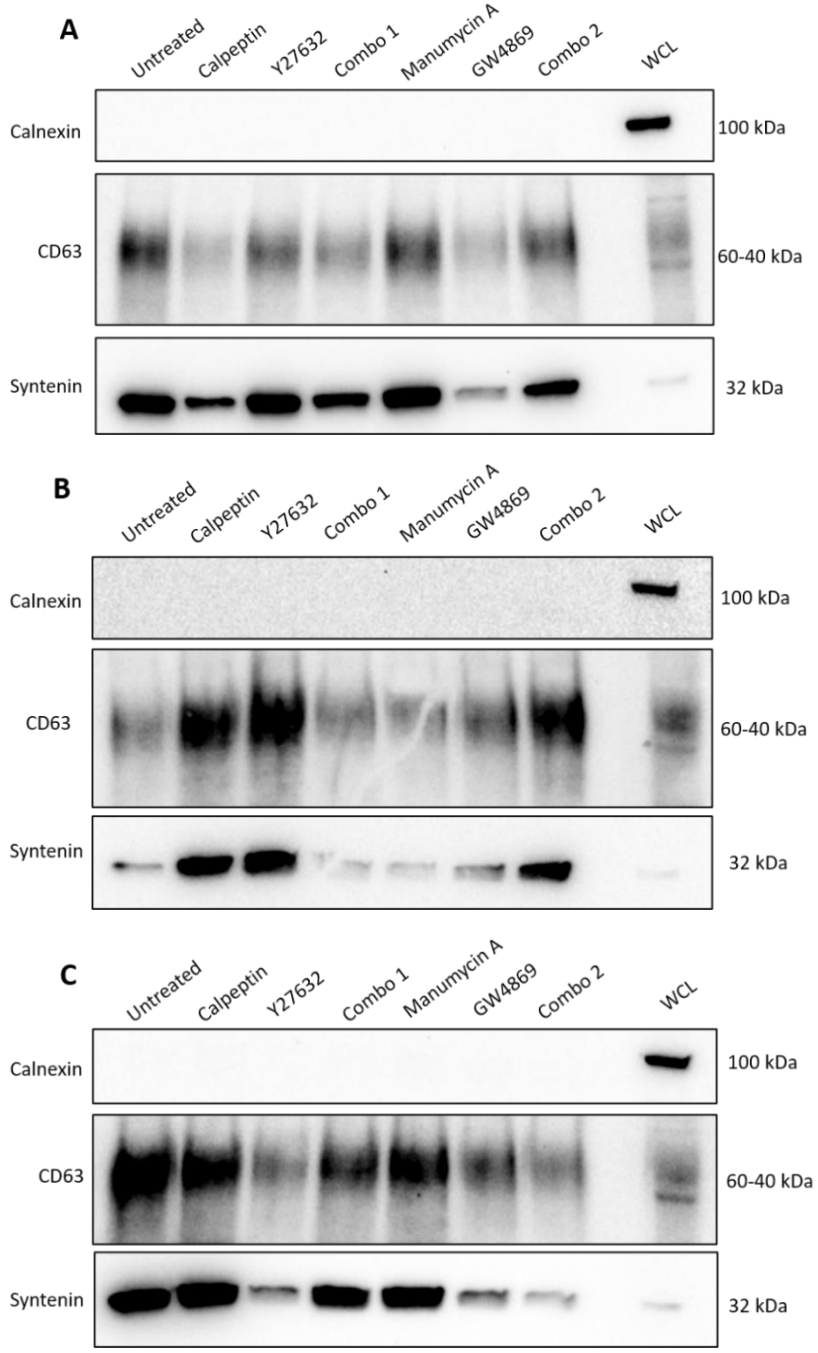

Figure 4.5: Immunoblot analysis of Hs578Ts(i)$_8$ EVs following inhibitor treatment of cells

Immunoblot analysis of EVs following inhibitor treatment. (A-C) are *n=3* independent biological repeats. Calnexin is a negative control. WCL = whole cell lysate of Hs578Ts(i)$_8$ cells is used as a positive control.

Overall, TEM analysis of Hs578Ts(i)$_8$ EVs show that after inhibitor treatment the more limited number of EVs were still intact. EVs released after no treatment had a size of approximately 100 nm, characteristic of small EVs (Fig. 4.6 (A)). EVs released after calpeptin treatment were in also within the size range of small EVs and homogenous in size (Fig. 4.6 (B)). EVs released after Y27632 treatment have a dirtier background, with the majority being within 100 nm in size (Fig. 4.6 (C)). EVs released after combo 1 treatment were mostly approximately 100 nm in size (Fig. 4.6 (D)). EVs released after manumycin A treatment have a very dirty background but show EVs are present (Fig. 4.6 (E)). EVs released after GW4869 treatment had a size of approximately 100 nm but were present in very low numbers (Fig. 4.6 (F)). EVs released after combo 2 treatment had a clear background, and most EVs were 100 nm or smaller in size (Fig. 4.6 (G)).

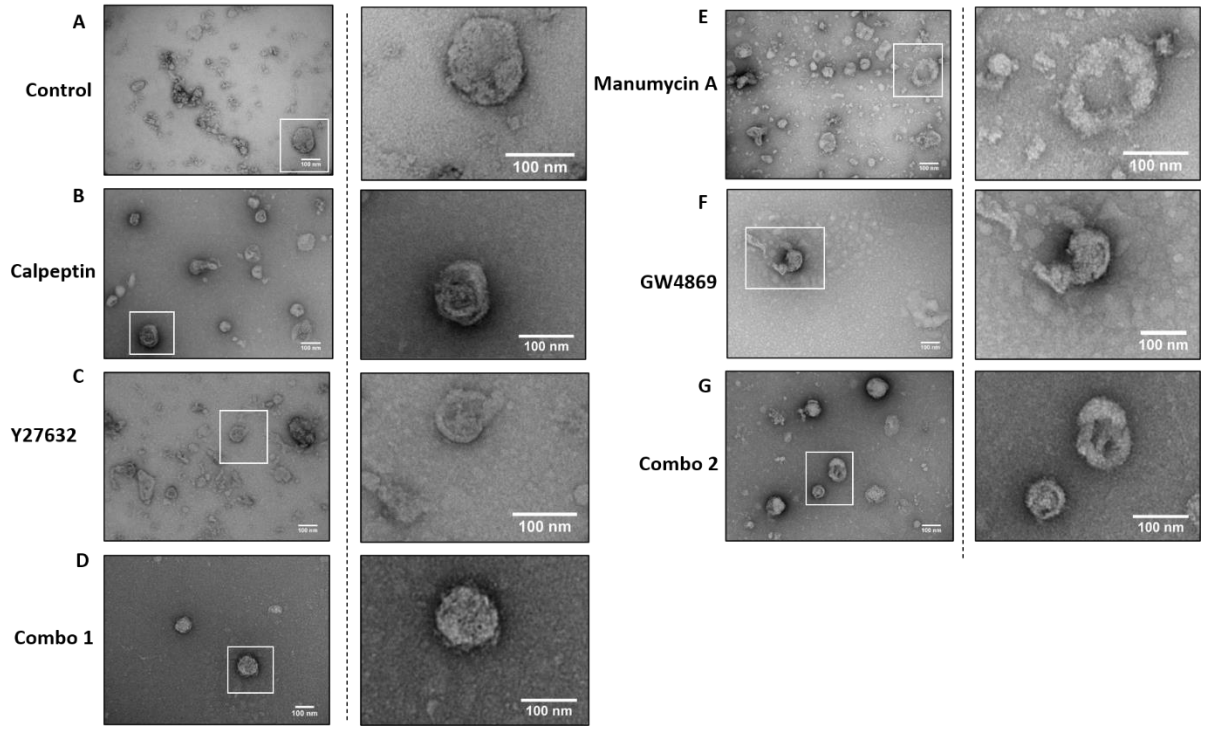

Figure 4.6: TEM analysis of Hs578Ts(i)$_8$ EVs following inhibitor treatment of cells

TEM analysis of EVs after inhibitor treatment of (B) Calpeptin, (C) Y27632, (D) Combo 1, (E) Manumycin A, (F) GW4869, (G) Combo 2. Control EVs (A) are also shown. Images were taken at a magnification of 30000X. Scale=100 nm.

4.3.3 Functional analysis of EVs following inhibitor treatment with adjusted protocol

For the following assays, three quantities of EVs were added to TNBC cells, based on NTA analysis. This method of adding EVs to the assays allowed the decrease of EV release caused by inhibitor treatment to be considered. This allowed the true monitoring of the EVs' effects on recipient cells, as EVs were added to each assay in the same amounts as they were released from the Hs578Ts(i)$_8$ cells. BT549 cells were used instead of MDA-MB-468 as the have similar growth rates as the Hs578T cells and can be monitored over the same length of time.

EVs released from Hs578Ts(i)$_8$ cells following inhibitor treatment were used to treat Hs578T and BT549 cells to determine if there was an effect cell proliferation. Three different EV doses were added (Fig. 4.7 (A)). Overall, the EVs had a limited effect on Hs578T (Fig. 4.7 (B-D)) and BT549 (Fig. 4.7 (E-G)) cell proliferation. Hs578T proliferation was significantly (*p=0.020*) reduced when treated with 1.27 x 10^6 of EVs released after combo 2 treatment when compared to untreated cells (Fig. 4.7 (D)). Similarly, BT549 cell proliferation was significantly decreased with EVs released after combo 2 treatment at a quantity of 1.27 x 10^4 (*p=0.032*) and 1.27 x 10^6 (*p=0.001*) compared to untreated cells (Fig. 4.7 (E and G)).

A

	Control EVs	Calpeptin EVs	Y27632 EVs	Combo 1 EVs	Manumycin A EVs	GW4869 EVs	Combo 2 EVs
Dose 1	8.33 x 10^4	9.88 x 10^3	3.66 x 10^3	4.21x 1 0^3	3.03 x 10^4	2.07 x 1 0^3	1.27 x 10^4
Dose 2	8.33 x 10^5	9.88 x 10^4	3.66 x 10^4	4.21 x 10^4	3.03 x 10^5	2.07 x 10^4	1.27 x 10^5
Dose 3	8.33 x 10^6	9.88 x 10^5	3.66 x 10^5	4.21 x 10^5	3.03 x 10^6	2.07 x 10^5	1.27 x 10^6

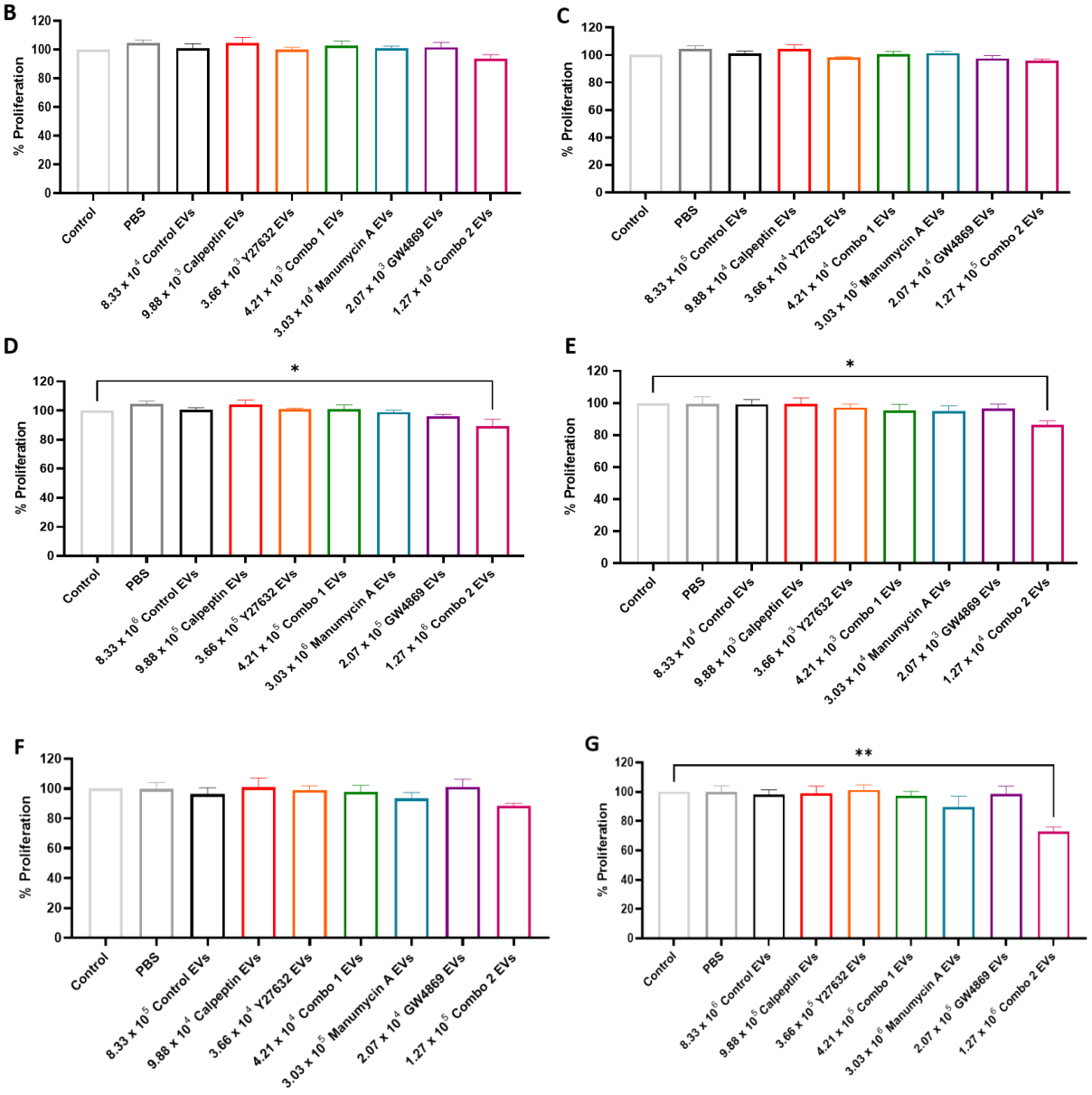

Figure 4.7: Proliferation assay with Hs578Ts(i)$_8$ EVs released following inhibitor treatment

Hs578T (B-D) and BT549 (E-G) cells were seeded in 96-well plates and treated with three doses of EVs (A) separated from the Hs578Ts(i)$_8$ after inhibitor treatment for 72 hrs. Control is cells treated with cell medium alone. Graphs represent mean ± SEM of *n=4* independent biological experiments. One -way ANOVA was used as statistical test. *P<0.05, **P<0.01.

The EVs were also investigated for their ability to change cell migration. There was a 13.3-fold increase in Hs578T cells used for migration; therefore, a 13.3-fold increase in EVs were used (Fig. 4.8 (A)).
EVs released after no inhibitor treatment increased Hs578T migration compared to untreated control cells, which were treated with cell medium containing no EVs, although no dose-dependency was observed (Fig. 4.8 (B)). All Hs578Ts(i)$_8$ EVs that continued to be released following inhibitor treatment caused a minor decrease in Hs578T migration when compared to treatment with EVs that were released after no inhibitor treatment. Significance was only reached with EVs released after combo 2 treatment, at a dose of 1.70 x 10^7 EVs (*p=0.036*) (Fig. 4.8 (H)). Representative wound healing images show Hs578T migration after 24 hrs, treated with the highest dose of EVs from all conditions.

A

	Control EVs	Calpeptin EVs	Y27632 EVs	Combo 1 EVs	Manumycin A EVs	GW4869 EVs	Combo 2 EVs
Dose 1	1.08×10^6	1.28×10^5	4.76×10^4	5.47×10^4	3.94×10^5	2.70×10^4	1.65×10^5
Dose 2	1.11×10^7	1.32×10^6	4.87×10^5	5.60×10^5	4.03×10^6	2.75×10^5	1.67×10^6
Dose 3	1.11×10^8	1.32×10^7	4.88×10^6	5.61×10^6	4.04×10^7	2.76×10^6	1.70×10^7

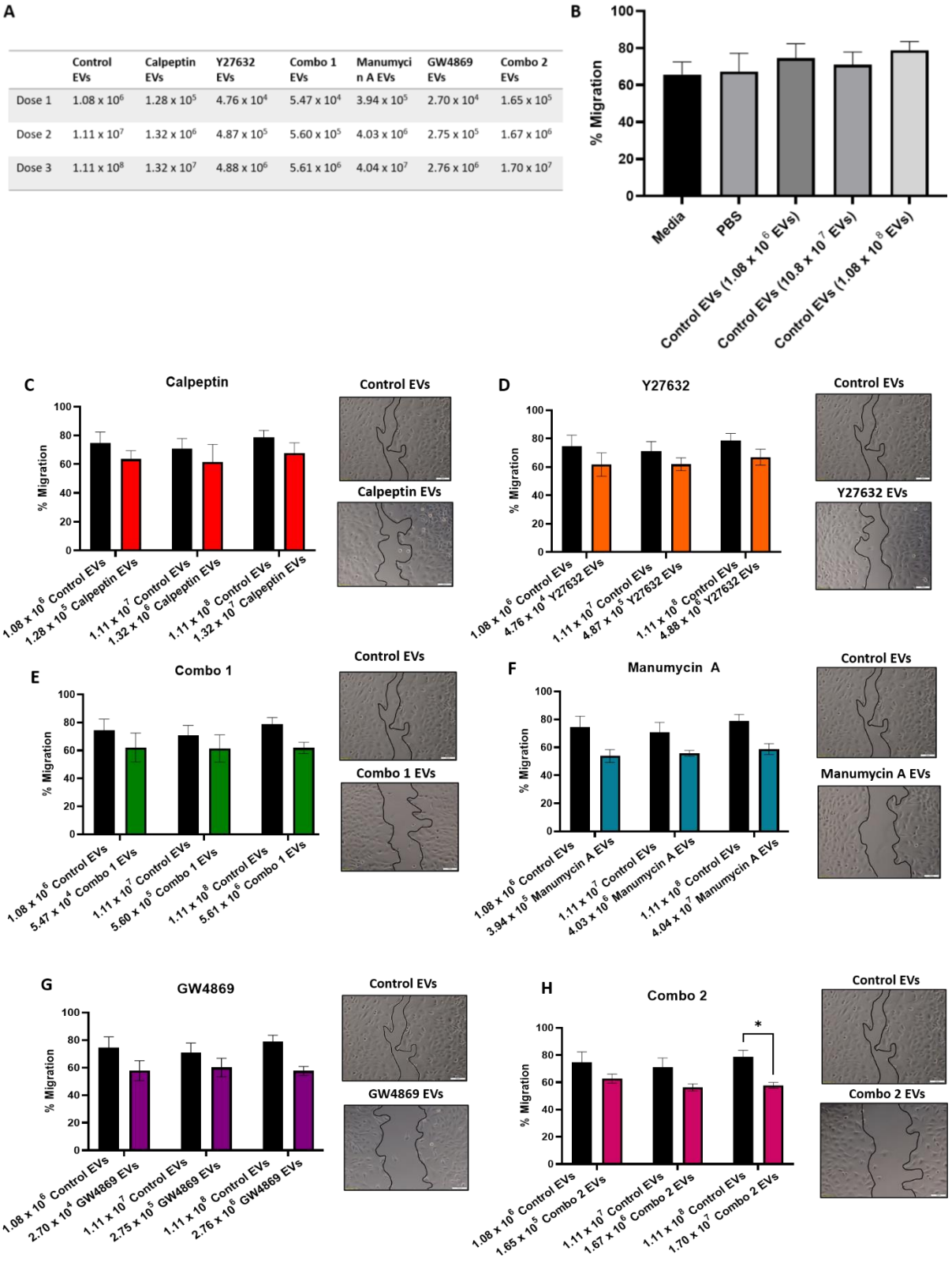

Figure 4.8: Hs578T migration with Hs578Ts(i)$_8$ EVs still released after inhibitor treatment

Hs578T migration was monitored over 24 hrs with (A) three increasing doses of EVs. (B) PBS control and Control EVs at three doses were graphed separately. Migration of Hs578T with (C) Calpeptin EVs, (D) Y27632 EVs, (E) Combo 1 EVs, (F) Manumycin A EVs, (G) GW4869 EVs and (H) Combo 2 EVs treatment was analysed. Representative wound healing images from the highest EV dose are shown. Scale bar is 100 µm. Graphs represent mean ± SEM of *n=3* independent experiments. Two-way ANOVA was used as statistical test. *P<0.05.

EVs released from Hs578Ts(i)$_8$ cells after inhibitor treatment were used to investigate the effect on BT549 migration. There was 10-fold increase in BT549 cells used for migration compared to the proliferation assay, therefore, 10-fold increase in EVs were used (Fig. 4.9 (A)).

EVs released after no inhibitor treatment significantly increased BT549 migration with 8.33 x 10^6 (*p=0.012*) and 8.33 x 10^7 (*p=0.005*) EVs compared to untreated control cells, in a dose-dependent manner (Fig. 4.9 (B)). EVs released after calpeptin treatment compared to EVs released after no treatment, significantly decreased BT549 migration at the two highest doses of, 9.88 x 10^5 EVs (*p=0.015*) and 9.88 x 10^6 EVs (*p=0.036*) (Fig. 4.9 (C)). EVs released after Y27632 treatment compared to EVs released after no treatment caused a significant decrease in BT549 migration at a dose of 3.66 x 10^5 (*p=0.0001*) and 3.66 x 10^6 EVs (*p=0.007*) (Fig. 4.9 (D)). EVs released after combo 1 treatment compared to EVs released after no treatment significantly decreased migration at a concentration of 4.21 x 10^5 (*p=0.019*) and 4.21 x 10^6 (*p=0.005*) EVs (Fig. 4.9 (E)). EVs released after manumycin A treatment compared to EVs released after no treatment also caused a significant decrease at a dose of 3.03 x 10^6 EVs (*p=0.008*) and 3.03 x 10^7 EVs (*p=0.005*) (Fig. 4.9 (F)). EVs released after GW4869 treatment had a limited effect at decreasing migration at the lower doses but at 2.07 x 10^6 EVs, there was a significant decrease (*p=0.005*) compared to the migration caused by EVs released after no treatment (Fig. 4.9 (G)). EVs released after combo 2 treatment compared to EVs released after no treatment decreased BT549 migration at all doses, however, only significantly at 1.27 x 10^7 EVs (*p=0.017*) (Fig. 4.9 (G)). Representative wound healing images show BT549 migration after 24 hrs, treated with the highest dose of EVs from all conditions.

A

	Control EVs	Calpeptin EVs	Y27632 EVs	Combo 1 EVs	Manumycin A EVs	GW4869 EVs	Combo 2 EVs
Dose 1	8.33×10^5	9.88×10^4	3.66×10^4	4.21×10^4	3.03×10^5	2.07×10^4	1.27×10^5
Dose 2	8.33×10^6	9.88×10^5	3.66×10^5	4.21×10^5	3.03×10^6	2.07×10^5	1.27×10^6
Dose 3	8.33×10^7	9.88×10^6	3.66×10^6	4.21×10^6	3.03×10^7	2.07×10^6	1.27×10^7

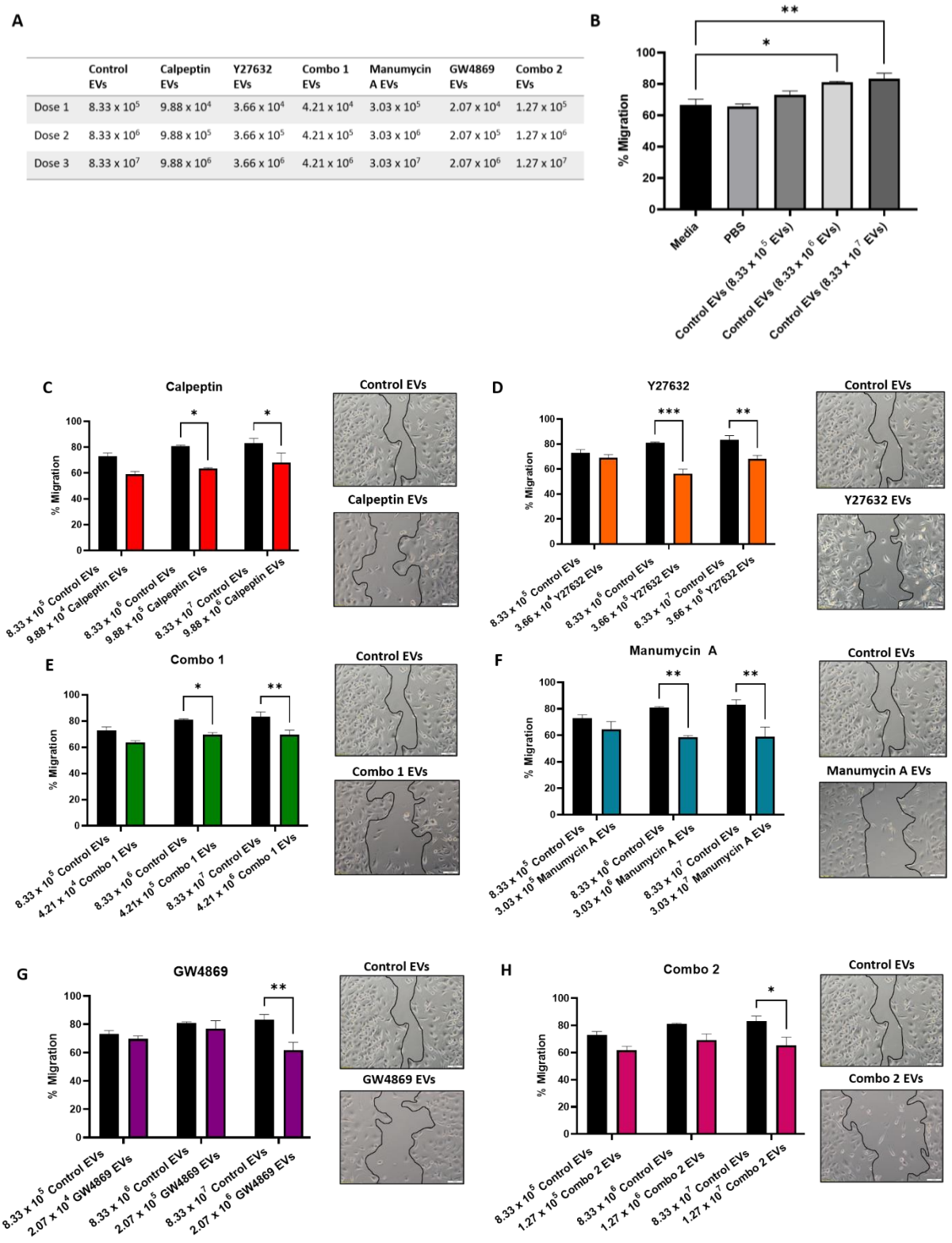

Figure 4.9: BT549 migration with Hs578Ts(i)$_8$ EVs still released after inhibitor treatment

BT549 migration was monitored over 24 hrs with (A) three increasing doses of EVs. (B) PBS control and Control EVs with three different doses were graphed separately. Migration of BT549 with (C) Calpeptin EVs, (D) Y27632 EVs, (E) Combo 1 EVs, (F) Manumycin A EVs, (G) GW4869 EVs and (H) Combo 2 EVs treatment was analysed. Representative wound healing images from the highest EV dose are shown. Scale bar is 100 µm. Graphs represent mean ± SEM of *n=3* independent experiments. One-way ANOVA was used for (A), Two-way ANOVA was used as statistical test for (C-H). *P<0.05, **P<0.01, ***P<0.001.

4.3.4 Toxicity of additional potential inhibitors in a panel of TNBC cell lines

An additional selection of drugs which included commonly used therapeutic drugs, neratinib, and carboplatin, a drug which had been demonstrated to both inhibit and increase EV release in two conflicting papers, sulfisoxazole and a drug which has shown to be effective in TNBC cell lines by activating mutant p53, COTI-2 were investigated in a panel of TNBC cell lines including Hs578Ts(i)$_8$, MDA-MB-468, HCC1143, BT549, and MDA-MB-231. GW4869 and manumycin A were also further investigated in the additional cell lines. Before continuing on, all cell lines were checked that they had mutant p53 [264].

A small-scale EV screening method was optimised in 24-well plates rather than full-scale T175 flasks, to increase the capacity of the drug screening to determine their effects on EV release in a higher throughput manner. This was done by collecting the conditioned medium (CM) from five TNBC cell lines that had been treated with the panel of six drugs for 48 hrs in 24-well plates. This CM was then pre-cleared by centrifugation at 300g and analysed by flow cytometry for presence of CD9. CD9 was chosen as it had the highest detection in a previous flow cytometry analysis of Hs578Ts(i)$_8$ EVs (see Fig. 4.6)

Initial cytotoxicity assays were performed to determine a non-toxic concentration of each potential inhibitor for each TNBC cell line (Fig. 4.16).

Potential inhibitor	Hs578Ts(i)$_8$		MDA-MB-468		HCC1143		BT549		MDA-MB-231	
	Concentration chosen	Viability (*n=3*)	Concentration chosen	Viability (*n=3*)	Concentration chosen	Viability (*n=3*)	Concentration chosen	Viability (*n=3*)	Concentration chosen	Viability (*n=3*)
Neratinib	**0.01 µM**	93.2 ± 4.3	**0.01 µM**	91.4 ± 3.3	**0.01 µM**	92.2 ± 2.3	**0.1 µM**	94.9 ± 2.6	**1 µM**	105.7± 16.8
Carboplatin	**10 µM**	93.4 ± 2.9	**0.5 µM**	94.6 ± 3.9	**10 µM**	96.7 ± 8.7	**50 µM**	96.3 ± 5.9	**100 µM**	95.0 ± 7.6
GW4869	**5 µM**	82.8 ± 6.0	**5 µM**	100.9 ± 1.6	**10 µM**	112.2 ± 6.5	**5 µM**	97.6 ± 5.9	**5 µM**	105.0 ± 12.6
Sulfisoxazole	**50 µM**	92.6 ± 4.3	**100 µM**	92.6 ± 0.8	**50 µM**	91.9 ± 4.8	**50 µM**	92.7 ± 0.9	**100 µM**	102.6 ± 7.1
Manumcyin A	**2 µM**	96.7 ± 2.6	**1.5 µM**	97.7 ± 3.5	**1.5 µM**	90.5 ± 4.2	**750 nM**	95.3 ± 10.2	**750 nM**	96.8 ± 7.0
COTI-2	**5 nM**	103.9 ± 11.8	**0.25 nM**	97.4 ± 0.9	**10 nM**	95.3 ± 4.4	**1 nM**	89.2 ± 4.5	**5 nM**	93.8 ± 7.8

Figure 4.10: Summary of cytotoxicity of potential inhibitors in TNBC cell line panel

TNBC cell lines were treated in 96-well plates for 48hrs with each inhibitor to determine a non-toxic concentration at which to treat the cells in subsequent experiments. Tabulated results are of mean ± SEM of *n=3* independent biological experiments.

4.3.5 Small-scale screening of inhibitor effects on TNBC cell line EV release

Following the selection of each drug concentration (see Fig. 4.16), Hs578Ts(i)$_8$ cells were treated for 48 hrs with each drug and the resulting conditioned medium (CM) was screened for CD9 by flow cytometry. COTI-2 significantly (*p<0.0001*) increased CD9 positivity of sEVs-gated particles compared to untreated cells (Fig. 4.11 (A)). When all three sub-populations events were added together, COTI-2 significantly (*p=0.032*) increased CD9 levels in the CM compared to that of untreated cells (Fig. 4.11 (B)). Although not significant, GW4869 and manumycin A decreased CD9. neratinib, sulfisoxazole and carboplatin increased CD9 (Fig. 4.11 (B)). A summary of the screening results is also shown (Fig. 4.11 (C)). Representative dot plots generated during the screening are shown (Fig. 4.11 (D)).

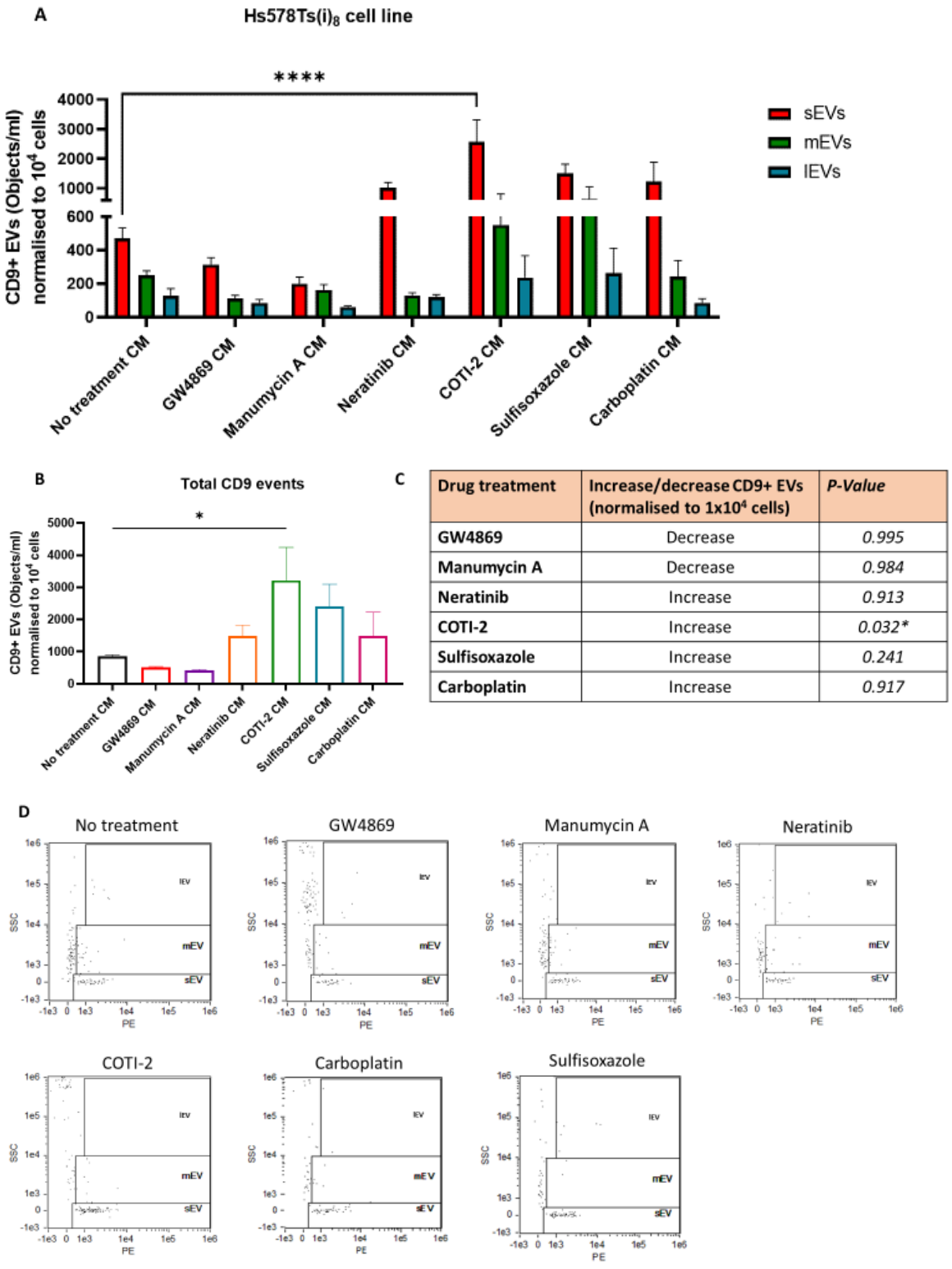

Drug treatment	Increase/decrease CD9+ EVs (normalised to 1x10^4 cells)	*P-Value*
GW4869	Decrease	*0.995*
Manumycin A	Decrease	*0.984*
Neratinib	Increase	*0.913*
COTI-2	Increase	*0.032**
Sulfisoxazole	Increase	*0.241*
Carboplatin	Increase	*0.917*

Figure 4.11: CD9 flow cytometry screening of Hs578Ts(i)$_8$ conditioned medium

Hs578Ts(i)$_8$ conditioned medium was screened for CD9 after 48 hrs drug treatment of the cells. (A) CD9 positive particles were detected and normalised as CD9 positive particles per 1x10^4 cells, from which the conditioned medium was collected. (B) All three sub-populations events were added together and graphed. (C) Summary of CD9 in conditioned medium after drug treatment compared to the control. (CD) Representative dot plots generated after analysis of each condition showing the side-scatter plotted against CD9 positivity Graphs represents mean ± SEM of *n=4* independent biological experiments. Two-way ANOVA was used as statistical test for graph (A) and one-way ANOVA was used for (B). * P<0.05, ****P<0.0001

In the CM of MDA-MB-468 cells after drug treatment, GW4869 significantly (*p=0.009*) decreased the CD9 positivity of mEV-gated particles compared to untreated cells (Fig, 4.12 (A)). COTI-2 also significantly (*p=0.002*) decreased the CD9 of mEV-gated particles in the CM compared to untreated cells (Fig. 4.12 (A)).

When all three sub-population events were added together, CD9 in the CM was decreased, although not significant, following GW4869, manumycin A, neratinib and COTI-2 compared to the untreated CM (Fig. 4.12 (B)). Sulfisoxazole and carboplatin did not have an effect of CD9 levels in the CM (Fig. 4.12 (B)). A summary of the drug's effects are tabulated (Fig. 4.12 (C)). Representative dot plot generated during the screen are shown (Fig. 4.12 (D)).

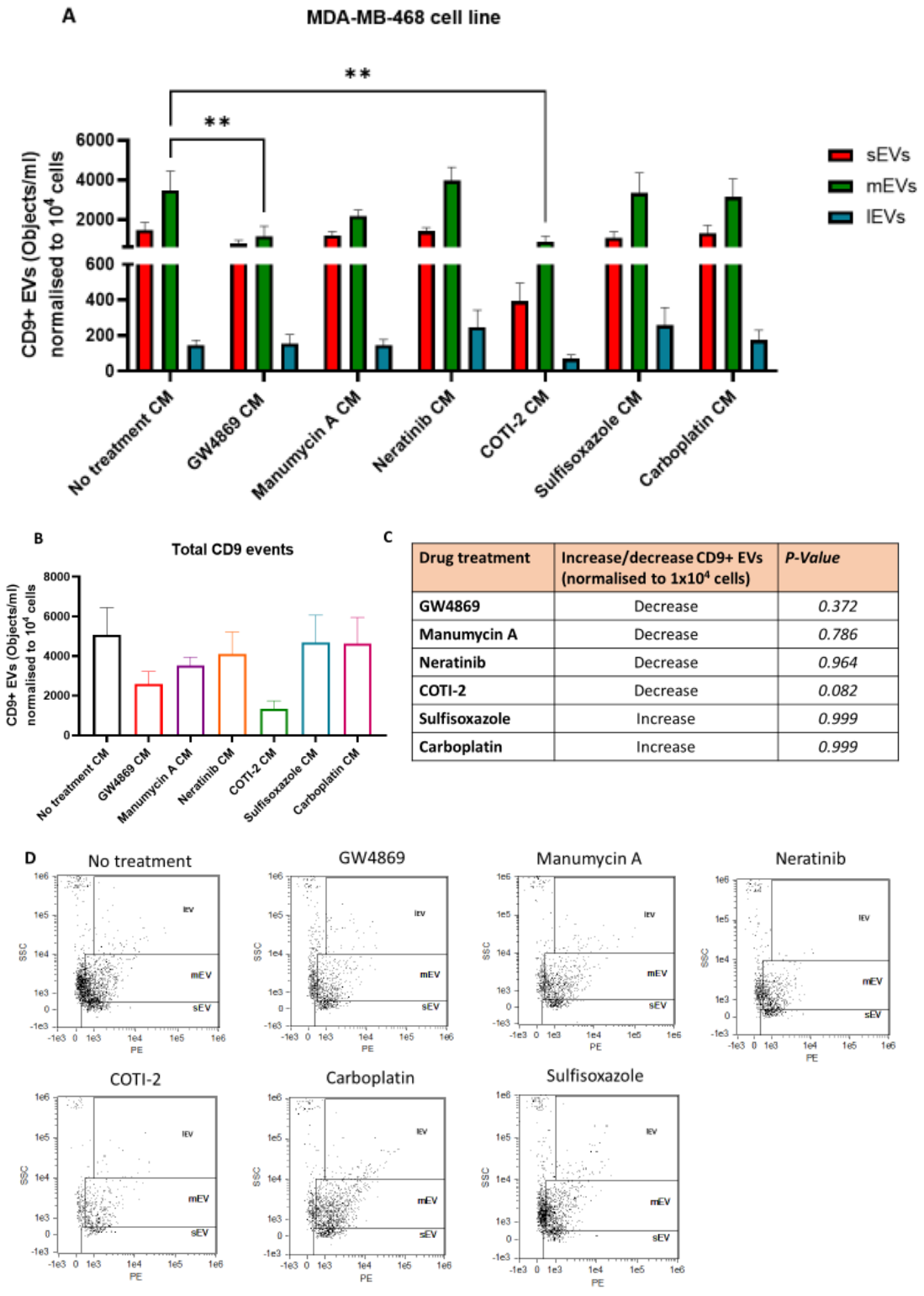

Drug treatment	Increase/decrease CD9+ EVs (normalised to 1x10^4 cells)	*P-Value*
GW4869	Decrease	*0.372*
Manumycin A	Decrease	*0.786*
Neratinib	Decrease	*0.964*
COTI-2	Decrease	*0.082*
Sulfisoxazole	Increase	*0.999*
Carboplatin	Increase	*0.999*

Figure 4.12: CD9 flow cytometry screening of MDA-MB-468 conditioned medium

MDA-MB-468 conditioned medium was screened for CD9 after 48 hrs drug treatment of the cells. (A) CD9 positive particles were detected and normalised as CD9 positive particles per 1x10^4 cells, from which the conditioned medium was collected. (B) All three sub-populations events were added together and graphed. (C) Summary of CD9 in conditioned medium after drug treatment compared to the control. (D) Representative dot plots generated after analysis of each condition showing the side-scatter plotted against CD9 positivity. Graphs represents mean ± SEM of *n=4* independent biological experiments. Two-way ANOVA was used as statistical test for graph (A). **P<0.01.

In the CM of HCC1143 cells, GW4869 significantly (*p=0.0007*) decreased the CD9 positivity of mEV-gated particles compared to untreated cells. (Fig. 4.13 (A)). When all three sub-population events were added together, CD9 was decreased, although not significant, after treatment with all inhibitors, with GW4869 having the biggest effect (Fig. 4.13 (B)). A summary of the drugs' effects are tabulated (Fig. 4.13 (C)). Representative dot plot generated during the screen are shown (Fig. 4.13 (D)).

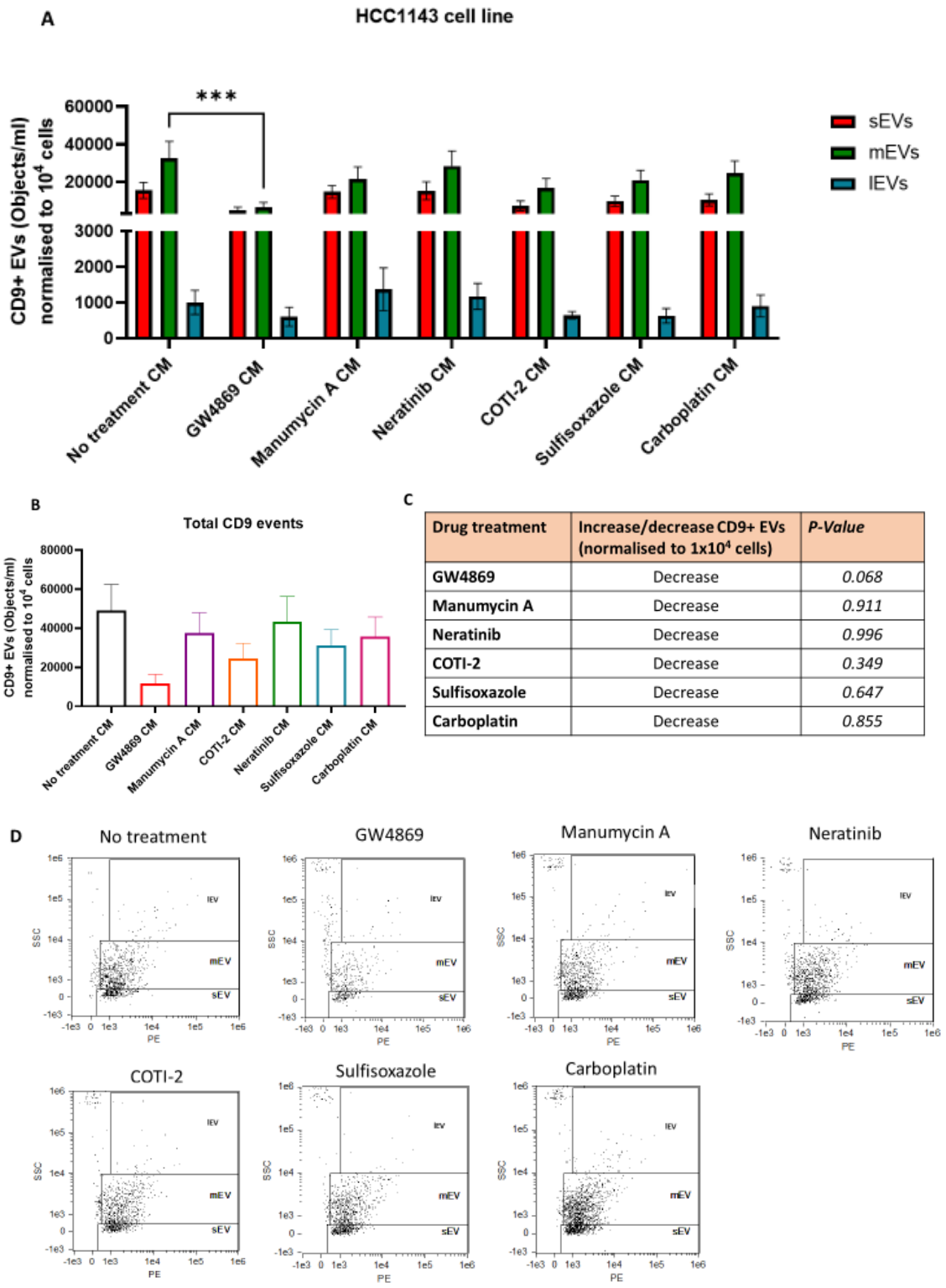

Drug treatment	Increase/decrease CD9+ EVs (normalised to 1x10^4 cells)	*P-Value*
GW4869	Decrease	*0.068*
Manumycin A	Decrease	*0.911*
Neratinib	Decrease	*0.996*
COTI-2	Decrease	*0.349*
Sulfisoxazole	Decrease	*0.647*
Carboplatin	Decrease	*0.855*

Figure 4.13: CD9 flow cytometry screening of HCC1143 conditioned medium

HCC1143 conditioned medium was screened for CD9 after 48 hrs drug treatment of the cells(A) CD9 positive particles were detected and normalised as CD9 positive particles per 1x10^4 cells, from which the conditioned medium was collected. (B) All three sub-populations events were added together and graphed. (C) Summary of CD9 in conditioned medium after drug treatment compared to the control. (D) Representative dot plots generated after analysis of each condition showing the side-scatter plotted against CD9 positivity. Graphs represents mean ± SEM of *n=4* independent biological experiments. Two-way ANOVA was used as statistical test for graph (A). ***P<0.001.

BT549 cells were treated for 48hrs, after which manumycin A significantly (*p<0.0001*) increased CD9 positivty of mEV-gated particles comared to untreated cells. (Fig. 4.14 (A).

When all three sub-population events were added together, CD9 was significantly (*p=0.002*) increased in the CM following manumycin A treatment compared to the untreated CM (Fig. 4.14 (B)). All other inhibitors also increased CD9 in the CM, although not significantly (Fig. 4.20 (B)). A summary of the drug's effects are tabulated (Fig. 4.14 (C)). Representative dot plot generated during the screen are shown (Fig. 4.14 (D)).

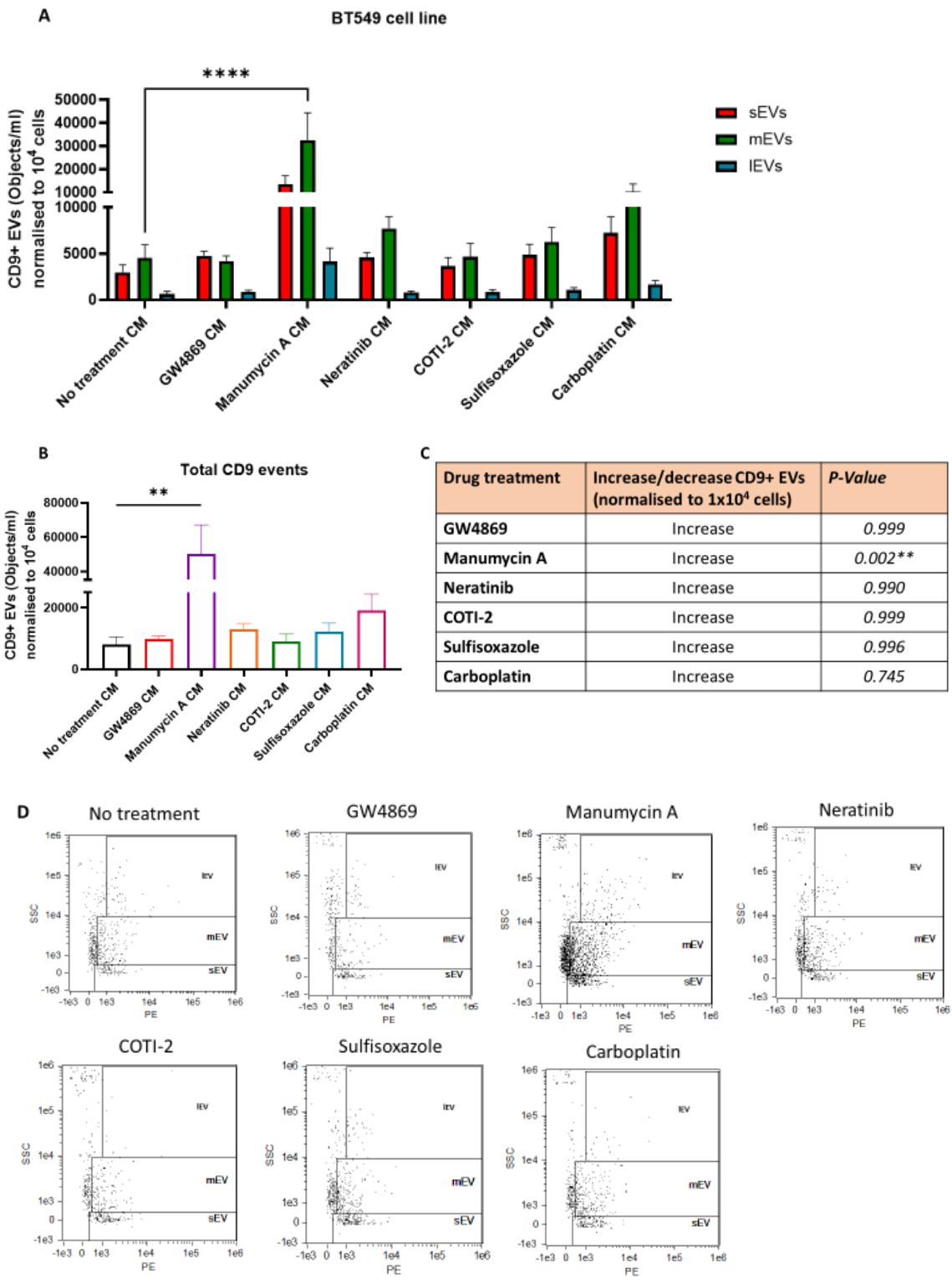

Drug treatment	Increase/decrease CD9+ EVs (normalised to 1x10^4 cells)	*P-Value*
GW4869	Increase	*0.999*
Manumycin A	Increase	*0.002***
Neratinib	Increase	*0.990*
COTI-2	Increase	*0.999*
Sulfisoxazole	Increase	*0.996*
Carboplatin	Increase	*0.745*

Figure 4.14: CD9 flow cytometry screening of BT549 conditioned medium

BT549 conditioned medium was screened for CD9 after 48 hrs drug treatment of the cells. (A) CD9 positive particles were detected and normalised as CD9 positive particles per 1x10^4 cells, from which the conditioned medium was collected. (B) All three sub-populations events were added together and graphed. (C) Summary of CD9 in conditioned medium after drug treatment compared to the control. (D) Representative dot plots generated after analysis of each condition showing the side-scatter plotted against CD9 positivity. Graphs represents mean ± SEM of *n=4* independent biological experiments. Two-way ANOVA was used as statistical test for graph (A) and One-way ANOVA was used for graph (B). *P<0.01, ****P<0.0001.

CD9 positivity of all three sub-popualtion gated was not substantially changed in the CM of MDA-MB-231 cells after drug treatment (Fig. 4.15 (A)). When all three sub-population events were added together, CD9 was decreased, although not significant, following manumycin A and COTI-2 compared to the untreated CM (Fig. 4.15 (B)). GW4869, neratinib, sulfisoxazole and carboplatin increased CD9 levels in the CM (Fig. 4.15 (B)). A summary of the drug's effects are tabulated (Fig. 4.15 (C)). Representative dot plot generated during the screen are shown (Fig. 4.15 (D)).

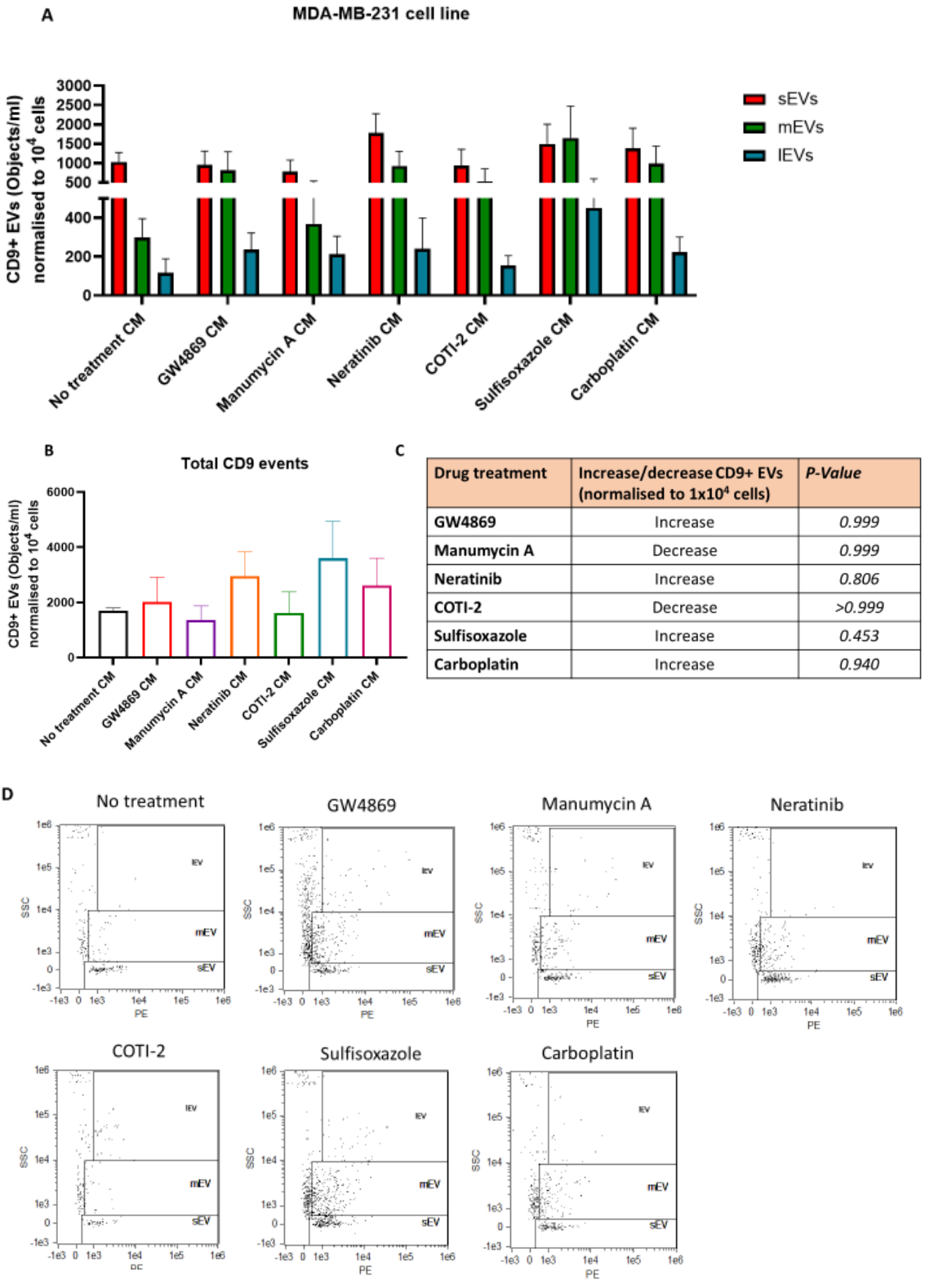

Drug treatment	Increase/decrease CD9+ EVs (normalised to 1x10^4 cells)	*P-Value*
GW4869	Increase	*0.999*
Manumycin A	Decrease	*0.999*
Neratinib	Increase	*0.806*
COTI-2	Decrease	*>0.999*
Sulfisoxazole	Increase	*0.453*
Carboplatin	Increase	*0.940*

Figure 4.15: CD9 flow cytometry screening of MDA-MB-231 conditioned medium

MDA-MB-231 conditioned medium was screened for CD9 after 48 hrs drug treatment of the cells. (A) CD9 positive particles were detected and normalised as CD9 positive particles per 1x10^4 cells, from which the conditioned medium was collected. (B) All three sub-populations events were added together and graphed. (C) Summary of CD9 in conditioned medium after drug treatment compared to the control. (D) Representative dot plots generated after analysis of each condition showing the side-scatter plotted against CD9 positivity. Graphs represents mean ± SEM of *n=4* independent biological experiments.

As a summary, each inhibitor caused different effects on detectable CD9 depending on the TNBC cell line under analysis. When comparing the effects of each inhibitor among all the TNBC cell lines with untreated control (i.e. black bars), GW4869 significantly (*p=0.0002*) decreased CD9 in the CM of the HCC1143 cell line (Fig. 4.16 (A)). Manumycin A caused a significant (*p=0.003*) increase in CD9 in the BT549 cells (Fig. 4.16 (B)). COTI-2 had different effects depending on the cell line. HCC1143 cells had significantly (*p=0.009*) less CD9 when treated with COTI-2 (Fig. 4.16 (C)). Neratinib caused either a slight increase in CD9 or almost no change when compared to untreated CM (Fig. 4.16 (D)). Sulfisoxazole and carboplatin treatment resulted in increased CD9 in the CM of all cell lines, with an exception of HCC1143 CM, although not significant (Fig. 4.16 (E-F)).

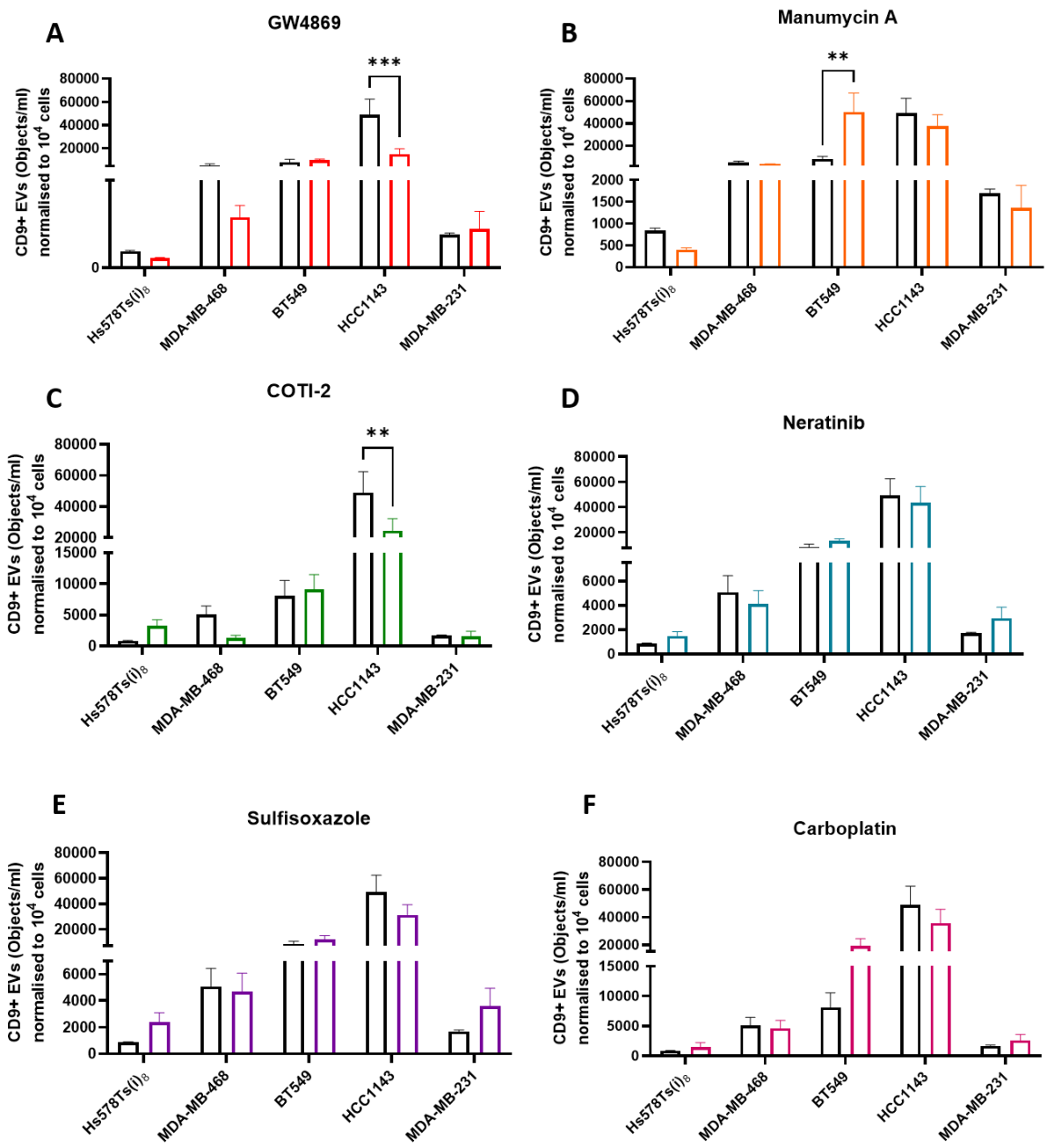

Figure 4.16: Overall summary of drug screening experiments

The results from the CD9 screening assay of all TNBC cell lines were compared together for each inhibitor to analyse the overall effects of each inhibitor in TNBC. The effects of (A) GW4869, (B) Manumycin A (C) COTI-2, (D) Neratinib, (E) Sulfisoxazole and (F) carboplatin are shown. Graphs represent mean ± SEM of *n=4* independent biological experiments. Two-way ANOVA was used as statistical test. **P<0.01, ***P<0.001.

4.4 Discussion

4.4.1 EV inhibitors study

By conducting toxicity experiments we first established the concentration of each inhibitor that was not toxic to the Hs578Ts(i)$_8$ cells. Both acid phosphatase and annexin V/PI FC assays were used, with the combination of GW4869 and manumycin A tested and calpeptin and Y27632 also tested by FC. Once the concentrations that would not cause the release of apoptotic bodies due to cell death were confirmed, we tested the ability of the inhibitors to decrease Hs578Ts(i)$_8$ cells' "aggressive" phenotype. Manumycin A significantly decreased Hs578Ts(i)$_8$ migration and GW4869 significantly decreased cell invasion. This points to a link between Hs578Ts(i)$_8$ cell motility with inhibition of nSMase and ras farnesyltrasnferase activity, by GW4869 and manumycin A, respectively. Although, there are no reported studies of manumycin A and anti-TNBC effects, there have been studies which show manumycin A can induce apoptosis *in vitro,* of various cancers such as oral squamous cell carcinoma [265], hepatocellular carcinoma [266] and prostate cancer [267]. Although GW4869 has not been studied in the context of TNBC drug treatment, either alone or in a combination. One study reported that GW4869 at a concentration of 5 µM, could decrease TNBC cells, MDA-MB-231 and MDA-MB-468, *in vitro* metastasis phenotype by decreasing 3D invasion, invasion through basement membrane and mammosphere formation [268].

After the EV separation protocol had been optimised by another PhD student in our group, Mariadelva Catalano, EVs were separated from Hs578Ts(i)$_8$ conditioned medium after the cells had been treated for 48hrs with each inhibitor. Full characterisation of the separated EVs was performed.

While other studies have used the inhibitors investigated in this project before, there are differences between this study and the others. In particular, the methods used to measure the reduction in EV release, and the methods used to characterise the EVs, which were performed to the MISEV guidelines**.** NTA analysis on the Hs578Ts(i)$_8$ EVs demonstrated that the inhibitors significantly decreased the release of EVs. GW4869 had the most substantial effect on Hs578Ts(i)$_8$ EV release. GW4869 has been used in multiple studies, as a biochemical tool to confirm that the effects observed are associated with EVs. Calpeptin has been used in multiple studies, particularly with platelet EVs, to inhibit their release. Calpeptin was shown to reduce "platelet microparticle" release in a dose-dependent manner from THP-1 monocytes [232]. However, it should be noted that EV release was measured by annexin V staining and not by particle concentration measurement techniques widely used by EV researchers. Y27632 effects on MV release from MDA-MB-231, HELA and U87 cells were determined by immunofluorescence staining for tissue transglutaminase (tTG), a protein previously

shown to be carried by MVs, with no NTA or similar technologies used [42]. Similarly, Y27632 inhibited blebbing from tumour cells, HT-1080 after stimulation with the matrikine, elastin degradation products, as visualised by phase-contrast microscopy [216]. Other studies used flow cytometry to measure the release of EVs, usually from platelets. For example, Wang *et al.* [226] measured "platelet microparticles" as annexin V+/CD61+ particles by flow cytometry. The researchers showed that when washed platelets were pre-treated with Y27632, followed by stimulation with high glucose and collagen, a decrease in annexin V+/CD61+ particles were released when compared to platelets not pre-treated with Y27632. There are only a few studies demonstrating manumycin A potential as an EV inhibitor. Jeong Oh *et al.* [113] showed while investigating neurogenesis, manumycin A inhibited the secretion of exosomes from differentiated F11 cells to undifferentiated F11 recipient cells by showing that the transfer of miR-193a was impaired and by tracking CD63-GFP labelled EVs in a microfluidic assay. EV release was inhibited by manumycin A during wound-healing processes of BUMPT cells [116]. NTA analysis showed that cell monolayers which had been wounded and subsequently treated with manumycin A had a decrease in EV release compared to wounded cells not treated. Finally, castration-resistant prostate cancer cells had decreased EV release when treated with manumycin A [114]. Specifically, they found that manumycin A targeted exosome release with a decrease in ALIX, hepatocyte growth factor-regulated tyrosine kinase substrate (Hrs) (i.e. a MVB marker) and Rab27a (i.e. a late endosome marker) was observed in C4-2B cells. Normal cell line, RWPE-1 was unaffected by manumycin A, suggesting a different pathway of exosome biogenesis between normal and prostate cancer cells.

There was no significant difference seen with protein levels of EVs after inhibitor treatment with the exception of combo 2, which significantly increased the protein levels. When comparing the EVs released as measured by NTA and the protein concentrations of the Hs578Ts(i)$_8$ EVs, there is no link between EV numbers and protein concentrations. Therefore, in our study protein concentration is a bad indicator of EV numbers. Other research groups have used a change in protein levels as a demonstration of the reduction in EV release. He *et al.* [249] measured the protein concentration of EVs from VSC 4.1 neurons after GW4869 treatment to confirm the decrease in EV release, without measuring the actual EV concentration. In another study, GW4869 was shown to inhibit EV release from dental pulp stem cells by the decrease in protein concentration of the EVs separated after GW4869 treatment [250].

Immunoblot analysis identified the presence of CD63 and syntenin in the EVs after inhibitor treatment. Calnexin was used as a negative control. This fulfilled the MISEV guidelines which require the identification of a transmembrane or GPI-anchored protein, a cytosolic protein and to assess the presence of contaminants when analysing EV preparations. It was evident that there was no

substantial effect on EV markers in the Hs578Ts(i)$_8$ EVs after treatment with the inhibitors. There was also no correlation between immunoblot analysis and NTA results. This may be due to the loading of protein concentration instead of EV numbers. However, other papers have used immunoblot to determine whether inhibitors of EV release have stopped the release. Yue *et al.* [269] determined that GW4869 was inhibiting the release of EVs from HUVECs, by a reduction in CD9 and ALIX detected on immunoblots compared to EVs isolated from DMSO-treated cells. This reduction of EVs was preventing the protection of neuronal growth. The researchers also demonstrated that GW4869 increased apoptotic cells and therefore, the decrease in CD9 and ALIX could be due to cell death and not the decrease in EV release. In another study, the densitometry of CD9, ALIX and flotillin were used to confirm that a combination of TNFα and GW4869 reduced EV release from bronchial epithelial cells compared to TNFα treatment without any additional particle measurements [256]. Similarly, Faict *et al.* [258] used immunoblot without any additional characterisation to conclude that GW4869 was decreasing EV release from murine multiple myeloma 5TGM1 cells, by a downregulation in CD81 and TSG101 compared to untreated 5TGM1 cells on the immunoblots. Detection of HSP70 protein by immunoblot was also used as a method to establish that GW4869 was decreasing EV release from an endometrial adenocarcinoma cell line, Ishikawa [270]. The researchers observed a reduction in HSP90 detection in EVs release from GW4869 treated cells when compared to untreated and DMSO treated cells. Lastly, a study demonstrated that GW4869 reduced amyloid plaques *in vivo* through the reduction in exosome release from the brains of Alzheimer's mouse model [259]. They demonstrated a reduction in mouse serum exosomes after GW4869 treatment by a reduction in ALIX on immunoblots and a decrease in serum exosome pellet protein concentration compared to untreated mice. Although all these studies show that protein markers in the resulting EVs are decreased, there are no particle measurements that show that the total particle numbers are also reduced. By showing a decrease in protein markers, they show that a pathway is inhibited, or the loading of a particular protein into the EVs is inhibited rather than actual EV inhibition.

TEM analysis of the EVs released demonstrated the presence of EVs following inhibitor treatment of the Hs578Ts(i)$_8$ cells. Sebbagh *et al.* [221] also used microscopy to evaluate Y27632 effects on Jurkat cell membrane blebbing that were undergoing apoptosis by treating the cells with anti-Fas antibody. Using phase-contrast microscopy and Hoechst 33342 labelling, the researchers demonstrated that Jurkat cells pre-treated with Y27632 had an inhibition of membrane blebbing. In a similar study, Y27632 was shown to inhibit the membrane blebbing of NIH3T3 mouse fibroblasts, which had been treated with TNFα to stimulate apoptosis [223]. This was performed by a combination of phase-contrast microscopy and scanning electron microscopy.

Acetylcholinesterase (AChE) activity has been used in EV studies as a surrogate marker for EV release with a decrease in AChE activity correlating with a decrease in release. Matsuzaka *et al.* [218] used AChE activity measurements to determine if GW4869 decreased EV release from myoblasts. In 2019, a paper published by the Thery group, established that AChE was not a universal EV marker and was associated with non-vesicular structures [271]. EVs separated with density gradients demonstrated that AChE was associated with the fractions that contained the least number of particles and contained no other EV markers.

The effects of the EVs still released after inhibitor treatment was investigated in two TNBC recipient cell lines, Hs578T and BT549. This is the first reported study that has investigated the EVs that still remain after the inhibition. Proliferation was not substantially affected in either cell line after EV treatment. EVs released from combo 2-treated Hs578Ts(i)$_8$ cells reduced Hs578T and BT549 cell proliferation at the highest EV quantity added. A greater effect was seen on TNBC cell migration, with the BT549 cell line being significantly affected. EVs still released from all inhibitor treated Hs578Ts(i)$_8$ cells, significantly decreased BT549 cell migration at the highest dose, when compared to the effects of the EVs released from Hs578Ts(i)$_8$ cells without treatment. This demonstrates that Hs578Ts(i)$_8$ EVs could increase BT549 cell migration but when treated with different inhibitors, the profile of EVs released by Hs578Ts(i)$_8$ cells changes. This change in EV release caused a substantial decrease in BT549 cell migration, indicating that a decrease in EV release may affect the transfer of aggressive phenotypes to recipient, nearby cells. As there was no substantial effect on Hs578T migration, this phenomenon needs to be further investigated in more cell lines. An investigation is also needed to identify if the inhibitors are encapsulated inside the released EVs (i.e. by HPLC) and if the drugs play a role in the effects seen on the recipient cell migration.

The investigation of EV functional capabilities after inhibitor treatment has not been fully explored, with this study among the only one looking at the cellular effects of the EVs still released following inhibitor treatment. Calpeptin was shown to increase the susceptibility of prostate cancer, PC3 cells, to docetaxel by inhibiting the release of MVs and, therefore, the removal of docetaxel from the cells [104]. This allowed the lowering down of docetaxel dose *in vivo* while still reducing tumour burden. A study investigated if GW4869 can decrease cell migration and invasion. Colorectal cancer (CRC) cells, HT29 and HCT116, incubated with exosomes derived from hypoxic HT29 and HCT116 cells had increased migration and invasion when compared to treatment with exosomes from normoxic cells [241]. When cells are also treated with GW4869, there is a reduction in the migration and invasion seen with hypoxic exosomes. As the EVs from GW4869 treated cells are not investigated, this study does not definitively show that EVs released from GW4869 cells can decrease CRC migration.

Although, all these studies demonstrate and corroborate our results, that the inhibitors used in this project can effect EV release, we have also shown that EVs which are still released may be able to decrease the transfer of caner phenotype to recipient cells. Further investigation is needed in a larger panel of TNBC cells to determine if a decrease in BT549 migration can be replicated in more cells.

4.4.2 Screening assay for EV release measurements

A method to detect a change in EV release from TNBC cell lines *in vitro* was developed with the intention of creating a protocol that can quickly give information on whether an inhibitor or drug is affecting EV release from cancer cells. By combining *in vitro* cell culture and IFCM, a screening assay was used to determine if neratinib, carboplatin, GW4869, sulfisoxazole and COTI-2 were changing EV release from a panel of TNBC cell lines, Hs578Ts(i)$_8$, MDA-MB-468, HCC1143, BT549 and MDA-MB-231.

Similar to the other inhibitors, toxicity assays with each drug, for all five cell lines were performed to choose a concentration that would be non-toxic to the TNBC cells. Next, cells were treated with each inhibitor in a 24-well plate setup, to create a small-scale collection of the CM without the need of long, laborious separation of EVs. After 48hrs, the CM was removed and pre-cleared from debris. After, the CM was screened for CD9 by IFCM. This crude way of collecting the CM gave quick results on whether a particular inhibitor had an effect on EV release. GW4869 and manumycin A were used as positive controls as they had already been used to treat the Hs578Ts(i)$_8$ cells. Neratinib, is an oral, irreversible, pan-HER tyrosine kinase inhibitor that is being investigated for use in HER2+ breast cancer but may have benefits for TNBC patients as it can also target epidermal growth factor receptor (EGFR/HER1) and HER4 [272, 273]. Sulfisoxazole (SFX) is an FDA approved oral antibiotic and was reported to inhibit small EV secretion from breast cancer cells by targeting the endothelin receptor A (ETA) [274]. However, there is some dispute whether SFX really decreases small EV release. Fonseka *et al.* [275] reported that they saw an increase in small EV release when they replicated the experiments in the same cell line, MDA-MB-231, as the original authors and by using the same EV separation protocol. Therefore, SFX was chosen to investigate if we could see an increase or decrease in a panel of TNBC cells, not just MDA-MD-231 cells. Carboplatin is a platinum-based chemotherapy that is currently being trialled for treatment of TNBC in the neoadjuvant setting or in combination with other chemotherapeutic drugs such as paclitaxel as shown by the various published clinical trials [276-279]. COTI-2 is small molecule inhibitor that has shown good efficacy in multiple cancers *in vitro* and *in vivo,* reactivating mutant p53 to wild-type p53 [280]. In the context of TNBC, it was shown to be effective in mutant-p53 TNBC cell lines [264]. All the TNBC cell lines used in this screening have mutant p53.

The results from the screening demonstrates that the potential inhibitors and other drugs had different effects depending on the TNBC cell line. It was also evident that different cell lines released a different profile of EVs. For example, Hs578Ts(i)$_8$ cells released more sEV-sized particles, whereas MDA-MB-468 cells seemed to release more mEV-sized particles. After the addition of all three sub-population CD9 events the effects of the drugs on EV release was evaluated. Hs578Ts(i)$_8$ EV release, as monitored by CD9 levels, was increased by the drugs carboplatin, sulfisoxazole, COTI-2 and neratinib. GW4869 and manumycin A decreased EV release. MDA-MB-468 CM had a decrease of CD9 with manumycin A, GW4869, neratinib and COTI-2 treatment. Sufisoxazole and carboplatin increased CD9 in MDA-MB-468 CM. HCC1143 CM had a decrease in CD9 after all treatments, whereas all drugs increased CD9 detection in BT549 CM. Finally, manumycin A and COTI-2 decreased CD9 in MDA-MB-231 CM, whereas GW4869, neratinib, sulfisoxazole and carboplatin increased CD9. Overall, this is quick method to screen multiple drugs at once, to check if they have an effect on EV release, taking the most interesting results forward and performing a full-scale EV isolation. For example, the differential effects of COTI-2 are interesting, with a significant decrease in CD9 for HCC1143 cells but an increase in Hs578Ts(i)$_8$ cells. Similarly, carboplatin increases CD9 in BT549 CM but decreases CD9 in HCC1143 CM. With carboplatin currently being trialled for the treatment of TNBC, the consequences of carboplatin treatment on EV release in patients should be explored. The BT549 CM had a substantial increase in CD9 when treated with carboplatin but CD9 remained unchanged when BT549 cells treated with neratinib. This is an example of how a tumour treatment could be personalised. If the BT549 cells represented a patient's tumour, neratinib would be a better treatment option when compared to carboplatin, to avoid the increase in EVs released from tumour cells and thus hampering the effects of the drug. When the results from the Hs578Ts(i)$_8$ CM screening are compared to results from the full Optiprep density gradient EV isolation (see Fig. 4.4) after GW4869 and manumycin A treatment, the screening method shows a trend similar to the fully separated EVs. GW4869 caused a 98% decrease and manumycin A caused a 64% decrease of EV release from Hs578Ts(i)$_8$ cells based on NTA analysis (See. Fig. 4.4). The IFCM screening results using the crude CM demonstrated that GW4869 treatment resulted in a 48% decrease and manumycin A resulted in a 60% decrease in CD9 positivity. Both methods demonstrated similar trends although, the full EV isolation using the "gold standard" Optiprep density gradient method showed a significant reduction in EV release from the Hs578Ts(i)$_8$ cells. However, it must be noted that both methods cannot be directly compared to each other as the crude CM was used for CD9 analysis and therefore, measuring only CD9 may not detect all EVs in the CM and consequently, the effects of GW4869 and manumycin A. Further validation with more EV markers is therefore needed such as CD63.

There have been many studies that have demonstrated the detrimental effects of chemotherapy treatment and the propagation of the cancer due to increased EV release. The increase in EVs released after chemotherapeutic agent administration have shown to increase chemoresistance, increase tumour metastasis, and can change the cargo in the EVs released. Human oral epidermoid carcinoma, KB cells, resistant to vincristine, treated with the chemotherapeutic agent vincristine, had elevated EV release and increased ABCB1 protein on the EVs [281]. These EVs were able to transfer ABCB1 to recipient sensitive cells. Doxorubicin, a substrate of ABCB1 was pumped out of cells that had acquired ABCB1 from taken up EVs, spreading the chemoresistance of doxorubicin. MDA-MB-231 cells were treated with a physiological dose of paclitaxel which caused the redistribution of survivin into the cytosol and increased survivin protein in exosomes released when compared to DMSO treatment. These exosomes conferred a survival advantage to NIH3T3 fibroblasts and promoted the chemoresistance of SKBR3 cells to paclitaxel treatment [282]. Chemotherapy can also push the cancer cell derived EVs to become pro-metastatic. Myeloma cells, CAG-HPSE (i.e. CAG myeloma cells that overexpress heparanase) treated with proteasome inhibitors bortezomib, carfilzomib or melphalan had increased EV release along with increased heparanase on their corresponding EV surface which is able to degrade heparan sulfate in the ECM [283]. These EVs could deliver and increase heparanase activity in myeloma cells, CAG and RPMI 8226, which normally express low levels of heparanase and could also enhance RAW 264.7 murine macrophage migration and TNFα secretion *in vitro*, which has been shown to aid myeloma tumour growth. Ovarian cancer spheroids treated with cisplatin released EVs that promoted the pro-tumourigenic profile of bone marrow-mesenchymal stem cells (BM-MSCs), through increased migration and MMP2 activity, increased secretion of il-6 and VEGFA, increased induction of angiogenesis, and increased the invasion of the low-metastatic ovarian cancer cell line, Ovcar3 [284].

As described, chemotherapy can negatively impact the reduction in tumour growth by promoting EV release and activate signalling in the tumour microenvironment. The EVs themselves enhance tumour growth when exposed to certain therapeutics. Researchers are trying to use this to the patient's advantage, by using EVs as a monitoring tool for therapy response and as liquid biopsies to identify biomarkers that could potentially help stratify patients into different treatment arms that are more suitable for their tumour type.

In the future, this screening assay could be used to improve "personalised medicine" for patients. As well as the molecular subtyping of a patients' tumour to determine the best treatment option, a screening of EV release with a particular drug could also be assessed. This could minimise the added disadvantages that a therapy can have on EV release and further signalling of the cancer cells, evading the drugs' response.

4.5 Conclusion

4.5.1 EV inhibitor study

The aim to fully characterise proposed EV inhibitors in the TNBC cell line, Hs578Ts(i)$_8$ while keeping within the requirements set out by the MISEV guidelines was achieved. A thorough characterisation of the EVs by NTA, BCA assay, immunoblot analysis and TEM analysis was performed.

We concluded that the proposed EV inhibitors, calpeptin, Y27632, GW4869 and manumycin A, at non-toxic concentrations, decreased EVs released by Hs578Ts(i)$_8$ cells. The EVs that were still released after inhibitor treatments caused a substantial reduction in BT549 migration, which may be due to the change in EV profile released.

4.5.2 Screening assay for EV release measurements

It is well established that EVs released from tumour cells after treatment can have negative consequences on the clearance of the tumour and can help promote cancer cell growth through the development of resistance to the chemotherapy, escalating the metastasis of tumour cells and initiate the formation of pre-metastatic niche. Chemotherapy can induce changes in the cargo of the EVs released from cancer cells, which can be transferred to other cancer cells nearby, creating a vicious circle for treatment outcomes.

By developing a screening assay, that is quick and user-friendly, we determined whether potential inhibitors could affect EV release. Further validation is needed including a full-scale EV separation to determine if the screening results do reflect the actual effect on EV release.

Chapter 5: Triple-Negative Breast Cancer EVs and Platelet aggregation

5 Abstract

Tumour cell induced platelet aggregation (TCIPA), a mechanism whereby cancer cells activate platelets and enhance their aggregation and so is associated with thromboembolism, was investigated with the TNBC cell line variants, Hs578T and Hs578Ts(i)$_8$, and their EVs. Upon the discovery that TNBC cell line variants and their derived EVs induced platelet aggregation in a dose-dependent manner, proteomic analysis was performed on the EVs to identify proteins that may potentially be responsible for the aggregation seen.

Key proteins identified by proteomic analysis then investigated in the EVs by immunoblot were platelet-derived growth factor receptor β (PDGFRβ), Cyr61, Urokinase plasminogen activator receptor (uPAR), glypican-1, mucin 18 (MUC18) or CD146 and CD97. Densitometry revealed that Hs578T EVs had significantly (*p=0.020*) higher levels of Cyr61 compared to Hs578Ts(i)$_8$ EVs. CD97 was significantly (*p=0.045*) higher in Hs578Ts(i)$_8$ EVs compared to Hs578T EVs. Similarly, uPAR had significantly (*p=0.002*) higher quantities in the Hs578Ts(i)$_8$ EVs compared to the Hs578T EVs.

In conclusion, with cancer associated thrombosis a major problem, the proteins identified as cargo of the TNBC EVs, that may be involved in platelet interaction and aggregation, may provide further insight into the mechanisms by which cancer EVs contribute to thrombosis and may provide targets for new therapeutic interventions.

5.1 Introduction

Thrombosis has an annual incidence rate of 0.5% among cancer patients and 0.1% in the general population, with cancer patients accounting for 15-30% of all patients diagnosed with venous thromboembolism (VTE). Some risk factors of cancer-associated thrombosis (CAT) include age, gender, stage of cancer, chemotherapy, and increased levels of tissue factor (TF) [285]. Cancer cells contribute to the hypercoagulable state by releasing various coagulation factors including TF, cancer pro-coagulant, heparanase, and through the shedding of EVs that express high levels of TF and phosphatidylserine (PS) [286]. It has long been established that tumours express pro-coagulant TF which is main activator of the coagulation cascade and can promote tumour growth [287]. Following this, TF has been identified on EVs released by tumour cells and platelets, leading to CAT and aiding cancer metastasis. Although, the mechanisms by which this occurs is still poorly understood.

A study in gastric cancer patients (*n=109*) concluded that platelet microparticles were elevated in the plasma of stage IV patients compared to stage I or stage II/III [288]. Several studies have implicated TF present on EVs, mainly platelet EVs, and thrombin generation as two potential activators of platelet aggregation. The negatively charged surface of the EVs also provide a suitable surface for components of the coagulation cascade to bind. TF activity (i.e. measured by FXa generation) was higher in a sample consisting of platelets and microparticles from cancer patients plasma (*n=20*), including lung, prostate, pancreas, kidney, breast, soft tissue and colon cancer, compared with healthy individuals (*n=23*), indicating that TF on the EV surface and platelets can contribute to the hypercoagulable state in cancer patients [289]. Microparticles from plasma of patients with early stage prostate cancer (*n=68*) had higher TF-specific pro-coagulant activity (i.e. measured by clotting assay) compared with microparticles from the plasma of healthy control (*n=20*) [290].

EVs can interact with other blood-borne cells to promote CAT. Leal *et al.* [291] observed that 4T1 breast cancer cell derived exosomes, as termed by the authors, were elevated in the plasma of a thrombotic, tumour-bearing mouse model. The exosomes could induce neutrophil extracellular traps (NET) formation in G-CSF primed neutrophils *in vitro*. The researchers reported that 4T1-derived exosomes induced venous thrombus formation in tumour-free mice treated with G-CSF, to similar levels seen in tumour-bearing mice. This study demonstrates that EVs and neutrophils may act together during the induction of cancer thrombosis.

A summary of other studies that have implicated EVs in the development of CAT, by analysing cancer patient's samples, isolating EVs from cancer cell *in vitro* or using *in vivo* mouse models of thrombosis,

are tabulated below (see table 5.1). Although TF has been heavily implicated in CAT, many other proteins may play a role in platelet aggregation and signalling.

Cells/biofluid used	Isolation method	Characterisation methods	Aggregation measured	Ref
Plasma from 4T1-tumour bearing mice. 4T1 cells	100,000g spin (x2) and pellet filtered with 0.2 µm filter. Cell culture medium EVs isolated with ExoQuick.	NTA and BCA	• Clotting assay using platelet-poor plasma	[291]
Pancreatic cancer cells e.g. Capan-2, Panc-1 and MiaPaCa-2. Plasma from pancreatic cancer mouse models.	100,000g spin (x1) to isolate microparticles	None reported	• TF measured by FACs • PS measured using the Zymuphen MP-activity kit • FXa generation assay	[292]
C57BL/6J mice used for IVC stenosis model. Panc02 cells	20,000 g spin to isolate microparticles	BCA, and Flow cytometry	• Intravital microscopy to visualise thrombus • Measure thrombus weight and length	[293]
Plasma from ApoE knockout C57BL/6J mice used for atherosclerosis model	Platelets activated with thrombin and spin at 20,000g (microvesicles) and 120,000g (exosomes)	NTA, TEM and Immunoblot	• Immunohistochemistry of atherothrombotic artery	[294]
C57BL/6J mice. Pancreatic cancer cells, BxPc-3 and L3.6pl	Microvesicles isolated from cell culture medium by 20,000g spin	BCA and TEM	• TF activity assay • Platelet aggregometry after incubation with microvesicles • Thrombin generation measured using calibrated automated thrombogram • Measure thrombus size *in vivo*	[295]
C57BL/6J used for thrombosis model. Endothelial cells isolated from umbilical veins. Plasma from human donors.	Endothelial microparticles isolated by 100,000g spin (x1). Microparticles isolated from human plasma by 15,000g spin.	Flow cytometry	• Platelet aggregometry after incubation with microparticles • Thrombus visualisation by fluorescence microscopy • Platelet and microparticle binding by FACS	[296]
Plasma from patients with acute DVT (*n=25*), recurrent DVT (*n=25*) and healthy controls (*n=25*)	Microparticles were prepared by centrifuging platelet-free plasma 100,000g	FACS using annexin V, Cellular origin of MPs by FACS using CD14, CD41a, CD235b and CD144 antibodies	• TF Chromogenic Activity Assay used to measure TF pro-coagulant activity	[297]
Cancer cells, MDA-MB-231, MCF-7, A549 and NB4	Microvesicles isolated by 20,000g spin and exosomes isolated by 100,000g spin	TEM and Immunoblot	• Fibrin clot formation assay with platelet poor plasma	[298]

			• Clot lysis assay	
MDA-MB-231 and MCF-7 breast cancer cells	ExoQuick	BCA, NTA, TEM and Immunoblot	• Platelet and EV interaction by CSFE-staining of EVs • Washed platelet aggregation measurements • P-selectin exposure on platelets	[299]
Mixture of microparticle and platelets from cancer patients	Platelet-rich plasma prepared by 200g and 20,000g spin	TEM	• TF activity measured using chromogenic assay • Soluble p-selectin and D-dimer measured in plasma by ELISA	[289]
Human (SOJ-8) and mouse (Panc02) pancreatic cancer cells and mouse Lewis ling carcinoma, LLC1 cells. C57BL/6J mice used for $FeCl_3$-induced thrombosis model	Microparticles were isolated from cell culture medium by 20,000g spin	BCA, Annexin V flow cytometry	• TF activity measured by chromogenic assay • Washed platelet aggregation experiments • Visualise thrombus by intravital microscopy	[166]

Table 5.1: Summary of studies of EVs and cancer-associated thrombosis

BCA=Bradford colorimetric assay, NTA=Nanoparticle tracking analysis, TEM=Transmission electron microscopy, TF=Tissue factor, PS=Phosphatidylserine,

5.2 Aims of study

Here we aimed to determine if TNBC cell line variants, Hs578T and Hs578Ts(i)$_8$, and their corresponding EVs, can induce platelet aggregation. There has only been one previous study investigating MDA-MB-231-derived EVs. However, different analysis was performed to measure platelet aggregation.

The subsequent overall objective was to perform global proteomic profiling of the TNBC EVs, to identify proteins carried by the TNBC EVs, other than the well-established TF, that may be involved in platelet aggregation.

5.3 Results

5.3.1 Characterisation of EVs from TNBC cell line variants

EVs separated from isogenic triple-negative breast cancer cell line variants, Hs578T and Hs578Ts(i)$_8$ using protocol described in section 2.2.1, were characterised by NTA (Fig 5.1 (A-B)) to estimate the concentration and size of the EVs released by both cell line variants. BCA assay was used to measure the protein of the separated EVs (Fig. 5.1 (C)). There was no significant difference in protein levels between the two variants. Immunoblot analysis demonstrates the presence of EV with the detection of common EV markers such as flotillin and CD63 (Fig. 5.1 (D)). Calnexin was used as a negative control. TEM analysis also confirms the successful separation of EVs (Fig. 5.1 (E)).

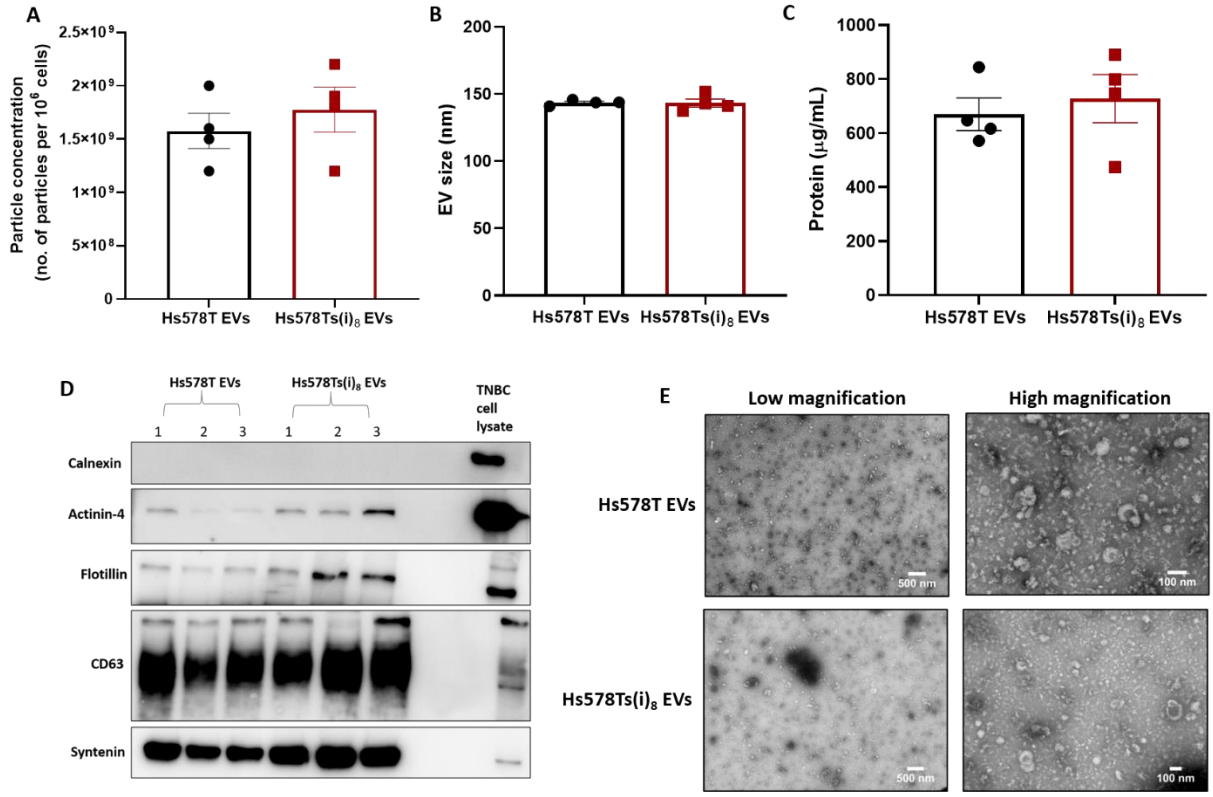

Figure 5.1: Characterisation of EVs from TNBC cell line variants

Extracellular vesicles separated from the Hs578T and Hs578Ts(i)$_8$ cell line variants were characterised by NTA (A-B) and BCA assay (C). A representative Immunoblot, with 1-3 representing 3 independent EV isolations (D), and TEM analysis (E) is shown. TEM images are taken at 5000X (i.e. low) and 20000X (i.e. high) magnification with scale bar of 500 nm and 100 nm, respectively. Graphs represent mean ± SEM of *n=4* independent experiments.

5.3.2 Tumour Cell Induced Platelet Aggregation (TCIPA) by TNBC cell line variants

Initial experiments were performed, as described in section 2.8.3, to determine if the TNBC cell line variants themselves cause TCIPA. Washed platelets were prepared from the blood of healthy donors and washed with Tyrode's buffer (see section 2.8.1). The lag phase or time taken for the induction of aggregation when the TNBC cells were incubated with washed platelets was measured. Both cell line variants caused a significant reduction in the time taken for induction of TCIPA compared to the control (*P< 0.0001*) (Fig. 5.2 (A-B)). When the two cell line variants were compared, there was no significant between their TCIPA-inducing effects (Fig. 5.2 (C)). Aggregated platelets were fixed and imaged under a light microscope after the experiments had ended (Fig. 5.2 (D)).

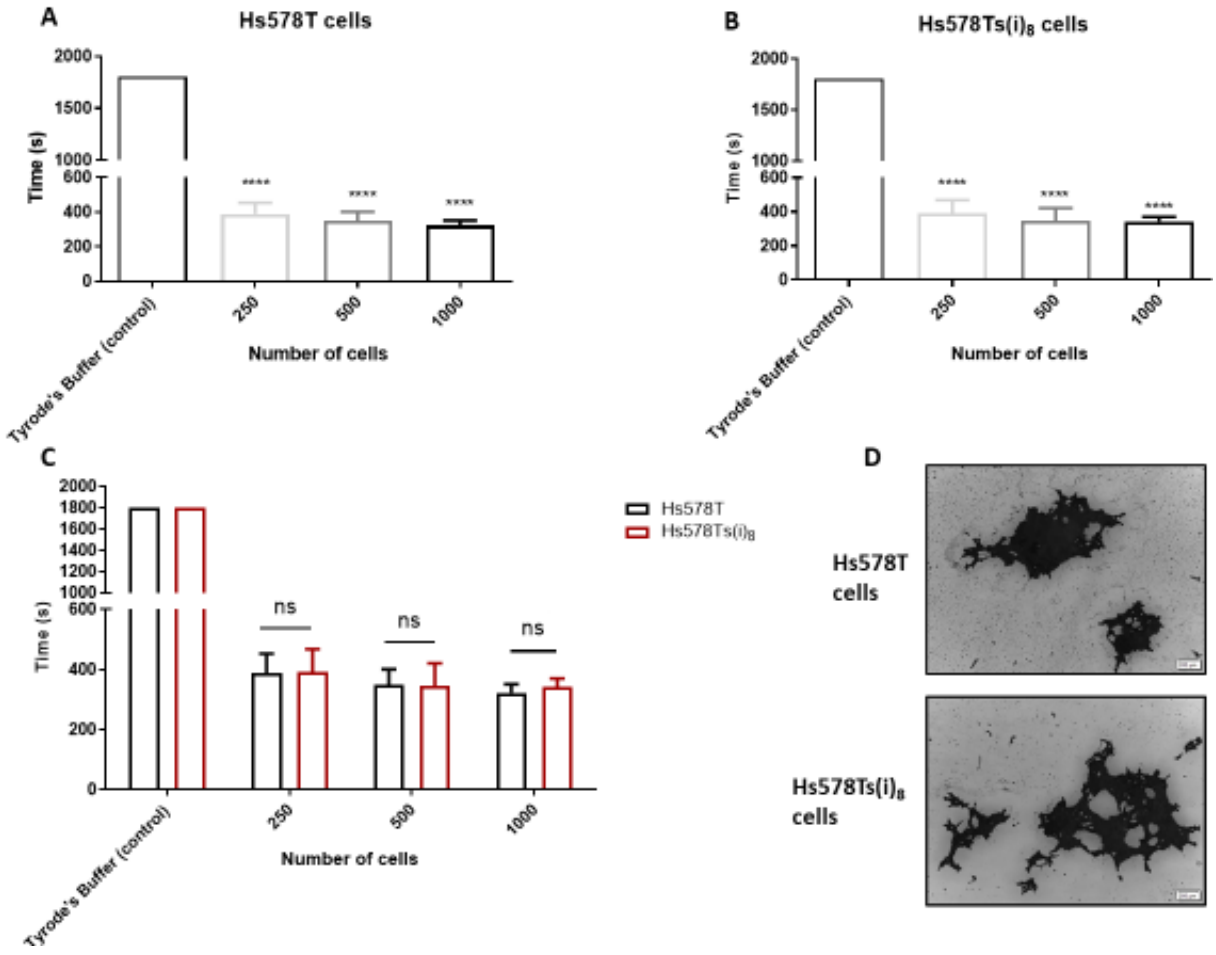

Figure 5.2: Measurements of platelet aggregation induced by TNBC cell line variants

The lag phase was measured upon (A) Hs578T or (B) Hs578Ts(i)$_8$ incubation with washed platelets. (C) Data generated with Hs578T and Hs578Ts(i)$_8$ cells was co-analysed together to determine if there was a significant difference in the lag phase between the two cell line variants. (D) Phase contrast microscopy was used to image aggregated platelets. Scale bar is 200 nm. Graphs represent mean ± SEM and are *n=4* independent experiments. One-way ANOVA performed for (A) and (B) and a two-way ANOVA performed for (C). ****P<0.0001.

5.3.3 TCIPA by EVs from TNBC cell line variants

As the cells induced TCIPA, EVs from each cell line variant were tested for their ability to induce platelet aggregation as described in section 2.8.3. EVs from both cell line variants significantly decreased the lag phase for the onset of platelet aggregation (*P<0.0001*). The more EVs were incubated with the washed platelets, the shorter the time for the induction of platelet aggregation (Fig. 5.3 (A-B)). As with their cells of origin, there was no significant difference when both EVs were compared (Fig. 5.3 (C)). Aggregated platelets were fixed and imaged under the microscope after the experiments had ended (Fig. 5.3 (D)).

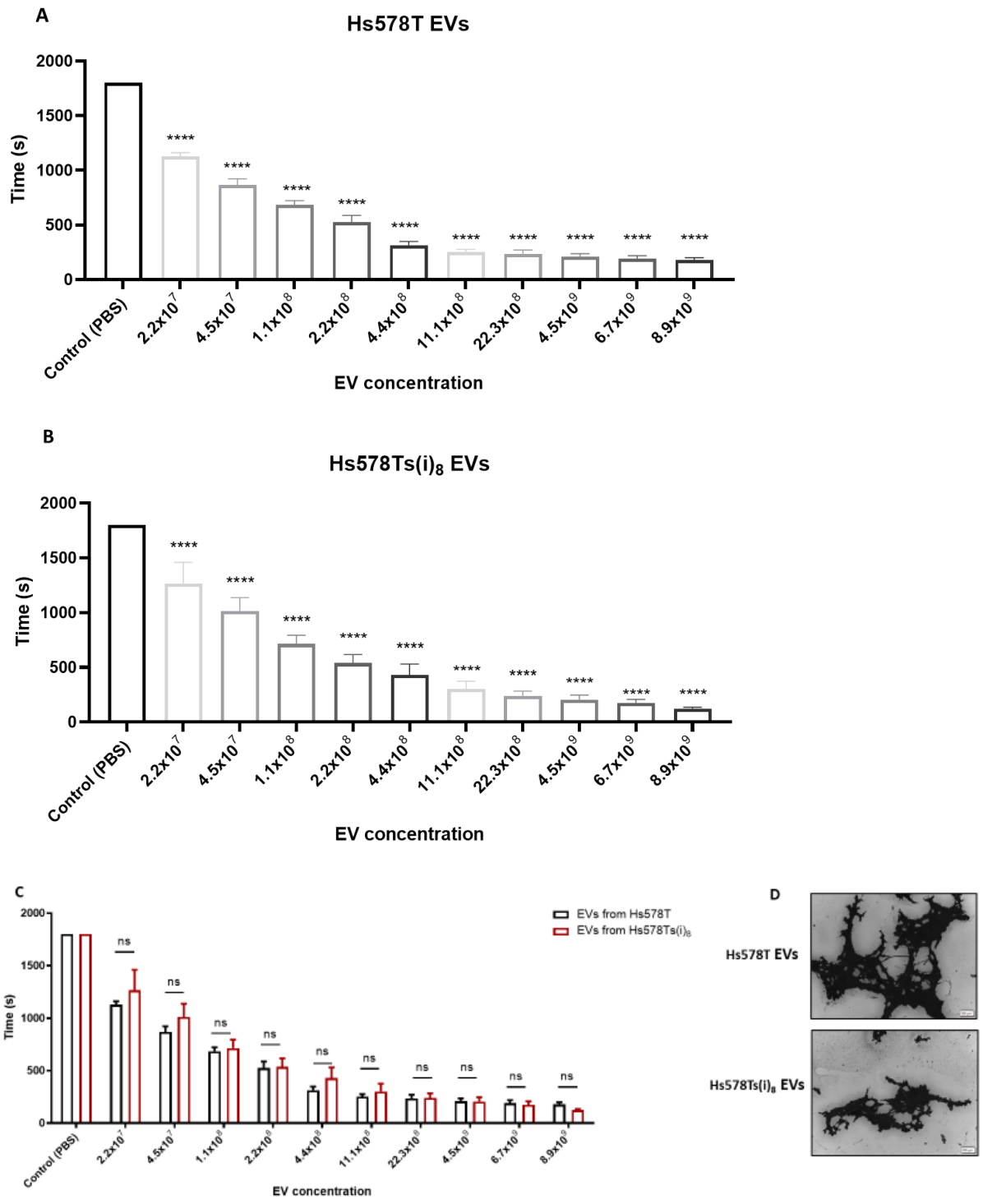

Figure 5.3: Measurements of platelet aggregation induced by EVs released from TNBC cell line variants

The lag phase was measured upon (A) Hs578T and (B) Hs578Ts(i)$_8$ EVs incubation with washed platelets. (C) Data generated with Hs578T and Hs578Ts(i)$_8$ EVs were analysed together to determine if there was a significant difference in the TCIPA-inducing effects between the two cell line variants. (D) Phase contrast microscopy was used to image aggregated platelets. Scale bar is 200 nm. Graphs represent mean ± SEM and are *n=4* independent experiments. One-way ANOVA performed for (A) and (B) and a two-way ANOVA performed for (C). ****P<0.0001.

5.3.4 Mass spectrometry analysis of protein cargo of EVs from TNBC cell line variants

Proteomic profiling was performed on EVs separated from the cell line variants. EVs were prepared by in-solution digestion of the EV protein (see Section 2.9.1). Unsupervised hierarchical clustering was performed, visually showing that EVs from the cell line variants have distinct patterns of protein levels, clearly demonstrated at the top and bottom of the heatmap, with green representing low intensity and red representing a higher intensity (Fig. 5.4 (A)). EVs from each cell variant contained five exclusive proteins each (Fig. 5.4 (B)). A Venn diagram illustrates that the EVs contained 760 proteins in total between the two variants (Fig 5.4 (C)). As a confirmation of successful proteomic analysis and comparison with other published EV research, the top 100 reported proteins identified in EVs from both the Exocarta and Vesiclepedia databases were downloaded and compared with the proteins identified in the TNBC EVs (Fig 5.4 (D)).

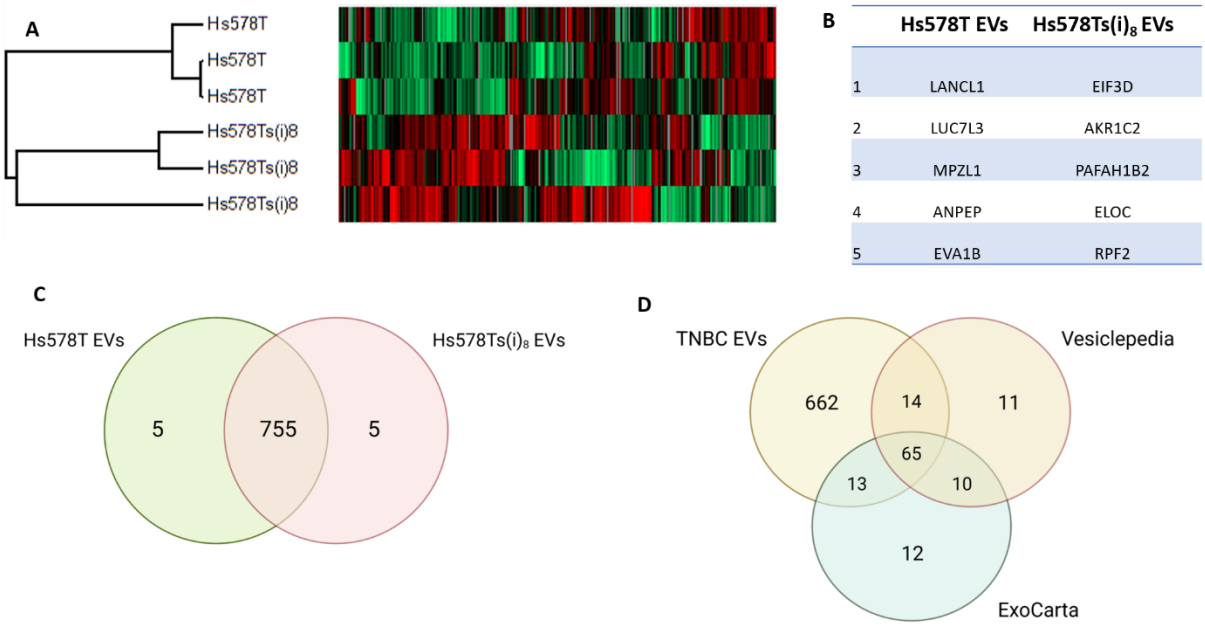

Figure 5.4: Identification of proteins in EVs and comparison with online databases

Perseus software was used to perform statistical analysis on the MS data. (A) Heatmap of unsupervised clustering of z-scored protein intensities. (B) Gene names of the 5 proteins identified exclusively in each cell line variant EV. (C) Venn diagram was created to represent the number of proteins identified in the EVs. (D) The online databases of Top 100 protein from "Vesiclepedia" and "Exocarta" were downloaded and compared with the total proteins detected in the EVs.

5.3.5 Investigation of potential function of proteins detected on EVs from TNBC cell line variants

Using FunRich, an EV functional enrichment tool, the proteins identified in the TNBC EVs were compared with the total number of proteins reported on the Vesiclepedia database, with thirty three proteins present in the TNBC EVs that have not been previously documented to exist in EVs (Fig. 5.5 (A)). Gene enrichment analysis identified that the following cellular components; exosomes, centrosomes, lysosomes, ribosomes, cytoplasm, mitochondrion, extracellular region and membrane are the most significantly associated with the proteins identified in the TNBC EVs (Fig. 5.5 (B)). Platelet-related signalling pathways that are associated with the proteins include, platelet degranulation, formation of fibrin clot and platelet-derived growth factor receptor β signalling pathway (Fig. 5.5 (C)).

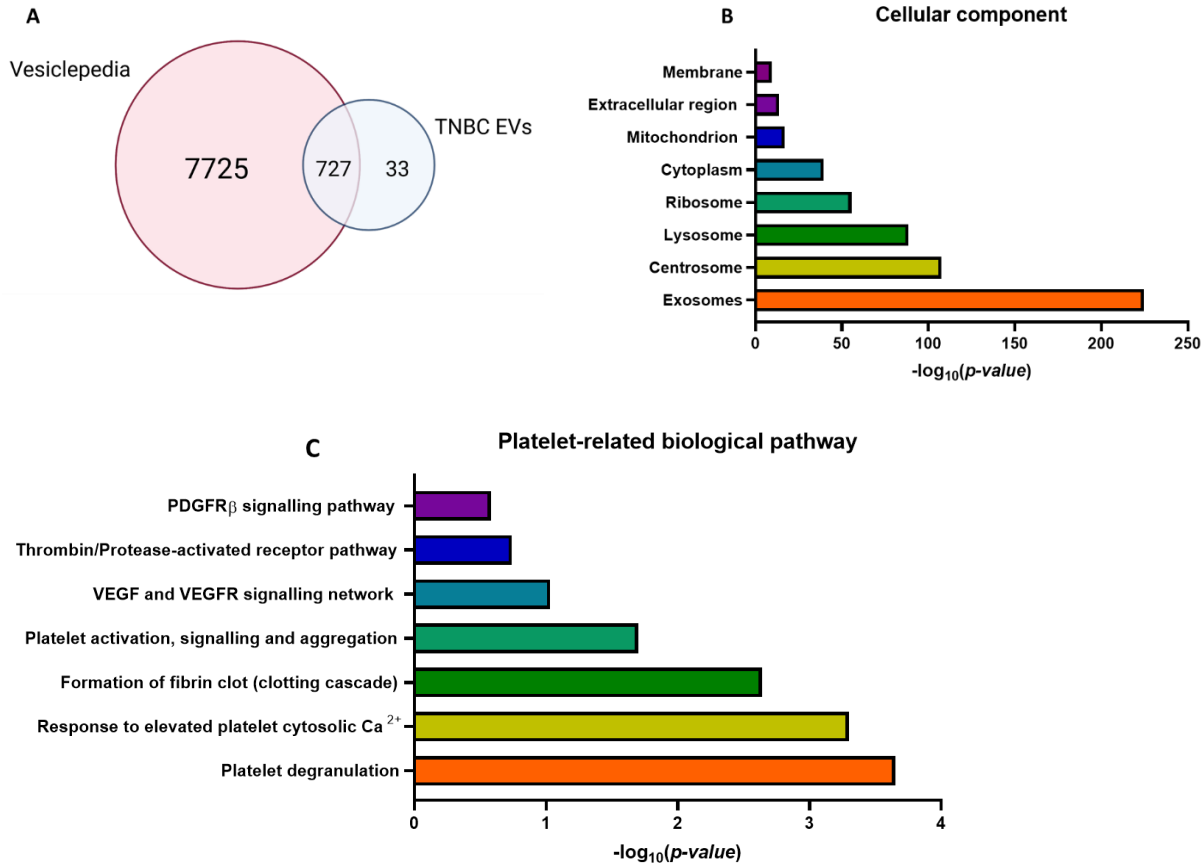

Figure 5.5: Functional enrichment using the FunRich analysis tool

Gene enrichment analysis was performed using FunRich. (A) Hs578T and Hs578Ts(i)$_8$ EVs proteins were compared to all reported EV proteins on the "Vesiclepedia" database. (B) Cellular component analysis was performed with substantially enriched components graphed. (C) platelet-related biological pathways that were significantly associated with the TNBC EVs were graphed.

5.3.6 Evaluation of mass spectrometry in EVs from TNBC cell line variants

Following their identification as present in the EVs by mass spectrometry analysis, several proteins which are related to platelet functions or TNBC disease were evaluated by immunoblot. Platelet-derived growth factor receptor β (PDGFRβ) was detected in both EVs by mass spectrometry. It was significantly (*p=0.001*) higher in the Hs578T EVs (Fig. 5.6 (A)). It was also higher in the Hs578T EVs by immunoblot analysis, although not significant, compared to Hs578Ts(i)$_8$ EVs (Fig. 5.6 (G)).

Protein Cyr61 was detected in both cell line variant EVs by mass spectrometry, with a higher quantity visible in the Hs578T EVs compared to the Hs578Ts(i)$_8$ EVs (Fig. 5.6 (B)). Densitometric analysis on Cyr61 immunoblot also demonstrated a significantly (*p=0.020*) higher quantity in the Hs578T EVs (Fig. 5.6 (H)).

Mass spectrometry identified a higher detection of CD97 in the Hs578Ts(i)$_8$ EVs compared to the Hs578T EVs (Fig. 5.6 (C)). Immunoblot and densitometry demonstrated that CD97 was significantly (*p=0.045*) higher in the Hs578Ts(i)$_8$ EVs compared to Hs578T EVs (Fig. 5.6 (I)).

Glypican-1 label-free quantification (LFQ) intensity was significantly (*p=0.012*) higher in the Hs578Ts(i)$_8$ EVs compared to the Hs578T EVs (Fig. 5.6 (D)). Greater levels were seen by immunoblot (Fig. 5.6 (J)).

Cell surface glycoprotein MUC18 (MUC18) or CD146 was detected in both TNBC EVs, with significantly (*p=0.028*) more in Hs578T EVs (Fig. 5.6 (E)). However, immunoblotting showed no significant difference between the two EVs (Fig. 5.6 (K)).

Urokinase-type plasminogen activator receptor (uPAR) was significantly (*p=0.0004*) higher in the mass spectrometry analysis of Hs578Ts(i)$_8$ EVs compared to Hs578T EVs (Fig. 5.6 (F)). Similarly, densitometric analysis on the immunoblots demonstrated a significantly (*p=0.002*) higher amounts of uPAR in the Hs578Ts(i)$_8$ EVs compared to Hs578T EVs (Fig. 5.5 L)). Immunoblots performed are shown (Fig 5.6 (M)). A summary of all protein levels detected by mass spectrometry and immunoblot is tabulated (N).

Mass spectrometry data:

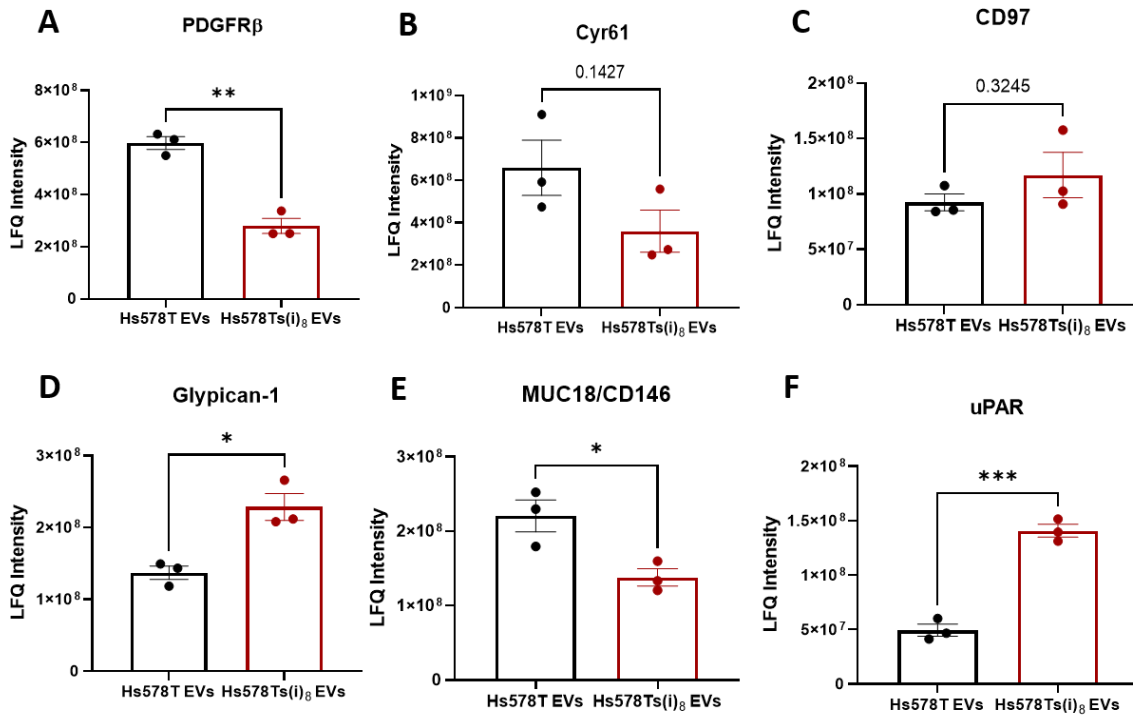

Immunoblotting data:

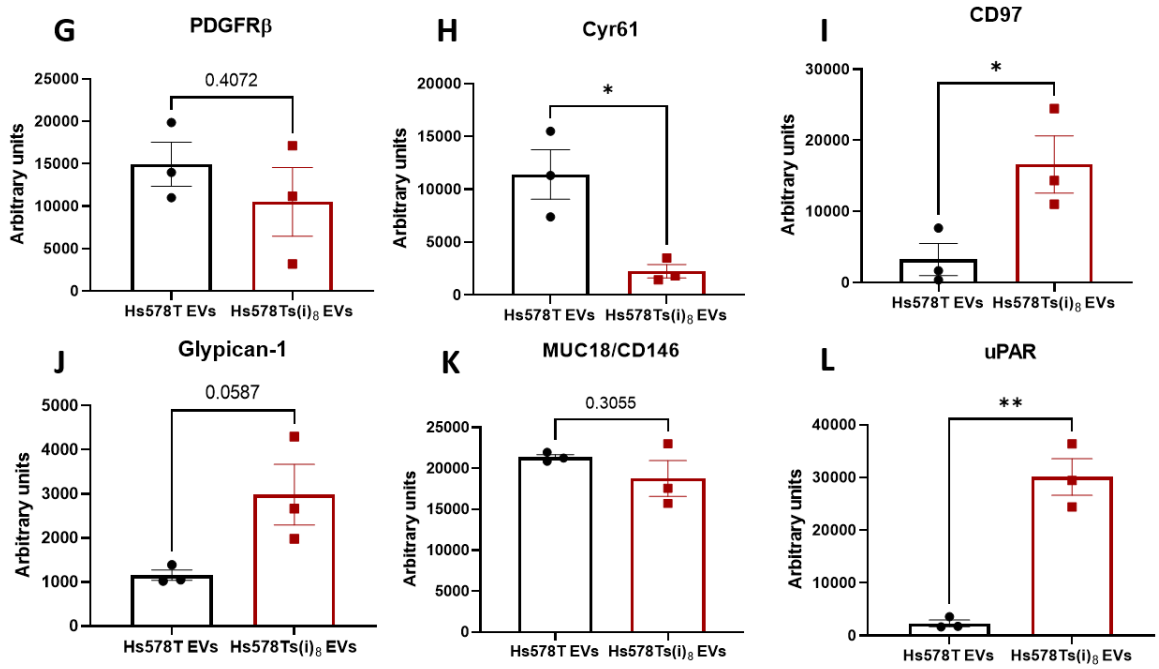

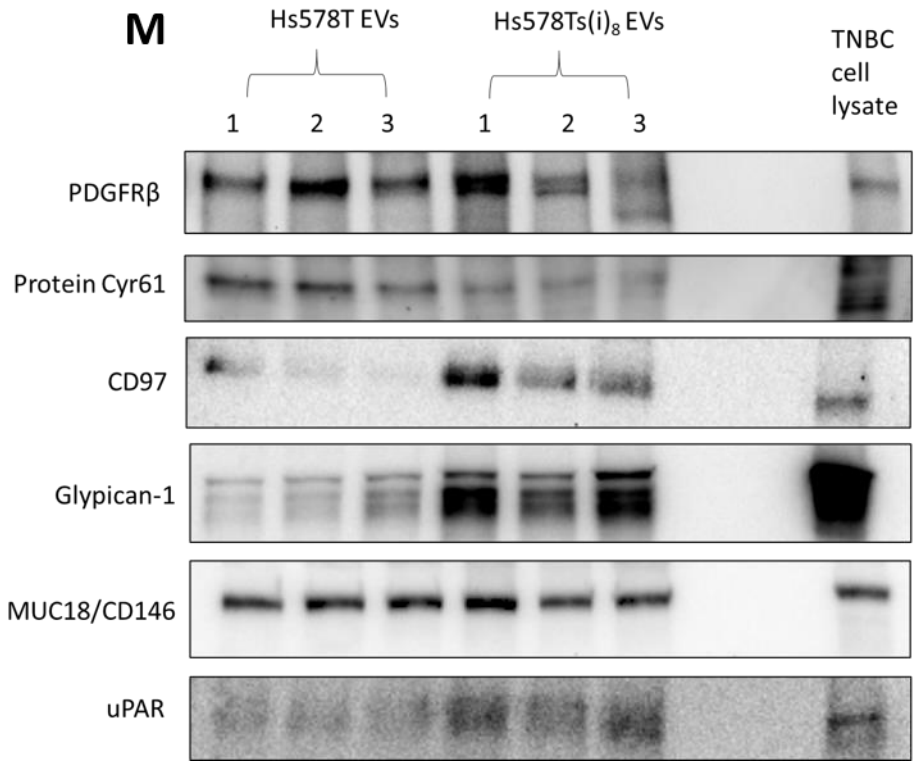

N

Name	Mass spectrometry	Immunoblot
PDGFRβ	Hs578T EVs (*p=0.001*)**	Hs578T EVs (*p=0.407*)
Cyr61	Hs578T EVs (*p=0.143*)	Hs578T EVs (*p=0.020*)*
CD97	Hs578Ts(i)$_8$ EVs (*p=0.325*)	Hs578Ts(i)$_8$ EVs (*p=0.045*)*
Glypican-1	Hs578Ts(i)$_8$ EVs (*p=0.012*)*	Hs578Ts(i)$_8$ EVs (*p=0.059*)
MUC18/CD146	Hs578T EVs (*p=0.028*)*	Hs578T EVs (*p=0.306*)
uPAR	Hs578Ts(i)$_8$ EVs (*p=0.0004*)***	Hs578Ts(i)$_8$ EVs (*p=0.002*)**
Increase Hs578T EVs means increased when compared to Hs578Ts(i)$_8$ EVs		

Figure 5.6: Mass spectrometry analysis and evaluation of selected EV proteins from TNBC cell line variants

Label-free quantification (LFQ) intensities from mass spectrometry analysis of the TNBC EVs are shown for (A) Platelet-derived growth factor receptor β, (B) Protein Cyr61, (C) CD97, (D) Glypican-1, (E) MUC18/CD146 and (F) urokinase-type plasminogen activator receptor. Immunoblot images are shown (M), along with densitometric analysis of (G) PDGFRβ, (H) Cyr61, (I) CD97, (J) Glypican-1, (K) MUC18/CD146 and (L) uPAR. (N) A summary Table of protein levels detected by mass spectrometry and immunoblot. Graphs represent mean ± SEM of *n*=3 independent biological experiments, shown as 1,2,3. Unpaired t-test was used as statistical test. * P<0.05, **P<0.01, ***P<0.001

5.3.7 Kaplan Meier curves of selected EV proteins

A search was conducted to determine if the selected proteins were associated with a worse prognosis in TNBC.

The gene name of each validated protein was inserted BreastMark, a collection of transcriptomic dataset and breast cancer outcome, to identify if the mRNA had a significant correlation to TNBC patient overall survival (OS). PDGFRβ (Fig 5.7 (A)) and glypican-1 (Fig 5.7 (D)) mRNA significantly correlated with patient outcome. Cyr61 (Fig. 5.7 (B)), CD97 (Fig. 5.7 (C)), MUC18/CD146 (Fig. 5.7 (E)) and uPAR (Fig. 5.7 (F)) were not significantly associated with patients' outcome.

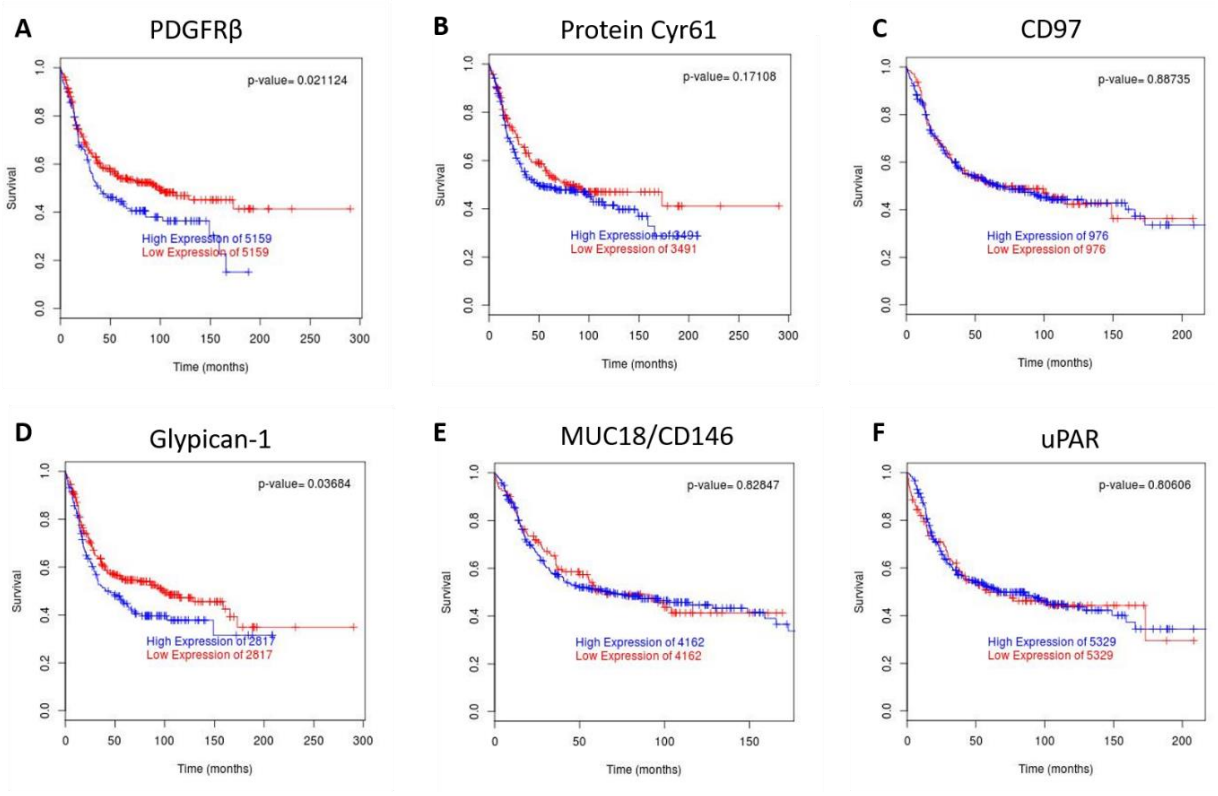

G

Gene transcript	*P-value*
PDGFRβ	0.021*
Cyr61	0.171
CD97	0.887
Glypican-1	0.037*
MUC18/CD146	0.828
uPAR	0.806

Figure 5.7: Kaplan Meier curves from BreastMark analysis of selected proteins in TNBC EVs

Gene names of selected EV proteins were inserted into the algorithm "BreastMark" to determine if mRNA expression was associated with TNBC patient outcome. (A) PDGFRβ, (B) Protein Cyr61, (C) CD97, (D) Glypican-1, (E) MUC18/CD146 and (F) uPAR were investigated. (G) *P-value* for each mRNA is tabulated.

The gene names were also inserted into Kaplan Meier Plotter (kmplot.com), a larger database of mRNA data from breast cancer patients. Patients with the ER-/PR-HER2- status were selected for the analysis.

CD97 (Fig 5.8 (C)) and MUC18/CD146 (Fig 5.7 (E)) mRNA significantly correlated with TNBC disease outcome. PDGFRβ (Fig. 5.8 (A)), Cyr61 (Fig. 5.7 (B)), glypican-1 (Fig. 5.7 (D)) and uPAR (Fig. 5.7 (F)) were not significantly associated with disease outcome.

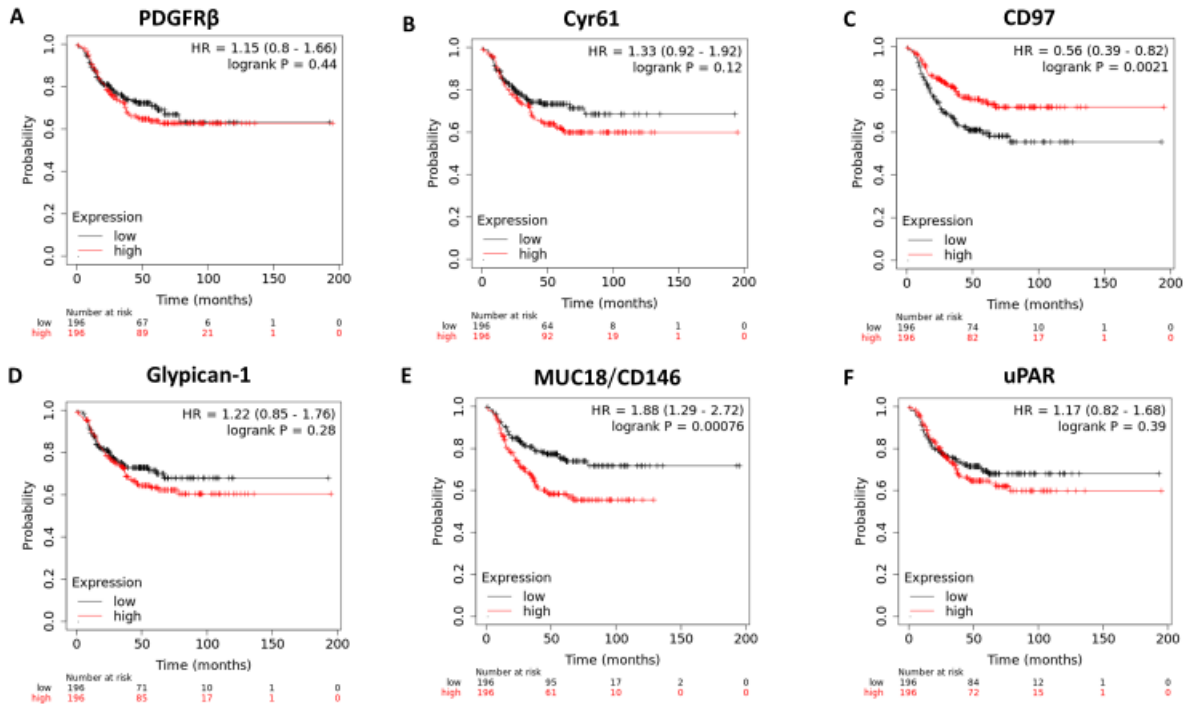

G

Gene transcript	*P-value*
PDGFRβ	0.438
Cyr61	0.123
CD97	0.002**
Glypican-1	0.279
MUC18/CD146	0.0008***
uPAR	0.387

Figure 5.8: Kaplan Meier curves from kmplot.com analysis of selected proteins in TNBC EVs

Gene names of validated EV proteins were searched on kmplot.com, to determine if mRNA expression was associated with ER-/PR-/HER2- breast cancer patient disease outcome. (A) PDGFRβ, (B) Cyr61, (C) CD97, (D) Glypican-1, (E) MUC18/CD146, (F) uPAR. (G) *p-value* for each mRNA is tabulated.

5.4 Discussion

We first set out to establish if the TNBC cell line variants caused platelet aggregation, also called TCIPA. Both cell line variants induced aggregation when incubated with washed platelets, although, there was no significant difference between the effects of the two cell line variants. TCIPA is a well-established phenomenon. In breast cancer in particular, MCF-7 cells have been shown to induce platelet aggregation via the GPIb-IX, ADP, GPIIb/IIIa pathways [300]. GPIb has been identified on the surface of MCF-7 cells and, by blocking its activity, researchers discovered that it plays a role in MCF-7 TCIPA [301]. This is of great interest to this study as GPIb has been identified *via* mass spectrometry analysis, to be present within the Hs578T and Hs578Ts(i)$_8$ EVs and therefore, may be involved in their platelet aggregation mechanism.

Next, the EVs derived from both variants were tested for their ability to induce aggregation. As for their cells of origin, the EVs released from both cell line variants caused platelet aggregation in a dose-dependent manner, with a higher concentration of EVs reducing the lag phase or time taken for induction of aggregation. This study is one of only few studies that have investigated the role of cancer cell EVs and platelet aggregation, with the majority of other studies investigating the role of EVs isolated from blood or plasma and could therefore, come from multiple cellular origins such as platelets. Of the studies that investigated cancer cell derived EVs, TF has been identified as a pro-coagulant protein carried by the EVs. Gomes *et al.* [299] used MDA-MB-231 and MCF-7 EVs to report breast cancer EVs are capable of causing platelet aggregation through direct platelet interaction. Although using different methods that we used to measure platelet aggregation, the main finding from their study was that both TF-dependent and TF-independent mechanisms were involved in MDA-MB-231 EV-induced platelet aggregation. The less aggressive MCF-7 EVs caused significantly less aggregation. Another group established that MDA-MB-231-derived "microvesicles" can generate thrombin due to the TF bound to negatively charged phospholipids on the surface of the microvesicles (MVs) [302]. Pancreatic tumour cell MVs deriving from BxPc-3 and L3.6pl cells also indirectly activated platelets through thrombin generation *via* TF- positive MVs and caused thrombus formation *in vivo* in C57Bl6/J mice. Pre-incubation of the MVs with anti-TF antibody, HTF-1, abolished the increase in thrombus size, thrombi formation and decreased mice death [169].

Global proteomic profiling of the Hs578T and Hs578Ts(i)$_8$ EVs showed that the EVs contain common EV protein markers including tetraspanins CD9 and CD81, and ADAM10, a metalloproteinase located on the surface of small EVs. Proteins that belong to the "lipid or membrane protein-binding ability" category in the MISEV 2018 guidelines were also identified such as ALIX, syntenin, RhoA and heat shock proteins (HSPs) such as Hsp90 and HCS70. Proteins categorised in "subtypes of EVs" according

to the MISEV2018 guidelines were present. These include multiple histones such as cytokeratin 18 and actinin-1/4. Lastly, proteins that are recovered with secreted EVs were identified including, galectin 3-binding protein, fibronectin, and collagen. Proteins related to the coagulation signalling cascade was also detected, including TF as well as those involved in platelet activation signalling such as prothrombin, coagulation factor X and fibronectin. Proteins carried by the EVs were associated with signalling pathways such as translation, metabolism and epithelial-to-mesenchymal transition signalling, a process that is crucial for tumour cell metastasis. Of particular interest to this study, platelet-related pathways were also associated with the EV proteins. Platelet degranulation and platelet activation, signalling and aggregation are two examples of such processes. Evaluation of the proteins that may be associated with the aggregation was performed. While TF, a known pro-coagulant protein was identified in both TNBC EVs, we selected other proteins which may also play a role in platelet aggregation.

PDGFRβ: is a tyrosine receptor kinase and belongs to the type III group. PDGFRβ binds specifically to PDGF-C and PDGF-D ligands. Upon ligand binding, two PDGFRβ receptors undergo dimerization. Ligand binding also induces a conformational change, stabilising the conformation and inducing transphosphorylation of the tyrosine residue [303]. The receptor is then fully activated and can activate its downstream substrates and activate signalling pathways. Label-free quantification intensities demonstrated that PDGFRβ was significantly higher in Hs578T EVs. However, although the trend is the same, by immunoblot this statistical significance was not achieved. This may be due to the biological repeats of EVs analysed by immunoblot not being as reproducible compared to mass spectrometry analysis of the three biological repeats. Another study has also reported PDGFRβ identification in melanoma cell-derived EVs [304]. PDGFRβ was shown to transfer resistance to the BRAF-inhibitor, PLX-4720, from drug-resistant melanoma cells (LM-MEL-64R3) to recipient drug-sensitive melanoma cells (LM-MEL-64) by activating the PI3K/AKT pathway. There are very few studies implicating PDGFRβ in platelet activation or thrombosis but with the release of PDGF from stimulated platelet α-granules, there may be a feedback loop of activation that can be explored [305].

Cyr61: Cysteine-rich angiogenic inducer 61 (Cyr61), a heparin-binding extracellular matrix-associated protein which belongs to the cysteine rich 61/connective tissue growth factor/nephroblastoma overexpressed (CNN) family of proteins, has been previously identified in TNBC cell lines including Hs578T cells [306]. Mass spectrometry analysis showed it was also present in TNBC EVs, with Hs578T EVs containing a higher amount compared to the Hs578Ts(i)$_8$ EVs, which was confirmed by immunoblot. Cyr61 has been shown to potentiate breast cancer metastases to the lung [307] and it has also been implicated in platelet adhesion. A study demonstrated that ADP-activated platelets showed a substantial increase in adhesion to Cyr61 protein that was coated on cell culture plates

compared to inactivated platelets [308]. They discovered, through the blocking of integrin $\alpha_{IIb}\beta_3$ with RGD-containing peptides and dodecapeptide H_{12}, the activated platelet integrin mediated the adhesion of platelets to Cyr61-coated wells. Overall, this study shows a potential role of Cyr61 in both homeostasis and thrombosis. With Cyr61 associated with the TNBC EVs, it may be postulated that platelets can bind to EVs via Cyr61, creating a functional link between TNBC EVs with platelet adhesion and aggregation.

CD97: Is an adhesion G-protein coupled receptor (GPCR) and it belongs to the epidermal growth factor-seven-span transmembrane (EGF-TM7) family of GPCRs that is mainly expressed on surface of lymphocytes. CD97 plays a role in T-cell activation and in driving cancer cell invasion with abnormal expression of CD97 identified in malignant tumours [309, 310]. It is still not fully understood if CD97 can activate platelets, however, immunoblot analysis showed it is substantially higher in Hs578Ts(i)$_8$ EVs, the more aggressive subclone of Hs578T, so further investigation is warranted. A previous study also highlighted the potential role of CD97 in tumour cell-platelet interaction. DU145/Ras prostate cells were shown to enable platelet activation *via* CD97; this was reduced when cells were depleted of CD97 [311]. This allowed the tumour cells to migrate through disrupted endothelial tight junctions upon lysophosphatidic acid release from activated platelets, promoting the metastasis of the cancer cells. Although, this study described did not investigate whether DU145/Ras-derived EVs could provide another source of CD97 for platelet activation, this interaction via CD97 could be another means by which platelets could become activated by cancer cell EVs and the development of thrombosis.

Glypican-1: Belongs to a family of heparan sulfate proteoglycans that are overexpressed on the surface of breast cancer cells, located on the cell membrane *via* GPI anchors, and shown to enhance the progression of tumour cell growth [312]. Glypican-1 was found in the TNBC EVs by mass spectrometry, with a higher detection level in the Hs578Ts(i)$_8$ EVs. This was followed up with immunoblotting, which showed an increase ($p=0.058$) in glypican-1 on Hs578Ts(i)$_8$ EVs when compared to Hs578T EVs. This is of particular interest in the context of TNBC, as glypican-1 has been thoroughly investigated, and confirmed as an early diagnostic biomarker in pancreatic cancer with high glypican-1 levels on exosomes derived from pancreatic patients [313]. Although there are no reports, that we are aware of, of glypican-1 having any role in platelet aggregation or cancer-associated thrombosis, the association between its expression and breast cancer progression makes it of interest to this study.

MUC18/CD146: MUC18, also called melanoma cell adhesion molecule (MCAM), is a cell surface glycoprotein that is involved in cell adhesion. It is also over-expressed in multiple carcinomas, including breast cancer, where it has been connected with increased EMT [314]. Shao *et al.* [315]

published a study showing that carcinoma mucins were involved in the formation of microthrombi in C57BL/6J mouse models, through the interaction of neutrophils that release neutrophil p-selectin glycoprotein ligand 1 (PSGL-1) and p-selectin from activated platelets. Here MUC18 was identified in the TNBC EVs, with more detected in the Hs578T EVs compared to Hs578Ts(i)$_8$ EVs by mass spectrometry. However, immunoblot analysis did not detect such a big difference between the EVs. MUC18 has already been identified on the surface of breast cancer EVs specifically. Ghoroghi *et al.* [316] demonstrated that MUC18, sorted into murine 4T1 cell line derived EVs by Ral GTPases, Ral A/B, affected the tropism of 4T1 tumour cells. By blocking MUC18 with a blocking antibody, the 4T1 EVs failed to reach the lung and establish a pre-metastatic niche *in vivo.* Another study, demonstrated that MUC18 and its soluble, secreted form was associated with increased TF activity and coagulation factor detection [317]. Using ovarian cancer HEY cells, and melanoma A375 cells in an *in vivo* mouse model, they report that the cancer cells secrete MUC18, up-regulating TF activity. When the cells were injected *in vivo* along with recombinant soluble MUC18, increased tumour metastasis occurred, along with increased pro-coagulant factors such as d-dimer and thrombin anti-thrombin complex (TAT) and an increase in circulating microparticles. Interestingly, when the cells were treated *in vitro* with soluble MUC18, increased TF was detected in the cell supernatants, implicating the microparticles as a mechanism of MUC18 secretion. A monoclonal antibody developed by the author to target MUC18, M2J-1 mAb, blocked the effects seen, decreasing pro-coagulant factors and microparticle numbers *in vivo.* Therefore, this study shows the potential of EV derived MUC18 and the development of thrombosis.

uPAR: Is a component of the plasminogen activation system. The uPAR ligand, urokinase-type plasminogen activator (uPA) activates plasmin, a blood enzyme, from its precursor plasminogen, allowing the activation of MMPs involved in cell migration and wound healing. This can become aberrant in disease such as cancer, causing cancer cell invasion and angiogenesis [318]. uPAR was identified by mass spectrometry in the TNBC EVs. It is substantially higher in amounts in the Hs578Ts(i)$_8$ EVs than the Hs578T EVs, confirmed by immunoblot analysis. One of the first studies to identify a link between uPAR and EVs demonstrated that uPA-uPAR had the ability to generate plasmin on endothelial derived microparticle surface [319]. Melanoma cell (i.e. A375 and the metastatic sub-clone, M6) EVs that contained uPAR, could be taken up by and promoted recipient endothelial cells proliferation, motility and increased tubule formation *in vitro* and *in vivo* by upregulating EGFR signalling in the endothelial cells [320]. Although there are no reports of platelet aggregation induced by uPAR activity, it has been noted as a biomarker of tumour progression and associated with a worse prognosis in TNBC [321, 322]. Therefore, uPAR was evaluated by immunoblot and may be studied further.

This study has demonstrated that there may be other proteins present within or on the surface of EVs from TNBC cells, that have not been previously identified to play a role in platelet aggregation.

While determining whether the evaluated proteins were associated with worse TNBC patient outcome we used two online databases with different publically-available datasets. BreastMark and kmplot.com were used. The results from both datasets gave different outcomes depending on the protein. For example, CD97 was not associated with TNBC patient outcome when searched on BreastMark database. However, by searching on kmplot.com we observed that low CD97 expression was significantly associated with worse patient outcome. Overall, none of the results were the same between both datasets.

5.5 Conclusion

Here we have demonstrated that TNBC cell line variants Hs578T and Hs578Ts(i)$_8$, and their corresponding EVs induce platelet aggregation. Based on proteomic profiling, there may be other proteins that are responsible for the aggregation other than TF, which has shown to have pro-coagulant properties. The next step in this study is to check the presence of these proteins in TNBC patient EVs compared to control EVs. In addition, the proteins will be blocked on the EVs and TCIPA experiments will be repeated to determine if the proteins are associated with platelet aggregation or causally involved.

With further investigation and confirmation if the proteins identified cause platelet aggregation, the proteins may be targeted to inhibit VTE and the EVs from cancer patients may be used to identify if a particular group of patients are more at risk of developing VTE.

Chapter 6: Comparison of different EV separation methods using cancer patients' and age-matched controls' sera

6 Abstract

With a specific focus on translation to clinical utility, a study was designed to investigate what is an optimal method of EV separation derived from cancer patient serum and age-matched controls without a reliance on ultracentrifugation (UC). The intention is that the selected method may potentially be used in a hospital setting to analyse patient as cancer diagnostic tools or help to decide upon a treatment regime.

The comparison of six methods included size-exclusion chromatography (SEC), the magnetic immunobeads kits, Miltenyi Biotec MACSplex (Miltenyi) and Stemcell Technologies EasySep (Stemcell), Nickel-based isolation (NBI) and polyethylene glycol precipitation (PEG). Initially, these methods were compared with density-gradient ultracentrifugation (dUC) until further characterisation revealed that dUC was not an appropriate method to use as a comparison and differential ultracentrifugation (Diff UC) was used.

Initially, two serum pools were created by pooling together ER+ breast cancer patient serum (*n=7*) and their age-matched control sera (*n=16*) to create two separate pools. Following characterisation of the methods, Stemcell was the most appropriate method for a clinical setting as it was fast to perform, separated non-contaminated EVs and can be easily replicated in a hospital laboratory environment without the necessity of specialised equipment. EVs were separated from breast cancer patient serum (*n=20*) and their age-matched sera (*n=20*) using the Stemcell method. BCA assay was used to measure the protein of the EVs, however, there was no significant difference between breast cancer patients and the healthy controls. The difference of EV cargo between breast cancer patients and healthy controls was investigated with glypican-1 and gremlin-1 levels measured by ELISA. There was significantly (*p=0.039*) more gremlin-1 protein in breast cancer EVs compared to the healthy controls.

Overall, we chose the magnetic immunobead Stemcell EasySep kit as a method that can separate serum EVs efficiently, can be used to distinguish between breast cancer and healthy controls by their protein cargo and may be used in a clinical setting.

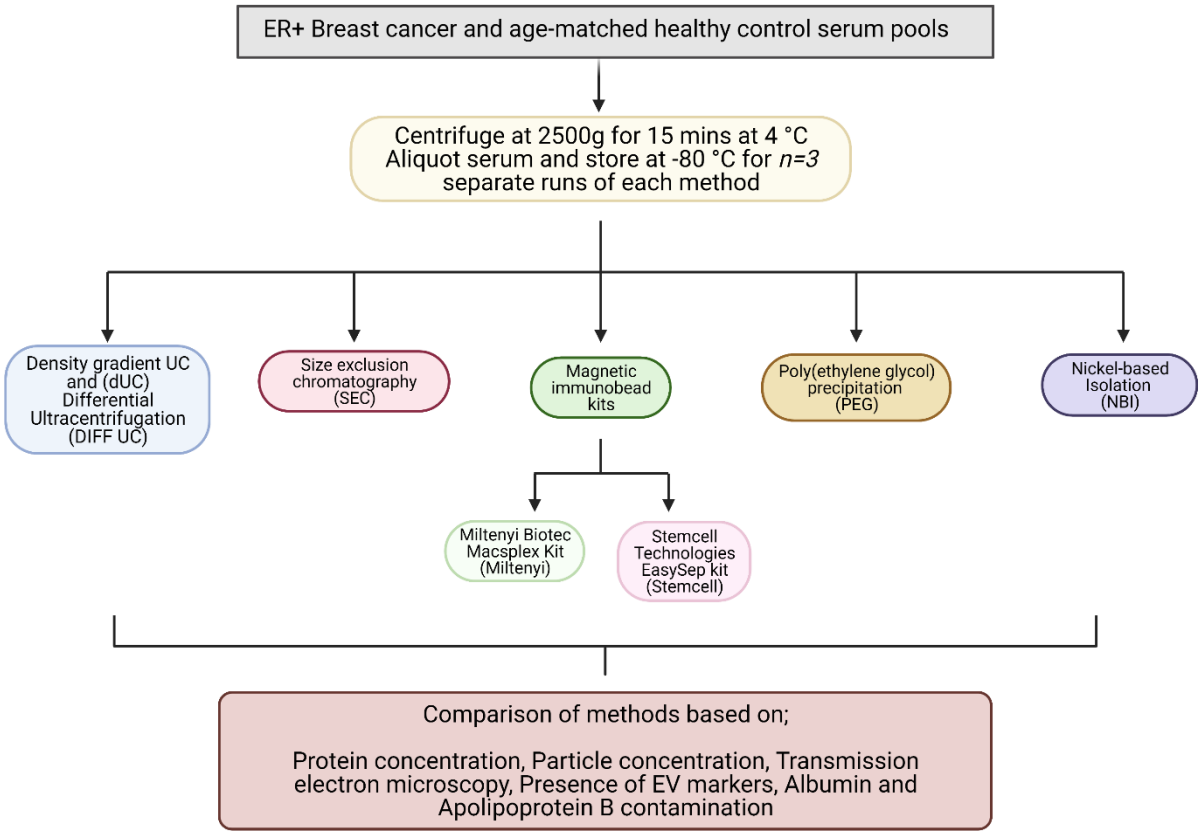

Figure 6.1: Study design for separation of serum EVs

Initially, two serum pools were created using ER+ breast cancer patient serum and their healthy controls to identify the optimal method of serum EV separation. The pools of serum were centrifuged at 2500 g for 15 mins at 4°C to pre-clear the serum. 500 µl aliquots were then frozen at -80°C until required. Three aliquots of both pools were used for each separation method to perform three independent experiments. These included SEC, magnetic immunobead kit from Miltenyi Biotec and Stemcell Technologies, PEG and NBI. Density gradient ultracentrifugation was initially used as control method but, after characterisation was performed, it was evident that it was not separating EVs efficiently. Diff UC was replaced as the control method. Comparison of methods was performed by characterisation methods such as NTA, BCA assay and TEM. Immunoblotting was also performed on the EVs for markers, CD63, CD9 and CD81. Albumin was also investigated as potential contamination. Apolipoprotein B was quantified for another source of contamination. Once the optimal method was chosen, breast cancer patient sera (*n=20*) and their age-matched healthy controls (*n=20*) were separated and studied further.

6.1 Introduction

Blood-based EVs have the potential to be used as diagnostic tools with recent studies demonstrating the presence of proteins and nucleic acid such as mRNA in patient serum and plasma with several different malignancies. Some studies have used EVs to distinguish between patients and healthy individuals as well as the different stages of cancers with ongoing research hoping to translate this to clinical use. Current diagnostic proteins for breast cancer include uPA and plasminogen activator inhibitor 1 (PAI-1), but are infrequently used as they require invasive biopsies to access the area of disease to obtain the fresh tissue needed to measure uPA and PAI-1 levels [323]. Others such as serum biomarkers CA 15-3, carcinoembryonic antigen (CEA) and tissue polypeptide antigen (TPA) are not sensitive enough to detect early-staged breast cancer [324]. Jesneck *et al.* [325] questioned whether a panel of 98 serum biomarkers (including, cytokeratin 19, CDP-2, il-8, EGFR, PAI-1, VEGF and RANTES) could actually decipher breast cancer in a cohort of breast cancer patients (*n=97*) and healthy controls (*n=68*). They concluded that the serum proteins could not definitively distinguish between benign and malignant lesions and it was difficult to ascertain if the proteins came from the cancer itself or was influenced by other factors such as an immune response, making them not sensitive or specific enough for breast cancer diagnostics. Serum EVs that are released by the tumour cells and therefore, making them cancer specific could represent an effective tool for diagnostic purposes. With distinct subtypes of breast cancer and further molecular subtypes of triple-negative breast cancer, serum EVs could, hypothetically, be used as non-invasive biomarkers that could differentiate between breast cancer patients and enable stratification in terms of prognosis and treatment options.

The potential of serum EVs at diagnosing several different cancers has been explored. For glioma cancer, Wang *et al*. [326] discovered that $EGFR^+$ serum EVs were at significantly higher amounts in cancer patients (*n=23*) compared to healthy controls (*n=12*), with higher grade gliomas carrying increased EGFR compared to lower grade gliomas. They also investigated if serum EVs could be used to track changes after surgery and demonstrated a dramatic decrease in $EGFR^+$ serum EVs in patients after surgical resection. Overall, this study demonstrated that serum EVs have the potential as non-invasive screening tool for brain tumours, aiding early detection. Our group investigated the relevance of miR-134 in breast cancer and found that miR-134 was reduced in breast tumours (via online database mining) and serum EV specimens compared to healthy controls [87]. Breast cancer serum EVs (*n=78*) had significantly ($p<0.01$) higher levels of small RNAs, isomiR of miR-21-5p and miR-23a-3p, when compared to cancer-free individuals (*n=72*) [327]. Another study reported that glypican-1 positive EVs (termed exosomes) from pancreatic ductal adenocarcinoma (PDAC) patients serum (*n=109*) had a strong correlation with cancer compared to those from healthy individuals (*n=100*).

Interestingly, glypican-1^{+} serum EVs could also distinguish between PDAC, pancreatic cancer precursor lesions (PCPL) and benign pancreatic disease (BPD) which, when compared to CA 19-9, a serum marker currently used for PDAC clinical diagnosis, demonstrating that serum EVs had a higher specificity as a biomarker for all stages of pancreatic cancer disease [313].

6.2 Aims of study

The aim of this study was to compare the separation of EVs from sera of breast cancer patients' and aged-matched controls using a method that is effective at separating the purest EVs which can be further analysed while also being a quick, cost-effective technique that realistically could be translated to clinical utility in a hospital setting towards patient care. Figure 6.1 illustrates the study design.

6.3 Results

6.3.1 Comparsion of six different separation methods using serum from breast cancer patients and their age-matched healthy controls

As TNBC is relatively rare compared to other breast cancer subtypes, the initial comparison was performed using ER$^+$ breast cancer sera as we had more of this availbale compared to TNBC serum.

Characterisation of ER$^+$ serum EVs and their age-matched healthy controls using six different separation methods (see Section 2.10.2 for protocols for each method) i.e. DIFF UC, PEG, SEC, NBI, miltenyi and stemcell was performed. Initial comparison used a crude measurement of protein concentration of non-lysed EVs (often used as a surrogate marker for EV quantity). The NBI method resulted in significantly (*p<0.0001*) more protein compared to all other separation methods with the age-matched healthy control EVs (Fig. 6.2 (A)). Similarly, with ER$^+$ patients' EVs, NBI had significantly (*p<0.0001*) more protein compared to the other methods, and DIFF UC separated EVs had significantly (*p=0.022*) less compared to PEG separated EVs (Fig. 6.2 (B)).

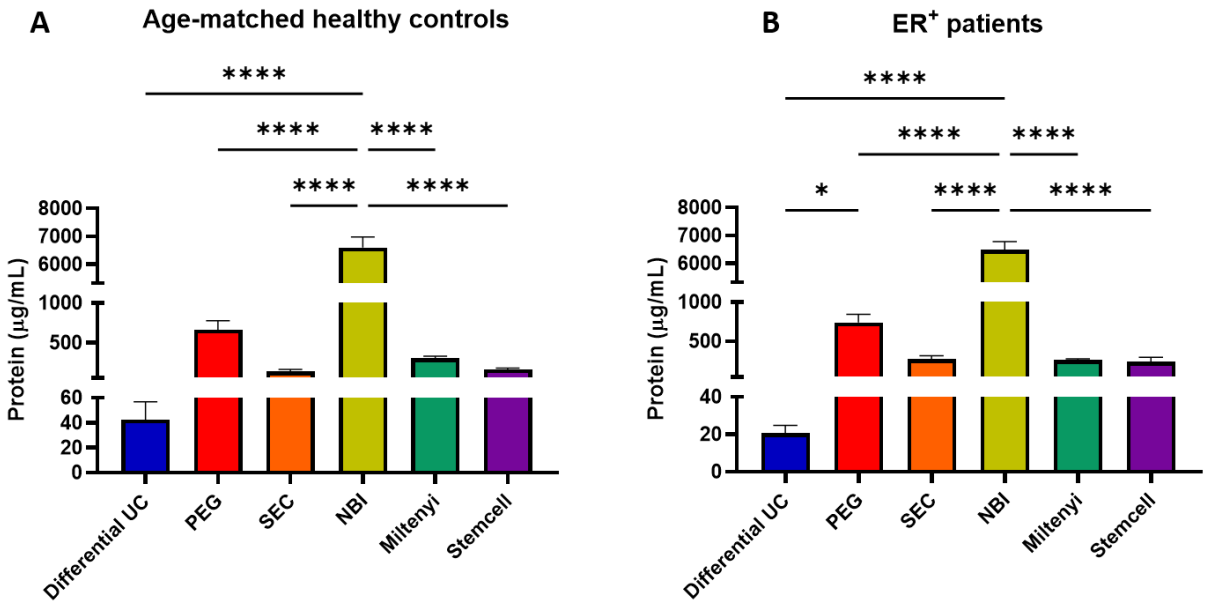

Figure 6.2: Comparison of protein concentrations of serum EVs separated with six methods

BCA assay was used to measure the protein concentration of (A) Age-matched healthy control and (B) ER+ patient serum EVs. Graphs represent mean ± SEM of *n=3* independent biological experiments. µg/mL reports the amount of EV protein per millilitre (mL) of EV suspension. One-way ANOVA was used as statistical test. *P<0.05, ****P<0.0001.

NTA analysis was subsequently used to compare the concentration and size of EVs obtained after each separation method. Both Stemcell and Miltenyi isolates still have beads attached to the EVs or at least present in the sample which effected the NTA results. Stemcell isolates were prone to produce high noise when being analysed and, therefore, may skew the results. Using the Miltenyi kit, both age-matched healthy control and ER$^+$ patient EVs had a significantly (*p<0.0001*) higher concentration when compared with every other method (Fig. 6.3 (A-B)). DIFF UC resulted in the lowest concentration in both pools of EVs (Fig. 6.3 (A-B)). EVs separated using the Stemcell kit had a significantly larger modal size when compared to EVs separated by DIFF UC for healthy control EVs (*p=0.0007*) and ER+ EVs (*p=0.0005*). Similarly, Stemcell EVs were significantly larger than PEG (*p=0.0002*), SEC (*p<0.0001*), NBI (*p<0.0001*) and Miltenyi (*p<0.0001*) (Fig. 6.3 (C-D)). This may be due to the high noise when analysing the EVs. All other methods resulted in particles with a modal size within the range of 60-142 nm.

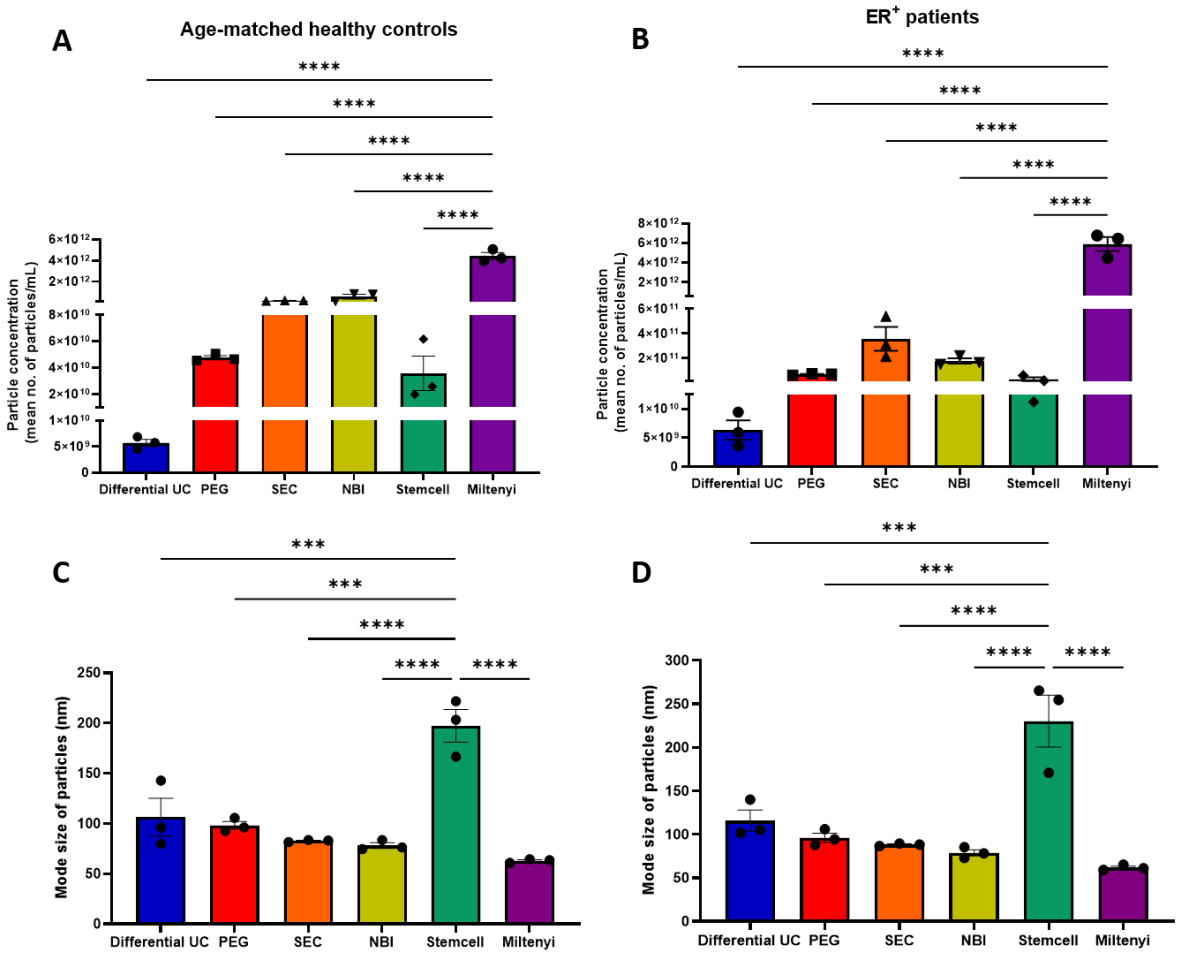

Figure 6.3: Comparison of particle concentration and size of serum EVs separated with six methods

NTA was used to measure the concentration (particles per mL) of (A) Age-matched healthy controls and (B) ER$^+$ patients' serum EVs. The modal size (nm) of (C) Age-matched healthy control and (D) ER$^+$ patients' serum EVs were also measured. Graphs represent mean ± SEM of *n=3* independent biological experiments. One-way ANOVA was used as statistical test. ***P<0.001, ****P<0.0001.

The protein (of lysed EVs) and particle concentrations were graphed against each other to deteremine if protein concentration was a good surrogate marker for particle quantification. The R^2 was calculated to determine the goodness of fit. Of all methods investigated, age-matched control isolates separated by Stemcell had a strong correlation (R^2=0.931) between protein and particle concentration (Fig 6.4 (E)). It was the only method that showed, with increased protein concentration there was a correlation with increased particle concentration. PEG (Fig. 6.4 (B)), SEC (Fig. 6.4 (C)), NBI (Fig. 6.4 (D)) and Miltenyi (Fig. 6.4 (F)) did not give a good correlation between protein and particle concentration of the isolates. Although DIFF UC gave a strong correlation, the increase in protein concentration correlated with decreased particle concentration, indicating the data was biased due to a small data entries when calulating the R^2 values (Fig. 6.4 (A)).

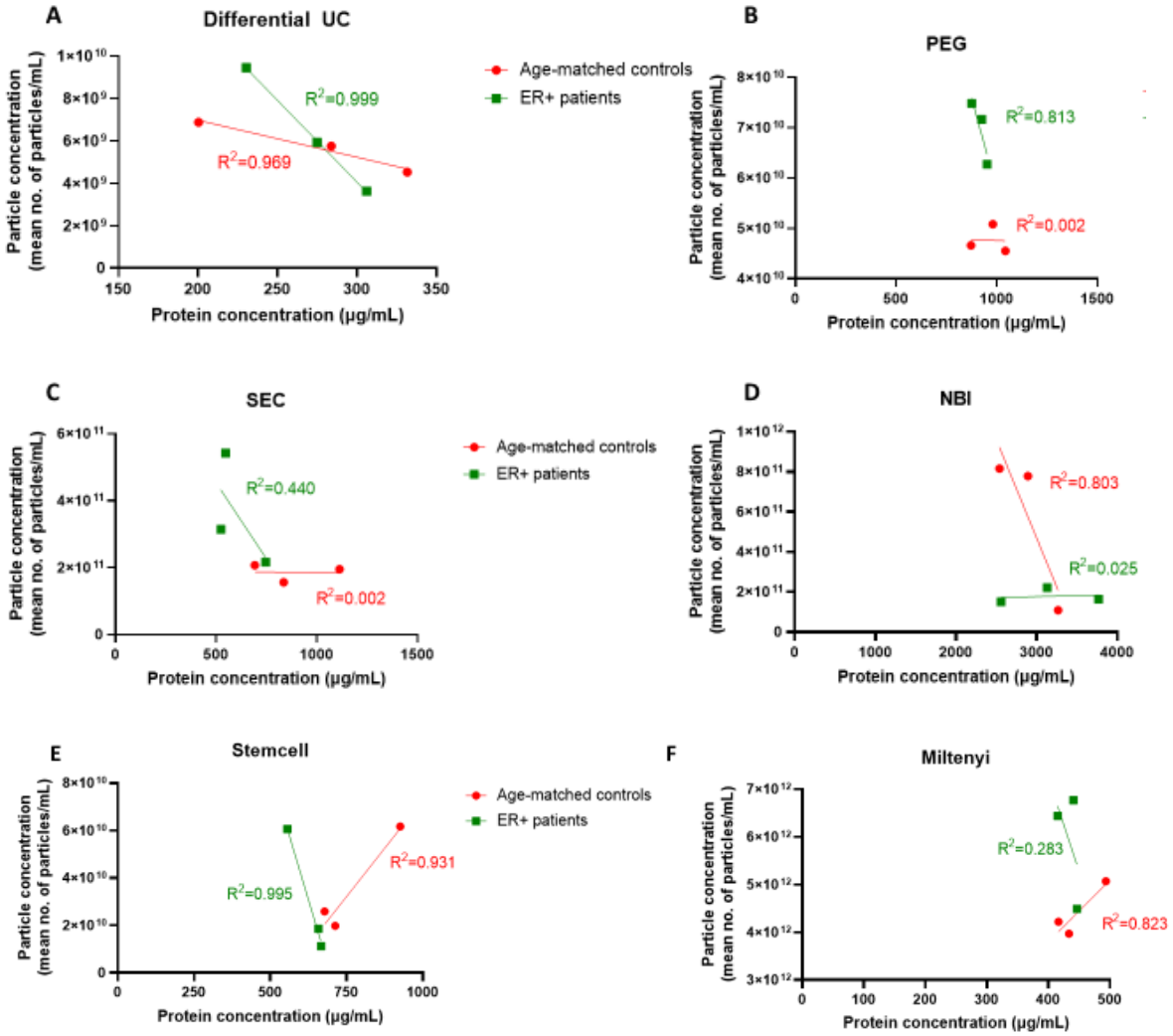

Figure 6.4: Determination if protein concentration is a good surrogate marker for EV concentration of each method of separation

Protein and particle concentration were plotted against each other to deteremine if protein concentration was a good surrogate marker for EV numbers for (A) DIFF UC, (B) PEG, (C) SEC, (D) NBI, (E) Stemcell and (F) Miltenyi separation methods. Simple linear regression was used to calculate the R^2 of the "goodness of fit". Each graph plots the individual biological replicates of *n=3* experiments.

The quantification of total protein after EV lysis and particle count as measured by NTA was used to create a particle number-to-protein concentration ratio as previously described [328]. This acts an estimation of EV purity by assessing the level of contaminating proteins. In both age-matched healthy controls and ER$^+$ patients' EVs, Stemcell isolates had a significantly (*p<0.0001*) higher particle-to-protein ratio compared to all other methods (Fig. 6.5 (A-B)). DIFF UC had the lowest ratio out of all methods, indicating high protein contaminating levels.

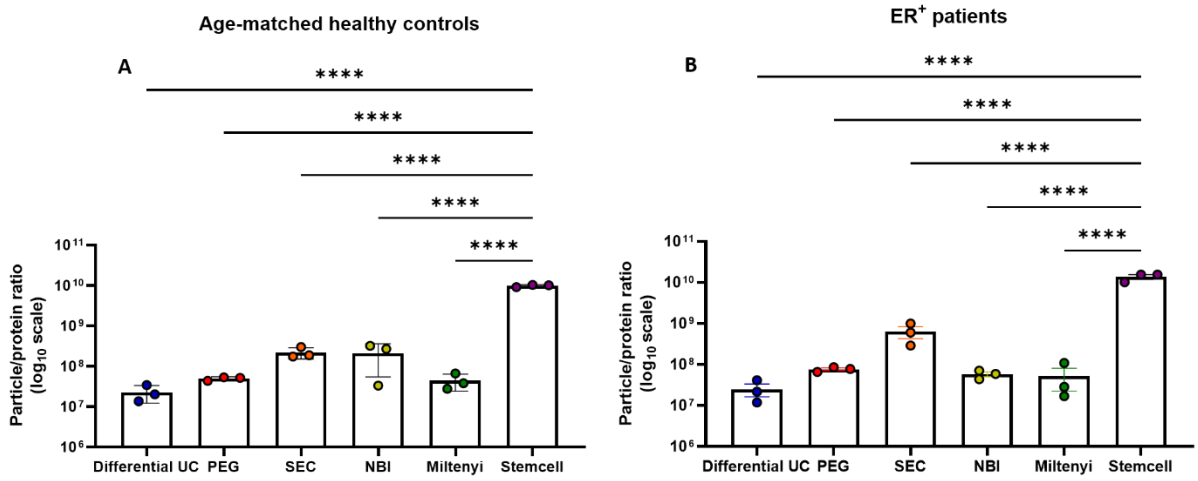

Figure 6.5: Particle number/protein concentration ratio of serum EVs separated by six methods

Purity was assessed by calculating a particle-to-protein ratio for (A) age-matched healthy control and (B) ER$^+$ patient serum EVs. This was calculated by dividing particle count (no. of particles/mL) and protein concentration (µg/mL) of lysed EVs. Log_{10} scale is used to graph data. Graphs represent mean ± SEM of *n=3* independent biological experiments. One-way ANOVA was used as statistical test. ****P<0.0001.

TEM analysis confirmed the presence of EVs when using each method of separation and had the characteristic EV shape and size. Diff UC EVs were low in numbers, as also seen by NTA (Fig. 6.6 (A)). TEM images of PEG isolates showed the presence of aggregates in the EV suspension (Fig. 6.6 (B)). SEC EVs were highly contaminated with other vesicular structures, possibly lipoproteins (Fig. 6.6 (C)). NBI isolates had a cleaner grid background compared with those separated by other methods. However, low numbers were visible (Fig. 6.6 (D)). Miltenyi and Stemcell EVs were seen attached to bead-like structures (Fig. 6.6 (E-F)).

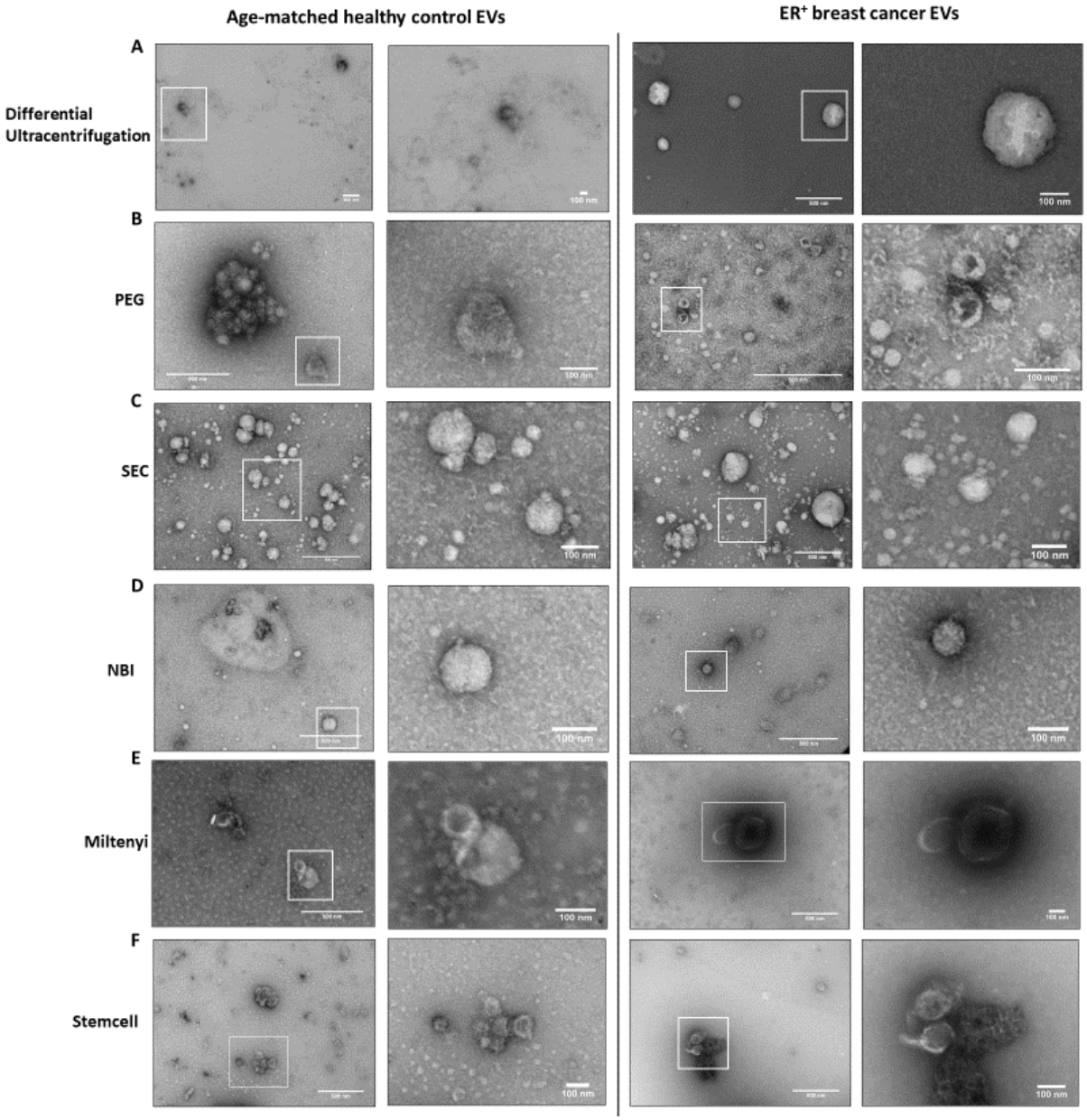

Figure 6.6: TEM analysis of serum EVs separated with six methods

TEM analysis of separated EVs from age-matched healthy control and ER$^+$ patient serum using (A) Differential UC, (B) PEG, (C) SEC, (D) NBI, (E), Miltenyi and, (F) Stemcell methods. Images were taken at a magnification of 15000X or 20000X. Scale bars are 500 nm (left images) and 100 nm (right images).

Immunoblot analysis of the EVs separated demonstrated the presence or absence of common EV markers and albumin contamination. The tetraspanins CD63, CD9 and CD81 and contaminant albumin were compared across the separation methods. These were chosen as the immunobead kits were specific for all three tetraspanins and therefore, we could compare the amount of CD63, CD9 and CD81 in all methods. Albumin was evaluated as it would allow us to assess the purity of the isolates. The isolates from density gradient contained none of the EV markers evaluated.

In age-matched healthy control EVs, CD63 was detected in all methods, CD9 was present in EVs separated by PEG and NBI. CD81 was detected in EVs separated with both the Stemcell and Miltenyi (Fig. 6.7 (A)). In ER^+ patient EVs, CD63 was detected in all methods, CD9 was present in EVs separated by PEG and NBI and CD81 was detected in EVs isolated by Stemcell and Miltenyi (Fig. 6.7 (B)). EVs isolated by NBI method was highly contaminated with albumin, followed by PEG and Miltenyi. SEC and Stemcell methods had almost undetectable albumin levels (Fig. 6.7 (A-B)).

DIFF UC was subsequently used as a "control" method. CD63 was the only EV marker detected along with albumin contamination (Fig. 6.7 (C)). A summary of EV markers detected in EVs after each separation method and level of albumin contamination is shown (Fig. 6.7 (D)).

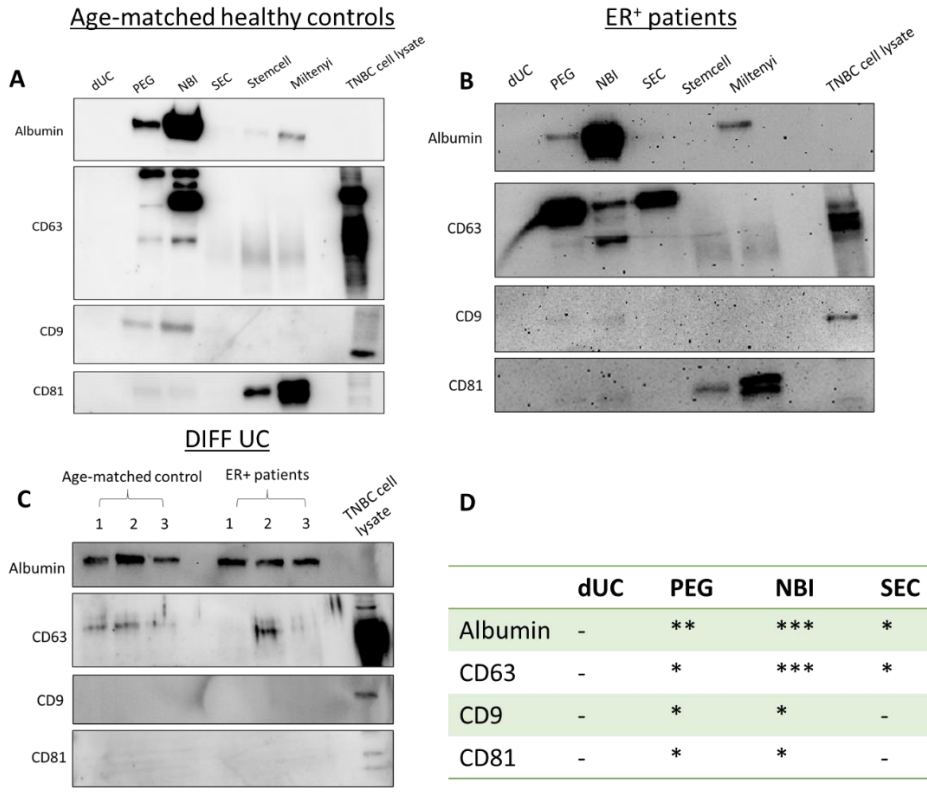

	dUC	PEG	NBI	SEC	Stemcell	Miltenyi
Albumin	-	**	***	*	-	**
CD63	-	*	***	*	**	**
CD9	-	*	*	-	-	-
CD81	-	*	*	-	**	***

Figure 6.7: Immunoblot analysis of serum EVs separated with six methods

Immunoblot was used to investigate the presence of EV markers, CD63, CD9 and CD81. Albumin was also investigated. Representative immunoblots are shown (A-C). A summary of EV marker levels from *n=3* independent immunoblots are tabulated (D). 1-3 are *n=3* biological independent DIFF UC isolations.

Apolipoprotein B (ApoB) contamination was also investigated. In the age-matched healthy controls' EVs, SEC separated EVs had significantly (*p<0.0001*) more ApoB compared to any other method (Fig. 6.8 (A)). PEG separated EVs also had significantly more ApoB compared with NBI (*p=0.0004*), Stemcell (*p=0.0009*) and Miltenyi (*p=0.002*) (Fig. 6.8 (A)).

Similarly, in ER$^+$ patient EVs, ApoB contamination was significantly higher in SEC separated EVs compared with all other isolation methods (*p<0.0001*) (Fig. 6.8 (B)). PEG separated EVs had significantly more ApoB compared with NBI (*p=0.010*), Stemcell *(p=0.006*) and Miltenyi separated EVs (*p=0.014*) (Fig. 6.8 (B)).

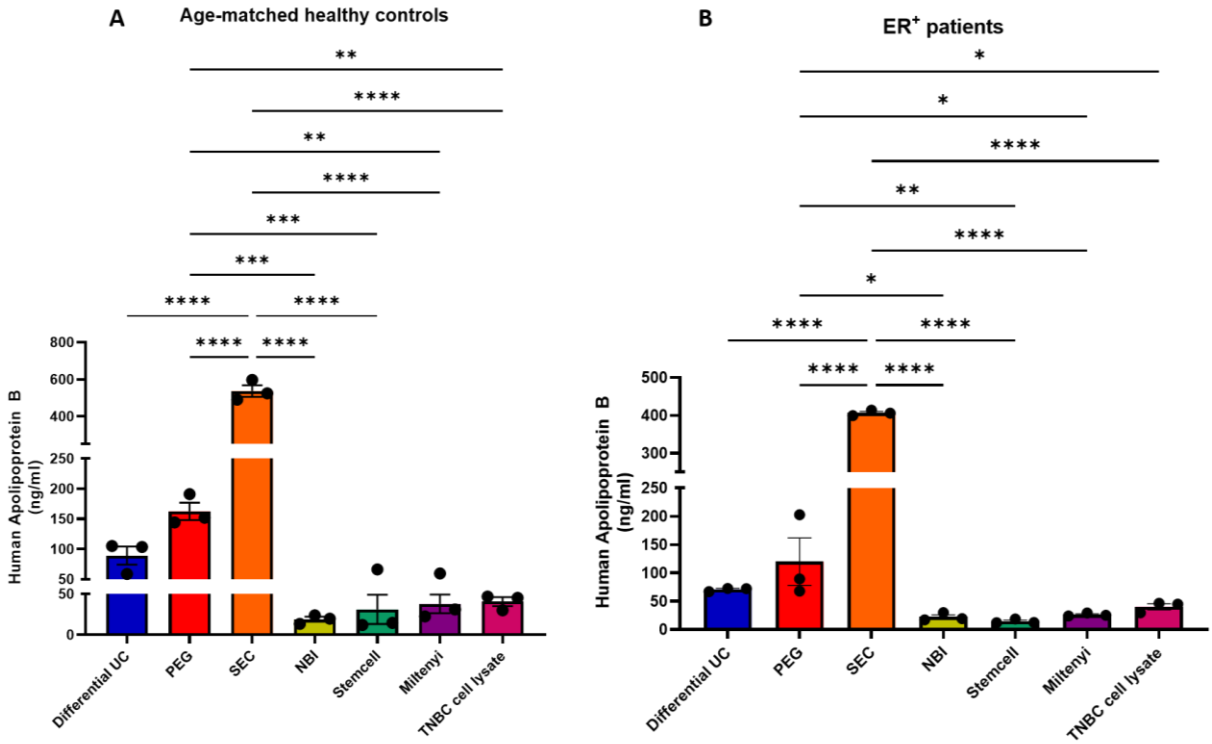

Figure 6.8: Apolipoprotein B measurement of serum EVs separated with six methods

Apolipoprotein B (ApoB) ELISA was performed to quantify the contamination of ApoB of the EVs isolated from the different EV isolation methods in age-matched healthy control (A) and ER$^+$ patients (B) serum. Cell lysate from the TNBC cell line, Hs578Ts(i)$_8$ was used as a positive control. Graphs represent mean ± SEM of *n=3* independent biological experiments. One-way ANOVA was used as statistical test. *P<0.05, **P<0.01, ***P<0.001,****P<0.0001.

In summary, six methods were compared by their resulting protein content, particle concentration, the presence of common EV markers and contamination from both albumin and ApoB (Fig. 6.9). Compared to DIFF UC, the control method, Stemcell separated EVs had a higher protein and particle concentration. TEM analysis showed the presence of EVs which had the characteristic EV shape and size, with SEC EVs having the highest and DIFF UC, Miltenyi and Stemcell EVs having the lowest EV concentration. Stemcell EVs had both CD81 and CD63 compared to CD63 only in the DIFF UC EVs. Stemcell EVs had less albumin and ApoB contamination. The time to separate EVs by the Stemcell kit was shorter compared to differential UC with a difference of 2hrs between the two methods.

PEG, NBI and SEC resulted in a high albumin and ApoB contamination. Miltenyi had similar results to Stemcell, however, it had a higher albumin contamination.

Separation method	Protein Concentration	Particle concentration	TEM imaging	EV markers	Albumin contamination	Apolipoprotein B contamination	Time to isolate
Differential UC	*	*	*	CD63	***	**	2.5hrs
PEG	**	**	**	CD63, CD9, CD81	***	***	3.25 hrs
NBI	****	**	**	CD63, CD9, CD81	****	*	50 mins
SEC	**	**	****	CD63	*	****	30 mins
Stemcell EasySep kit	**	**	*	**CD63, CD81**	*	*	**30 mins**
Miltenyi Macsplex beads	**	****	*	CD63, CD81	**	*	20 mins

Figure 6.9: Summary of the characterisation of six separation methods of serum EVs

A personal grading of each isolation method, with * corresponding to low, ** corresponding to medium, *** corresponding to high and **** corresponding to very high. Time to isolate was calculated based on time from having serum to a final resuspension of EVs/isolates.

6.3.2 Separation of breast cancer sera EVs and their age-matched healthy controls using the Stemcell EasySep Kit

Following the selection of Stemcell EasySep kit, 20 pairs of breast cancer patient EVs and their age-matched healthy control EVs were separated from sera samples. Protein concentration was measured to determine its suitability in distinguishing between breast cancer patients and healthy controls. A comparison of two different protein quantification assays was performed. Up until now, BCA assay had been used to measure protein concentration. MicroBCA was tested alongside the BCA assay to determine what method of protein measurement may be the best to use for Stemcell isolates.

Protein concentration in breast cancer patient isolates was higher when compared to their age-matched healthy controls. However, significance was not reached when using the standard BCA assay (Fig. 6.10 (A)), or microBCA assay (Fig. 6.10 (B)). When using the microBCA kit, the protein concentration of the age-matched healthy control isolates was higher compared to the breast cancer patients isolates (Fig. 6.10 (B)). Standard BCA assay and the microBCA kit demonstrated more comparable results, with the microBCA showing the highest protein concentrations between the two methods (Fig. 6.10 (C)).

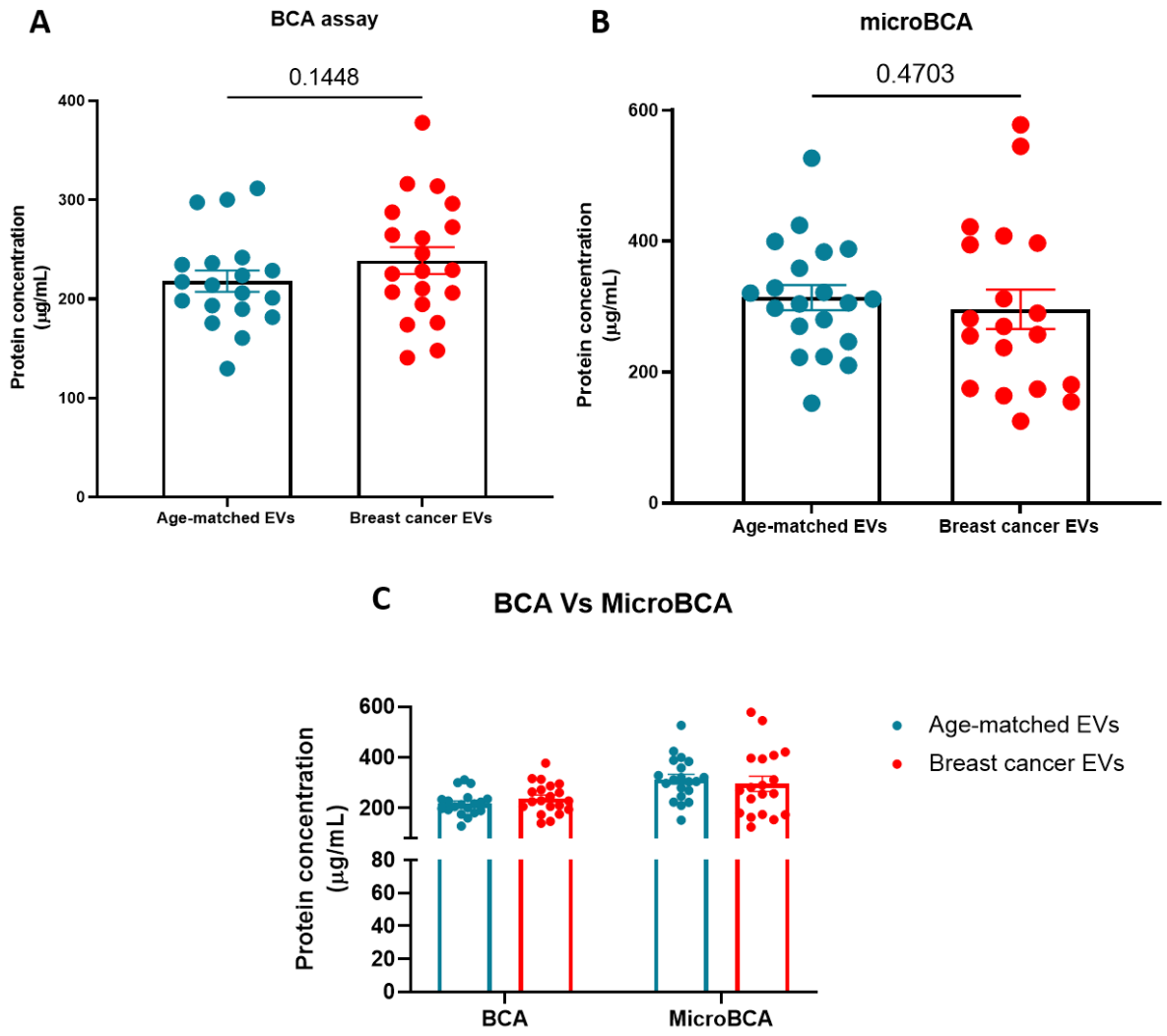

Figure 6.10: BCA analysis of breast cancer patients' sera isolates and age-matched healthy controls' isolates

Serum EVs were isolated using the Stemcell EasySep kit and protein concentration was measured using the (A) BCA assay and (B) MicroBCA kit. A comparison of both methods was made (C). Graphs represent mean ± SEM of *n=20* pairs of patients EVs. One significant outlier was removed from each of the graphs (A-B). Paired t-test (A-C) was used as statistical test.

The twenty pairs of serum EVs were lysed and analysed for the presence of two proteins known to be expressed by breast cancer cells [312, 329]. Glypican-1 was measured in both healthy control and breast cancer EVs, with no significant difference detected between them (Fig. 6.11 (A)). Patient EVs from different breast cancer subtypes were also investigated but there was no difference observed (Fig. 6.11 (B)). Gremlin-1 was measured in both healthy control and breast cancer patient EVs, with a significantly (*p=0.039*) higher amount in breast cancer EVs (Fig. 6.11 (C)). When EVs from breast cancer subtypes were compared with healthy control EVs, TNBC EVs had significantly (p=0.005) more gremlin-1 compared to control EVs (Fig. 6.11 (D)). However, the small sample number and substantial variability between sera EVs from the TNBC (*n=5*) samples, indicate that this result should be taken cautiously.

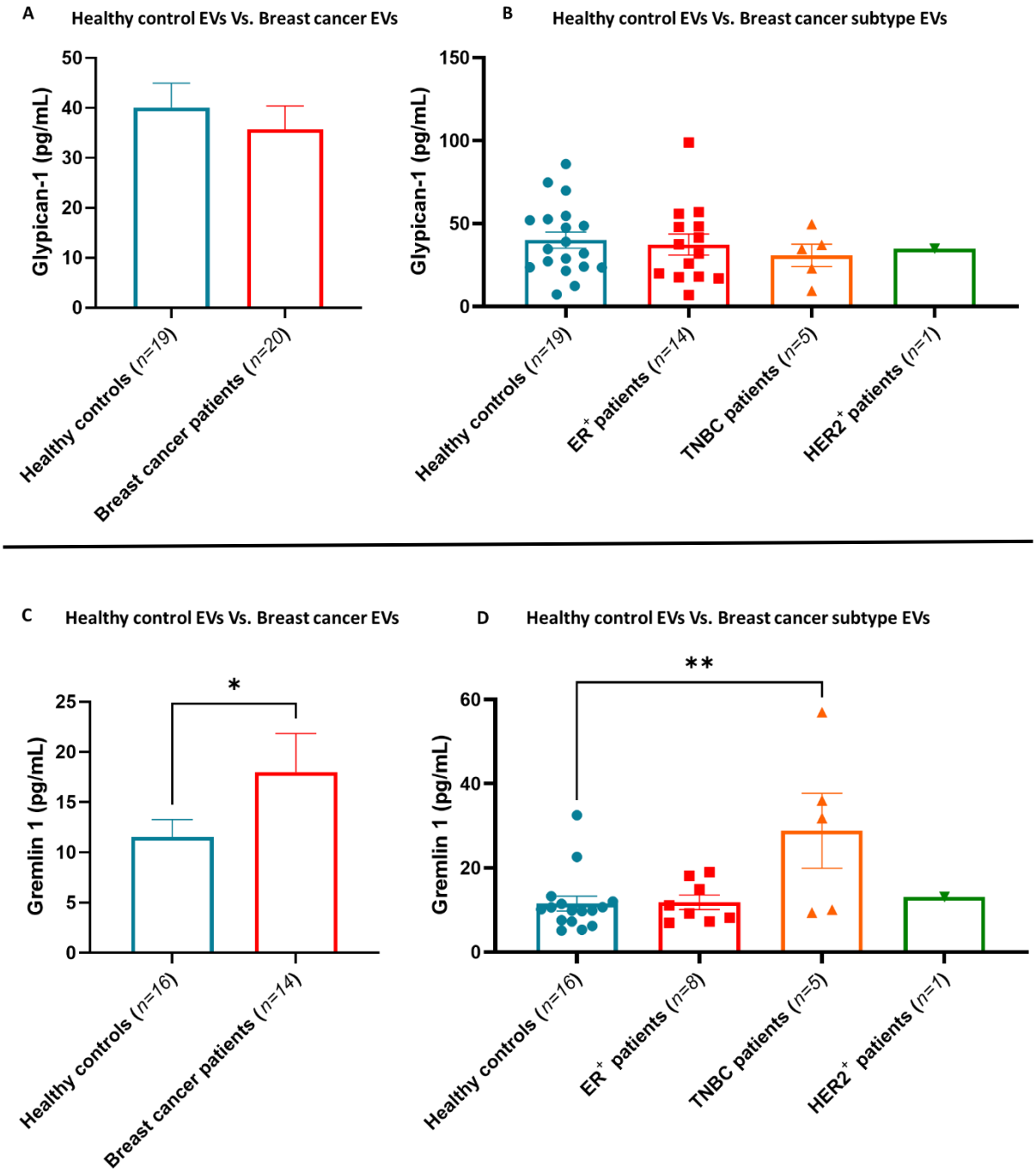

Figure 6.11: Glypican-1 and gremlin-1 in breast cancer patients' and their age-matched control sera EVs measured by ELISA

Glypican-1 and gremlin-1 was measured in age-matched healthy control and breast cancer EVs by ELISA. 10 µg and 5 µg of EV protein was used for glypican-1 and gremlin-1 ELISAs, respectively. Glypican-1 was compared in healthy control versus breast cancer EVs (A) and with individual breast cancer subtypes (B). Similarly, gremlin-1 was compared in healthy control versus breast cancer EVs (C) and with individual breast cancer subtypes (D). Graphs represent mean ± SEM and show the numbers of healthy control and breast cancer patient EVs which had detectable levels of each protein. Paired t-test (C) and one-way ANOVA (D) were used as statistical tests.*P<0.05, **P<0.01.

6.4 Discussion

After an extensive investigation with six different EV separation methods, we concluded that the Stemcell method separated EVs that met most of the criteria needed for an acceptable EV isolation according to the MISEV2018 guidelines. The method can be performed in as little as 30 minutes making it suitable for clinical settings. Stemcell EVs had the least albumin contamination and apolipoprotein B levels were relatively low when compared to other methods such as SEC. The protein concentration of Stemcell EVs was comparable to other methods such as Miltenyi, PEG and SEC. NBI EVs had high protein concentrations, which may be due to high amounts of albumin contamination, as seen by immunoblot. Although the EV concentrations by NTA were reproducible, Stemcell and Miltenyi EVs readings can be altered due to the presence of immunobeads still attached to the EVs. However, a particle-to-protein concentration ratio was still calculated to measure the purity of the separated EVs, which have been used in other EV studies [330-332]. Stemcell EVs had the highest ratio, indicating that they had the highest purity out of all EVs. DIFF UC had the lowest ratio, indicating a high amount of proteins that co-pellet and contaminate the final EV isolates. Immunoblot demonstrated that Stemcell EVs had almost no albumin contamination while isolates also expressing CD81 and CD63. Although PEG and NBI isolates contained all three tetraspanins, high levels of albumin contamination was present with the separated EVs.

Others have compared different EV separation methods for serum. Ju Ryu *et al.* [333] reported that small EVs could be separated from breast cancer patient-derived serum (*n=30*) with high yield and not compromising on purity by performing ultracentrifugation (UC) prior to precipitation kits, Total Exosome Isolation (TEI) and ExoQuick (EQ). The researchers compared four UC steps with combination two UC steps with a precipitation kit. A lower albumin contamination was achieved while detecting EV miR-21 and miR-155 in comparable amounts to the four rounds of UC. Our group has also reviewed the viability of EVs derived from breast cancer patients' blood as diagnostic tools [334]. Another study compared five UC spins with SEC alone and a UC spin before loading onto a SEC column using serum from healthy donors (no n number reported) [335]. They concluded that depending on your downstream use, each method had it pros and cons. They found that SEC had more contaminating serum proteins (i.e. apolipoprotein B) compared to the other two methods. In our study we also observed that SEC separated EVs had a substantial amount of ApoB contamination and, therefore, made it harder to detect any EV protein markers by immunoblot. A 2015 study demonstrated that serum EVs isolated from commercially available normal human sera (no n number reported) using five UC steps (i.e. 110000 g) had comparable results to five centrifugation steps (i.e. 40000 g) in terms of

protein yield, EV marker detection and TEM analysis [336]. The researchers demonstrated that a speed of 40000 g can separate EVs from serum identical to UC, giving a more affordable option for clinical use, as a benchtop Sorvall™ centrifuge was used for the 40,000 g spin. In our study, UC separated EVs had a high albumin contamination with CD63 barely detectable. With ApoB levels relatively high compared to other methods such as NBI and Stemcell, this made it difficult to detect any EV protein markers. Similar contamination issues are reported in a study that compared the reproducibility of UC with a density cushion and EQ kit for isolation of serum EVs (*n=2*) [337]. The study showed that contaminating proteins such as albumin affect the reproducibility of the UC method. The EQ method co-precipitated less albumin from the starting serum material and was found to be more reproducible. By performing two rounds of EQ they showed that the addition of a second round of EQ, reduced the albumin contamination and still maintained similar levels of EV marker, LAMP2. This study highlights the need for checking the reproducibility of methods chosen for serum EV separation and that albumin, lipoprotein or IgG contamination is a major factor in skewing the reproducibility. Brennan *et al.* [338] compared eight different separation methods (i.e. using serum from 5 healthy non-fasting adults) including EQ-Plus, SEC, SEC combined with density gradient UC (SEC-DG), UC alone, Density cushion UC (CUC), Density gradient and UC (DG-UC), and Density cushion with density gradient and UC combined (CUC-DG-UC). They report that careful considerations are needed before choosing your method of separation and should be based on your downstream applications. CD63 was detected in all methods by immunoblot, with EVs separated with different methods carrying either the 60kDa glycosylated form or the 50, 75 kDa forms. TSG101 was only detected in the UC alone method. By performing a particle count and protein concentration ratio, they identified SEC and DG-UC had the highest ratios, i.e. less soluble proteins co-isolating with the EVs. Performing UC resulted in a lower particle-to-protein ratio, indicating a higher co-isolation of contaminating proteins. All the methods included in the above study require an ultracentrifugation step with a lot of hands-on isolation time and therefore, are more suitable for research purposes rather than clinical settings. Lastly, Buschmann *et al.* [339] compared several EV isolation kits for serum EV separation and compared them to UC with the purpose of identify the most suitable method for miRNA profiling. They used serum from sepsis patients (*n=4*), patients in septic shock (*n=5*) and healthy volunteers (*n=10*). These included a precipitation-based kit, miRCURY exosome kit, a size-exclusion based kit, Exo-spin columns as well as Izon SEC columns, and a membrane affinity-based kit, exoRNeasy kit. Like our study, no EV markers were detected in UC isolates by immunoblot except for high albumin contamination. Overall, the researchers state that the precipitation based method gave the best results in stratifying disease versus healthy patients, although they state that another purification step may be required to fully understand if the miRNA identified are truly encapsulated in EVs and not separated with the EVs

through the binding with co-isolated proteins such as argonaute-2. While all the studies above compared methods of serum EV separation and tried to improve the purity of the serum isolates, the purpose of our study was to determine a method that could be easily translated to the clinic for breast cancer diagnosis, by using only one method for each separation and included methods that have, to the best of our knowledge, not been assessed on human sera. NBI separation has not been tested for serum EV separation for the purpose of clinical application while Stemcell immunobead kit has only been launched in 2020.

Upon measuring the protein concentration of Stemcell isolates, we observed that there was no significant difference in protein concentration between age-matched control and breast cancer isolates.

Glypican-1 and gremlin 1 were chosen to investigate whether breast cancer serum EVs had higher amounts compared to healthy control EVs. There was no difference in glypican-1 levels between healthy and breast cancer EVs. This result was unexpected as it has been shown that glypican-1 is over-expressed in breast cancer [312]. It must be noted that this study measured glypican-1 by RNA by northern blot analysis and therefore, is not the same as our study. Glypican-1 has been identified in other cancer cell derived EVs. Researchers identified glypican-1 in EVs released by colorectal cancer cells, MC38 which over-expressed Snail [340]. Risha *et al*. [341] performed proteomic profiling of MDA-MB-231 and MCF-7 EVs. They found that glypican-1 was carried by MDA-MB-231 EVs but not MCF-7 EVs. However, they did not further validate their findings in breast cancer patient samples.

Gremlin-1 was shown to be at a higher quantity in breast cancer patient EVs compared to healthy controls. When we analysed individual breast cancer subtypes of the patients' EVs, TNBC had substantially more gremlin-1 compared to health control EVs. This is the first study, to the best of our knowledge to demonstrate the presence of gremlin 1 in EVs. Gremlin-1 is a member of the cysteine knot superfamily and a bone morphogenetic protein antagonist. It plays a role during embryonic development and has been shown to be overexpressed in human cancers [329, 342]. Gremlin-1 has been implicated in the promotion of breast cancer metastasis. Using female BALB/c mice injected orthotopically with breast cancer cells, MTV/TM-011 transfected with gremlin 1 they demonstrate that an increase in lung metastases compared to mice injected with MTV/TM-011 cells that had silenced gremlin-1 gene [343]. Another study showed that gremlin-1 was elevated in breast cancer cell lines compared to normal breast cells, MCF-10A [344]. They also showed that gremlin-1 increased colony formation and viability of the breast cancer cells, MDA-MB-468, MDA-MB-453 and SKBR3 *in vitro* as well as increasing tumour growth in BALB/c nu/nu athymic mice injected with SKBR3 cells

through the increase in EGFR signalling. Therefore, gremlin-1-carrying serum EVs may be a potential marker of breast cancer disease.

6.5 Conclusion

We have successfully compared six different EV separation methods using breast cancer patient serum and age-matched healthy controls. We chose the Stemcell EasySep isolation kit as the best method for separating EVs from serum. Although a limitation to this method is the unsuitability to analyse the EVs by NTA, the Stemcell method can be easily translated to clinical utility while also performing well against the other methods.

We also identified that gremlin-1 levels were higher in breast cancer serum EVs compared to healthy control EVs. We identified, for the first time that serum EVs carry gremlin-1 and it may be a marker of breast cancer disease. Further work is needed to verify that this method can be clinically used to separate EVs from patients' sera and as a diagnostic tool.

Chapter 7: Discussion, Conclusions, and Future Directions

7.1 Discussion

7.1.1 Investigation of TNBC EV sub-population the inhibition of EV release with proposed inhibitors

As discussed in Chapter 1, breast cancer is the most commonly diagnosed cancer in the world, as of 2020. TNBC is an aggressive subtype of breast cancer that is heterogeneous in nature and is often detected at later stages, in younger women. It has the worst prognosis as there is currently no targeted treatment like other subtypes such as HER2+ breast cancer which can be treated with Herceptin.

EVs are released by many different cells in the body, in both normal and diseased states. In the context of cancer, our group was the first to show that EVs released from drug resistant cells can spread the resistance to drug-sensitive cells. EVs have also been implicated in TNBC disease progression through various mechanisms (as discussed in Section 1.2.2). Our group showed that a heterogeneous pool of EVs from TNBC cell line variant Hs578Ts(i)$_8$ could transmit aggressive phenotypic traits to recipient breast cancer cells, both TNBC and HER2+ cell lines. To continue on from this work, we sought to identify what sub-population of EV, if any, was responsible for these effects. We first separated out the sub-populations from the Hs578Ts(i)$_8$ cell conditioned medium (CM) using differential ultracentrifugation and performed a full characterisation of each sub-population. We concluded that we had obtained four sub-populations that had individual characteristics and could be used to treat the recipient parental cell line, Hs578T. By performing various assays including, proliferation, migration, invasion and *anoikis*, we observed that all the four sub-populations that were isolated from Hs578Ts(i)$_8$ CM were all responsible and acted together to transmit the effects of altered proliferation, migration, invasion and *anoikis* to Hs578T cells. In summary, we did not identify one single sub-population that was mostly involved and therefore, the next aim was to test a panel of proposed EV inhibitors with the aim to block the release of the EVs and in turn, their aggressive effects.

To decrease the transfer of the aggressive effects, we investigated proposed EV inhibitors and their ability to decrease EV release from TNBC cell line variant, Hs578Ts(i)$_8$. Calpeptin, Y27632, manumycin A and GW4869 were investigated, making sure that non-toxic doses of each inhibitor were used, something which had been left out of many studies involving these inhibitors. We found that all four inhibitors substantially decreased EV release compared to untreated cells. The EVs that were still released were thoroughly characterised, according to the MISEV2018 guidelines, something that is also not always performed in other studies that have used these inhibitors. We determined that there was no difference in protein concentration of EVs released after inhibitor treatment (i.e. with the exception of combo 2 which caused an increase compared to untreated cells) and protein markers carried in the EVs. To determine if the EVs still released after inhibitor treatment could be reduced

when compared to the negative effects caused by the heterogenous pool of EVs previously seen, we treated Hs578T and BT549 cells with increasing doses of remaining EVs and investigated their effects on recipient cell proliferation and migration. While there was a limited effect on cell proliferation, BT549 migration was substantially decreased when the cells were treated with the EVs released following inhibitor treatment when compared to the EVs released after no treatment. These experiments have shown that by inhibiting the release of EVs from TNBC cells, we could see a decrease in the migration of recipient TNBC cells. While others have studied these inhibitors before, this study investigates four different inhibitors at once, something which has not been performed. There has also been no other study that has investigated the effects of the cell derived EVs after EV inhibitor treatment.

7.1.2 TNBC EVs and platelet aggregation

Tumour cell induced platelet aggregation is a well-established phenomenon whereby tumour cells can interact with platelets and promote their activation. In the context of cancer in particular, this may lead to the development of heightened platelet aggregation and eventual thrombosis. Studies have also identified that cancer patients have elevated levels of circulating EVs and have been shown to play a role in aggregation by using *in vivo* mouse models. As discussed in Section 1.3, platelets can enhance cancer growth and evasion from cell death while cancer patients have an increased risk of developing venous thromboembolism (VTE). Therefore, we sought to investigate whether the TNBC cell line variants, Hs578T and Hs578Ts(i)$_8$ could also induce platelet aggregation and if their EVs also play a role, adding another mechanism by which TNBC EVs may enhance tumour growth and spread. Both TNBC cell line variants substantially reduced the amount of time it took for platelets to begin aggregating compared to the control without TNBC cells. Even more interesting, both cell line derived EVs induced platelet aggregation, with the higher the amount of EVs added to the washed platelets, the quicker they began to aggregate. Following this observation, we wanted to identify new proteins targets that may be carried by the EVs or on the EV surface and be potentially involved in this aggregation. Although TF and phosphatidylserine has already been established as pro-coagulant proteins carried by EVs, we aimed to identify other proteins carried by the TNBC EVs that also have platelet aggregation potential. Global proteomic analysis was performed on the TNBC EVs by mass spectrometry. Following data analysis, we selected six proteins including, PDGFRβ, Cyr61, glypican-1, CD97, MUC18/CD146 and MUC18, to undergo further investigation into their role in platelet aggregation. Immunoblotting was used to evaluate the six proteins. All six proteins were identified in both cell line derived EVs and densitometry measurements showed the same trend to the proteomic

data. A more detailed investigation is now warranted to determine if these proteins are involved in the platelet aggregation observed through the blocking of the proteins on the EVs and subsequent platelet aggregation measurements.

7.1.3 Serum EV separation

A study was designed to find a method of EV separation suitable for breast cancer patients' sera and their age-matched healthy controls that could potentially be translated into clinical use for diagnostic purposes. We sought to compare five different methods and included differential ultracentrifugation as a control method upon which to compare against. We chose poly (ethylene glycol) precipitation, size-exclusion chromatography, nickel-based isolation and two immunobead based kits (i.e. Stemcell technologies and Miltenyi Biotec) that selected for CD9/63/81^{+} EVs. By using several characterisation methods including BCA assay, NTA, TEM and immunoblot and investigating the levels of contamination of each separation method by apolipoprotein B ELISA, we determined that the Stemcell EasySep kit resulted in the purest EVs with the least amount of contaminating albumin and apolipoprotein B. One disadvantage of this method is the unsuitability of NTA which cannot accurately determine the particle concentration due to the immunobeads remaining in the isolate. However, this method can be easily translated to clinical use and is both time and cost effective without the need for a laborious EV isolation

Once a method was chosen, we wanted to investigate whether the isolated EVs could distinguish between breast cancer and cancer-free individuals, giving them a clinical relevance. Measuring the protein concentration of the EVs isolated from *n=20* breast cancer patients' sera and their age-matched healthy controls showed that there was no difference between the two groups. Next, we wanted to assess the EV cargo of the isolates to determine if they may be suitable for biomarker discovery. Glypican-1 and gremlin-1 were chosen as they been identified as having a role in breast cancer tumorigenesis. Glypican-1 has also been identified in EVs and shown to effective at distinguishing between different stages of the development pancreatic cancer. While glypican-1 levels were not different between breast cancer and healthy control isolates, gremlin-1 was substantially higher in breast cancer EVs compared to healthy controls. When the subtypes of the breast cancer patients were further analysed, TNBC patients' EVs carried the highest levels of gremlin-1 compared to the other subtypes. This is the first study to report the presence of gremlin-1 in EVs. More investigation is now needed to include more markers of breast cancer including miRNA, to determine if serum EVs isolated with our translatable method may be suitable for future diagnostic purposes.

7.2 Conclusions

7.2.1 Investigation of TNBC EV sub-population the inhibition of EV release with proposed inhibitors

We determined that all four sub-populations separated from the heterogeneous pool of EVs released from Hs578Ts(i)$_8$ cells were responsible for the transmission of aggressive traits to recipient parental Hs578T cells. This indicated that it was not simply one "rogue" sub-population that was responsible, but the EV pool collectively.

The proposed EV inhibitors, calpeptin, Y27632, manumycin A and GW4869 decreased the release of EVs from the Hs578Ts(i)$_8$ cells. Treating recipient TNBC cells, Hs578T and BT549 we discovered that the EVs still released after inhibitor treatment had a reduced ability to promote the migration of the recipient cells. With further studies performed, the inhibitors may be used in combination with other treatments to inhibit the progression of TNBC disease through the blocking of EV release that propagate the aggressive traits to other cells.

We have developed a protocol allows a faster way to check if a potential inhibitor is blocking EV release. It allows a higher throughput EV release screening without the need of a laborious separation method for a "first check" screening. With further validation, it may be an effective way to test new potential inhibitor in a shorter timeframe.

7.2.2 TNBC EVs and platelet aggregation

We showed that TNBC cell line variants, Hs578T and Hs578Ts(i)$_8$, and their corresponding EVs can induce platelet aggregation. Proteomic profiling of the TNBC EVs allowed us to select and evaluate proteins carried in the EVs that may be causing the platelet aggregation seen. Future experiments including blocking these proteins will determine if these proteins are the main cause or if they are causally involved.

7.2.3 Serum EV separation

In conclusion, by comparing several methods we have identified a quick, user-friendly method of serum EV separation that may be translated to a clinical setting. We also found that the serum EVs from breast cancer patients had higher gremlin-1 compared to healthy control. With further patient samples analysed to increase data confidence and more biomarkers investigated, this method may be

used to separate serum EVs from breast cancer patients and used as diagnostic tools without the need for invasive biopsies.

7.3 Future directions

A. Investigate EV inhibitors in more TNBC cell lines

The proposed EV inhibitors, calpeptin, Y27632, GW4869 and manumycin A should be tested in a larger panel of TNBC cell lines, to determine if their effects can be seen across multiple tumour types. TNBC cell lines including MDA-MB-231, HCC1143, BT549, MDA-MB-468 and also the non-tumorigenic breast cell line, MCF10A can be used. This would be a pre-requisite of an *in vivo* investigation.

B. Further development of high throughput screening assay

The addition of more EV markers such as CD81, CD63 and ADAM10 would be investigated in the CM of TNBC cells. Other cancer cells may also be used to develop the assay. A direct comparison with the "gold standard" EV separation method will be used to determine if the screening assay is a reliable method as a "first check" of EV release.

C. Assessment of EV inhibitors in patient-derived xenografts (PDX) models

If the proposed EV inhibitors successfully decrease EV release across a panel of TNBC cell lines *in* vitro, the next may be the use of a PDX model, to determine if the inhibitors have the potential to decrease tumour growth, in combination with another anti-cancer therapy. By implanting the original tissue or cells of the TNBC patient tumour in immunocompromised mice, the results seen with the TNBC cell lines *in vitro* can be investigated in a more realistic tumour environment. We could assess the release of EVs from the tumour *in vivo*.

D. Block proteins identified in TNBC EVs

The next part of the EV and platelet aggregation study would involve the blocking of key proteins identified by proteomic profiling using antibodies against the particular protein. As tissue factor and phosphatidylserine are known pro-coagulant proteins, they would be investigated too. The blocking of PDGFRβ, protein Cyr61, MUC18, CD97, glypican-1 and uPAR, would evaluate whether these proteins play a role in activating platelets. By repeating the experimental setup used with the TNBC EVs but comparing antibody blockage of individual proteins, we would use light transmission aggregometry to test the effects of inhibiting the proteins on platelet aggregation.

E. More in-depth investigation of breast cancer patient-derived serum EVs

Following the observation of different gremlin-1 levels carried in breast cancer EVs compared to age-matched control EVs, more biomarkers of breast cancer disease will be investigated with the addition of more breast cancer serum to increase the confidence of the data and help progress towards patient care. Other global profiling methods may also be used such as metabolomics or investigate the potential differences in glycoprotein signatures between breast cancer patients and healthy controls.

References

1. Perou, C.M., et al., *Molecular portraits of human breast tumours.* Nature, 2000. **406**: p. 747.
2. Sørlie, T., et al., *Gene expression patterns of breast carcinomas distinguish tumor subclasses with clinical implications.* Proceedings of the National Academy of Sciences of the United States of America, 2001. **98**(19): p. 10869-10874.
3. Yersal, O. and S. Barutca, *Biological subtypes of breast cancer: Prognostic and therapeutic implications.* World journal of clinical oncology, 2014. **5**(3): p. 412-424.
4. Creighton, C.J., *The molecular profile of luminal B breast cancer.* Biologics : targets & therapy, 2012. **6**: p. 289-297.
5. Cheang, M.C., et al., *Ki67 index, HER2 status, and prognosis of patients with luminal B breast cancer.* J Natl Cancer Inst, 2009. **101**(10): p. 736-50.
6. Inic, Z., et al., *Difference between Luminal A and Luminal B Subtypes According to Ki-67, Tumor Size, and Progesterone Receptor Negativity Providing Prognostic Information.* Clinical Medicine Insights. Oncology, 2014. **8**: p. 107-111.
7. Abdel-Hafiz, A.H., *Epigenetic Mechanisms of Tamoxifen Resistance in Luminal Breast Cancer.* Diseases, 2017. **5**(3).
8. Figueroa-Magalhães, M.C., et al., *Treatment of HER2-positive breast cancer.* Breast (Edinburgh, Scotland), 2014. **23**(2): p. 128-136.
9. Slamon, D., et al., *Adjuvant trastuzumab in HER2-positive breast cancer.* The New England journal of medicine, 2011. **365**(14): p. 1273-1283.
10. Tortora, G., *Mechanisms of Resistance to HER2 Target Therapy.* JNCI Monographs, 2011. **2011**(43): p. 95-98.
11. Dai, X., et al., *Breast cancer intrinsic subtype classification, clinical use and future trends.* American journal of cancer research, 2015. **5**(10): p. 2929-2943.
12. Herschkowitz, J.I., et al., *Identification of conserved gene expression features between murine mammary carcinoma models and human breast tumors.* Genome Biol, 2007. **8**(5): p. R76.
13. Prat, A., et al., *Phenotypic and molecular characterization of the claudin-low intrinsic subtype of breast cancer.* Breast Cancer Res, 2010. **12**(5): p. R68.
14. Livasy, C.A., et al., *Phenotypic evaluation of the basal-like subtype of invasive breast carcinoma.* Modern Pathology, 2005. **19**: p. 264.
15. Kreike, B., et al., *Gene expression profiling and histopathological characterization of triple-negative/basal-like breast carcinomas.* Breast cancer research : BCR, 2007. **9**(5): p. R65-R65.
16. Bastien, R.R.L., et al., *PAM50 breast cancer subtyping by RT-qPCR and concordance with standard clinical molecular markers.* BMC medical genomics, 2012. **5**: p. 44-44.
17. M Perou, C., *Molecular Stratification of Triple-Negative Breast Cancers*. Vol. 16 Suppl 1. 2011. 61-70.
18. Sorlie, T., et al., *Repeated observation of breast tumor subtypes in independent gene expression data sets.* Proceedings of the National Academy of Sciences of the United States of America, 2003. **100**(14): p. 8418-8423.
19. Dent, R., et al., *Triple-Negative Breast Cancer: Clinical Features and Patterns of Recurrence.* Clinical Cancer Research, 2007. **13**(15): p. 4429.
20. Bauer, K.R., et al., *Descriptive analysis of estrogen receptor (ER)-negative, progesterone receptor (PR)-negative, and HER2-negative invasive breast cancer, the so-called triple-negative phenotype.* Cancer, 2007. **109**(9): p. 1721-1728.
21. Haffty, B.G., et al., *Locoregional Relapse and Distant Metastasis in Conservatively Managed Triple Negative Early-Stage Breast Cancer.* Journal of Clinical Oncology, 2006. **24**(36): p. 5652-5657.
22. Harris, L.N., et al., *Molecular subtypes of breast cancer in relation to paclitaxel response and outcomes in women with metastatic disease: results from CALGB 9342.* Breast cancer research : BCR, 2006. **8**(6): p. R66-R66.

23. Stefansson, I.M., et al., *Germline BRCA1 Mutations and a Basal Epithelial Phenotype in Breast Cancer.* JNCI: Journal of the National Cancer Institute, 2003. **95**(19): p. 1482-1485.
24. Yin, L., et al., *Triple-negative breast cancer molecular subtyping and treatment progress.* Breast Cancer Research, 2020. **22**(1): p. 61.
25. Jiang, Y.-Z., et al., *Molecular subtyping and genomic profiling expand precision medicine in refractory metastatic triple-negative breast cancer: the FUTURE trial.* Cell Research, 2021. **31**(2): p. 178-186.
26. Lehmann, B.D., et al., *Identification of human triple-negative breast cancer subtypes and preclinical models for selection of targeted therapies.* The Journal of Clinical Investigation, 2011. **121**(7): p. 2750-2767.
27. Lehmann, B.D., et al., *Refinement of Triple-Negative Breast Cancer Molecular Subtypes: Implications for Neoadjuvant Chemotherapy Selection.* PloS one, 2016. **11**(6): p. e0157368.
28. Burstein, M.D., et al., *Comprehensive Genomic Analysis Identifies Novel Subtypes and Targets of Triple-Negative Breast Cancer.* Clinical Cancer Research, 2015. **21**(7): p. 1688.
29. Hackett, A.J., et al., *Two Syngeneic Cell Lines from Human Breast Tissue: The Aneuploid Mammary Epithelial (Hs578T) and the Diploid Myoepithelial (Hs578Bst) Cell Lines2.* JNCI: Journal of the National Cancer Institute, 1977. **58**(6): p. 1795-1806.
30. Kenny, P.A., et al., *The morphologies of breast cancer cell lines in three-dimensional assays correlate with their profiles of gene expression.* Molecular Oncology, 2007. **1**(1): p. 84-96.
31. Hughes, L., et al., *Characterisation of breast cancer cell lines and establishment of a novel isogenic subclone to study migration, invasion and tumourigenicity.* Clin Exp Metastasis, 2008. **25**(5): p. 549-57.
32. O'Neill, S., et al., *2-Deoxy-D-Glucose inhibits aggressive triple-negative breast cancer cells by targeting glycolysis and the cancer stem cell phenotype.* Sci Rep, 2019. **9**(1): p. 3788.
33. Espinosa Fernandez, J.R., et al., *Identification of triple-negative breast cancer cell lines classified under the same molecular subtype using different molecular characterization techniques: Implications for translational research.* PloS one, 2020. **15**(4): p. e0231953.
34. Johnstone, R.M., et al., *Vesicle formation during reticulocyte maturation. Association of plasma membrane activities with released vesicles (exosomes).* J Biol Chem, 1987. **262**(19): p. 9412-20.
35. Mathivanan, S., H. Ji, and R.J. Simpson, *Exosomes: Extracellular organelles important in intercellular communication.* Journal of Proteomics, 2010. **73**(10): p. 1907-1920.
36. Cocucci, E., G. Racchetti, and J. Meldolesi, *Shedding microvesicles: artefacts no more.* Trends in Cell Biology, 2009. **19**(2): p. 43-51.
37. D'Souza-Schorey, C. and J.W. Clancy, *Tumor-derived microvesicles: shedding light on novel microenvironment modulators and prospective cancer biomarkers.* Genes Dev, 2012. **26**(12): p. 1287-99.
38. Clark, M.R., *Flippin' lipids.* Nature Immunology, 2011. **12**(5): p. 373-375.
39. van Niel, G., G. D'Angelo, and G. Raposo, *Shedding light on the cell biology of extracellular vesicles.* Nat Rev Mol Cell Biol, 2018. **19**(4): p. 213-228.
40. Del Conde, I., et al., *Tissue-factor-bearing microvesicles arise from lipid rafts and fuse with activated platelets to initiate coagulation.* Blood, 2005. **106**(5): p. 1604-11.
41. Muralidharan-Chari, V., et al., *ARF6-regulated shedding of tumor cell-derived plasma membrane microvesicles.* Curr Biol, 2009. **19**(22): p. 1875-85.
42. Li, B., et al., *RhoA triggers a specific signaling pathway that generates transforming microvesicles in cancer cells.* Oncogene, 2012. **31**(45): p. 4740-4749.
43. Théry, C., L. Zitvogel, and S. Amigorena, *Exosomes: composition, biogenesis and function.* Nature Reviews Immunology, 2002. **2**: p. 569.
44. Raiborg, C. and H. Stenmark, *The ESCRT machinery in endosomal sorting of ubiquitylated membrane proteins.* Nature, 2009. **458**: p. 445.

45. Colombo, M., G. Raposo, and C. Théry, *Biogenesis, Secretion, and Intercellular Interactions of Exosomes and Other Extracellular Vesicles.* Annual Review of Cell and Developmental Biology, 2014. **30**(1): p. 255-289.
46. Piper, R.C. and D.J. Katzmann, *Biogenesis and function of multivesicular bodies.* Annual review of cell and developmental biology, 2007. **23**: p. 519-547.
47. Wollert, T. and J.H. Hurley, *Molecular mechanism of multivesicular body biogenesis by ESCRT complexes.* Nature, 2010. **464**: p. 864.
48. Babst, M., B.A. Davies, and D.J. Katzmann, *Regulation of Vps4 during MVB sorting and cytokinesis.* Traffic, 2011. **12**(10): p. 1298-305.
49. Baietti, M.F., et al., *Syndecan–syntenin–ALIX regulates the biogenesis of exosomes.* Nature Cell Biology, 2012. **14**(7): p. 677-685.
50. Roucourt, B., et al., *Heparanase activates the syndecan-syntenin-ALIX exosome pathway.* Cell Research, 2015. **25**(4): p. 412-428.
51. Trajkovic, K., et al., *Ceramide Triggers Budding of Exosome Vesicles into Multivesicular Endosomes.* Science, 2008. **319**(5867): p. 1244.
52. Menck, K., et al., *Neutral sphingomyelinases control extracellular vesicles budding from the plasma membrane.* Journal of extracellular vesicles, 2017. **6**(1): p. 1378056.
53. van Niel, G., et al., *The tetraspanin CD63 regulates ESCRT-independent and -dependent endosomal sorting during melanogenesis.* Dev Cell, 2011. **21**(4): p. 708-21.
54. Hristov, M., et al., *Apoptotic bodies from endothelial cells enhance the number and initiate the differentiation of human endothelial progenitor cells in vitro.* Blood, 2004. **104**(9): p. 2761.
55. Halicka, H.D., E. Bedner, and Z. Darzynkiewicz, *Segregation of RNA and Separate Packaging of DNA and RNA in Apoptotic Bodies during Apoptosis.* Experimental Cell Research, 2000. **260**(2): p. 248-256.
56. Crescitelli, R., et al., *Distinct RNA profiles in subpopulations of extracellular vesicles: apoptotic bodies, microvesicles and exosomes.* Journal of extracellular vesicles, 2013. **2**: p. e20677.
57. Holmgren, L., et al., *Horizontal Transfer of DNA by the Uptake of Apoptotic Bodies.* Blood, 1999. **93**(11): p. 3956.
58. Bergsmedh, A., et al., *Horizontal transfer of oncogenes by uptake of apoptotic bodies.* Proceedings of the National Academy of Sciences, 2001. **98**(11): p. 6407.
59. Al-Nedawi, K., et al., *Intercellular transfer of the oncogenic receptor EGFRvIII by microvesicles derived from tumour cells.* Nature Cell Biology, 2008. **10**: p. 619.
60. Di Vizio, D., et al., *Oncosome formation in prostate cancer: association with a region of frequent chromosomal deletion in metastatic disease.* Cancer research, 2009. **69**(13): p. 5601-5609.
61. Minciacchi, V.R., et al., *Large oncosomes contain distinct protein cargo and represent a separate functional class of tumor-derived extracellular vesicles.* Oncotarget, 2015. **6**(13): p. 11327-41.
62. Morello, M., et al., *Large oncosomes mediate intercellular transfer of functional microRNA.* Cell cycle (Georgetown, Tex.), 2013. **12**(22): p. 3526-3536.
63. Di Vizio, D., et al., *Large oncosomes in human prostate cancer tissues and in the circulation of mice with metastatic disease.* The American journal of pathology, 2012. **181**(5): p. 1573-1584.
64. Muralidharan-Chari, V., et al., *Microvesicles: mediators of extracellular communication during cancer progression.* J Cell Sci, 2010. **123**(Pt 10): p. 1603-11.
65. Sidhu, S.S., et al., *The microvesicle as a vehicle for EMMPRIN in tumor-stromal interactions.* Oncogene, 2004. **23**(4): p. 956-63.
66. Menck, K., et al., *Characterisation of tumour-derived microvesicles in cancer patients' blood and correlation with clinical outcome.* Journal of Extracellular Vesicles, 2017. **6**(1): p. 1340745.
67. Grange, C., et al., *Microvesicles Released from Human Renal Cancer Stem Cells Stimulate Angiogenesis and Formation of Lung Premetastatic Niche.* Cancer Research, 2011. **71**(15): p. 5346.

68. Castellana, D., et al., *Membrane microvesicles as actors in the establishment of a favorable prostatic tumoral niche: a role for activated fibroblasts and CX3CL1-CX3CR1 axis.* Cancer Res, 2009. **69**(3): p. 785-93.
69. Al-Nedawi, K., et al., *Endothelial expression of autocrine VEGF upon the uptake of tumor-derived microvesicles containing oncogenic EGFR.* Proceedings of the National Academy of Sciences of the United States of America, 2009. **106**(10): p. 3794-3799.
70. Kang, M., S. Kim, and J. Ko, *Roles of CD133 in microvesicle formation and oncoprotein trafficking in colon cancer.* The FASEB Journal, 2018: p. 4248-4260.
71. Suwakulsiri, W., et al., *Proteomic profiling reveals key cancer progression modulators in shed microvesicles released from isogenic human primary and metastatic colorectal cancer cell lines.* Biochimica et Biophysica Acta (BBA) - Proteins and Proteomics, 2018.
72. Raposo, G., et al., *B lymphocytes secrete antigen-presenting vesicles.* The Journal of Experimental Medicine, 1996. **183**(3): p. 1161.
73. Morvan, J., B. Rinaldi, and S. Friant, *Pkh1/2-dependent phosphorylation of Vps27 regulates ESCRT-I recruitment to endosomes.* Mol Biol Cell, 2012. **23**(20): p. 4054-64.
74. Lee, T.H., et al., *Oncogenic ras-driven cancer cell vesiculation leads to emission of double-stranded DNA capable of interacting with target cells.* Biochem Biophys Res Commun, 2014. **451**(2): p. 295-301.
75. Abd Elmageed, Z.Y., et al., *Neoplastic reprogramming of patient-derived adipose stem cells by prostate cancer cell-associated exosomes.* Stem Cells, 2014. **32**(4): p. 983-97.
76. Ramteke, A., et al., *Exosomes secreted under hypoxia enhance invasiveness and stemness of prostate cancer cells by targeting adherens junction molecules.* Mol Carcinog, 2015. **54**(7): p. 554-65.
77. Martinez, V.G., et al., *Resistance to HER2-targeted anti-cancer drugs is associated with immune evasion in cancer cells and their derived extracellular vesicles.* Oncoimmunology, 2017. **6**(12): p. e1362530.
78. Cereghetti, D.M. and P.P. Lee, *Tumor-Derived Exosomes Contain microRNAs with Immunological Function: Implications for a Novel Immunosuppression Mechanism.* Microrna, 2014. **2**(3): p. 194-204.
79. Peinado, H., et al., *Melanoma exosomes educate bone marrow progenitor cells toward a pro-metastatic phenotype through MET.* Nature Medicine, 2012. **18**: p. 883.
80. Smith, J.A., et al., *Extracellular vesicles and their synthetic analogues in aging and age-associated brain diseases.* Biogerontology, 2015. **16**(2): p. 147-185.
81. van Niel, G., et al., *Exosomes: A Common Pathway for a Specialized Function.* The Journal of Biochemistry, 2006. **140**(1): p. 13-21.
82. Kowal, J., et al., *Proteomic comparison defines novel markers to characterize heterogeneous populations of extracellular vesicle subtypes.* Proceedings of the National Academy of Sciences, 2016. **113**(8): p. E968.
83. Baietti, M.F., et al., *Syndecan–syntenin–ALIX regulates the biogenesis of exosomes.* Nature Cell Biology, 2012. **14**: p. 677.
84. D'Souza-Schorey, C. and P. Chavrier, *ARF proteins: roles in membrane traffic and beyond.* Nat Rev Mol Cell Biol, 2006. **7**(5): p. 347-58.
85. Théry, C., et al., *Minimal information for studies of extracellular vesicles 2018 (MISEV2018): a position statement of the International Society for Extracellular Vesicles and update of the MISEV2014 guidelines.* Journal of extracellular vesicles, 2018. **7**(1): p. 1535750.
86. O'Brien, K., et al., *Exosomes from triple-negative breast cancer cells can transfer phenotypic traits representing their cells of origin to secondary cells.* Eur J Cancer, 2013. **49**(8): p. 1845-59.
87. O'Brien, K., et al., *miR-134 in extracellular vesicles reduces triple-negative breast cancer aggression and increases drug sensitivity.* Oncotarget, 2015. **6**(32): p. 32774-32789.

88. Kavanagh, E.L., et al., *Protein and chemotherapy profiling of extracellular vesicles harvested from therapeutic induced senescent triple negative breast cancer cells.* Oncogenesis, 2017. **6**: p. e388.
89. Ozawa, P.M.M., et al., *Extracellular vesicles from triple-negative breast cancer cells promote proliferation and drug resistance in non-tumorigenic breast cells.* Breast Cancer Research and Treatment, 2018. **172**(3): p. 713-723.
90. Rabe, D.C., et al., *Tumor extracellular vesicles are required for tumor-associated macrophage programming.* bioRxiv, 2018: p. 375022.
91. Piao, Y.J., et al., *Breast cancer cell-derived exosomes and macrophage polarization are associated with lymph node metastasis.* Oncotarget, 2018. **9**(7): p. 7398-7410.
92. Medeiros, B., et al., *Triple-Negative Primary Breast Tumors Induce Supportive Premetastatic Changes in the Extracellular Matrix and Soluble Components of the Lung Microenvironment.* Cancers, 2020. **12**(1).
93. Ramírez-Ricardo, J., et al., *Circulating extracellular vesicles from patients with breast cancer enhance migration and invasion via a Src-dependent pathway in MDA-MB-231 breast cancer cells.* Molecular medicine reports, 2020. **22**(3): p. 1932-1948.
94. Catalano, M. and L. O'Driscoll, *Inhibiting extracellular vesicles formation and release: a review of EV inhibitors.* Journal of Extracellular Vesicles, 2020. **9**(1): p. 1703244.
95. Im, E.-J., et al., *Sulfisoxazole inhibits the secretion of small extracellular vesicles by targeting the endothelin receptor A.* Nature Communications, 2019. **10**(1): p. 1387.
96. Kosgodage, U.S., et al., *Chloramidine/Bisindolylmaleimide-I-Mediated Inhibition of Exosome and Microvesicle Release and Enhanced Efficacy of Cancer Chemotherapy.* International journal of molecular sciences, 2017. **18**(5): p. 1007.
97. Kholia, S., et al., *A novel role for peptidylarginine deiminases in microvesicle release reveals therapeutic potential of PAD inhibition in sensitizing prostate cancer cells to chemotherapy.* Journal of Extracellular Vesicles, 2015. **4**(1): p. 26192.
98. Tarcsa, E., et al., *Protein unfolding by peptidylarginine deiminase. Substrate specificity and structural relationships of the natural substrates trichohyalin and filaggrin.* J Biol Chem, 1996. **271**(48): p. 30709-16.
99. Tsujinaka, T., et al., *Synthesis of a new cell penetrating calpain inhibitor (calpeptin).* Biochem Biophys Res Commun, 1988. **153**(3): p. 1201-8.
100. Storr, S.J., et al., *The calpain system and cancer.* Nature Reviews Cancer, 2011. **11**(5): p. 364-374.
101. Sorimachi, H., S. Hata, and Y. Ono, *Expanding members and roles of the calpain superfamily and their genetically modified animals.* Exp Anim, 2010. **59**(5): p. 549-66.
102. Huang, Y. and K.K. Wang, *The calpain family and human disease.* Trends Mol Med, 2001. **7**(8): p. 355-62.
103. Leloup, L. and A. Wells, *Calpains as potential anti-cancer targets.* Expert Opin Ther Targets, 2011. **15**(3): p. 309-23.
104. Jorfi, S., et al., *Inhibition of microvesiculation sensitizes prostate cancer cells to chemotherapy and reduces docetaxel dose required to limit tumor growth in vivo.* Scientific reports, 2015. **5**: p. 13006.
105. Mallick, R.L., et al., *Prion protein fragment (106–126) induces prothrombotic state by raising platelet intracellular calcium and microparticle release.* Cell Calcium, 2015. **57**(4): p. 300-311.
106. Fox, J.E., et al., *Evidence that agonist-induced activation of calpain causes the shedding of procoagulant-containing microvesicles from the membrane of aggregating platelets.* Journal of Biological Chemistry, 1991. **266**(20): p. 13289-13295.
107. Amano, M., M. Nakayama, and K. Kaibuchi, *Rho-kinase/ROCK: A key regulator of the cytoskeleton and cell polarity.* Cytoskeleton (Hoboken, N.J.), 2010. **67**(9): p. 545-554.
108. Kureishi, Y., et al., *Rho-associated kinase directly induces smooth muscle contraction through myosin light chain phosphorylation.* J Biol Chem, 1997. **272**(19): p. 12257-60.

109. Maekawa, M., et al., *Signaling from Rho to the actin cytoskeleton through protein kinases ROCK and LIM-kinase.* Science, 1999. **285**(5429): p. 895-8.
110. Latham, S.L., et al., *Cooperation between β-and γ-cytoplasmic actins in the mechanical regulation of endothelial microparticle formation.* The FASEB Journal, 2013. **27**(2): p. 672-683.
111. Abid Hussein, M.N., et al., *Inhibition of microparticle release triggers endothelial cell apoptosis and detachment.* Thromb Haemost, 2007. **98**(5): p. 1096-107.
112. Logsdon, C.D. and W. Lu, *The Significance of Ras Activity in Pancreatic Cancer Initiation.* International journal of biological sciences, 2016. **12**(3): p. 338-346.
113. Oh, H.J., et al., *Convective exosome-tracing microfluidics for analysis of cell-non-autonomous neurogenesis.* Biomaterials, 2017. **112**: p. 82-94.
114. Datta, A., et al., *Manumycin A suppresses exosome biogenesis and secretion via targeted inhibition of Ras/Raf/ERK1/2 signaling and hnRNP H1 in castration-resistant prostate cancer cells.* Cancer Letters, 2017. **408**: p. 73-81.
115. Yang, Y., et al., *Dysregulation of miR-212 Promotes Castration Resistance through hnRNPH1-Mediated Regulation of AR and AR-V7: Implications for Racial Disparity of Prostate Cancer.* Clinical Cancer Research, 2016. **22**(7): p. 1744.
116. Zhou, X., et al., *Exosome production and its regulation of EGFR during wound healing in renal tubular cells.* American journal of physiology. Renal physiology, 2017. **312**(6): p. F963-F970.
117. Luhtala, N., et al., *Secreted Glioblastoma Nanovesicles Contain Intracellular Signaling Proteins and Active Ras Incorporated in a Farnesylation-dependent Manner.* J Biol Chem, 2017. **292**(2): p. 611-628.
118. Shamseddine, A.A., M.V. Airola, and Y.A. Hannun, *Roles and regulation of neutral sphingomyelinase-2 in cellular and pathological processes.* Advances in biological regulation, 2015. **57**: p. 24-41.
119. Essandoh, K., et al., *Blockade of exosome generation with GW4869 dampens the sepsis-induced inflammation and cardiac dysfunction.* Biochimica et biophysica acta, 2015. **1852**(11): p. 2362-2371.
120. Huang, Y., et al., *Zika virus propagation and release in human fetal astrocytes can be suppressed by neutral sphingomyelinase-2 inhibitor GW4869.* Cell Discovery, 2018. **4**(1): p. 19.
121. Hu, Y., et al., *Fibroblast-Derived Exosomes Contribute to Chemoresistance through Priming Cancer Stem Cells in Colorectal Cancer.* PLOS ONE, 2015. **10**(5): p. e0125625.
122. Cao, Y.-L., et al., *Exosomal DNMT1 mediates cisplatin resistance in ovarian cancer.* Cell Biochemistry and Function, 2017. **35**(6): p. 296-303.
123. Menck, K., et al., *Neutral sphingomyelinases control extracellular vesicles budding from the plasma membrane.* Journal of extracellular vesicles, 2017. **6**(1): p. 1378056-1378056.
124. Menter, D.G., et al., *Platelet "first responders" in wound response, cancer, and metastasis.* Cancer metastasis reviews, 2017. **36**(2): p. 199-213.
125. Jackson, S.P., N. Mistry, and Y. Yuan, *Platelets and the Injured Vessel Wall— "Rolling into Action": Focus on Glycoprotein Ib/V/IX and the Platelet Cytoskeleton.* Trends in Cardiovascular Medicine, 2000. **10**(5): p. 192-197.
126. Witkowski, M., U. Landmesser, and U. Rauch, *Tissue factor as a link between inflammation and coagulation.* Trends in Cardiovascular Medicine, 2016. **26**(4): p. 297-303.
127. Owens, A.P., 3rd and N. Mackman, *Tissue factor and thrombosis: The clot starts here.* Thrombosis and haemostasis, 2010. **104**(3): p. 432-439.
128. Nieswandt, B., et al., *Lysis of Tumor Cells by Natural Killer Cells in Mice Is Impeded by Platelets.* Cancer Research, 1999. **59**(6): p. 1295.
129. Rachidi, S., et al., *Platelets subvert T cell immunity against cancer via GARP-TGFβ axis.* Sci Immunol, 2017. **2**(11).
130. Haemmerle, M., et al., *Platelets reduce anoikis and promote metastasis by activating YAP1 signaling.* Nature Communications, 2017. **8**(1): p. 310.

131. Labelle, M., S. Begum, and R.O. Hynes, *Direct signaling between platelets and cancer cells induces an epithelial-mesenchymal-like transition and promotes metastasis.* Cancer cell, 2011. **20**(5): p. 576-590.
132. Bottsford-Miller, J., et al., *Differential platelet levels affect response to taxane-based therapy in ovarian cancer.* Clinical cancer research : an official journal of the American Association for Cancer Research, 2015. **21**(3): p. 602-610.
133. Radziwon-Balicka, A., et al., *Platelets increase survival of adenocarcinoma cells challenged with anticancer drugs: mechanisms and implications for chemoresistance.* British Journal of Pharmacology, 2012. **167**(4): p. 787-804.
134. Di Vito, C., et al., *Platelets from glioblastoma patients promote angiogenesis of tumor endothelial cells and exhibit increased VEGF content and release.* Platelets, 2017. **28**(6): p. 585-594.
135. Jiang, L., et al., *Platelet releasate promotes breast cancer growth and angiogenesis via VEGF-integrin cooperative signalling.* Br J Cancer, 2017. **117**(5): p. 695-703.
136. Zarà, M., et al., *Molecular mechanisms of platelet activation and aggregation induced by breast cancer cells.* Cellular Signalling, 2018. **48**: p. 45-53.
137. Heinmöller, E., et al., *Tumor Cell-Induced Platelet Aggregation in Vitro by Human Pancreatic Cancer Cell Lines.* Scandinavian Journal of Gastroenterology, 1995. **30**(10): p. 1008-1016.
138. Mitrugno, A., et al., *A novel and essential role for FcγRIIa in cancer cell–induced platelet activation.* Blood, 2014. **123**(2): p. 249-260.
139. Medina, C., et al., *Platelet Aggregation-Induced by Caco-2 Cells: Regulation by Matrix Metalloproteinase-2 and Adenosine Diphosphate.* Journal of Pharmacology and Experimental Therapeutics, 2006. **317**(2): p. 739.
140. Alonso-Escolano, D., et al., *Membrane type-1 matrix metalloproteinase stimulates tumour cell-induced platelet aggregation: role of receptor glycoproteins.* British Journal of Pharmacology, 2004. **141**(2): p. 241-252.
141. Heinmöller, E., et al., *Studies on tumor-cell-induced platelet aggregation in human lung cancer cell lines.* Journal of Cancer Research and Clinical Oncology, 1996. **122**(12): p. 735-744.
142. Vernieri, C., et al., *The neutrophil-to-lymphocyte and platelet-to-lymphocyte ratios predict efficacy of platinum-based chemotherapy in patients with metastatic triple negative breast cancer.* Scientific reports, 2018. **8**(1): p. 8703.
143. Romero-Cordoba, S., et al., *Decoding Immune Heterogeneity of Triple Negative Breast Cancer and Its Association with Systemic Inflammation.* Cancers, 2019. **11**(7): p. 911.
144. Khorana, A.A., et al., *Development and validation of a predictive model for chemotherapy-associated thrombosis.* Blood, 2008. **111**(10): p. 4902-4907.
145. Verso, M., et al., *A modified Khorana risk assessment score for venous thromboembolism in cancer patients receiving chemotherapy: the Protecht score.* Intern Emerg Med, 2012. **7**(3): p. 291-2.
146. Khorana, A.A., *Venous thromboembolism and prognosis in cancer.* Thrombosis research, 2010. **125**(6): p. 490-493.
147. Kyriazi, V. and E. Theodoulou, *Assessing the risk and prognosis of thrombotic complications in cancer patients.* Arch Pathol Lab Med, 2013. **137**(9): p. 1286-95.
148. Horsted, F., J. West, and M.J. Grainge, *Risk of Venous Thromboembolism in Patients with Cancer: A Systematic Review and Meta-Analysis.* PLOS Medicine, 2012. **9**(7): p. e1001275.
149. Ahlbrecht, J., et al., *Tumor Grade Is Associated With Venous Thromboembolism in Patients With Cancer: Results From the Vienna Cancer and Thrombosis Study.* Journal of Clinical Oncology, 2012. **30**(31): p. 3870-3875.
150. Mellema, W.W., et al., *Retrospective evaluation of thromboembolic events in patients with non-small cell lung cancer treated with platinum-based chemotherapy.* Lung Cancer, 2014. **86**(1): p. 73-77.

151. Lechner, D., et al., *Chemotherapy-induced thrombin generation via procoagulant endothelial microparticles is independent of tissue factor activity.* Journal of Thrombosis and Haemostasis, 2007. **5**(12): p. 2445-2452.
152. Sciacca, F.L., et al., *Genetic and Plasma Markers of Venous Thromboembolism in Patients with High Grade Glioma.* Clinical Cancer Research, 2004. **10**(4): p. 1312.
153. Bollen, L., et al., *Active PAI-1 as marker for venous thromboembolism: Case–control study using a comprehensive panel of PAI-1 and TAFI assays.* Thrombosis Research, 2014. **134**(5): p. 1097-1102.
154. Chen, N., et al., *Bevacizumab promotes venous thromboembolism through the induction of PAI-1 in a mouse xenograft model of human lung carcinoma.* Mol Cancer, 2015. **14**: p. 140.
155. Key, N.S., et al., *Venous Thromboembolism Prophylaxis and Treatment in Patients With Cancer: ASCO Clinical Practice Guideline Update.* Journal of Clinical Oncology, 2019. **38**(5): p. 496-520.
156. Carrier, M., et al., *Apixaban to Prevent Venous Thromboembolism in Patients with Cancer.* New England Journal of Medicine, 2018. **380**(8): p. 711-719.
157. Levine, M.N., et al., *A randomized phase II trial of apixaban for the prevention of thromboembolism in patients with metastatic cancer.* Journal of Thrombosis and Haemostasis, 2012. **10**(5): p. 807-814.
158. Raskob, G.E., et al., *Edoxaban for the Treatment of Cancer-Associated Venous Thromboembolism.* N Engl J Med, 2018. **378**(7): p. 615-624.
159. Agnelli, G., et al., *Semuloparin for Thromboprophylaxis in Patients Receiving Chemotherapy for Cancer.* New England Journal of Medicine, 2012. **366**(7): p. 601-609.
160. Zwicker, J.I., et al., *Prediction and prevention of thromboembolic events with enoxaparin in cancer patients with elevated tissue factor-bearing microparticles: a randomized-controlled phase II trial (the Microtec study).* British journal of haematology, 2013. **160**(4): p. 530-537.
161. Prandoni, P., et al., *Recurrent venous thromboembolism and bleeding complications during anticoagulant treatment in patients with cancer and venous thrombosis.* Blood, 2002. **100**(10): p. 3484-3488.
162. Khorana, A.A., et al., *Tissue Factor Expression, Angiogenesis, and Thrombosis in Pancreatic Cancer.* Clinical Cancer Research, 2007. **13**(10): p. 2870.
163. Vormittag, R., et al., *High Factor VIII Levels Independently Predict Venous Thromboembolism in Cancer Patients.* Arteriosclerosis, Thrombosis, and Vascular Biology, 2009. **29**(12): p. 2176-2181.
164. Faille, D., et al., *Biomarkers for the risk of thrombosis in pancreatic adenocarcinoma are related to cancer process.* Oncotarget; Vol 9, No 41, 2018.
165. Mauracher, L.M., et al., *Citrullinated histone H3, a biomarker of neutrophil extracellular trap formation, predicts the risk of venous thromboembolism in cancer patients.* Journal of thrombosis and haemostasis : JTH, 2018. **16**(3): p. 508-518.
166. Thomas, G.M., et al., *Cancer cell–derived microparticles bearing P-selectin glycoprotein ligand 1 accelerate thrombus formation in vivo.* Journal of Experimental Medicine, 2009. **206**(9): p. 1913-1927.
167. Davila, M., et al., *Tissue factor-bearing microparticles derived from tumor cells: impact on coagulation activation.* Journal of Thrombosis and Haemostasis, 2008. **6**(9): p. 1517-1524.
168. Al Saleh, H.A., et al., *Thrombotic characteristics of extracellular vesicles derived from prostate cancer cells.* The Prostate, 2018. **78**(13): p. 953-961.
169. Geddings, J.E., et al., *Tissue factor-positive tumor microvesicles activate platelets and enhance thrombosis in mice.* Journal of thrombosis and haemostasis : JTH, 2016. **14**(1): p. 153-166.
170. Heijnen, H.F.G., et al., *Activated Platelets Release Two Types of Membrane Vesicles: Microvesicles by Surface Shedding and Exosomes Derived From Exocytosis of Multivesicular Bodies and ・-Granules.* Blood, 1999. **94**(11): p. 3791-3799.

171. Hoogland, G., et al., *Thrombin-stimulated glutamate uptake in human platelets is predominantly mediated by the glial glutamate transporter EAAT2.* Neurochemistry International, 2005. **47**(7): p. 499-506.
172. Gautam, D., et al., *Glutamate induces synthesis of thrombogenic peptides and extracellular vesicle release from human platelets.* Scientific Reports, 2019. **9**(1): p. 8346.
173. Tripisciano, C., et al., *Different Potential of Extracellular Vesicles to Support Thrombin Generation: Contributions of Phosphatidylserine, Tissue Factor, and Cellular Origin.* Scientific Reports, 2017. **7**(1): p. 6522.
174. Berckmans, R.J., et al., *Extracellular vesicles and coagulation in blood from healthy humans revisited.* Journal of extracellular vesicles, 2019. **8**(1).
175. Berckmans, R.J., et al., *Cell-derived microparticles circulate in healthy humans and support low grade thrombin generation.* Thromb Haemost, 2001. **85**(4): p. 639-46.
176. Görgens, A., et al., *Optimisation of imaging flow cytometry for the analysis of single extracellular vesicles by using fluorescence-tagged vesicles as biological reference material.* Journal of Extracellular Vesicles, 2019. **8**(1).
177. Tyanova, S., T. Temu, and J. Cox, *The MaxQuant computational platform for mass spectrometry-based shotgun proteomics.* Nature Protocols, 2016. **11**(12): p. 2301-2319.
178. Cox, J. and M. Mann, *MaxQuant enables high peptide identification rates, individualized p.p.b.-range mass accuracies and proteome-wide protein quantification.* Nat Biotechnol, 2008. **26**(12): p. 1367-72.
179. Cox, J., et al., *Andromeda: A Peptide Search Engine Integrated into the MaxQuant Environment.* Journal of Proteome Research, 2011. **10**(4): p. 1794-1805.
180. Cox, J., et al., *Accurate proteome-wide label-free quantification by delayed normalization and maximal peptide ratio extraction, termed MaxLFQ.* Mol Cell Proteomics, 2014. **13**(9): p. 2513-26.
181. Pathan, M., et al., *A novel community driven software for functional enrichment analysis of extracellular vesicles data.* Journal of Extracellular Vesicles, 2017. **6**(1): p. 1321455.
182. Notarangelo, M., et al., *Rapid Nickel-based Isolation of Extracellular Vesicles from Different Biological Fluids.* Bio-protocol, 2020. **10**(3): p. e3512.
183. O'Brien, K., et al., *Exosomes from triple-negative breast cancer cells can transfer phenotypic traits representing their cells of origin to secondary cells.* European Journal of Cancer, 2013. **49**(8): p. 1845-1859.
184. Rontogianni, S., et al., *Proteomic profiling of extracellular vesicles allows for human breast cancer subtyping.* Communications biology, 2019. **2**: p. 325.
185. Keerthikumar, S., et al., *Proteogenomic analysis reveals exosomes are more oncogenic than ectosomes.* Oncotarget, 2015. **6**(17): p. 15375-15396.
186. Muhsin-Sharafaldine, M.-R., et al., *Procoagulant and immunogenic properties of melanoma exosomes, microvesicles and apoptotic vesicles.* Oncotarget, 2016. **7**(35): p. 56279-56294.
187. Théry, C., et al., *Minimal information for studies of extracellular vesicles 2018 (MISEV2018): a position statement of the International Society for Extracellular Vesicles and update of the MISEV2014 guidelines.* Journal of extracellular vesicles, 2018. **7**(1): p. 1535750-1535750.
188. Falchi, A.M., et al., *Astrocytes shed large membrane vesicles that contain mitochondria, lipid droplets and ATP.* Histochemistry and Cell Biology, 2013. **139**(2): p. 221-231.
189. Paggetti, J., et al., *Exosomes released by chronic lymphocytic leukemia cells induce the transition of stromal cells into cancer-associated fibroblasts.* Blood, 2015. **126**(9): p. 1106.
190. Akers, J.C., et al., *miRNA contents of cerebrospinal fluid extracellular vesicles in glioblastoma patients.* Journal of neuro-oncology, 2015. **123**(2): p. 205-216.
191. Willms, E., et al., *Cells release subpopulations of exosomes with distinct molecular and biological properties.* Scientific Reports, 2016. **6**: p. 22519.

192. Spinelli, C., et al., *Large extracellular vesicles carry most of the tumour DNA circulating in prostate cancer patient plasma AU - Vagner, Tatyana.* Journal of Extracellular Vesicles, 2018. **7**(1): p. 1505403.
193. Zhang, H., et al., *Identification of distinct nanoparticles and subsets of extracellular vesicles by asymmetric flow field-flow fractionation.* Nature Cell Biology, 2018. **20**(3): p. 332-343.
194. Milani, G., et al., *Expression Profiling of Circulating Microvesicles Reveals Intercellular Transmission of Oncogenic Pathways.* Molecular Cancer Research, 2017. **15**(6): p. 683.
195. Hong, B.S., et al., *Colorectal cancer cell-derived microvesicles are enriched in cell cycle-related mRNAs that promote proliferation of endothelial cells.* BMC genomics, 2009. **10**: p. 556.
196. Franzen, C.A., et al., *Urothelial cells undergo epithelial-to-mesenchymal transition after exposure to muscle invasive bladder cancer exosomes.* Oncogenesis, 2015. **4**(8): p. e163-e163.
197. Rahman, M.A., et al., *Lung cancer exosomes as drivers of epithelial mesenchymal transition.* Oncotarget, 2016. **7**(34): p. 54852-54866.
198. Chen, L., et al., *HCC-derived exosomes elicit HCC progression and recurrence by epithelial-mesenchymal transition through MAPK/ERK signalling pathway.* Cell Death Dis, 2018. **9**(5): p. 513.
199. Harris, D.A., et al., *Exosomes Released from Breast Cancer Carcinomas Stimulate Cell Movement.* PLOS ONE, 2015. **10**(3): p. e0117495.
200. Xue, X., et al., *Exosomal miR-93 promotes proliferation and invasion in hepatocellular carcinoma by directly inhibiting TIMP2/TP53INP1/CDKN1A.* Biochemical and Biophysical Research Communications, 2018. **502**(4): p. 515-521.
201. Sakha, S., et al., *Exosomal microRNA miR-1246 induces cell motility and invasion through the regulation of DENND2D in oral squamous cell carcinoma.* Scientific Reports, 2016. **6**: p. 38750.
202. Singh, R., et al., *Exosome-mediated transfer of miR-10b promotes cell invasion in breast cancer.* Molecular cancer, 2014. **13**: p. 256.
203. Paoli, P., E. Giannoni, and P. Chiarugi, *Anoikis molecular pathways and its role in cancer progression.* Biochimica et Biophysica Acta (BBA) - Molecular Cell Research, 2013. **1833**(12): p. 3481-3498.
204. Wei, F., et al., *Exosomes derived from gemcitabine-resistant cells transfer malignant phenotypic traits via delivery of miRNA-222-3p.* Molecular Cancer, 2017. **16**(1): p. 132.
205. Urciuoli, E., et al., *Osteosarcoma-derived extracellular vesicles induce a tumor-like phenotype in normal recipient cells.* Journal of Cellular Physiology, 2018. **233**(8): p. 6158-6172.
206. Corcoran, C., et al., *Docetaxel-resistance in prostate cancer: evaluating associated phenotypic changes and potential for resistance transfer via exosomes.* PloS one, 2012. **7**(12): p. e50999.
207. Oushy, S., et al., *Glioblastoma multiforme-derived extracellular vesicles drive normal astrocytes towards a tumour-enhancing phenotype.* Philosophical transactions of the Royal Society of London. Series B, Biological sciences, 2018. **373**(1737): p. 20160477.
208. Crescitelli, R., et al., *Subpopulations of extracellular vesicles from human metastatic melanoma tissue identified by quantitative proteomics after optimized isolation.* Journal of extracellular vesicles, 2020. **9**(1): p. 1722433.
209. Lázaro-Ibáñez, E., et al., *DNA analysis of low- and high-density fractions defines heterogeneous subpopulations of small extracellular vesicles based on their DNA cargo and topology.* Journal of extracellular vesicles, 2019. **8**(1): p. 1656993.
210. Hosseinkhani, B., et al., *(Sub)populations of extracellular vesicles released by TNF-α -triggered human endothelial cells promote vascular inflammation and monocyte migration.* Journal of extracellular vesicles, 2020. **9**(1): p. 1801153.
211. Dalla, P.V., et al., *Selectively-Packaged Proteins in Breast Cancer Extracellular Vesicles Involved in Metastasis.* International journal of molecular sciences, 2020. **21**(14): p. 4990.
212. Keklikoglou, I., et al., *Chemotherapy elicits pro-metastatic extracellular vesicles in breast cancer models.* Nature cell biology, 2019. **21**(2): p. 190-202.

213. Campos, A., et al., *Caveolin-1-containing extracellular vesicles transport adhesion proteins and promote malignancy in breast cancer cell lines.* Nanomedicine, 2018. **13**(20): p. 2597-2609.
214. Nishida-Aoki, N., et al., *Disruption of Circulating Extracellular Vesicles as a Novel Therapeutic Strategy against Cancer Metastasis.* Molecular Therapy, 2017. **25**(1): p. 181-191.
215. Matsumoto, A., et al., *Accelerated growth of B16BL6 tumor in mice through efficient uptake of their own exosomes by B16BL6 cells.* Cancer science, 2017. **108**(9): p. 1803-1810.
216. Brassart, B., et al., *Tumour cell blebbing and extracellular vesicle shedding: key role of matrikines and ribosomal protein SA.* British journal of cancer, 2019. **120**(4): p. 453-465.
217. Yang, C., et al., *Highly-expressed micoRNA-21 in adipose derived stem cell exosomes can enhance the migration and proliferation of the HaCaT cells by increasing the MMP-9 expression through the PI3K/AKT pathway.* Arch Biochem Biophys, 2020. **681**: p. 108259.
218. Matsuzaka, Y., et al., *Characterization and Functional Analysis of Extracellular Vesicles and Muscle-Abundant miRNAs (miR-1, miR-133a, and miR-206) in C2C12 Myocytes and mdx Mice.* PLOS ONE, 2016. **11**(12): p. e0167811.
219. Kim, M., et al., *The Volatile Anesthetic Isoflurane Increases Endothelial Adenosine Generation via Microparticle Ecto-5'-Nucleotidase (CD73) Release.* PLOS ONE, 2014. **9**(6): p. e99950.
220. Sapet, C., et al., *Thrombin-induced endothelial microparticle generation: identification of a novel pathway involving ROCK-II activation by caspase-2.* Blood, 2006. **108**(6): p. 1868-1876.
221. Sebbagh, M., et al., *Caspase-3-mediated cleavage of ROCK I induces MLC phosphorylation and apoptotic membrane blebbing.* Nature Cell Biology, 2001. **3**(4): p. 346-352.
222. NM, A.H., et al., *Inhibition of microparticle release triggers endothelial cell apoptosis and detachment*. 2007: Thromb Haemost. p. 1096-1107.
223. Coleman, M.L., et al., *Membrane blebbing during apoptosis results from caspase-mediated activation of ROCK I.* Nat Cell Biol, 2001. **3**(4): p. 339-45.
224. Tramontano, A.F., et al., *Statin decreases endothelial microparticle release from human coronary artery endothelial cells: implication for the Rho-kinase pathway.* Biochem Biophys Res Commun, 2004. **320**(1): p. 34-8.
225. Chen, J., et al., *Tetramethylpyrazine alleviates LPS-induced inflammatory injury in HUVECs by inhibiting Rho/ROCK pathway.* Biochem Biophys Res Commun, 2019. **514**(1): p. 329-335.
226. Wang, G.H., et al., *Caspase 3/ROCK1 pathway mediates high glucose-induced platelet microparticles shedding.* Biochemical and Biophysical Research Communications, 2019. **509**(2): p. 596-602.
227. Chen, P., et al., *Neurokinin 1 receptor mediates membrane blebbing and sheer stress-induced microparticle formation in HEK293 cells.* PloS one, 2012. **7**(9): p. e45322.
228. Crespin, M., et al., *Activation of PAK1/2 during the shedding of platelet microvesicles.* Blood Coagul Fibrinolysis, 2009. **20**(1): p. 63-70.
229. Miyoshi, H., et al., *Calpain activation in plasma membrane bleb formation during tert-butyl hydroperoxide-induced rat hepatocyte injury.* Gastroenterology, 1996. **110**(6): p. 1897-904.
230. Yano, Y., et al., *The effects of calpeptin (a calpain specific inhibitor) on agonist induced microparticle formation from the platelet plasma membrane.* Thromb Res, 1993. **71**(5): p. 385-96.
231. Atanassoff, A.P., et al., *Microvesicle shedding and lysosomal repair fulfill divergent cellular needs during the repair of streptolysin O-induced plasmalemmal damage.* PloS one, 2014. **9**(2): p. e89743.
232. Grant, R., et al., *A filtration-based protocol to isolate human Plasma Membrane-derived Vesicles and exosomes from blood plasma.* Journal of Immunological Methods, 2011. **371**(1): p. 143-151.
233. O'Connell, D.J., N. Rozenvayn, and R. Flaumenhaft, *Phosphatidylinositol 4,5-bisphosphate regulates activation-induced platelet microparticle formation.* Biochemistry, 2005. **44**(16): p. 6361-70.

234. Siljander, P., et al., *Platelet adhesion enhances the glycoprotein VI-dependent procoagulant response: Involvement of p38 MAP kinase and calpain.* Arterioscler Thromb Vasc Biol, 2001. **21**(4): p. 618-27.
235. Richards, K.E., et al., *Cancer-associated fibroblast exosomes regulate survival and proliferation of pancreatic cancer cells.* Oncogene, 2017. **36**(13): p. 1770-1778.
236. Li, X.Q., et al., *Exosomes derived from gefitinib-treated EGFR-mutant lung cancer cells alter cisplatin sensitivity via up-regulating autophagy.* Oncotarget, 2016. **7**(17): p. 24585-95.
237. Vilette, D., et al., *Efficient inhibition of infectious prions multiplication and release by targeting the exosomal pathway.* Cell Mol Life Sci, 2015. **72**(22): p. 4409-27.
238. Charrier, A., et al., *Exosomes mediate intercellular transfer of pro-fibrogenic connective tissue growth factor (CCN2) between hepatic stellate cells, the principal fibrotic cells in the liver.* Surgery, 2014. **156**(3): p. 548-55.
239. Lyu, L., et al., *A critical role of cardiac fibroblast-derived exosomes in activating renin angiotensin system in cardiomyocytes.* J Mol Cell Cardiol, 2015. **89**(Pt B): p. 268-79.
240. Guo, B.B., S.A. Bellingham, and A.F. Hill, *The neutral sphingomyelinase pathway regulates packaging of the prion protein into exosomes.* J Biol Chem, 2015. **290**(6): p. 3455-67.
241. Huang, Z., et al., *Exosomes Derived from Hypoxic Colorectal Cancer Cells Transfer Wnt4 to Normoxic Cells to Elicit a Prometastatic Phenotype.* International journal of biological sciences, 2018. **14**(14): p. 2094-2102.
242. Xu, Z.H., et al., *Brain microvascular endothelial cell exosome-mediated S100A16 up-regulation confers small-cell lung cancer cell survival in brain.* Faseb j, 2019. **33**(2): p. 1742-1757.
243. Gong, X.H., et al., *Exosomes derived from SDF1-overexpressing mesenchymal stem cells inhibit ischemic myocardial cell apoptosis and promote cardiac endothelial microvascular regeneration in mice with myocardial infarction.* J Cell Physiol, 2019. **234**(8): p. 13878-13893.
244. Tsutsumi, R., et al., *Involvement of exosomes in dopaminergic neurodegeneration by microglial activation in midbrain slice cultures.* Biochem Biophys Res Commun, 2019. **511**(2): p. 427-433.
245. Munson, P.B., et al., *Exosomal miR-16-5p as a target for malignant mesothelioma.* Sci Rep, 2019. **9**(1): p. 11688.
246. Wu, B., et al., *Exosomes isolated from CAPS1-overexpressing colorectal cancer cells promote cell migration.* Oncol Rep, 2019. **42**(6): p. 2528-2536.
247. Nath, S., et al., *The extracellular role of DNA damage repair protein APE1 in regulation of IL-6 expression.* Cell Signal, 2017. **39**: p. 18-31.
248. Yue, K.-Y., et al., *Neurons can upregulate Cav-1 to increase intake of endothelial cells-derived extracellular vesicles that attenuate apoptosis via miR-1290.* Cell Death & Disease, 2019. **10**(12): p. 869.
249. Wang, H., et al., *MiR-126-3p-Enriched Extracellular Vesicles from Hypoxia-Preconditioned VSC 4.1 Neurons Attenuate Ischaemia-Reperfusion-Induced Pain Hypersensitivity by Regulating the PIK3R2-Mediated Pathway.* Molecular Neurobiology, 2021. **58**(2): p. 821-834.
250. Zhou, H., et al., *The proangiogenic effects of extracellular vesicles secreted by dental pulp stem cells derived from periodontally compromised teeth.* Stem Cell Research & Therapy, 2020. **11**(1): p. 110.
251. Jin, Q., et al., *Extracellular vesicles derived from human dental pulp stem cells promote osteogenesis of adipose-derived stem cells via the MAPK pathway.* J Tissue Eng, 2020. **11**: p. .
252. Niu, Z., et al., *Polymer-based precipitation preserves biological activities of extracellular vesicles from an endometrial cell line.* PloS one, 2017. **12**(10): p. e0186534.
253. Guarino, B.D., et al., *Extracellular Vesicles From Pathological Microenvironment Induce Endothelial Cell Transformation and Abnormal Angiogenesis via Modulation of TRPV4 Channels.* Frontiers in Cell and Developmental Biology, 2019. **7**: p. 344.
254. Wooff, Y., et al., *Small-Medium Extracellular Vesicles and Their miRNA Cargo in Retinal Health and Degeneration: Mediators of Homeostasis, and Vehicles for Targeted Gene Therapy.* Frontiers in Cellular Neuroscience, 2020. **14**: p. 160.

255. Liu, A., et al., *Macrophage-derived small extracellular vesicles promote biomimetic mineralized collagen-mediated endogenous bone regeneration.* International Journal of Oral Science, 2020. **12**(1): p. 33.
256. Sohda, M., Y. Misumi, and K. Oda, *TNFα triggers release of extracellular vesicles containing TNFR1 and TRADD, which can modulate TNFα responses of the parental cells.* Archives of Biochemistry and Biophysics, 2015. **587**: p. 31-37.
257. Montermini, L., et al., *Inhibition of Oncogenic Epidermal Growth Factor Receptor Kinase Triggers Release of Exosome-like Extracellular Vesicles and Impacts Their Phosphoprotein and DNA Content *.* Journal of Biological Chemistry, 2015. **290**(40): p. 24534-24546.
258. Faict, S., et al., *Exosomes play a role in multiple myeloma bone disease and tumor development by targeting osteoclasts and osteoblasts.* Blood cancer journal, 2018. **8**(11): p. 105.
259. Dinkins, M.B., et al., *Exosome reduction in vivo is associated with lower amyloid plaque load in the 5XFAD mouse model of Alzheimer's disease.* Neurobiol Aging, 2014. **35**(8): p. 1792-800.
260. Bai, L., et al., *Renoprotective effects of artemisinin and hydroxychloroquine combination therapy on IgA nephropathy via suppressing NF-κB signaling and NLRP3 inflammasome activation by exosomes in rats.* Biochemical Pharmacology, 2019. **169**: p. 113619.
261. Wang, X., et al., *Hsp20-Mediated Activation of Exosome Biogenesis in Cardiomyocytes Improves Cardiac Function and Angiogenesis in Diabetic Mice.* Diabetes, 2016. **65**(10): p. 3111-3128.
262. Aubertin, K., et al., *Massive release of extracellular vesicles from cancer cells after photodynamic treatment or chemotherapy.* Scientific Reports, 2016. **6**(1): p. 35376.
263. König, L., et al., *Elevated levels of extracellular vesicles are associated with therapy failure and disease progression in breast cancer patients undergoing neoadjuvant chemotherapy.* OncoImmunology, 2018. **7**(1): p. e1376153.
264. Synnott, N.C., et al., *COTI-2 reactivates mutant p53 and inhibits growth of triple-negative breast cancer cells.* Breast Cancer Res Treat, 2020. **179**(1): p. 47-56.
265. Cho, J.J., et al., *Manumycin A from a new Streptomyces strain induces endoplasmic reticulum stress-mediated cell death through specificity protein 1 signaling in human oral squamous cell carcinoma.* Int J Oncol, 2015. **47**(5): p. 1954-62.
266. Zhou, J.M., et al., *Manumycin inhibits cell proliferation and the Ras signal transduction pathway in human hepatocellular carcinoma cells.* Int J Mol Med, 2003. **11**(6): p. 767-71.
267. Li, J.-G., et al., *Manumycin induces apoptosis in prostate cancer cells.* OncoTargets and therapy, 2014. **7**: p. 771-777.
268. Lin, Q., et al., *ASPH-notch Axis guided Exosomal delivery of Prometastatic Secretome renders breast Cancer multi-organ metastasis.* Molecular Cancer, 2019. **18**(1): p. 156.
269. Yue, K.Y., et al., *Neurons can upregulate Cav-1 to increase intake of endothelial cells-derived extracellular vesicles that attenuate apoptosis via miR-1290.* Cell Death Dis, 2019. **10**(12): p. 869.
270. Niu, Z., et al., *Polymer-based precipitation preserves biological activities of extracellular vesicles from an endometrial cell line.* PloS one, 2017. **12**(10): p. e0186534-e0186534.
271. Liao, Z., et al., *Acetylcholinesterase is not a generic marker of extracellular vesicles.* Journal of extracellular vesicles, 2019. **8**(1): p. 1628592.
272. Nasrazadani, A. and A. Brufsky, *Neratinib: the emergence of a new player in the management of HER2+ breast cancer brain metastasis.* Future Oncology, 2020. **16**(7): p. 247-254.
273. Kim, S., et al., *Berberine down-regulates IL-8 expression through inhibition of the EGFR/MEK/ERK pathway in triple-negative breast cancer cells.* Phytomedicine, 2018. **50**: p. 43-49.
274. Im, E.J., et al., *Sulfisoxazole inhibits the secretion of small extracellular vesicles by targeting the endothelin receptor A.* Nat Commun, 2019. **10**(1): p. 1387.
275. Fonseka, P., et al., *Sulfisoxazole does not inhibit the secretion of small extracellular vesicles.* Nature Communications, 2021. **12**(1): p. 977.

276. Zhang, P., et al., *Better pathologic complete response and relapse-free survival after carboplatin plus paclitaxel compared with epirubicin plus paclitaxel as neoadjuvant chemotherapy for locally advanced triple-negative breast cancer: a randomized phase 2 trial.* Oncotarget, 2016. **7**(37): p. 60647-60656.
277. Yu, K.-D., et al., *Effect of Adjuvant Paclitaxel and Carboplatin on Survival in Women With Triple-Negative Breast Cancer: A Phase 3 Randomized Clinical Trial.* JAMA oncology, 2020. **6**(9): p. 1390-1396.
278. Sharma, P., et al., *Efficacy of Neoadjuvant Carboplatin plus Docetaxel in Triple-Negative Breast Cancer: Combined Analysis of Two Cohorts.* Clinical Cancer Research, 2017. **23**(3): p. 649.
279. Chen, X.-s., et al., *Both carboplatin and bevacizumab improve pathological complete remission rate in neoadjuvant treatment of triple negative breast cancer: a meta-analysis.* PloS one, 2014. **9**(9): p. e108405.
280. Salim, K.Y., et al., *COTI-2, a novel small molecule that is active against multiple human cancer cell lines in vitro and in vivo.* Oncotarget; Vol 7, No 27, 2016.
281. Wang, X., et al., *Chemotherapeutic drugs stimulate the release and recycling of extracellular vesicles to assist cancer cells in developing an urgent chemoresistance.* Molecular cancer, 2019. **18**(1): p. 182.
282. Kreger, B.T., et al., *The Enrichment of Survivin in Exosomes from Breast Cancer Cells Treated with Paclitaxel Promotes Cell Survival and Chemoresistance.* Cancers, 2016. **8**(12).
283. Bandari, S.K., et al., *Chemotherapy induces secretion of exosomes loaded with heparanase that degrades extracellular matrix and impacts tumor and host cell behavior.* Matrix Biology, 2018. **65**: p. 104-118.
284. Vera, N., et al., *Small Extracellular Vesicles Released from Ovarian Cancer Spheroids in Response to Cisplatin Promote the Pro-Tumorigenic Activity of Mesenchymal Stem Cells.* International journal of molecular sciences, 2019. **20**(20): p. 4972.
285. Sud, R. and A.A. Khorana, *Cancer-associated thrombosis: risk factors, candidate biomarkers and a risk model.* Thrombosis Research, 2009. **123**: p. S18-S21.
286. Falanga, A., et al., *Mechanisms and risk factors of thrombosis in cancer.* Critical Reviews in Oncology/Hematology, 2017. **118**: p. 79-83.
287. Lee, A.Y.Y., *Thrombosis and Cancer: The Role of Screening for Occult Cancer and Recognizing the Underlying Biological Mechanisms.* Hematology, 2006. **2006**(1): p. 438-443.
288. Kim, H.K., et al., *Elevated levels of circulating platelet microparticles, VEGF, IL-6 and RANTES in patients with gastric cancer: possible role of a metastasis predictor.* European Journal of Cancer, 2003. **39**(2): p. 184-191.
289. Tilley, R.E., et al., *Tissue factor activity is increased in a combined platelet and microparticle sample from cancer patients.* Thrombosis Research, 2008. **122**(5): p. 604-609.
290. Haubold, K., et al., *Tissue factor procoagulant activity of plasma microparticles is increased in patients with early-stage prostate cancer.* Thromb Haemost, 2009. **101**(6): p. 1147-55.
291. Leal, A.C., et al., *Tumor-Derived Exosomes Induce the Formation of Neutrophil Extracellular Traps: Implications For The Establishment of Cancer-Associated Thrombosis.* Scientific reports, 2017. **7**(1): p. 6438-6438.
292. Wang, J.-G., et al., *Tumor-derived tissue factor activates coagulation and enhances thrombosis in a mouse xenograft model of human pancreatic cancer.* Blood, 2012. **119**(23): p. 5543-5552.
293. Thomas, G.M., et al., *Tissue factor expressed by circulating cancer cell-derived microparticles drastically increases the incidence of deep vein thrombosis in mice.* Journal of thrombosis and haemostasis : JTH, 2015. **13**(7): p. 1310-1319.
294. Li, J., et al., *Thrombin-activated platelet-derived exosomes regulate endothelial cell expression of ICAM-1 via microRNA-223 during the thrombosis-inflammation response.* Thrombosis Research, 2017. **154**: p. 96-105.
295. Geddings, J.E., et al., *Tissue factor–positive tumor microvesicles activate platelets and enhance thrombosis in mice.* Journal of Thrombosis and Haemostasis, 2016. **14**(1): p. 153-166.

296. Ghosh, A., et al., *Platelet CD36 mediates interactions with endothelial cell–derived microparticles and contributes to thrombosis in mice.* The Journal of Clinical Investigation, 2008. **118**(5): p. 1934-1943.
297. Ye, R., et al., *Circulating tissue factor positive microparticles in patients with acute recurrent deep venous thrombosis.* Thrombosis Research, 2012. **130**(2): p. 253-258.
298. Durrieu, L., A. Bharadwaj, and D.M. Waisman, *Analysis of the thrombotic and fibrinolytic activities of tumor cell-derived extracellular vesicles.* Blood advances, 2018. **2**(10): p. 1054-1065.
299. Gomes, F.G., et al., *Breast-cancer extracellular vesicles induce platelet activation and aggregation by tissue factor-independent and -dependent mechanisms.* Thromb Res, 2017. **159**: p. 24-32.
300. Lian, L., et al., *Inhibition of MCF-7 breast cancer cell-induced platelet aggregation using a combination of antiplatelet drugs.* Oncology letters, 2013. **5**(2): p. 675-680.
301. Oleksowicz, L., et al., *Characterization of tumor-induced platelet aggregation: the role of immunorelated GPIb and GPIIb/IIIa expression by MCF-7 breast cancer cells.* Thromb Res, 1995. **79**(3): p. 261-74.
302. Gheldof, D., et al., *Thrombin generation assay and transmission electron microscopy: a useful combination to study tissue factor-bearing microvesicles.* Journal of Extracellular Vesicles, 2013. **2**(1): p. 19728.
303. Yang, Y., S. Yuzawa, and J. Schlessinger, *Contacts between membrane proximal regions of the PDGF receptor ectodomain are required for receptor activation but not for receptor dimerization.* Proc Natl Acad Sci U S A, 2008. **105**(22): p. 7681-6.
304. Vella, L.J., et al., *Intercellular Resistance to BRAF Inhibition Can Be Mediated by Extracellular Vesicle-Associated PDGFRβ.* Neoplasia (New York, N.Y.), 2017. **19**(11): p. 932-940.
305. Wei, C.-K., et al., *Inhibition of the interactions between metastatic human breast cancer cells and platelets by β-nitrostyrene derivatives.* Life Sciences, 2015. **143**: p. 147-155.
306. Tsai, M.-S., et al., *Expression and Function of CYR61, an Angiogenic Factor, in Breast Cancer Cell Lines and Tumor Biopsies.* Cancer Research, 2000. **60**(20): p. 5603.
307. Huang, Y.-T., et al., *The matricellular protein CYR61 promotes breast cancer lung metastasis by facilitating tumor cell extravasation and suppressing anoikis.* Oncotarget; Vol 8, No 6, 2016.
308. Jedsadayanmata, A., et al., *Activation-dependent Adhesion of Human Platelets to Cyr61 and Fisp12/Mouse Connective Tissue Growth Factor Is Mediated through Integrin αIIbβ3.* Journal of Biological Chemistry, 1999. **274**(34): p. 24321-24327.
309. Wang, T., et al., *CD97, an adhesion receptor on inflammatory cells, stimulates angiogenesis through binding integrin counterreceptors on endothelial cells.* Blood, 2005. **105**(7): p. 2836-2844.
310. Safaee, M., et al., *CD97 is a multifunctional leukocyte receptor with distinct roles in human cancers (Review).* Int J Oncol, 2013. **43**(5): p. 1343-1350.
311. Ward, Y., et al., *Platelets Promote Metastasis via Binding Tumor CD97 Leading to Bidirectional Signaling that Coordinates Transendothelial Migration.* Cell reports, 2018. **23**(3): p. 808-822.
312. Matsuda, K., et al., *Glypican-1 Is Overexpressed in Human Breast Cancer and Modulates the Mitogenic Effects of Multiple Heparin-binding Growth Factors in Breast Cancer Cells.* Cancer Research, 2001. **61**(14): p. 5562.
313. Melo, S.A., et al., *Glypican-1 identifies cancer exosomes and detects early pancreatic cancer.* Nature, 2015. **523**(7559): p. 177-182.
314. Wang, Z. and X. Yan, *CD146, a multi-functional molecule beyond adhesion.* Cancer Letters, 2013. **330**(2): p. 150-162.
315. Shao, B., et al., *Carcinoma mucins trigger reciprocal activation of platelets and neutrophils in a murine model of Trousseau syndrome.* Blood, 2011. **118**(15): p. 4015-4023.
316. Ghoroghi, S., et al., *Ral GTPases promote breast cancer metastasis by controlling biogenesis and organ targeting of exosomes.* eLife, 2021. **10**: p. e61539.

317. Stalin, J., et al., *Therapeutic targeting of soluble CD146/MCAM with the M2J-1 monoclonal antibody prevents metastasis development and procoagulant activity in CD146-positive invasive tumors.* International Journal of Cancer, 2020. **147**(6): p. 1666-1679.
318. Lijnen, H.R., *Elements of the fibrinolytic system.* Ann N Y Acad Sci, 2001. **936**: p. 226-36.
319. Lacroix, R., et al., *Activation of plasminogen into plasmin at the surface of endothelial microparticles: a mechanism that modulates angiogenic properties of endothelial progenitor cells in vitro.* Blood, 2007. **110**(7): p. 2432-2439.
320. Biagioni, A., et al., *uPAR-expressing melanoma exosomes promote angiogenesis by VE-Cadherin, EGFR and uPAR overexpression and rise of ERK1,2 signaling in endothelial cells.* Cellular and Molecular Life Sciences, 2020.
321. Huber, M.C., et al., *uPAR enhances malignant potential of triple-negative breast cancer by directly interacting with uPA and IGF1R.* BMC Cancer, 2016. **16**(1): p. 615.
322. Huber, M.C., et al., *Cyr61 and YB-1 are novel interacting partners of uPAR and elevate the malignancy of triple-negative breast cancer.* Oncotarget; Vol 7, No 28, 2016.
323. Duffy, M.J., et al., *uPA and PAI-1 as biomarkers in breast cancer: validated for clinical use in level-of-evidence-1 studies.* Breast Cancer Research, 2014. **16**(4): p. 428.
324. Duffy, M.J., *Serum Tumor Markers in Breast Cancer: Are They of Clinical Value?* Clinical Chemistry, 2006. **52**(3): p. 345-351.
325. Jesneck, J.L., et al., *Do serum biomarkers really measure breast cancer?* BMC Cancer, 2009. **9**(1): p. 164.
326. Wang, H., et al., *Evaluation of serum extracellular vesicles as noninvasive diagnostic markers of glioma.* Theranostics, 2019. **9**(18): p. 5347-5358.
327. Koi, Y., et al., *Predicting the presence of breast cancer using circulating small RNAs, including those in the extracellular vesicles.* Cancer science, 2020. **111**(6): p. 2104-2115.
328. Webber, J. and A. Clayton, *How pure are your vesicles?* J Extracell Vesicles, 2013. **2**.
329. Namkoong, H., et al., *The bone morphogenetic protein antagonist gremlin 1 is overexpressed in human cancers and interacts with YWHAH protein.* BMC Cancer, 2006. **6**(1): p. 74.
330. Pang, B., et al., *Quality Assessment and Comparison of Plasma-Derived Extracellular Vesicles Separated by Three Commercial Kits for Prostate Cancer Diagnosis.* International journal of nanomedicine, 2020. **15**: p. 10241-10256.
331. Dong, L., et al., *Comprehensive evaluation of methods for small extracellular vesicles separation from human plasma, urine and cell culture medium.* Journal of Extracellular Vesicles, 2020. **10**(2): p. e12044.
332. Stranska, R., et al., *Comparison of membrane affinity-based method with size-exclusion chromatography for isolation of exosome-like vesicles from human plasma.* Journal of translational medicine, 2018. **16**(1): p. 1-1.
333. Ryu, K.J., et al., *Isolation of Small Extracellular Vesicles From Human Serum Using a Combination of Ultracentrifugation With Polymer-Based Precipitation.* Annals of laboratory medicine, 2020. **40**(3): p. 253-258.
334. Daly, R. and L. O'Driscoll, *Extracellular vesicles in blood: are they viable as diagnostic and predictive tools in breast cancer?* Drug Discovery Today, 2021. **26**(3): p. 778-785.
335. An, M., et al., *Comparison of an Optimized Ultracentrifugation Method versus Size-Exclusion Chromatography for Isolation of Exosomes from Human Serum.* Journal of proteome research, 2018. **17**(10): p. 3599-3605.
336. Kim, J., Z. Tan, and D.M. Lubman, *Exosome enrichment of human serum using multiple cycles of centrifugation.* Electrophoresis, 2015. **36**(17): p. 2017-2026.
337. Caradec, J., et al., *Reproducibility and efficiency of serum-derived exosome extraction methods.* Clinical Biochemistry, 2014. **47**(13): p. 1286-1292.
338. Brennan, K., et al., *A comparison of methods for the isolation and separation of extracellular vesicles from protein and lipid particles in human serum.* Scientific reports, 2020. **10**(1): p. 1039.

339. Buschmann, D., et al., *Evaluation of serum extracellular vesicle isolation methods for profiling miRNAs by next-generation sequencing.* Journal of extracellular vesicles, 2018. **7**(1): p. 1481321.
340. Papiewska-Pająk, I., et al., *Glypican-1 Level Is Elevated in Extracellular Vesicles Released from MC38 Colon Adenocarcinoma Cells Overexpressing Snail.* Cells, 2020. **9**(7): p. 1585.
341. Risha, Y., et al., *The proteomic analysis of breast cell line exosomes reveals disease patterns and potential biomarkers.* Scientific reports, 2020. **10**(1): p. 13572-13572.
342. Topol, L.Z., et al., *Biosynthesis, Post-translation Modification, and Functional Characterization of Drm/Gremlin*.* Journal of Biological Chemistry, 2000. **275**(12): p. 8785-8793.
343. Sung, N.J., et al., *Gremlin-1 Promotes Metastasis of Breast Cancer Cells by Activating STAT3-MMP13 Signaling Pathway.* International journal of molecular sciences, 2020. **21**(23): p. 9227.
344. Park, S.-A., et al., *Gremlin-1 augments the oestrogen-related receptor α signalling through EGFR activation: implications for the progression of breast cancer.* British Journal of Cancer, 2020. **123**(6): p. 988-999.

Appendix I

(A) Chapter 4 appendix: Investigation of the use of proposed Extracellular Vesicle (EV) inhibitors to block triple-negative breast cancer (TNBC) EVs

i) Determination of Staurosporine concentration for Annexin V /PI flow cytometry

Staurosporine was used as positive control of cell death for Annexin V/PI flow cytometry. The concentration of Staurosporine needed to induce cell apoptosis was determined (Fig. A.1). The concentration of 1000 nM was selected for use.

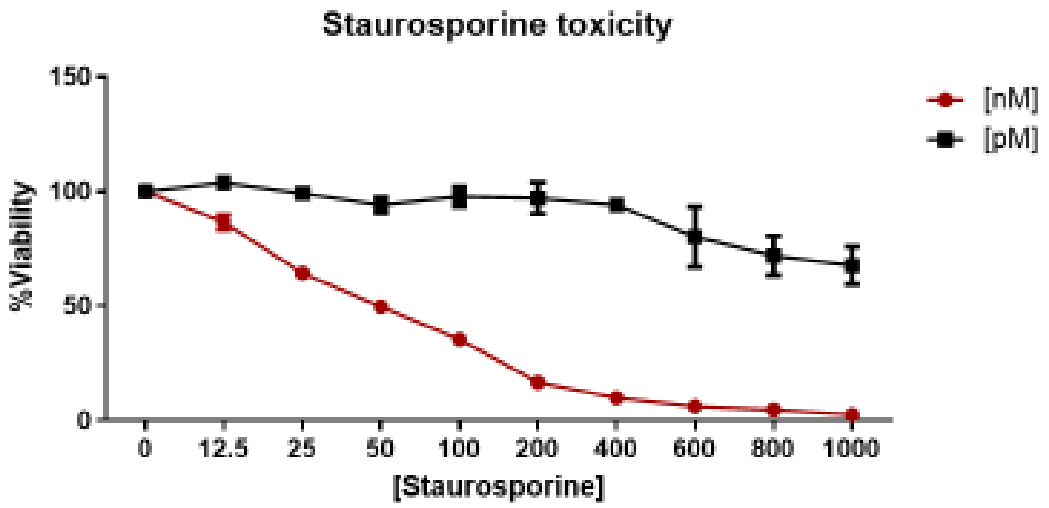

Figure A.1: Staurosporine toxicity in Hs578Ts(i)$_8$ cell line variant
An acid phosphatase assay was performed to determine the concentration of Staurosporine to use to treat the Hs578Ts(i)$_8$ cells. Graph represents mean ± SEM of n=3 biological repeats.

ii) Characterisation of EVs still released from Hs578Ts(i)$_8$ cells after inhibitor treatment

EVs were originally separated from the conditioned medium of Hs578Ts(i)$_8$ cells with or without inhibitor treatment by density gradient ultracentrifugation. The EV-enriched gradient fractions were pooled and cleaned by one round of ultracentrifugation (120,000g for 2hrs).

Initial characterisation of EVs included NTA analysis of EVs released after 48hrs of inhibitor treatment versus EVs released after 48 hrs of no inhibitor treatment (i.e. control). While calpeptin and Y27632 increased EVs compared to control, combo 1, manumycin A and GW4869 decreased EV release compared to the control (Fig. A.2 (A)). The percentage of increase or decrease is shown (Fig. A.2 (B)). There was no significant change in the size (nm) of the EVs released following inhibitor treatment (Fig. A.2 (C)). The EVs ranged from 126 ± 3.9 nm, for control-EVs to 134 ± 3.9 nm, manumycin A EVs. Protein measurement (as a surrogate marker for EVs) of the EVs after inhibitor treatment demonstrates a change compared to the control, however, not significantly (Fig. A.2 (D)).

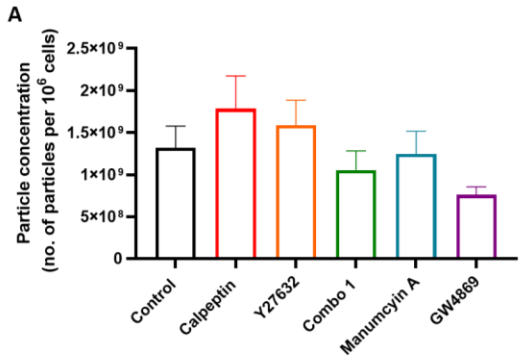

B

Potential inhibitor	Average EV concentration	Increase/reduction compared to control
Control	1.32 x 10^9	-
Calpeptin	1.78 x 10^9	+35%
Y27632	1.59 x 10^9	+16%
Combo 1	1.06 x 10^9	-20%
Manumycin A	1.25 x 10^9	-17%
GW4869	7.60 x 10^8	-43%

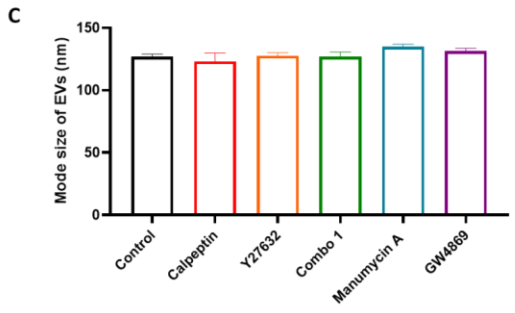

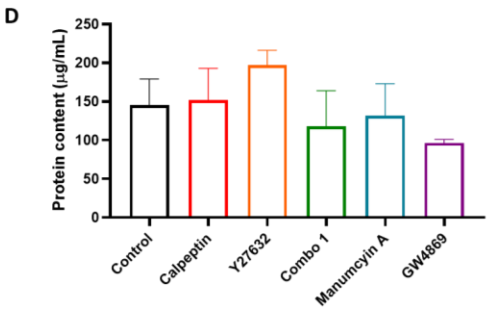

Figure A.2: Particle release and protein measurements of EVs after inhibitor treatment

The release of EVs were measured by (A) NTA and (B) the % of release was calculated compared to the untreated control. The (C) size of EVs released was measured by NTA and (D) the protein (µg/mL) was measured by BCA. Graphs (A) and (C) represent mean ± SEM of *n=5* independent biological experiments. Graph (D) is representative of mean ± SEM of *n=3* independent biological experiments. One-way ANOVA was used as statistical test.

Overall, none of the inhibitor significantly reduced the quantities of EVs. The size of the EVs released after inhibitor treatment was also not changed.

Given that the proposed inhibitors did not significantly reduce EVs release, immunoblot analysis was performed on the released lysed-EVs. A representative immunoblot is shown (Fig. A.3 (A)). Common EV markers indicated in the MISEV guidelines were investigated (Fig. A.3 (B-E)). Densitometry was performed as a semi-quantitative measurement of each EV marker with arbitrary units graphed. CD63 was significantly decreased in EV released following combo 2 treatment (*p=0.019*) (Fig. A.3 (B)). Syntenin-1 was significantly increased following combo 1 treatment (*p=0.033*) (Fig. A.3 (D)).

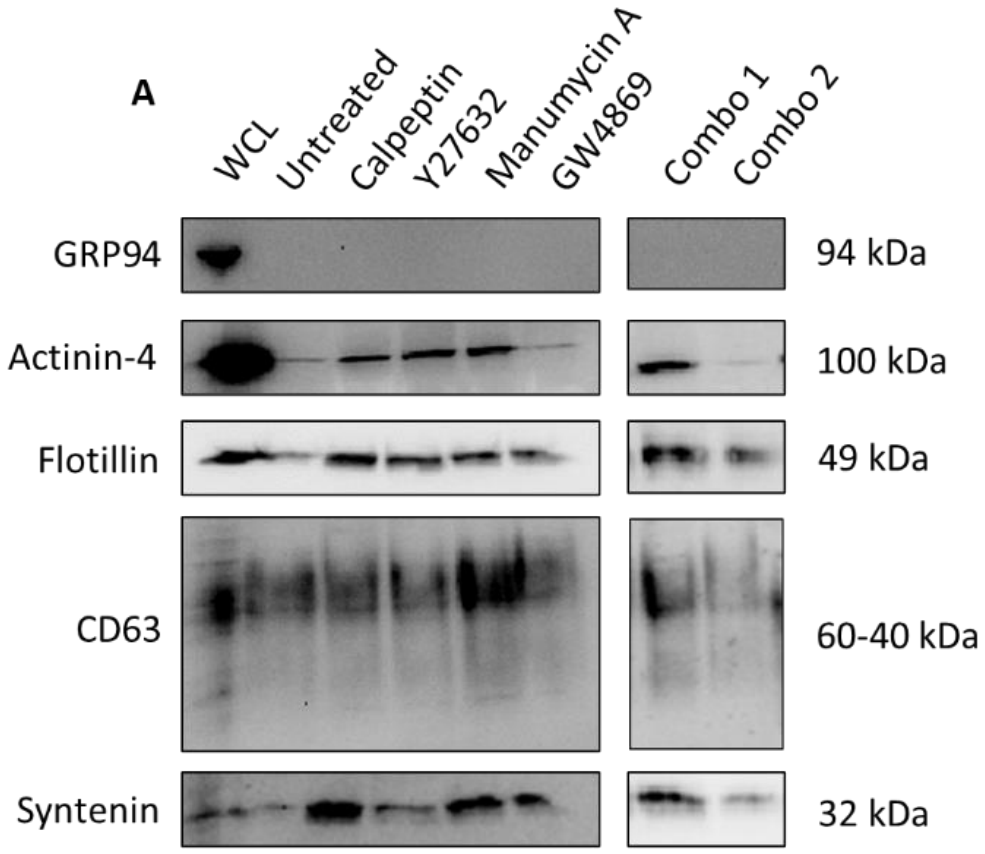

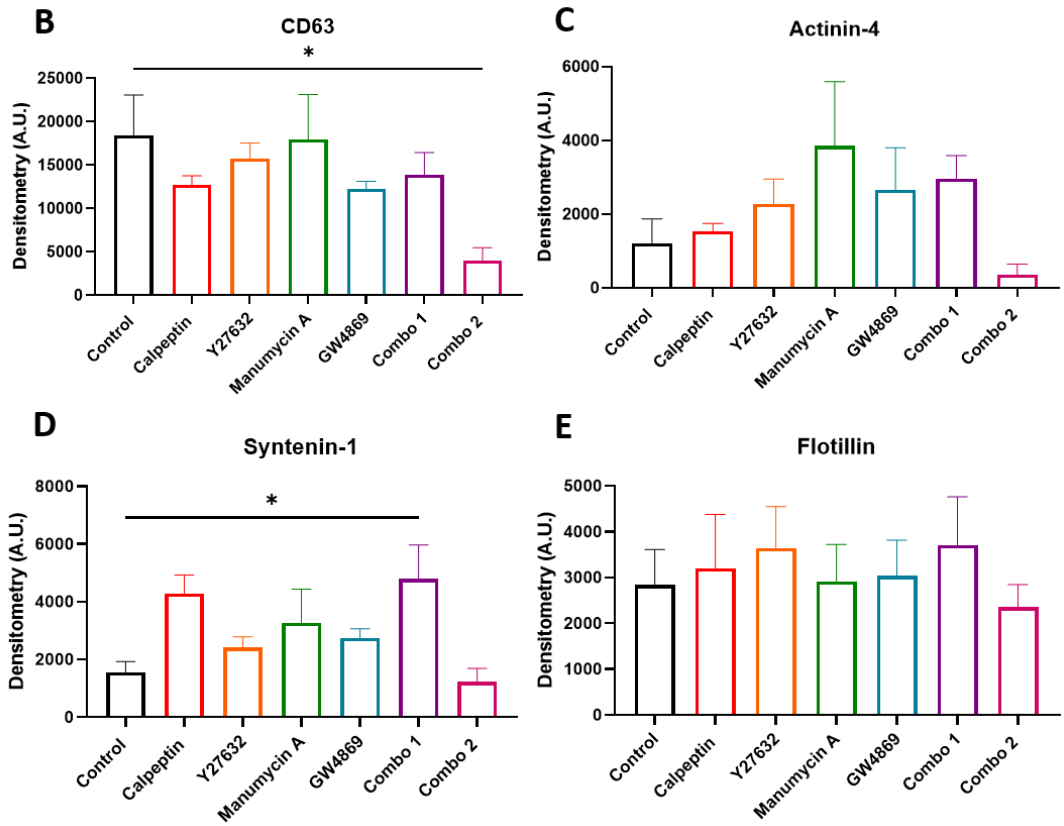

Figure A.3: Immunoblot analysis of EVs after inhibitor treatment

EV markers were used to characterise the EVs following inhibitor treatment. (A) Shows a representative immunoblot. EV markers analysed include (B) CD63, (C) Actinin-4 (D) syntenin-1 and (E) Flotillin. WCL=Whole cell lysate of Hs578Ts(i)[8] cells. Graphs represent mean ± SEM of n=3 independent biological experiments. One-way ANOVA was used as statistical test. * P< 0.05.

Overall, immunoblot analysis of the EVs released after inhibitor treatment showed that EV markers were mostly unchanged, with the exception of CD63 on combo 2-EVs and syntenin-1 on combo 1-EVs.

Imaging flow cytometry (IFCM) analysis of surface EV markers was performed. These included tetraspanins CD9, CD63 and CD81 and the membrane metalloproteinase, ADAM10. These proteins were selected as they are on the surface of the EVs. CD9, CD63 and CD81 are most frequently reported as EV markers and ADAM10 is also a marker of sEVs, according to MISEV guidelines. EVs released after all inhibitor treatments significantly decreased CD9 positivity compared to the control, including calpeptin (*p=0.006*) , Y27632 (*p=0.002*), combo 1 (*p=0.003*), manumycin A (*p=0.021*) , GW4869 (*p=0.004*) , combo 2 (*p=0.017*) (Fig. A.4 (A)). Y27632 (*p=0.025*) and combo 1 (*p=0.030*) treatment caused a significant decrease in CD63. Similarly, Y27632 (*p=0.030*) and combo 1 (*p=0.018*) significantly decreased CD81 positivity of EVs released (Fig. A.4 (B-C)). Although not significant, ADAM10 positivity was also altered following inhibitor treatment (Fig. A.4 (D)).

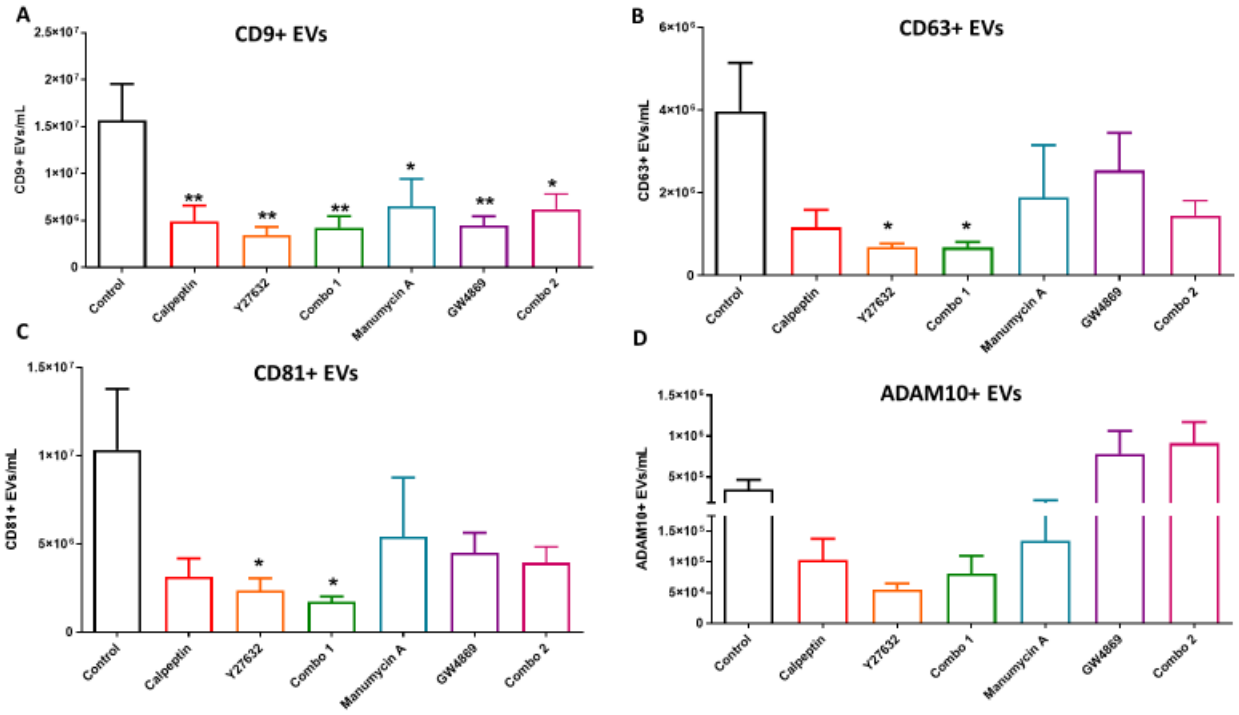

Figure A.4: Flow cytometry analysis of surface EV markers

Amnis ImageStream flow cytometer was used to quantify the surface EV marker of EVs released following inhibitor treatment. These included (A) CD9, (B) CD63 (C) CD81 and (D) ADAM10. Graphs represent mean ± SEM of *n=5* independent biological experiments. One- way ANOVA was used as statistical test. * P<005, **P<0.01.

Overall, CD9 detection on the surface of EVs released after all inhibitor treatment was significantly reduced. CD63 and CD81 was significantly reduced after Y27632 and combo 1. Although, ADAM10 was increased or decreased depending on the inhibitor treatment, it was not statistically significant.

iii) Functional analysis of EVs still released after inhibitor treatment

After characterisation of the EVs released from the Hs578Ts(i)$_8$ cell line variant after inhibitor treatment, functional analysis of the EVs was investigated in recipient TNBC cell lines, Hs578T and MDA-MB-468.

Initially, effects of three EV quantities on TNBC cell proliferation was investigated. Hs578T cell proliferation was not affected with EV treatment (Fig A.5 (A-C)). Similarly, EV treatment had limited effect on MDA-MB-468 cell proliferation (Fig. A.5 (D-F)). Although not significant, EVs released after calpeptin treatment and EV released after GW4869 treatment, decreased MDA-MB-468 proliferation at all three EV quantities compared to the control.

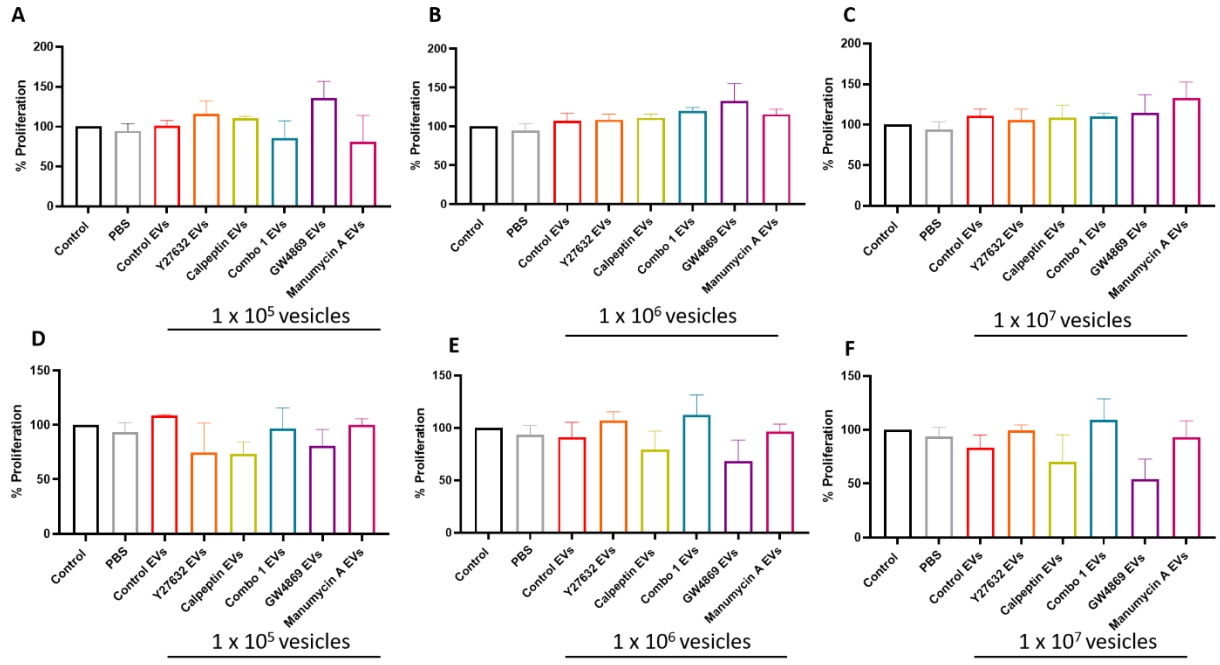

Figure A.5: Proliferation assay with Hs578Ts(i)$_8$ EVs after inhibitor treatment of the cells

Hs578T (A-C) and MDA-MB-468 (E-F) cells were seeded in 96-well plates and treated with three quantities of EVs (i.e. 1 x 10^5, 1 x 10^6 and 1 x 10^7) for 72 hrs. Graphs represent mean ± SEM of *n=3* independent biological experiments.

Overall, none of the EVs released following cell treatment with any inhibitors significantly changed recipient cell proliferation.

The effect of the EVs on Hs578T cell migration was also evaluated. The same quantity of EVs were added based on the number of cells seeded for each cell line as for the proliferation assays, with three doses tested. The percentage of EV increase/decrease seen with NTA analysis, compared to control EVs, was also taken into account when adding EVs to the assay (Fig. A.6 (A)). For example, if 8.3 x 10^5 EVs from untreated Hs578Ts(i)$_8$ cells (i.e. control EVs) were added, 9.9 x 10^5 EVs released after Y27632 treatment (i.e. Y27632 EVs) was added, taking the 16% increase of EV release following Y27632 treatment compared to the control into account.

Although, significance was not reached, all EVs released following inhibitor treatment decreased Hs578T migration compared to treatment with EVs released from untreated cells (Fig. A.6 (B-D)).

A

EVs after treatment	Concentration of EVs added to Hs578T wound healing assay		
Control EVs	$8.3x10^5$	$8.3x10^6$	$8.3x10^7$
Y27632 EVs	$9.9x10^5$	$9.9x10^6$	$9.9x10^7$
Calpeptin EVs	$1.1x10^5$	$1.1x10^6$	$1.1x10^7$
Combo 1 EVs	$6.6x10^5$	$6.6x10^6$	$6.6x10^7$
GW4869 EVs	$4.7x10^5$	$4.7x10^6$	$4.7x10^7$
Manumycin A EVs	$4.2x10^5$	$4.2x10^6$	$4.2x10^7$

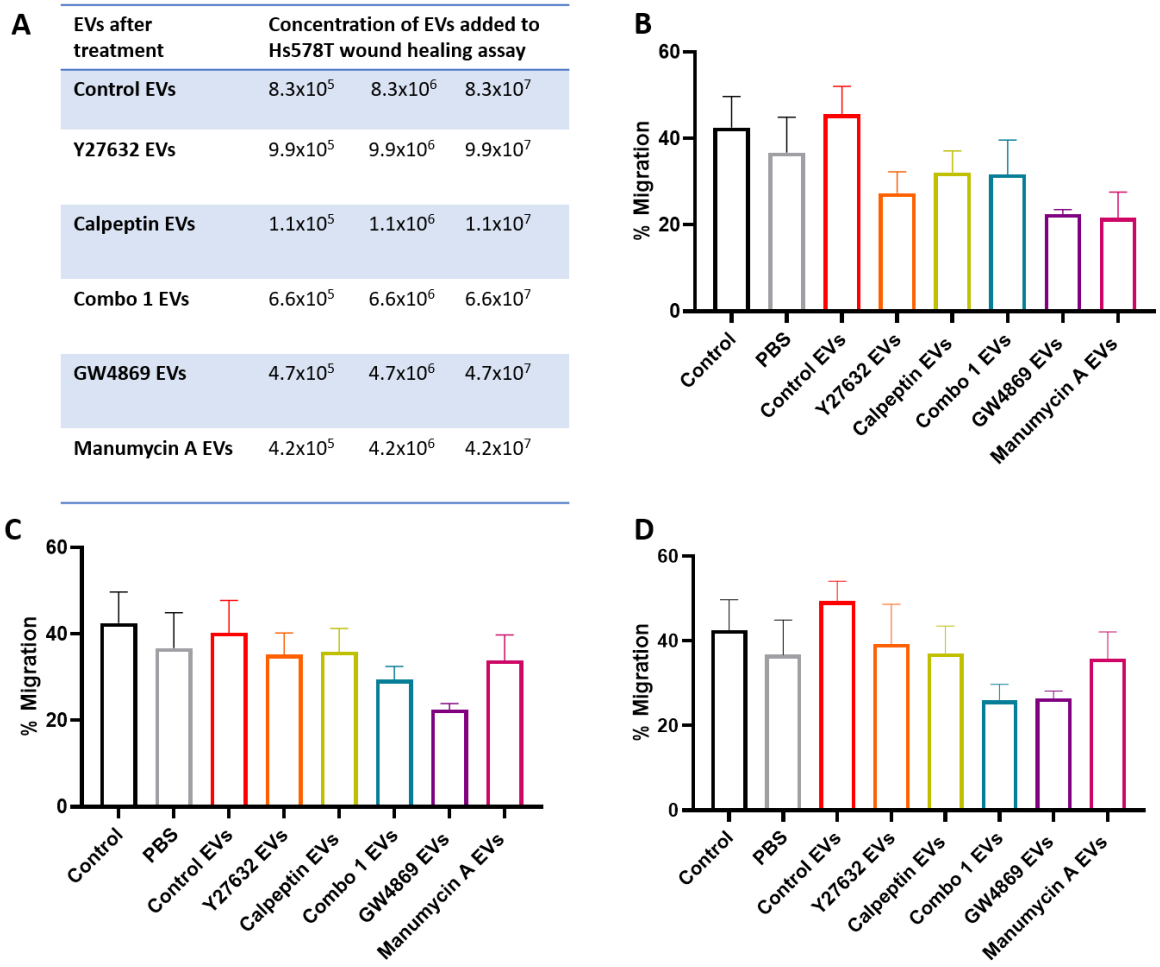

Figure A.6: Hs578T cell migration with Hs578Ts(i)$_8$ EV treatment

Hs578T cells were treated with EVs released after inhibitor treatment to investigate their ability to affect cell migration. (A) Amount of EVs added was kept constant between assays. Wound healing was monitored over 24 hrs (B-D) with three increasing quantities of EVs. Control is Hs578T cells treated with medium alone. Graphs represent mean ± SEM of *n=3* independent experiments.

Overall, Hs578T migration was not significantly reduced when treated with EVs released from Hs578Ts(i)$_8$ cells after treatment with any inhibitor

MDA-MB-468 cell migration was investigated, keeping the EV quantities constant between both assays (Fig. A.7 (A)). Cell migration was monitored over 48hrs, with images taken at 0hrs, 24 hrs and 48hrs after treatment. EVs released from untreated Hs578Ts(i)$_8$ cells increased cell migration compared to the control with three increasing doses of EVs after 24hrs, with significance at the highest dose (*p=0.035*) (Fig. A.7 (B-D)). EVs released after all inhibitor treatments decreased MDA-MB-468 migration when compared to EVs released after no inhibitor treatment after 24hrs, with the quantities of 5.4 x 10^6 EVs released after Y27632 treatment (*p=0.032*) (Fig. A.7 (B)), 3.6 x 10^8 EVs released after combo 1 treatment (*p=0.017*) (Fig. A.7 (C)) and 4.2 x 10^8 EVs released after manumycin A treatment (*p=0.022*) (Fig. A.7 (C)) significantly decreasing migration. However, none of them maintained significance across all EV quantities tested. After 48 hrs, all EVs inhibited migration compared to EV released after no inhibitor treatment, but no significance was reached (Fig. A.7 (B-G)).

A

Potential inhibitor	Quantity of EV added to MDA-MB-468 wound healing assay		
Control EVs	$4.5x10^6$	$4.5x10^7$	$4.5x10^8$
Y27632 EVs	$5.4x10^6$	$5.4x10^7$	$5.4x10^8$
Calpeptin EVs	$6.0x10^6$	$6.0x10^7$	$6.0x10^8$
Combo 1 EVs	$3.6x10^6$	$3.6x10^7$	$3.6x10^8$
GW4869 EVs	$2.6x10^6$	$2.6x10^7$	$2.6x10^8$
Manumycin A EVs	$4.2x10^6$	$4.2x10^7$	$4.2x10^8$

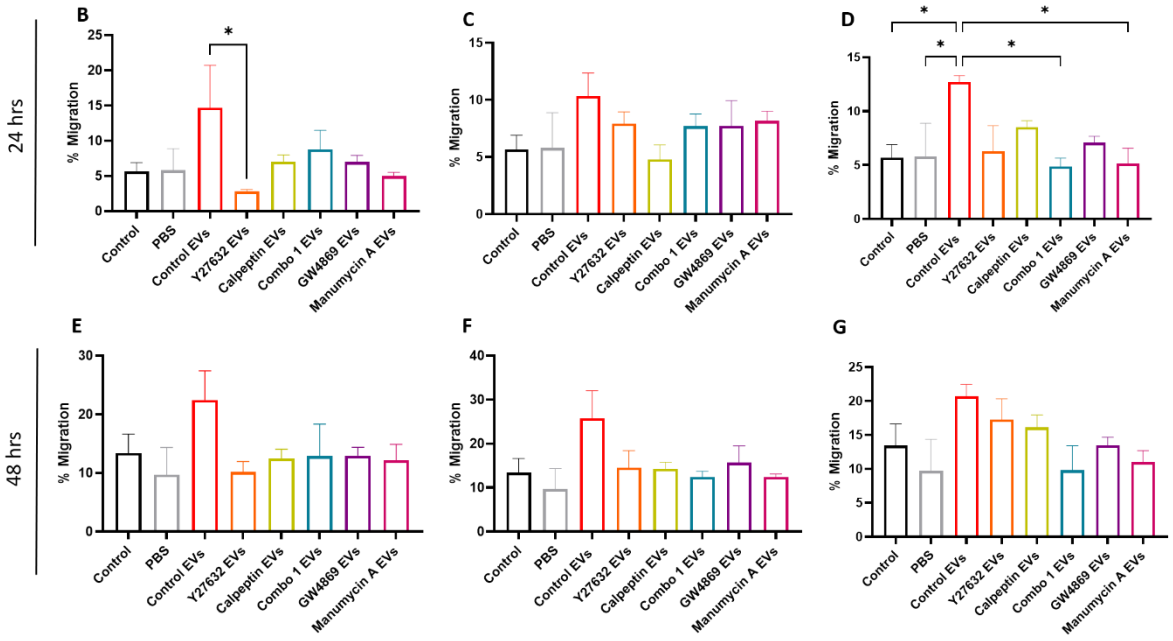

Figure A.*7*: MDA-MB-468 cell migration with Hs578Ts(i)$_8$ EV treatment

MDA-MB-468 cells were treated with EVs released after inhibitor treatment of Hs578Ts(i)$_8$ cells to investigate their ability to affect cell migration. (A) EV quantities added was kept constant between assays. Cell migration was monitored over 24 hrs (B-D) and 48 hrs (E-G) with three increasing quantities of EVs. Control is MDA-MB-468 cells treated with medium alone. Graphs represent mean ± SEM of *n=3* independent experiments. One-way ANOVA was used as statistical test. *P<0.05.

Overall, MDA-MB-468 migration was increased by EVs released from Hs578Ts(i)$_8$ cells after no inhibitor treatment compared to control cells treated with cell medium. After 24 hrs, the lowest dose of EVs released after Y27632 treatment significantly decreased MDA-MB-468 migration compared to EVs released after no treatment. At the highest dose of EVs, MDA-MB-468 migration was significantly reduced by EVs released after combo 1 treatment and EVs released after manumycin A treatment. Both Hs578T and MDA-MB-468 migration was affected by the EVs, however, significance was not achieved across both cell lines and across all EV quantities added.

iv) Comparison of single and double washed EVs

After the addition of a second PBS washing step a comparison was made between EVs separated with a single or double PBS wash. There was no significant difference in EV numbers for control-EVs and GW4869-EVs. However, there was significantly less EVs after a double wash for calpeptin-EVs (*p<0.0001*), Y27632-EVs (*p=0.0001*), combo 1-EVs (*p=0.017*) and manumycin A-EVs (*p=0.03*) (Fig. A.8 (A)). There was also significantly (p=*0.005*) less protein in Y27632-EVs after the double PBS wash (Fig. A.8 (B)).

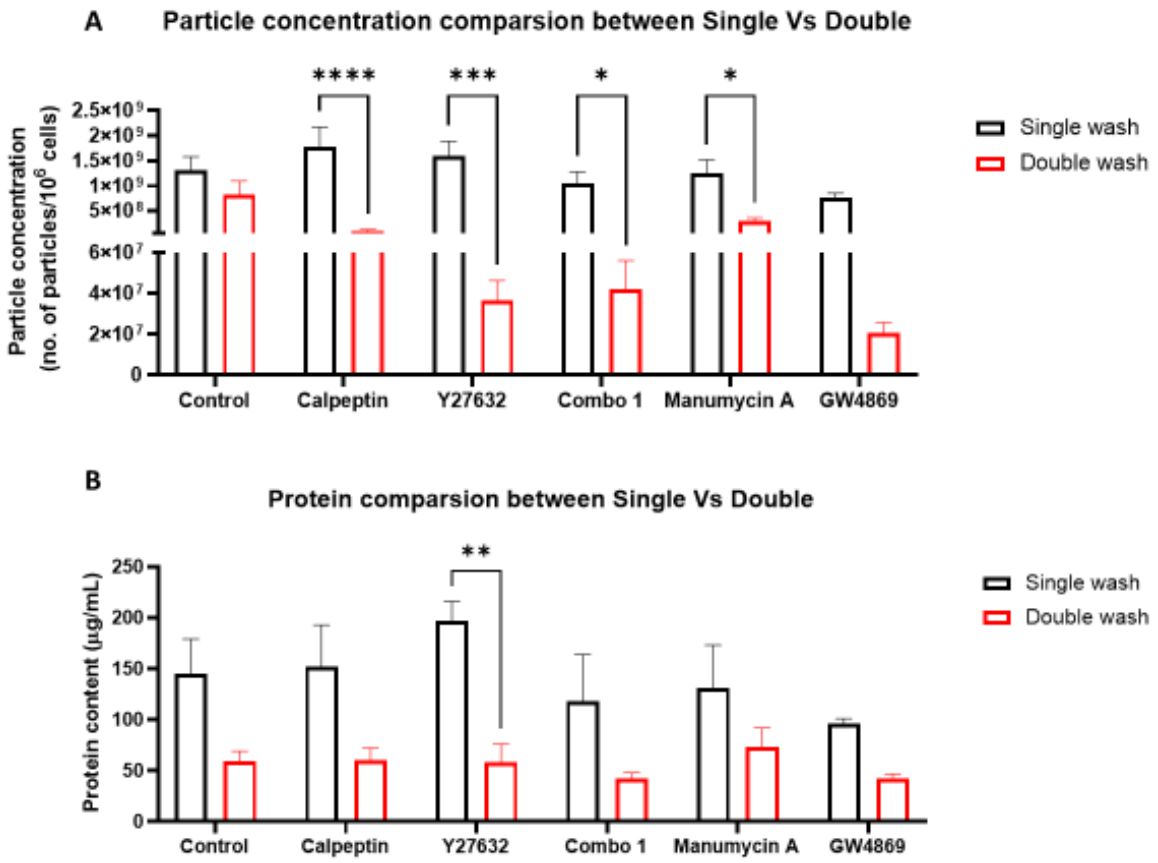

Figure A.8: Single versus double EV particle and protein measurements

A comparison of single and double washed EV (A) particle concentration and (B) protein concentration. Graphs represent mean ± SEM of (A) *n=4* and (B) *n=3* independent biological repeats. Two-way ANOVA was used as statistical test. *P<0.05, **P<0.01, ***P<0.001, P<0.0001.

v) Cytotoxicity assays for small-screening assay

The initial cytotoxicity assays were performed, to determine a concentration for each drug at which cell death did not occur after 48 hrs of treatment. The following drugs, including COTI-2 (Fig. A.9 (A)), carboplatin (Fig. A.9 (B)), neratinib (Fig. A.9 (C)) and sulfisoxazole (Fig. A.9 (D)) were tested in the Hs578Ts(i)$_8$ cell line variant. The concentrations chosen and the viability are given (Fig. A.9 (E)).

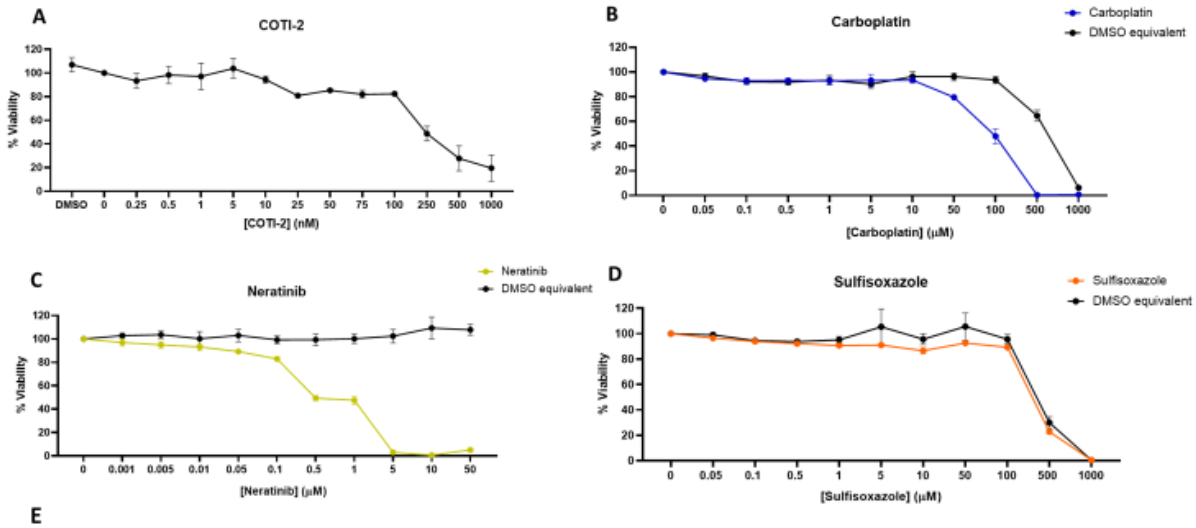

E

Inhibitor	Concentration chosen	Viability (%) (n=3)
COTI-2	5 nM	103.9 ± 11.8
Carboplatin	10 μM	93.4 ± 2.9
Neratinib	0.01 μM	93.2 ± 4.3
Sulfisoxazole	50 μM	92.6 ± 0.8

Figure A.9: Cytotoxicity assay in Hs578Ts(i)$_8$ cell line variant

Cytotoxicity assay were performed on the Hs578Ts(i)$_8$ cell line variant using (A) COTI-2, (B) carboplatin, (C) neratinib, and (D) sufisoxazole. (E) The concentration chosen are displayed along with the percent of viability at that given concentration. Graphs represent mean ± SEM of *n=3* independent biological experiments.

Next the cell line MDA-MB-468 was tested for cytotoxicity when treated with neratinib (Fig. A.10 (A)), carboplatin (Fig. A.10 (B)), GW4869 (Fig. 4.16 (C)), Sulfisoxazole (Fig. 4.17 (D)), manumycin A (Fig. A.10 (E)) and COTI-2 (Fig. A.10 (F)). The chosen concentration and the viability are given (Fig. A.10 (G)).

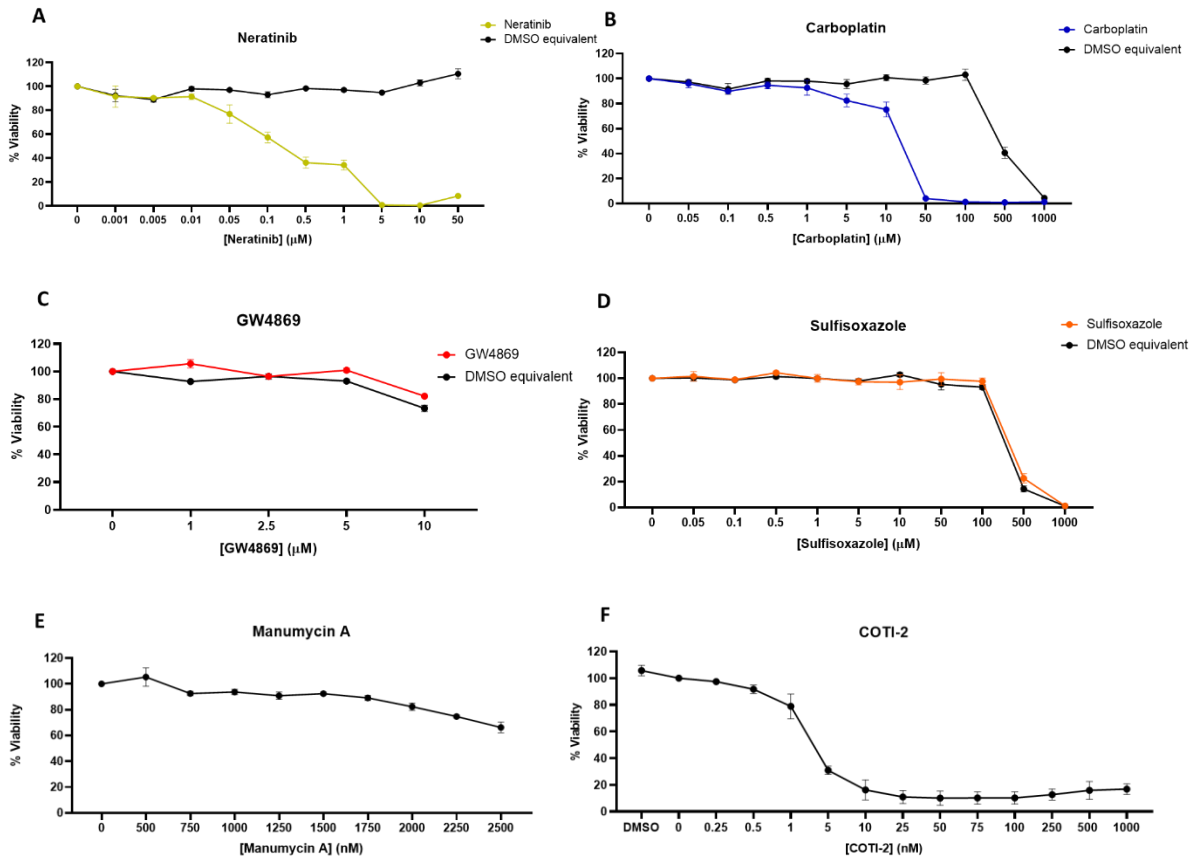

G

Inhibitor	Concentration chosen	Viability (%) (n=3)
Neratinib	0.01 μM	91.4 ± 3.3
Carboplatin	0.5 μM	94.6 ± 3.9
GW4869	5 μM	100.9 ± 1.6
Sulfisoxazole	100 μM	92.6 ± 0.8
Manumycin A	1.5 μM	97.7 ± 3.5
COTI-2	0.25 nM	97.4 ± 0.9

Figure A.10: Cytotoxicity assay in MDA-MB-468 cell line

Cytotoxicity assay were performed on the MDA-MB-468 cell line using (A) neratinib, (B) carboplatin, (C) GW4869, (D) sufisoxazole, (E) manumycin A, and (F) COTI-2. (G) The concentration chosen are displayed along with the percent of viability at that given concentration. Graphs represent mean ± SEM of *n=3* independent biological experiments.

The HCC1143 cell line was also treated with neratinib (Fig. A.11 (A)), carboplatin (Fig. A.11 (B)), GW4869 (Fig. A.11 (C)), sulfisoxazole (Fig.A.11 (D)), manumycin A (Fig. A.11 (E)) and COTI-2 (Fig. A.11 (F)). The chosen concentration and the viability are given (Fig. A.11 (G)).

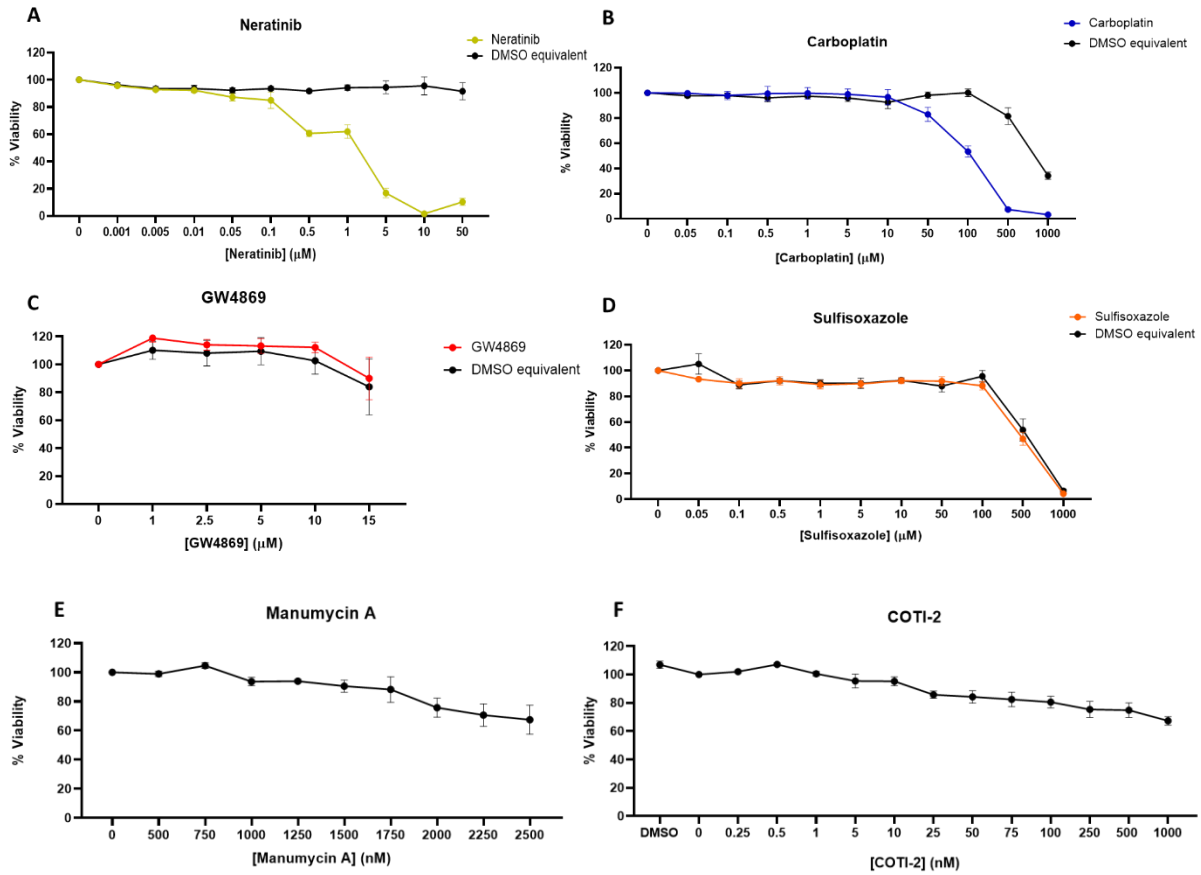

G

Inhibitor	Concentration chosen	Viability (%) (n=3)
Neratinib	0.01 µM	92.2 ± 2.3
Carboplatin	10 µM	96.7 ± 8.7
GW4869	10 µM	112.2 ± 6.5
Sulfisoxazole	50 µM	91.9 ± 4.8
Manumycin A	1.5 µM	90.5 ± 4.2
COTI-2	10 nM	95.3 ± 4.4

Figure A.11: Cytotoxicity assay in HCC1143 cell line

Cytotoxicity assay were performed on the HCC1143 cell line using (A) neratinib, (B) carboplatin, (C) GW4869, (D) sufisoxazole, (E) manumycin A, and (F) COTI-2. (G) The concentration chosen are displayed along with the percent of viability at that given concentration. Graphs represent mean ± SEM of *n=3* independent biological experiments.

MDA-MB-231 cells were treated with neratinib (Fig. A.12 (A)), carboplatin (Fig. A.12 (B)), GW4869 (Fig. A.12 (C)), sulfisoxazole (Fig. A.12 (D)), manumycin A (Fig. A.12 (E)) and COTI-2 (Fig. A.12 (F)). The chosen concentration and the viability are given (Fig. A.12 (G)).

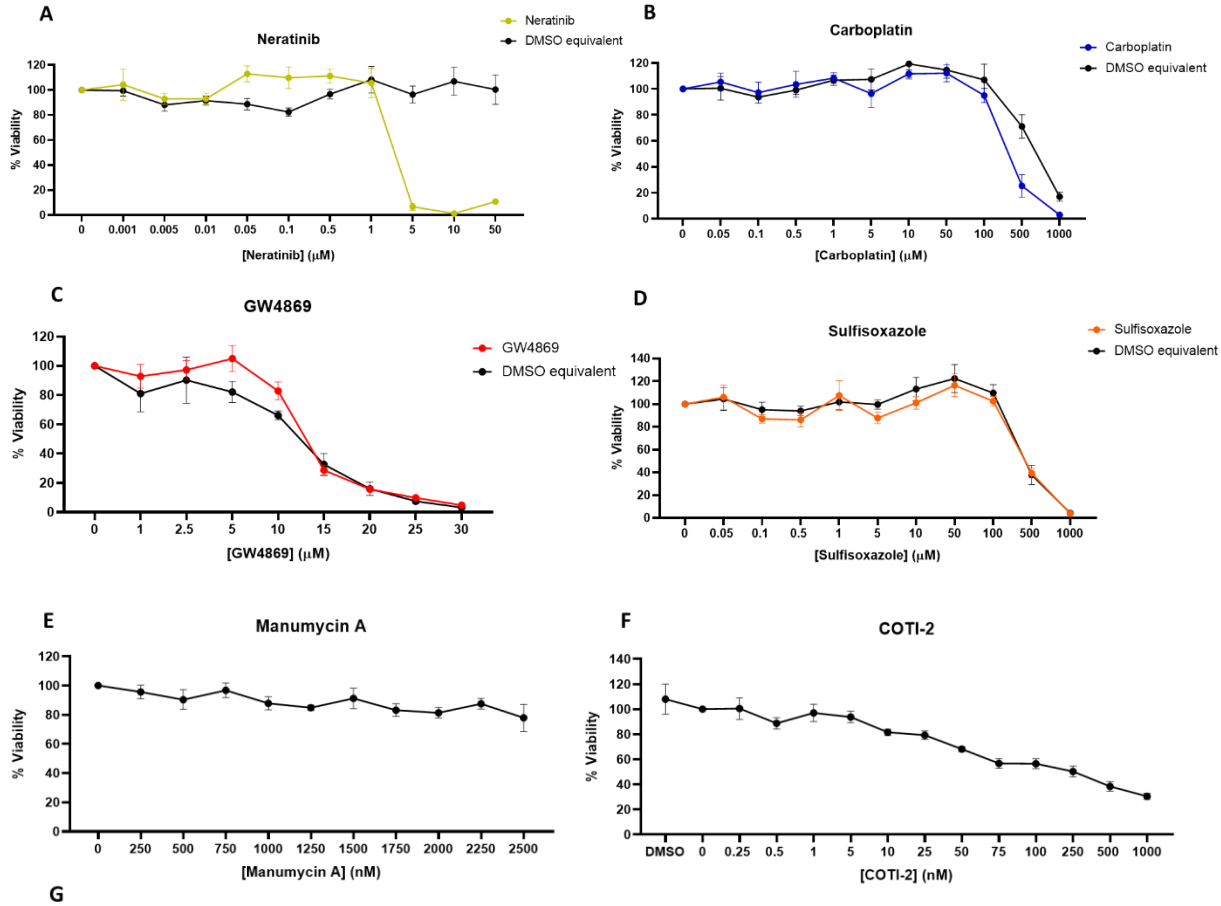

G

Inhibitor	Concentration chosen	Viability (%) (n=3)
Neratinib	1 µM	105.7 ± 16.8
Carboplatin	100 µM	95.0 ± 7.6
GW4869	5 µM	105.0 ± 12.6
Sulfisoxazole	100 µM	102.6 ± 7.1
Manumycin A	750 nM	96.8 ± 7.0
COTI-2	5 nM	93.8 ± 7.8

Figure A.12: Cytotoxicity assay in MDA-MB-231 cell line

Cytotoxicity assay were performed on the MDA-MB-231 cell line using (A) neratinib, (B) carboplatin, (C) GW4869, (D) sufisoxazole, (E) manumycin A, and (F) COTI-2. (G) The concentration chosen are displayed along with the percent of viability at that given concentration. Graphs represent mean ± SEM of *n=3* independent biological experiments.

Lastly, the BT549 cell line was also treated with neratinib (Fig. A.13 (A)), carboplatin (Fig. A.13 (B)), GW4869 (Fig. A.13 (C)), sulfisoxazole (Fig. A.13 (D)), manumycin A (Fig. A.13 (E)) and COTI-2 (Fig. A.13 (F)). The chosen concentration and the viability are given (Fig. A.13 (G)).

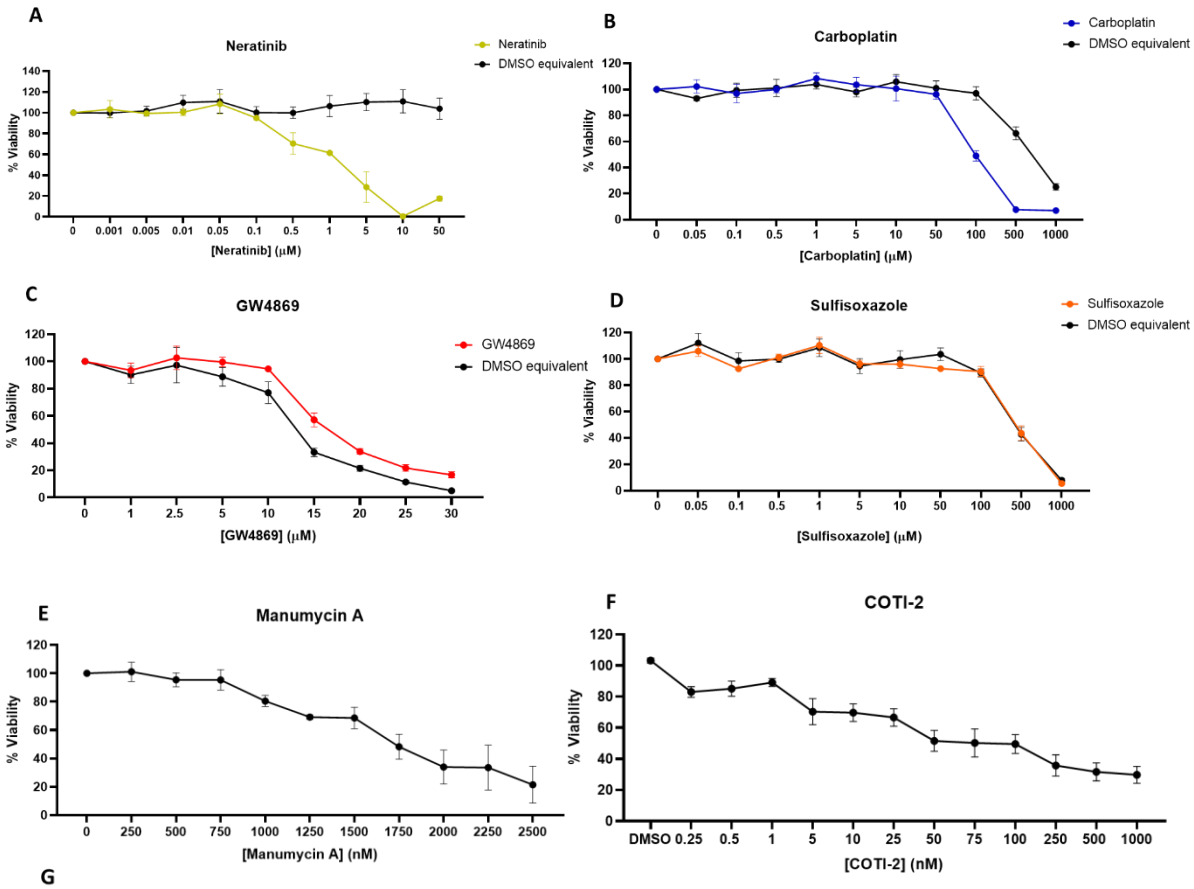

G

Inhibitor	Concentration chosen	Viability (%) (n=3)
Neratinib	0.1 μM	94.9 ± 2.6
Carboplatin	50 μM	96.3 ± 5.9
GW4869	5 μM	97.6 ± 5.9
Sulfisoxazole	50 μM	92.7 ± 0.9
Manumycin A	750 nM	95.3 ± 10.2
COTI-2	1 nM	89.2 ± 4.5

Figure A.13: Cytotoxicity assay in BT549 cell line

Cytotoxicity assay were performed on the BT549 cell line using (A) neratinib, (B) carboplatin, (C) GW4869, (D) sulfisoxazole, (E) manumycin A, and (F) COTI-2. (G) The concentration chosen are displayed along with the percent of viability at that given concentration. Graphs represent mean ± SEM of *n=3* independent biological experiments.

vi) Experimental controls for IFCM small-scale screening

Experimental controls used for IFCM analysis of TNBC CM for CD9 positivity are shown. Unstained control and PBS controls were included (Fig. A.14 (A-B)). Media used for each cell line that were set up the same but were not conditioned by TNBC cells were also included in the analysis to determine background CD9 positivity in the media for Hs578Ts(i)$_8$ cells (Fig. A.14 (C)), HCC1143 and BT549 cells (Fig. A.14 (D)), and MDA-MB-468 ad MDA-MB-231 media (Fig. A.14 (E)). NP-40 controls were included to determine if the CD9 positivity detected was derived from EVs in the CM. There was a decrease in CD9 in the CM when comparing untreated CM and NP-40 control of HCC1143 cells (Fig. A.14 (F-G)), MDA-MB-468 cell (Fig. A.14 (H-I)), Hs578Ts(i)$_8$ (Fig. A.14 (J-K)), BT549 cells (Fig. A.14 (L-M)) and MDA-MB-231 cells (Fig. A.14 (N-O)).

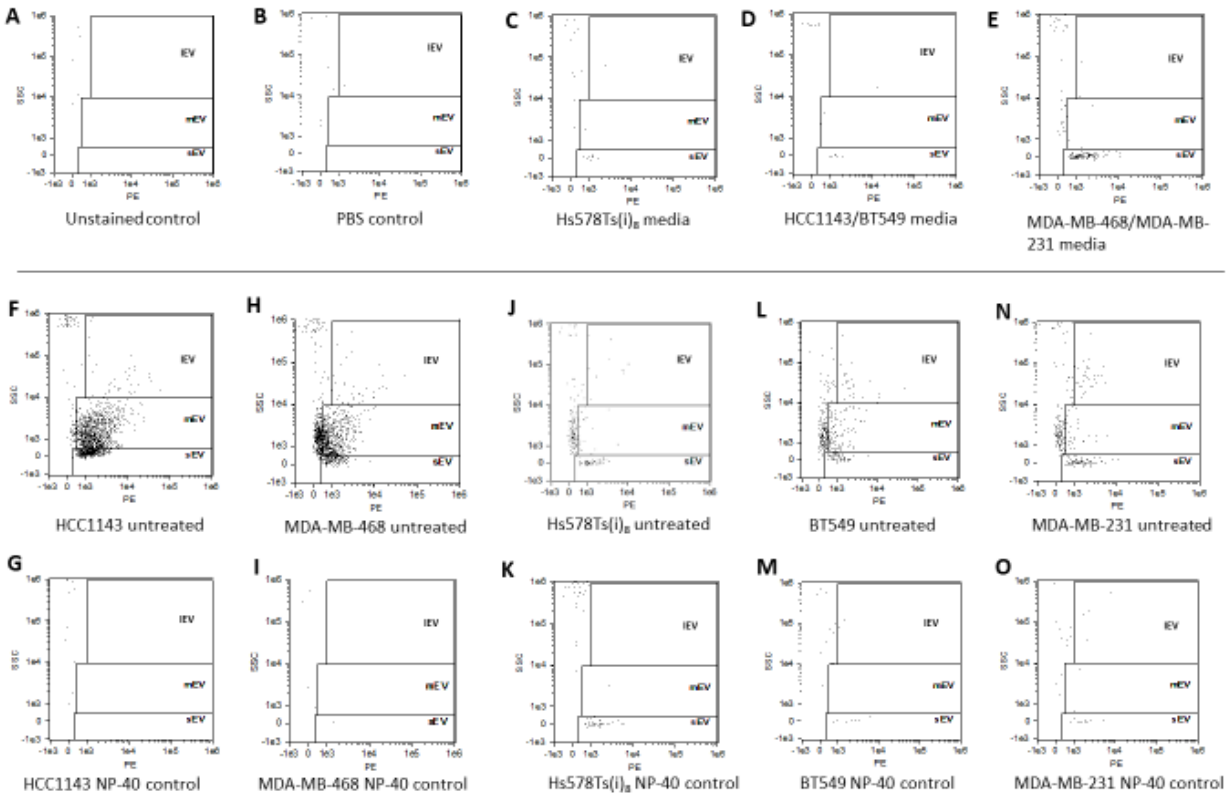

Figure A.14: Experimental controls for IFCM small-scale screening assay
Representative dot plots from IFCM experimental controls including (A) Unstained control, (B) PBS control, (C-E) Media controls, (F-G) HCC1143 NP-40 control, (H-I) MDA-MB-468 NP-40 control, (J-K) Hs578Ts(i)$_8$ NP-40 control, (L-M) BT549 NP-40 control, and (N-O) MDA-MB-468 NP-40 control. A final concentration of 2% NP-40 was used.

vii) Associated Discussion

Figure A.1

Acid phosphatase assay demonstrated that 1000 nM (or 1 μM) of staurosporine induced sufficient apoptosis in the Hs578Ts(i)$_8$ cells that it could be used as positive cell death control in the Annexin V/PI flow cytometry experiments.

Figure A.2-A.7

EV inhibitors were originally investigated after the EVs had been isolated by density gradient ultracentrifugation following which the EV-enriched fractions were pooled and washed once, by ultracentrifugation. The results differ when compared to EVs isolated with two washing steps after density gradient ultracentrifugation. No inhibitor caused a significant decrease in EV release from the Hs578Ts(i)$_8$ cells, nor a substantial change in EV size or protein concentration. Immunoblot analysis demonstrated that actinin-1, flotillin, CD63 and syntenin was carried by EVs following inhibitor treatment with only combo 2 treatment (i.e. manumycin A and GW4869) decreasing CD63 and combo 1 (i.e. calpeptin and Y27632) increasing syntenin in the EVs still released. IFCM demonstrated that the EVs still released after inhibitor treatment had a substantial decrease in CD9 positivity and Y27632 and combo 1 decreased the CD63 and CD81 positivity of the EVs still released. The investigation of the transfer of aggressive traits to recipient cells, Hs578T and MDA-MB-468 revealed that the EVs had a limited effect on their proliferation. The biggest effect was seen on MDA-MB-468 migration. The lowest dose of EVs released after Y27632 treatment substantially decreased MDA-MB-468 migration compared to EVs released after no treatment. At the highest dose of EVs, MDA-MB-468 migration was substantially reduced by EVs released after combo 1 treatment and EVs released after manumycin A treatment.

After the addition of the second washing step in the isolation protocol, the characterisation of the resulting EVs, by NTA (see Fig. 4.4 (A)) in particular gave differing results. The double washed EVs also had a bigger effect on recipient cell migration, as seen in BT549 migration (see Fig. 4.9).

Figure A.8

There was a change in the final EV particle and protein concentrations after adjusting the protocol and including a second PBS wash after the Optiprep density gradient. There was less EV particles and protein measured after the second wash compared to single washed EVs. We hypothesise that remining particle of Optiprep after just one wash may be contributing to the increased particle concentration in single washed samples.

Figure A.9-A.13

Cytotoxicity assay were performed to determine a concentration for each inhibitor that would not be toxic to the panel of TNBC cells.

Figure A.14

The controls were run in parallel with each experiment. Unstained control and PBS controls were used to detect background signals that may also be detected when the CM was analysed. Media controls that underwent the same processing as CM but did not have contact with any TNBC cells was also analysed. Hs578Ts(i)$_8$ DMEM and BT549 and HCC1143 RPMI media had very little CD9 signal. MDA-MB-468 and MDA-MB-231 DMEM had relatively higher background CD9 detection. NP-40 was used to lyse the EVs present in the CM, to understand if the CD9 positivity was associated with membrane-enclosed EVs or with protein complexes within the CM. All of the TNBC CM had greatly reduced CD9 detection following incubation with NP-40 with the exception of Hs578Ts(i)$_8$ CM. A recent study determined that smaller EVs may be more resistant to detergent lysis and this may explain the remaining CD9 signal in the Hs578Ts(i)$_8$ CM.

(B) Chapter 5 appendix: Triple-Negative Breast Cancer EVs and Platelet aggregation

i) Example of light transmission aggregometry (LTA) tracings

Examples of light transmission aggregometry tracings of TNBC cell line variants (Fig B.1 (A-B)) and Hs578Ts(I)$_8$ EVs (Fig. B.1 (C-D)). Platelet aggregation is recorded as a function of time.

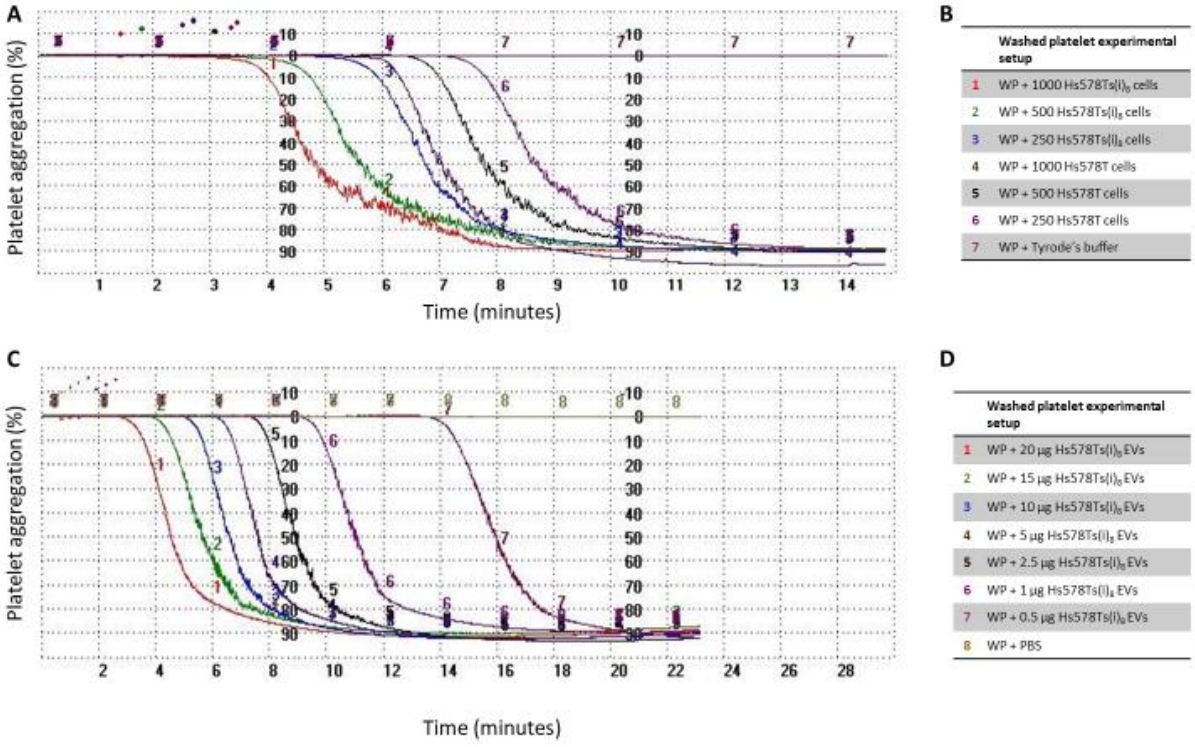

Figure B.1: Examples of light transmission aggregometry tracings
LTA tracings of (A) TNBC cell line variants and (C) Hs578Ts(i)$_8$ EVs induced platelet aggregation. Tyrode's buffer is used as control for cells and PBS is used as control for EV experiments.

ii) Associated discussion

LTA is a "gold standard" method for investigating platelet function. The transmission of light through the washed platelet suspension is increased as the platelet aggregate. From the tracings, the downward trend of the line indicates the onset of platelet aggregation and is measured as a function of time.

Appendix II
Publications, achievements, and presentations

A. Publications

Research article and review

O'Neill S, Porter RK, **McNamee N**, Martinez VG, O'Driscoll L. 2-Deoxy-D-Glucose inhibits aggressive triple-negative breast cancer cells by targeting glycolysis and the cancer stem cell phenotype. Sci Rep. 2019; 9(1):3788. Doi: 10.1038/s41598-019-39789-9.

McNamee N, O'Driscoll L. Extracellular vesicles and anti-cancer drug resistance. *Biochem Biophys Acta Rev Cancer*. 2018;1870(2):123-136. Doi: 10.1016/j.bbcan.2018.07.003.

Book chapter

McNamee, N. and L. O'Driscoll, *Miniaturized In Vitro Assays to Study Cellular Phenotypic Characteristics: Proliferation, Migration, Invasion, and Anoikis-Resistance.* Methods Mol Biol, 2021. 2283: p. 225-232.

Published abstracts

McNamee N, Rodriguez de la Fuente L, Santos-Martinez MJ, O'Driscoll. Extracellular vesicles associated with triple-negative breast cancer induce platelet aggregation. ISEV2021 Abstract Book. Journal of Extracellular Vesicles, 2021. 10(S1): p. e12083.

McNamee N, Catalano M, Mukhopadhya A, O'Driscoll L. Inhibition of extracellular vesicles release in triple negative breast cancer. ISEV2020 Abstract Book. Journal of Extracellular Vesicles, 2020. 9(S2): p. 1806576.

B. Awards and other

ISEV2020 Early Career Investigator Scholarship

C. International and national conferences

McNamee N, Rodriguez de la Fuente L, Santos-Martinez MJ, O'Driscoll**.** Extracellular vesicles associated with triple-negative breast cancer induce platelet aggregation. International Society for Extracellular Vesicles (ISEV) Conference 2021, Virtual (18th-21st May 2021).

McNamee N, Catalano M, Mukhopadhya A, O'Driscoll L. Reduction of aggressiveness of triple-negative breast cancer by blocking extracellular vesicle release. Biomedical Sciences Section of the Royal Academy of Medicine in Ireland (RAMI) meeting, Virtual (3rd February 2021)

McNamee N, Catalano M, Mukhopadhya A, O'Driscoll. Inhibition of extracellular vesicles release in triple negative breast cancer. International Society for Extracellular Vesicles (ISEV) Conference 2020, Virtual (20th-22nd July 2020).

McNamee N, O'Driscoll L. Extracellular vesicle subpopulations in triple negative breast cancer. All-Ireland Schools of Pharmacy Conference, Trinity College Dublin (17th-18th April 2019).